A Study of Photon Counters for X-Ray Astronomy.

A Thesis presented to the
University of Leicester for
the Degree of Doctor of Philosophy
by David George Smith.

1968.

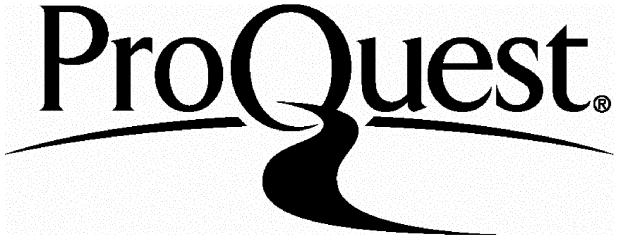

ERRATA

Page 59 line 24	The limiting charge density of 4.10^7 electrons per cm was predicted for a channel possessing an internal diameter of 1 mm and a voltage gradient of 800 volts per cm.
Page 132 line 22	The Bryant and Johnstone space charge maximum amounted to $6.4.\ 10^{-13}$ coulomb (not 6.10^{-14}) which therefore agrees with the measured mean value.

Declaration

I declare that this thesis is my own work and is based on investigations carried out by myself at the University of Leicester, except where otherwise stated. This work has not been presented as a thesis to any other university.

D.G. Smith.

Acknowledgements

This work has been carried out as part of the research programme of the X-Ray Astronomy Group in the Department of Physics. I would like to record my thanks to the Group for the financial and technical support and to the members of the Group, past and present, for their generous help.

Special thanks go to my supervisor, Professor E.A. Stewardson for his encouragement and interest in the work and to Dr. K.A. Pounds who originally suggested the investigations.

It is with pleasure that I record my gratitude to Dr. E. Mathieson of the University of Leicester and to Dr. J.H. Underwood of the Solar Physics Branch, NASA GSFC, Washington, D.C., for many valuable and stimulating discussions.

Part of the work was carried out with the support of a Science Research Council Studentship.

Introduction to Thesis

The work is concerned with the techniques of X-ray detection in the wavelength range 1 Å – 100 Å and was undertaken primarily as a laboratory investigation into the suitability of new detectors for future experiments by the X-ray Astronomy Group of the University of Leicester in its programme of study of solar and non-solar X-ray emissions. Part of the work is related directly to experiments already under development, several of which represent a collaborative effort with the University College, London Space Research Group, headed by Professor R.L.F. Boyd.

Much of the work is concerned with the establishment of the operating characteristics of a comparatively new family of electron multipliers and the application of these devices to the photo-electric detection of X-radiation. In the course of the work it also became necessary to investigate the use of the proportional counter as an absolute photometer in the ultra-soft X-ray region.

In the first two chapters the field of X-ray Astronomy is reviewed and the detection techniques available are surveyed. X-ray image devices and polarimeters are briefly considered although, to date, these devices have seen little use in the X-ray region.

In Chapter 3 the methods developed for the experimental work carried out are described and, where necessary, justified on the basis of subsidiary investigations.

Chapter 4 contains the experimental results, their analysis and interpretation. In the case of the photo-electric yield measurements, some comparison is made with previously reported measurements based on different techniques.

In Chapter 5 the significance of the experimental work is discussed with regard both to the estimated accuracy of the methods used and the practical implications in the case of specific X-ray astronomical experiments. Recommendations for the continuation of the work are also given.

Four Appendices develop further, subsidiary points arising in the main body of the work and the thesis is concluded with reprints of two publications based on part of the research.

Chapter 1. X-Ray Astronomy

Chapter 2. Photon counters for X-ray astronomical experiments.

Chapter 3. The Experimental Work - Apparatus and Procedure.

Chapter 4. The experimental results and their analysis

4.3. The Calibration of satellite proportional counters.

Chapter 5. The Significance of the Experimental Work

Appendices

Chapter 1. X-Ray Astronomy.

1.1. Introduction

X-Ray Astronomy is that branch of astrophysics concerned with the study of the X-ray emissions from stars. As might be expected, X-ray astronomy originated with the discovery, above the earth's atmosphere, of solar x-radiation. This took place in 1948.* In 1962 it became evident that other cosmic X-ray sources existed and, since then, the list of reported sources has grown steadily. At the present time the first optical identifications of cosmic X-ray sources are beginning to appear.

Since the sun is so much nearer the earth than all other stars, it is perhaps not surprising that X-ray astronomy is often quoted as having its origin in 1962; the previous work thereby being relegated to the field of solar physics. However, there is very little philosophical support for such a division, since the only differences that exist in practice between the two fields are those of optical brightness and angular extent.

The name X-ray astronomy is to a certain extent arbitrary for, although γ-ray astronomy also exists, the distinction between the two is not one of photon origin, as in the case of laboratory radiations, but one of

---

* See Chapter 2 for references and details of experiments.

photon energy. Thus X-ray astronomy is the study of cosmic electro-magnetic radiation up to photon energies of the order 10^4 - 10^5 eV and γ-ray astronomy that at higher photon energies. Although the laboratory designation could never have been adopted prior to the establishment of the origins of the cosmic radiation, the energy division is a rather more natural one, since the radiation/matter interaction behaviour, and therefore the observational techniques, are strongly photon energy dependent.

While there is no upper energy limit inherent in X-ray astronomy, (photon energies up to 10^{18} eV. and beyond must be expected, since primary cosmic ray energies of this order have been inferred from experimental measurements on cosmic ray showers), there is what amounts to a natural lower energy limit to non-solar X-ray astronomy. This is set by the absorption of cosmic x-radiation by inter-stellar material. This effect becomes increasingly important at energies below 10^3 eV. and will almost certainly exclude from detection all non-solar radiation below 10^2 eV.

Thus X-ray astronomy extends over at least two, and possibly three, orders of photon energy magnitude. This range may be compared with one order of magnitude for the combined optical region from the far ultra-violet (10 eV.) through visible to the near infra-red (1eV.).

Although the larger observational 'window' will itself allow more spectral information to be gathered, there is extra information to be obtained from X-ray astronomical studies.

1. The onset of inter-stellar absorption allows, in principle, measurements to be made on the nature and density of the inter-stellar medium.
2. Local abundances of the elements in certain of the X-ray emitting regions may be determined from the atomic emission line intensities with less ambiguity of interpretation than exists in the u.v. and optical regions.
3. The fundemental telescope resolutions under diffraction limitation will be much higher than at optical wavelength. Thus at 10 Å, a 4" telescope has the same angular limit as a 200" telescope at 5,000 Å, although it is certain that, as yet, no X-ray telescope has achieved spatial resolutions of this order.

Gould (1967) has recently reviewed the observational results of non-solar X-ray astronomy and gives a comprehensive bibliography of previous review articles.

1.2. Experimental Methods

Owing to the opacity of the earth's atmosphere astronomical observations cannot be made at wavelengths below about 3,000 Å. In the soft X-ray region (< 10 kev) the atmosphere would still be opaque even if composed

solely of molecular hydrogen. Thus X-ray astronomical observations must of necessity be carried out at altitudes at which the X-ray absorption of the residual atmosphere is reduced to a tolerably low level. This height is naturally dependent on the wavelength of observation.

Balloons have a ceiling of about 30 km, which limits their use to photon energies above 15 kev. There is, in effect, also an upper limit of about 50 kev at which level the decreasing cosmic photon count equals the cosmic ray induced atmospheric background. The restriction of balloon experiments to this comparatively narrow spectral range is partly off-set by the launching flexibility of the vehicle, which may conveniently be sent up much closer to the laboratory than the nearest available rocket range. There is also a useful absence of vibration during launch and reliable recovery of the experiment is usually possible.

Sounding rockets have provided by far most of the X-ray astronomical information obtained up to the present time. The principle behind rocket-borne observations is to fire the vehicle high enough above the atmosphere absorption threshold to give observation times typically of the order 10^2 - 10^3 secs. In this period the instrumentation on board follows a sequence of operation according to a pre-programmed set of instructions. The rotational movement of the instrumentation about the centre of gravity of the rocket is usually limited to an extent

dependent on the type of rocket used. For the simplest rockets, this limitation is solely that imposed by the dynamical stability, the most useful outcome of which is a degree of stabilisation in pitch and yaw arising from the roll (or spin) of the rocket about its longitudinal axis. Greater control can be achieved with attitude control units, which combine directional sensors and torque generators, in negative feedback, to maintain the attitude of the rocket to within specified limits. The choice of control unit for a particular experiment depends on the astronomical objectives of the experiment. Thus for a sky-scanning experiment two-axis control would usually be sufficient, whereas for a high (spatial) resolution study of a selected region of the sky three-axis control is required.

Orbiting artificial satellites have, as yet, seen relatively little use in X-ray astronomy. This is partly a result of the natural sequence of technological development, since a satellite is far more complex than a sounding rocket. Considerable delays have arisen in the U.S. OAO and OSO Satellite programmes as a result of technical problems and the mounting cost of the AOSO Satellite has resulted in its cancellation. These delays have been complemented by an increased use of rockets. This took place when it was recognised that rocket experiments were really more suited to the field of research as it stood at the time. Thus against the obvious advantages of a satellite, which include the

availability of superior attitude (or pointing) tolerances and long repeatable observation periods, were set factors such as the greater design flexibility allowed by the higher electrical power allowances, the short commissioning time from conception to launch and the direct use of photographic film.

In the case of a satellite the choice of orbit is fixed by the requirements of the observational programme. Thus, in the case of solar investigation, constant 'illumination' of the satellite will occur in a polar retrograde orbit. As well as providing the maximum observing time, these conditions are necessary in the case of a high-resolution telescope because of the need to maintain thermal stability of the structure.

All experimental information must be transferred by the telemetry system to ground at suitable points in orbit. This involves the 'dumping', on command, of information tape-recorded in orbit from the various experiments on board. Although the use of photographic film is not precluded, it is obvious that processing and analysis must be carried out in the satellite. This method was employed in the U.S. Orbiter Satellites.

1.3 The Information provided by X-Ray Astronomical Studies.

1.3.1. Thermal X-Ray Emission.

Thermal X-ray emission is the description applied to radiation originating under source conditions at, or near, kinetic equilibrium. The general requirement for these conditions to arise is that electron energy-sharing collisions occur sufficiently frequently.

In the case of a source which is optically dense (or opaque), the radiation emerging will gradually become thermal-like, or 'thermalised', regardless of the nature of the original energy processes within the source. Thus such a source will radiate like a black-body and its spectral emission function will be given by Planck's Law:

$$E(d\gamma) = \frac{8\pi h \gamma^5}{c^4(e^{h\gamma/KT}-1)} \, d\gamma \qquad \text{ergs/cm}^2\text{/sec.}$$

Where T is the electron temperature in the outer layers of the source.

This function has a maximum at $h\gamma = 2.82\ K\ T$.

(An equivalent expression giving the distribution as a function of wavelength interval has a maximum at $h\gamma = 4.96$ KT. and, if both distributions are expressed in terms of photon density, then these maxima become re-located at $h\gamma = 1.59$ KT and $h\gamma = 3.92$ KT respectively).

For an optically thin (or transparent) source the effects of self absorption, which lead to the long

wavelength cut-off in the case above , are absent and the spectral profile is found to be that of the electron energy distribution i.e. of Maxwell Boltzmann, or exponential, form:

$$E(d\gamma) = E_0 \, e^{-h\gamma/KT} . d\gamma \text{ erg/sq.cm./sec.}$$

Manley (1966), for example, finds that the spectrum of SCO X-1, the cosmic X-ray source first discovered, is compatible with that of a tenuous cloud of hot hydrogenic plasma in which free-free, or bremsstrahlung, transitions predominate. The works of Karzas and Latter (1961) and of Kvasnica (1960) are cited; the latter with reference to the contribution to the total of the electron-electron bremsstrahlung:

$$\frac{I \text{ (electron-electron)}}{I \text{ (electron-proton)}} = \frac{K T}{m c^2}$$

(This shows clearly that the electron-electron component is negligible here for $T < 10^8$. ^oK.)

Gould in his review paper (1967) has also summarised the experimental evidence for the origin of the X-ray emission from SCO X -1 and gives $T = 5.10^7$ ^oK to fit the data over the whole range (1 - 100 Kev) while at lower energies around 10 Kev $T = 4.0 \times 10^7$ ^oK appears to fit.

It is found that only the atomic interactions give an appreciable X-ray flux at electron energies corresponding to plasma temperatures below 10^8 ^oK (which seems to be the highest considered theoretically

to-date).

Tucker (1967), following previous work (Burbidge et al 1965, Tucker and Gould 1966), has examined the energy loss (or cooling) mechanisms for a hot optically transparent gas at temperatures between 10^6 and 10^8 ^oK under equilibrium conditions. These conditions represent the balance between collisional ionization and excitation by thermal electrons of the atomic species present and the subsequent recombination and de-excitation processes. Unlike in previous works, the effects of dielectronic recombination have been included, since this has been shown to be very important at high temperatures (Burgess 1964 and 1965).

The contributions to the X-ray emission in the spectral range 2 - 8 Å resulting from bremsstrahlung radiation, radiative recombination and line emission are computed for three models each having a different abundance distribution for the elements in the source.

(i) For the cosmic abundances (Aller 1961)

(ii) For a low mass Super Nova Shell.

(iii) For a massive Super Nova Shell.

Both the total emission and the line components are shown to vary considerably from model to model and it is concluded that experimental spectral information will enable several important points to be resolved. The most important of these is the confirmation of thermal conditions in a particular source (as distinct from non-thermal conditions q.v.) and the measure of local

abundance values. This information may be obtained by identifying emission lines and /or recombination edges in the source spectrum, (the latter are to be expected at the ionization energies of the ions present). The author notes that there is an irregularity in the spectrum of SCO-X1 obtained by Grader et al (1966) at about the Fe ^{26} Recombination Edge.

1.3.2. Non-Thermal X-Ray Emission

Introduction.

The principal mechanisms for the generation of non-thermal cosmic x-radiation are Bremsstrahlung generation, the Synchrotron process and the Compton process. These mechanisms result respectively from the interactions of energetic electrons with atomic nuclei, magnetic fields and starlight photons.

In the last two cases, relativistic electron energies are required to give significant emission at X-ray wavelengths (and much higher energies again are required in the first of these than in the second). In general, the emission rates of the synchrotron and Compton processes depend on the relative magnitudes of the magnetic and stellar photon energy densities in the source region (Felten and Morrison, 1966 - eqn. 31).

Synchrotron Radiation

Synchrotron radiation may be considered to be the higher harmonic components of the Larmor (or gyro-) frequency of the relativistic electrons in the magnetic

field and is named after the class of particle accelerator that provides these conditions in the laboratory. These components are very close together and have the appearance of a continuum. It is also referred to as magnetic bremsstrahlung. For a given electron the radiation is emitted in a cone in the forward direction of movement.

Schwinger (1949) has calculated theoretically from classical relativistic considerations a description of the synchrotron radiation characteristics. The frequency distribution of the radiation is dependent on the electron energy E and the magnetic field strength H. The energy radiated into unit frequency interval is found to increase with frequency up to a maximum and then to decrease rapidly. The position of this maximum is slightly higher than the characteristic(or critical)frequency of the radiations ν_c where:

$$\nu_c = \frac{3}{4\pi} \cdot \frac{He}{m} \cdot \left(\frac{E}{mc^2}\right)^2 \quad \left(\frac{He}{2\pi m} = \text{Larmor Frequency}\right)$$

Schwinger shows that the energy density per unit wavelength interval has the form

$$P(d\lambda) = \frac{3^{5/2}}{16\pi^2} \cdot \left(\frac{e^2 c}{R^3}\right) \cdot \left(\frac{E}{mc^2}\right)^7 \cdot G\left(\frac{\lambda_c}{\lambda}\right) \cdot d\lambda$$

Where $G(\lambda_c/\lambda)$ is a universal spectral distribution curve involving Bessel functions of imaginary argument and fractional order.

If a substitution is made for R, the radius of the electron orbit, which under relativistic conditions $V \sim C$, $E \gg mc^2$, is given by $R = \frac{E}{HeC}$, this expression becomes:

$$P(d\lambda) = \frac{3^{5/2}}{16\pi^2} \cdot \left(\frac{e^5}{m^3c^2}\right) \cdot H^3 \cdot \left(\frac{E}{mc^2}\right)^4 \cdot G\left(\frac{\lambda_c}{\lambda}\right)$$

Thus $\nu_c \propto HE^2$ (See Fig. 1.1) and $P(d\lambda) \propto H^3E^4$. Therefore the distribution has everywhere a spectral density increasing steeply with H and E, but with the maximum steadily moving towards shorter wavelengths.

Tomboulian and Hartman (1956) and Bathow et al (1966) have reported on experimental investigations into the characteristics of laboratory synchrotron radiation in the spectral ranges 200 ev. and below, and 15 - 300 kev. respectively. It is claimed that, within the accuracy of measurement, agreement was found with the synchrotron theory (See also Section 1.3.3. on Polarisation). More recently Madden et al (1967) have described new instrumentation for e.u.v. spectroscopic investigations using synchrotron radiation but do not present results.

In the case of cosmic sources of synchrotron radiation, it is most unlikely that mono-energetic electrons will be present. In general, the only type of electron spectrum to be expected is a continuous one, with either a flat or decreasing electron density towards higher energies. (This very fact, incidentally, represents a difficulty when an X-ray source, proposed as a synchrotron emitter, is not also optically visible

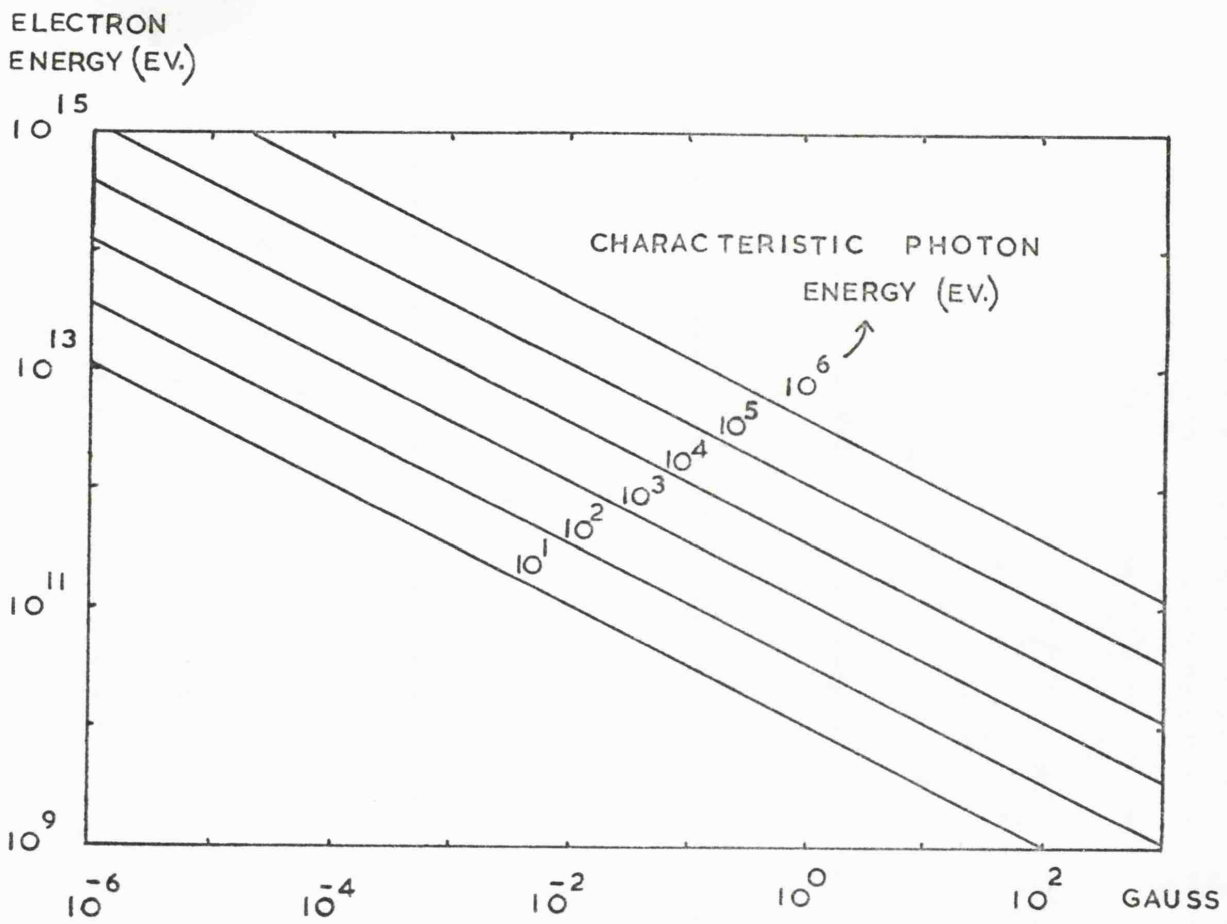

FIG 1.1 SYNCHROTRON RADIATION

(Burbidge et al. 1965)). Thus the spectral profile of an optically thin synchrotron source will be the convolute of the electron energy spectrum and the characteristic synchrotron spectra appropriate to the critical frequencies involved. The spectrum may therefore be expected to be continuous and to broadly reflect the electron energy distribution.

To-date the classical X-ray source of synchrotron appearance is the Crab Nebula (Tau XR - 1), although there is as yet no definite model of the source available.

Evidence for the existence of the source was first offered by Gursky et al (1963) and then by Bowyer et al (1964). The source was positively identified by Bowyer et al (1965a) by means of a rocket-borne lunar occultation experiment. The results presented were claimed to show that the source was 1 arc min. in extent, centered within 30" of the optical centre of the nebula. A subsequent reanalysis of the results, however, has shown that the source is 2 arc. min. in extent, i.e. about the same size as the optical source, and centered 30" the other side of the optical centre (Finn et al 1966).

In astrophysics the Crab is important for many reasons, including the fact that it was the first object to provide clear-cut evidence that the synchrotron process was a significant means of energy dissipation in celestial objects. The source has about the same size and brightness in the optical and radio regions and both radiations are polarised (q.v.) to about the same

extent. Historically the nebula is the expanding remnant of the super nova of 1054 A.D. and dynamical effects are still visible in the form of a fluctuating brightness. In X-ray astronomy the Crab has particular. importance as a possible model of a certain class of source.

The Compton Effect.

The Compton Effect describes the elastic photon-electron interaction. Under laboratory conditions, the photon energy is usually greater than that of the electron, which therefore acquires energy as a result of the interaction. On the cosmic scale, these conditions can become reversed and starlight photons, previously at optical wavelengths, may be blue-shifted to the X-ray region. As with synchrotron radiation, Compton radiation may be conveniently described in terms of a characteristic frequency ν_c where now,

$$\nu c = \left(\frac{E}{mc^2} \right)^2 \cdot \nu$$

for $\frac{mc^2}{h\nu} \gg \frac{E}{mc^2} \gg 1$ (Conditions appropriate to X-ray astronomy)

Where ν = Starlight frequency

E = Electron energy

m = Electron mass

For many electrons, the index of the differential Compton spectrum p is related to that of the electron density spectrum q by:

$$q = 2p - 1$$

(See for example Felten and Morrison 1966).

The process has been proposed by Felten and Morrison (1963) to account in part for the diffuse cosmic X-ray Flux (q.v.). For 5 Kev. X-rays electron energies of 20 - 30 Mev. are required. In their later paper (1966),the authors conclude that the form of the diffuse spectrum in the range 10^3 - 10^6 ev. can be explained in terms of the Inverse Compton radiation from a sufficiently intense power law energy distribution of relativistic electrons in the meta-galaxy.

In what is at present a separate field of study, that of Quasars, Rees and Sciama (1966) have shown that the Compton process is also likely to be an important source of radio emission. Further, since the original photons may possess polarisation from synchrotron origin, the Compton radiation may be wrongly attributed to direct synchrotron processes,which would require much higher electron energies.

Non-Thermal Bremsstrahlung

This class of radiation may be thought of as the 'X-ray tube' type of continuum. The radiation will arise as a result of the interactions of energetic electrons with atomic nuclei (producing free-free energy transitions). Burbidge et al (1965) state that this process is very inefficient compared with the thermal bremsstrahlung case, since about 10^5 times as much energy is lost in inelastic atomic collisions. Giacconi and Gursky (1965) also comment on this. With regard to the generation of electron-electron non-thermal Bremsstrahlung,there do not

appear to be any predictions of the intensities to be expected in the X-ray region commonly available.

1.3.3. Polarised X-Rays.

A preferred plane of X-Ray polarisation may be expected to arise as the result of any constraint on the planes of acceleration of the source electrons. Thus in the absence of significant Stark and Zeeman Effects, for which extremely intense electric and magnetic fields are required (Dolan 1967), atomic line radiations should be unpolarised. Synchrotron radiation, by its very nature, should exhibit a high degree of polarisation. The theoretical prediction given by Schwinger (1949) was verified by Bathow et al(1966) in their experimental synchrotron investigations. Thomson scattering from a polyethylene target was chosen as the polarisation sensitive interaction(The detection techniques available in polarimetry are mentioned in Chapter 2 of this thesis).

Compton scattered radiation will retain the polarisation of the original photons and is not therefore polarised by the interaction itself.

Non-thermal bremsstrahlung, however, should possess polarisation dependent on the degree of uniformity of the electron velocity directions. Korchak (1967) has discussed the information provided by measurements of cosmic X-ray polarisation in general and considers the case of the bremsstrahlung process in particular.

As yet no polarimetric measurements appear to have been reported in X-ray astronomy. This may be taken as an indication of the difficulties associated with such measurements. In the case of the Crab Nebula, it will be surprising if the X-ray emission does not prove to be polarised, in view of the evidence supporting a synchrotron mechanism at optical and radio wavelengths. However, the lack of any experimental measurements represents a conspicious gap in X-ray astronomy.

In the case of the sun (q.v.), the relatively high spatial resolutions available in principle will certainly make polarisation studies worthwhile. Thus, the high velocity particle streams, thought to be associated with the flash phase of a solar flare and other transients, represent possible sources of polarised X-radiation via the Synchrotron and/or Bremsstrahlung processes.

1.3.4. The diffuse background component of cosmic X-radiation.

All measured fluxes not appearing to originate in discrete sources are attributed to this component. Since all experimental measurements of source locations become limited by the quantum statistics of radiation detection when the sources become faint and numerous, the possibility exists that the background is simply the radiation from all unresolved sources (Gould and Burbidge 1963). The other explanation seems to be that

the mechanism of the radiation is the Compton Effect in extra-galactic space (Felten and Morrison 1963 and 1966).

Gould (1967) has summarised the experimentally obtained spectral information which indicates clearly a power law spectrum (energy density per unit photon energy per unit solid angle of sky). He continues to discuss the calculations of the expected intensity and emphasises that these allow potential tests of hypotheses on all of the following questions:

1. The large-scale structure of the Universe,
2. The Universal Cosmic Ray Postulate.
3. The problem of the value of the density of intergalactic matter.
4. The existence of the Cosmic $3^{o}K$ black body radiation.

Felten (1967) has argued that the observed diffuse Flux is compatible with a universal 3^{o} K black body radiation.

1.3.5. Interstellar Absorption.

The most recent estimate of the spectral dependence of the X-ray absorption in interstellar matter has been that of Felten and Gould (1966). In this work the general cosmic abundances of Aller (1961) were adopted. The results differ from those of previous calculations (Strom and Strom 1961), based on the

abundances given by Cameron (1959), mainly in the appearance of distinct K absorption edges of neon and oxygen at 14.2 Å and 23.3 Å respectively. * Felten and Gould proceed to apply their results to the case of the spectrum of SCO X - 1 as measured by Grader et al (1966), which exhibits an absorption-like turnover at about 1 Kev., but conclude that even though the results are consistent with other interstellar material data, the method is not necessarily reliable in the absence of detailed information concerning the source emission spectrum.

In general, measurements of the interstellar absorption will enable estimates to be made of the density of interstellar hydrogen and of the relative abundances of the heavier elements (Felten and Gould showed that these elements dominated the absorption in the energy range considered, 0.1 - 10 Kev.). The case of hydrogen is particularly interesting since only estimates of the atomic component may be obtained from 21 cm. radio observations, whereas the X-ray absorption will be dependent on the total hydrogen content.

---

* The predicted size of the neon edge has already prompted a proposal for its measurement by means of a rocket borne proportional counter. (University of Leicester 1967).

1.4. The Special Case of the Sun

1.4.1. Introduction

That the sun is a special case in X-ray astronomy is evident in several respects, all of which result from the proximity of the object to earth. With the sun, the X-ray astronomer is confronted by a main sequence star of average size still at the Hydrogen burning stage. Conditions of spherical symmetry are evident on a large scale but complex surface structure is a feature of the optical disc and active coronal regions are commonplace. At X-ray wavelengths it is to be expected that, purely on the basis of temperature, the emission arises in the corona (10^6 - 10^7 ^oK) rather than the photosphere ($\sim$6,000 ^oK). This has been borne out by X-ray experiments.

An idea of the experimental possibilities open in the case of the sun, but virtually closed in the case of other cosmic sources, may be obtained by considering the relative magnitudes of the photon fluxes. The X-ray flux from the sun in the wavelength range 2 – 8 Å varies from 10^{-5} erg/sq cm/sec to 10^{-3} erg/sq cm/sec (Bowles et al 1967). In photons this flux amounts to $\sim 10^3 \rightarrow \sim 10^5$ /sq.cm./sec. and dispersing techniques, based on crystals and gratings, can clearly be considered with only moderate collection areas. (To longer wavelengths the solar flux density is much higher and therefore even high-resolution spectroscopy becomes possible).

These solar fluxes may be compared with that of the brightest cosmic X-ray source, SCO X - 1, as given by Friedman (1967). (Flux (2 - 8 Å) = 18.7 photons/sq.cm./sec.).

If we consider also the question of spatial resolution, it is evident that even a 10 arc sec. telescope would resolve the solar disc into about 2.5×10^4 incremental areas or 'picture points', whereas stellar features would remain unresolved at this level of dissection.

The sun represents a special case in other respects, particularly in its role as nucleus of the solar system. Thus, the interaction between the sun and the earth is the seat of all ionospheric phenomena and the study of ionospheric physics must, of necessity, involve knowledge of, or assumptions concerning, solar activity.

The history of solar X-ray astronomy divides fairly naturally into four generations, the last of which is commencing at the present time. (In parallel with this sequence, which is not strictly chronological, are the X-ray film camera programmes mentioned in Chapter 2.)

1. Broad Band Spectrometry (Film, Geiger Counters and Ion Chambers).
2. Narrow Band Spectrometry (Proportional Counters)
3. Moderate resolution crystal spectrometers employing conventional detectors.
4. High resolution crystal spectrometers employing new detectors.

Culhane (1966) has described some X-ray studies of the sun using proportional counter spectrometers. One of the experiments is currently in orbit in the OSO - D satellite and part of the experimental work described in Chapters 3 and 4 concerns the calibration of the proportional counters used. Together with other work, Culhane describes the X-ray development of a class - 2 flare as observed from the UK 1 satellite on 27th April, 1962, and continues to show that the source mechanism here was unlikely to be of a synchrotron nature and suggests a thermal origin instead.

In experiments in which the detectors have a broad field of view, only the whole sun can be observed and locations of source regions on the disc must be inferred from other information obtained in the optical or radio region. Evans et al (1967) have described a counter crystal spectrometer experiment, the results of which have been interpreted in terms of the X-ray line emission from two principal regions of coronal activity as indicated by a 9.1 cm. Radioheliograph. A further quantitative analysis of the spectra is obtained using the equations of Pottasch (1964) and shown to yield values for the electron temperatures of the active regions, abundance values for elements in these regions and estimates for the sizes (Ne^2V) of the active regions and the whole corona (Evans and Pounds 1968).

Other solar emission line studies have been described by Blake et al (1964), Mandelstam (1965 and 1967), Neupert (1965) and Neupert et al (1967).

Blake and House (1967) have discussed the significance of the K_{α} characteristic line emissions with regard to the degree of stripping of the outer atomic electrons.

1.4.2. High Resolution Studies of Solar Emission Line Spectra.

In Chapter 5 a fourth generation crystal spectrometer is described. This instrument was proposed for the OSO - H satellite and is designed to observe selected local regions of the sun (40 arc.sec. square), at wavelengths in the region of 10 Å with a view to measuring the spectral line profiles of certain emission lines. The instrument achieves high spectral resolution ($>3,500$) by means of a crystal spectrometer following up a planar symmetrical parabolic X-ray mirror.

The primary objective is to study emissions from solar active regions and flares and it is anticipated that the possible information content of such a study will include:

1. The measurement of thermal broadening, hence temperature, via the symmetrical Doppler spreading of the emission line (vide infra).

2. The line assymmetries resulting from the Doppler displacement of complete lines by the high velocity transport of solar material (vide infra).

3. The investigation of non-thermal conditions via. the observation of characteristic K emissions.

4. A search, via excess population of higher excitation levels, for evidence for the presence of di-electronic recombination in the corona.

5. The unfolding of regions of the solar X-ray line spectrum too complex to be resolved by instruments of lower resolution.

1.4.3. The natural (or intrinsic) widths of spectral X-ray emission lines.

These widths will define the ultimate sensitivity of any experiment devoted to the mensuration of line profiles and an estimate of the importance of this with regard to X-ray studies now follows.

The natural energy width δE of a spectral line is the uncertainty conjugate of the mean life-time of the state transition involved, τ_{fi} say.

Thus $\delta E \cdot \tau_{fi} \simeq h/4\pi$ (1)

Now $\frac{1}{\tau_{fi}} = A_{fi} = \frac{8\pi}{3h} \left(\frac{2\pi\nu}{c}\right)^3 \cdot |e\, r_{fi}|^2$ (2)

Where A_{fi} = Transition probability per unit time.

ν = Emission frequency.

$|e\, r_{fi}|$ = Matrix element of the Electric Dipole Moment.

Values of A_{fi} can be computed theoretically when the atomic wave functions are available to allow quantal calculations of the relevant matrix elements. (For example see the treatment of Hydrogen by Bethe and Salpeter).

For convenience, it is better to express τ_{fi} in terms of a parameter more commonly used in plasma physics. This is the Oscillator Strength (or f - value) of the transition, f_{fi}, say

$$f_{fi} = \frac{8\pi^2 m\nu}{he^2} \left| e r_{fi} \right|^2 \qquad (3)$$

Now (3) $\div$ (2) gives:

$$\frac{f_{fi}}{A_{fi}} = \frac{3\, mc^3}{2e^2(2\pi\nu)^2} = \frac{3\, C}{2\, r_o(2\pi\nu)^2}$$

(Where $r_o = \frac{e^2}{mc^2}$, The classical electron radius).

This may be re-written as

$$\underline{\tau_{fi} \cdot f_{fi} \cdot E^2} = \frac{c\, h^2}{2\, r_o} = \underline{6.92 \times 10^{-8}\ ev^2 . sec.} \qquad (4)$$

(Where E = photon energy (ev))

Equation (4) represents the elementary relationship between the quantities of interest here. (Gold and Knox (1959) also quote this result).

If β is the fractional line width

From (1) we get $4\pi\beta = \frac{h}{e \cdot \tau_{fi} \cdot E}$

From (4), eliminating τ_{fi}. E, we get

$$\beta = 6.0 \times 10^{-8} \; E \cdot f_{fi} \div 4\pi \qquad (5)$$

or, in terms of wavelength:

$$\beta = 7.4 \times 10^{-4} \; f_{fi} / \lambda\,(\text{Å}) \div 4\pi \qquad (6)$$

Two points of interest follow from these relationships:-

1. In given wavelength region which is not too wide $\beta \propto f_{fi}$ (for all emission lines). Thus the most intense lines (high f-values)will generally be the broadest.
2. For any isoelectronic ion sequence we have for a given transition

$$\nu \tilde{\propto} Z^2$$

and $|e\, r_{fi}| \tilde{\propto} \frac{1}{Z}$

Thus from (3) f_{fi} is approximately constant and from (6) we have

$$d\lambda / \lambda \propto 1/\lambda$$

Therefore $d\lambda$ (Å) also remains approximately constant for the sequence.

Equation (6) is displayed graphically in Fig.1.2. for the spectral region of interest in X-ray astronomical experiments. The significance of these widths is discussed in the following section.

$4\pi\beta = \frac{\Delta\lambda}{\lambda} \cdot 4\pi$

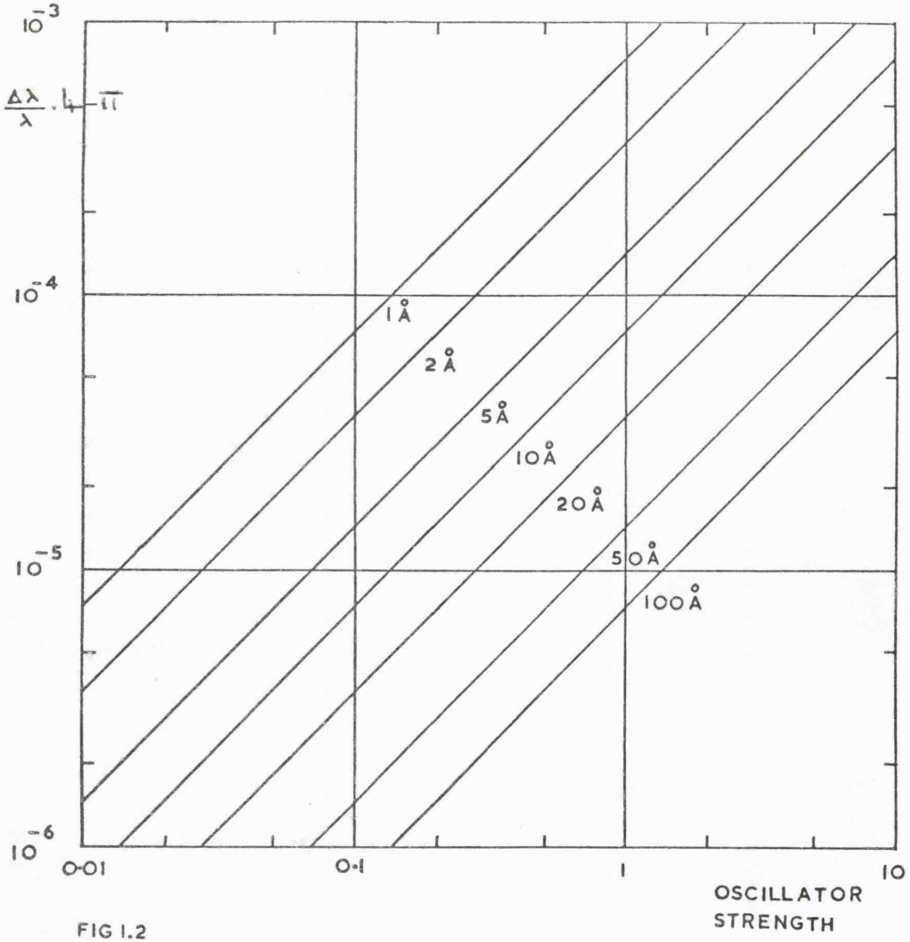

FIG 1.2

1.4.4. Doppler Effects.

a). Bulk Transport

For an ion with a line of sight velocity component V_n the line shift will be given simply by $\frac{d\lambda}{\lambda} = \pm \frac{V_n}{C}$ and displacement of the whole line will occur. The shift is plotted on Fig. 1.3. against V_n.

b). Thermal Broadening.

In the case of thermal velocities, the Doppler shifts will be random, according to the observer, and line broadening will result.

It is assumed that the parent ions are in mutual thermodynamic equilibrium.

Then the velocity distribution is given by

$$n(V) = n(o)\, e^{-\frac{MV^2}{2kT}}$$

Where T is the Ion Temperature (Not necessarily equal to the electron temperature).

This distribution is shown in Fig. 1.4. and would represent the Doppler spectrum if the thermal ions were all travelling along the line of sight.

This is not so and it is necessary to integrate the line of sight Doppler effects over ion velocities in 4π. Complete isotropy is assumed for this purpose.

For ions within $\Phi \rightarrow (\Phi + d\Phi)$ of the line of sight we have:

$$n(Vn) = \frac{n(o)}{4\pi}\, e^{-\frac{MVn^2}{2kT\cos^2\Phi}} \cdot 2\pi \sin\Phi \,.$$

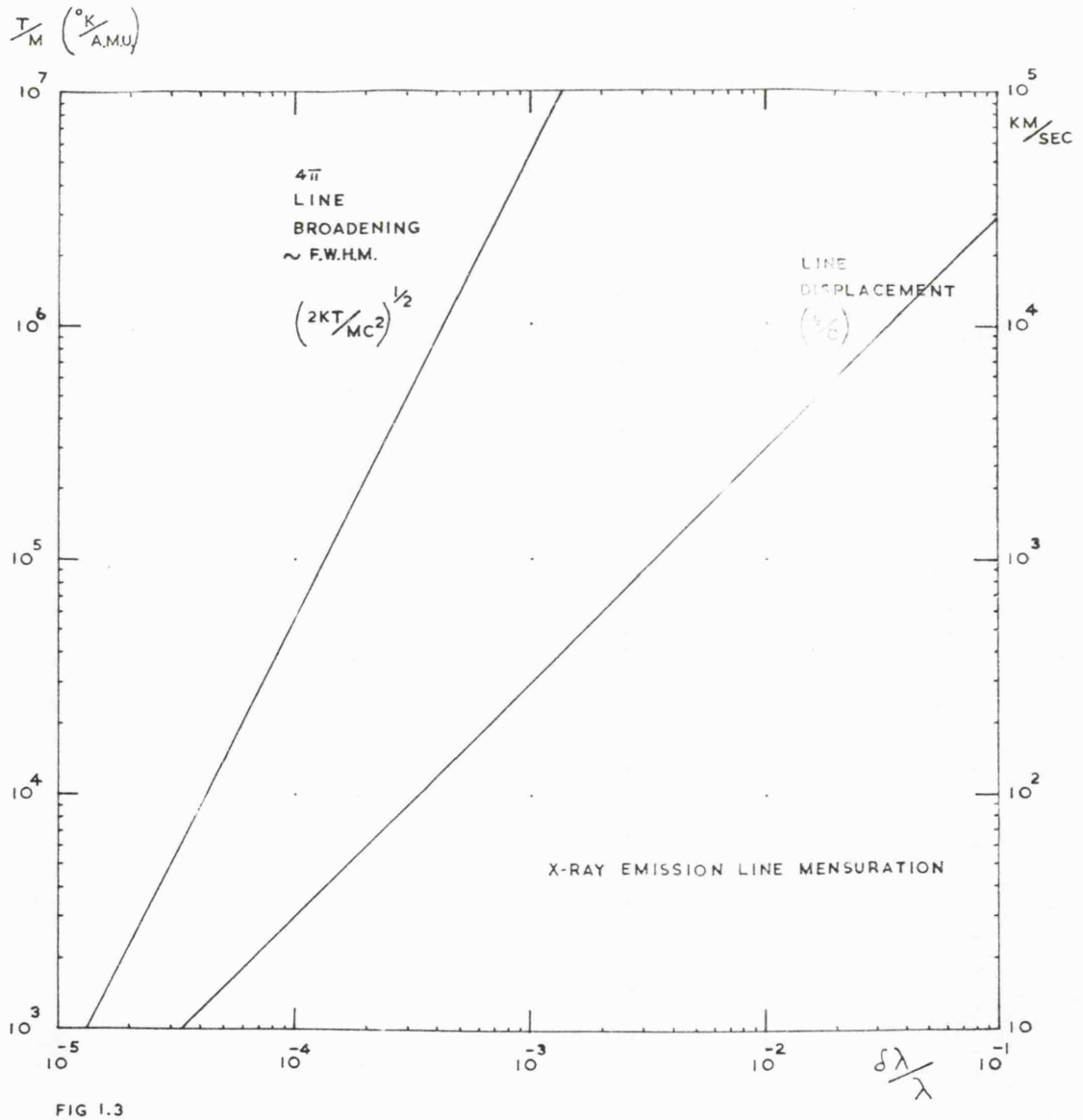
T/M (°K/A.M.U.)
10^7
10^6
10^5
10^4
10^3
10^5
KM/SEC
10^4
10^3
10^2
10
4π
LINE
BROADENING
~ F.W.H.M.
(2KT/MC^2)^1/2
LINE
DISPLACEMENT
(v/c)
X-RAY EMISSION LINE MENSURATION
10^-5
10^-4
10^-3
10^-2
10^-1
δλ/λ

FIG 1.3

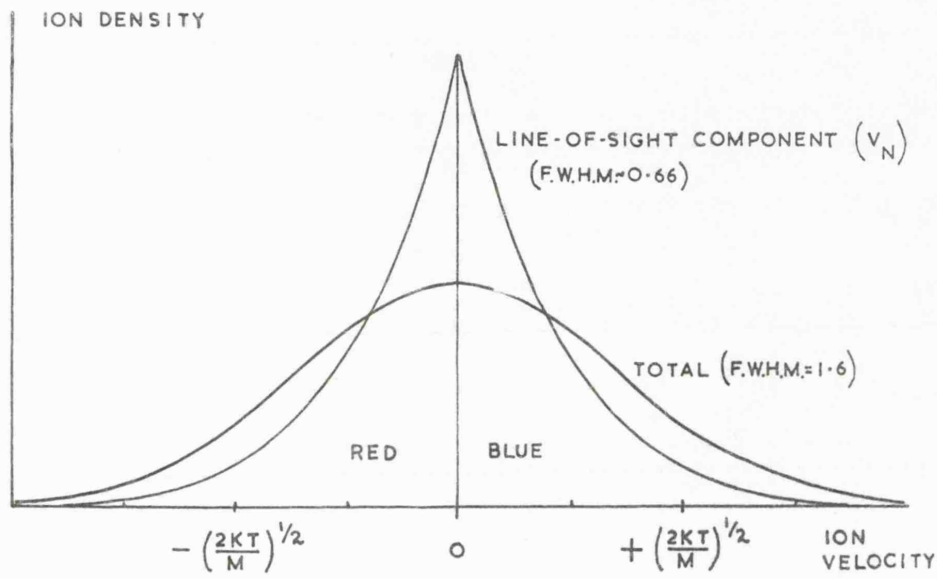
ION DENSITY
LINE-OF-SIGHT COMPONENT (V_N)
(F.W.H.M.=0·66)
TOTAL (F.W.H.M.=1·6)
RED
BLUE
$-\left(\frac{2KT}{M}\right)^{1/2}$
0
$+\left(\frac{2KT}{M}\right)^{1/2}$
ION VELOCITY

FIG 1.4

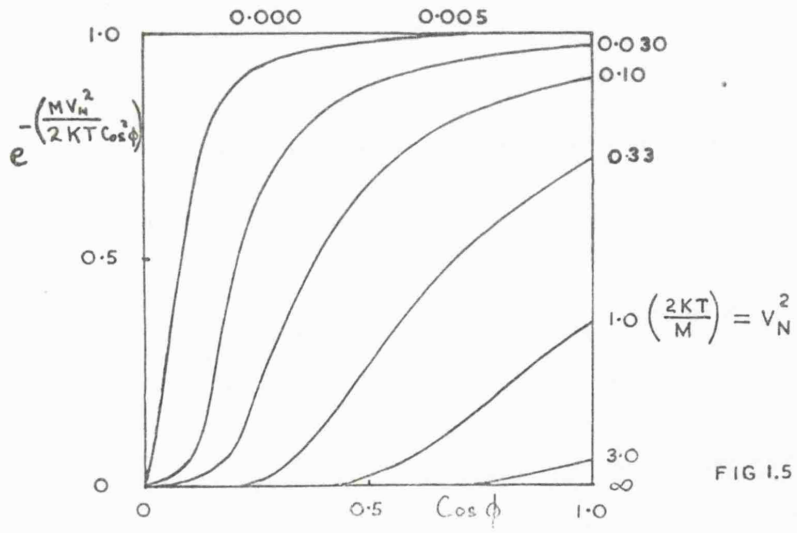
1·0
0·5
0
$e^{-\left(\frac{MV_N^2}{2KT\cos^2\phi}\right)}$
0·000
0·005
0·030
0·10
0·33
1·0 $\left(\frac{2KT}{M}\right) = V_N^2$
3·0
∞
0
0·5
Cos ϕ
1·0

FIG 1.5

Therefore over 2π (to or away from observer) we have for the total electron flux in an increment dVn (Vn is the line of sight velocity component)

$$n(Vn) = \frac{n(o)}{2} \int_0^{\pi/2} e^{-\frac{MVn^2}{2KT\cos^2\Phi}} \sin\Phi \, .d\Phi$$

This distribution of electron density is of the form $\int_0^1 e^{-\frac{A}{x^2}} . \, dx$ Where $A = \frac{MVn^2}{2KT}$

and $x = \cos\Phi$

This integral can be reduced to the error function form $\int e^{-Ky^2} .dy$ but, since tabulated figures must then be used, it is more convenient to integrate directly graphically.

This was carried out on Fig. 1.5 and the new profile is plotted on Fig. 1.4.

The fractional f.w.h.m. is seen to be significantly reduced from about $1.6\sqrt{\frac{2KT}{Mc^2}}$. for the thermal velocity distribution, to about $0.66\sqrt{\frac{2KT}{Mc^2}}$.

In at least one recent text this reduction has not been taken into account (Walker and Straw (1962) p.338).

Values of $1.0\sqrt{\frac{2KT}{Mc^2}}$ are plotted on Fig.1.3. to give the line width as a function of T/M. (The f.w.h.m. was increased by 50% to give a realistic indication of the apparent width of the line since, because the profile is cusp-like, it is not likely to be fully resolved in a measurement).

Fig. 1.3. may be used in conjunction with Fig.1.2. to assess the minimum temperatures necessary to displace or to broaden the intrinsic width of any line to a theoretically measurable value.

Thus, for example, for the Ne X line observed by Evans and Pounds (1968)

($1s^2S_{\frac{1}{2}} - 2p^2P_{\frac{1}{2},\frac{3}{2}}$, $\lambda = 12.13$ Å, assumed f - value = 0.42) we have $4\pi\beta = 2.6 \times 10^{-5}$ from Fig. 1.2.

If the line is now appreciably broadened to, say, $\gtrsim 10^{-45}$ we have, from Fig.1.3.,

$T/M \gtrsim 5.5 \times 10^{42}$

For Ne, $M = 20$. $\therefore T \gtrsim 1.1 \times 10^{64}\ ^{o}K.$

Similarly, taking now the most intense of the Fe XVII lines observed ($1s^22s^22p^6\ ^1S_o - 1s^22s^22p^53s\ ^3P_1$, $\lambda = 17.05$ Å, assumed f - value = 0.11) we obtain

$\beta = 4.8 \times 10^{-6}$. $\div 4\pi$

For a four-fold increase in width, $T/M \gtrsim 2.5 \times 10^{31}$,

For Fe, $M = 56$ $\therefore T \gtrsim 1.4 \times 10^{33}\ ^{o}K$

It will be shown in Chapter 5 that these minimum temperatures will be raised considerably by performance limitations in the instrumentation described.

Chapter 2. Photon Counters for X-ray Astronomical Experiments.

2.1. Introduction

The primary processes in any X-ray detector will be the interaction events between the x-radiation and the detector material. These events will result in a total or partial transfer of energy from the incident radiation to the detector. In general, the nature of the predominant process will depend on the atomic number of the detector medium and/or the photon energy (See for example R.D.Evans, p.712 (1955)).

The photoelectric absorption cross section is dominant in the soft X-ray region over all Z and the process defines the techniques to be adopted for photon registration. The variation of the cross-section τ on the nature of the absorbing material and of photon energy E, is given approximately by:

$$\tau \propto N.Z^5.E^{-8/3}$$

Where N = the No. of atoms of atomic No. Z per unit volume.

The total physical effects of a photo-electric interaction will include the existence of the primary photo electron, which generally will then be re-absorbed via atomic ionization processes in the detector. A finite probability exists for the ejection from the surface of one or more of the electrons acquiring kinetic energy directly or indirectly from the original interaction, this probability defining the external

photoelectric yield of the material. The Auger electrons produced in the photo-effect in other atoms and the fluorescence photons, if re-absorbed, will also contribute to this ionization.

2.2. A Review of Photon Counting Techniques and their application to X-ray Astronomical Experiments.

2.2.1. Introduction

In principle, all detectors are photon counters in that the basic photo-interactions are quantum effects. In practice, however, there are detector noise thresholds below which it is not possible to discern the discrete photon registrations and therefore only the aggregate effects of a large number of photons may then be observed at the detector output. At any given photon energy, the distinction between a counting and a non-counting detector is not a clear one, particularly when the limiting noise level of the non-counting detector is not solely a function of the detector itself but of the equipment that follows. Therefore this section will include brief discussions of the detection techniques not necessarily associated at present with single photon registration.

Boyd (1965) has reviewed techniques for the measurement of extra-terrestrial soft x-radiation.

2.2.2. The Photographic Method.

Atkinson and Pounds (1965) have reported soft X-ray sensitivity calibrations on photographic film in the range 2 - 14 Å. They give photon (per grain) equivalences at 2.1 Å for Ilford G and Kodak SC5 of 1.8 and 1.4 respectively, and suggest that unity equivalence would be expected to shorter wavelengths.

Pounds (1965) also shows that the information density of such film is comparable to the telemetric capacity of a conventional Skylark sender for one flight. Russian measurements on film soft X-ray quantum sensitivities have also been reported (Lukirskii and Karpovich 1959 and Rumsh et al 1964). Tomboulian (1964) presents film calibrations at longer wavelengths (115 - 304 Å) made with thin-window Geiger counters.

In solar X-ray astronomy the use of photographic film has been extensive. Since Burnight (1949) reported the blackening of a piece of film, shielded from visible and ultraviolet light by metal foil, carried on board a sounding rocket, several film pin-hole camera programmes have been carried out (see, for example, the work of Russell (1965 - a and b) and Russell and Pounds (1966)). More sensitive film cameras employing grazing incidence optics to obtain increased collection areas have also been used (Giacconi et al (1965) and Underwood and Muney (1967)). The development of a slitless spectrometer, based on the combination of such a camera and a transmission diffraction grating, has been reported (Gursky and Zehnpfennig 1966). The preliminary laboratory results presented indicate a spectral resolution ($\lambda/d\lambda$) of about 20 in the range 1 — 10 Å (Zehnpfennig 1966).

2.2.3. Gaseous Ionization Methods

With the Geiger mode of operation ionization events are recorded as a sequence of electrical pulses of uniform amplitude. The use of Geiger Counters for soft X-ray detection in the laboratory is well established. Its use for soft X-ray detection was first reported by Neufeldt (1931). In principle, the photon detection efficiency of the counter is defined by the optical transmission factors of the window and of the gas filling. The manufacture of usefully transmissive windows for use beyond 15 Å becomes difficult even with compounds of the lightest elements, however, and care must be taken if absolute flux determinations are required. The problem has been discussed by Lukirskii et al (1960 a) and by Lukirskii and Brytov (1965). It is pointed out in the second paper that it is possible to determine the efficiency of gas counters using thin nitrocellulose windows out to wavelengths of around 400 Å. The problem of the presence of a dead region behind the window is mentioned but not dealt with in detail.

Tomboulian (1964) mentions another correction that must be made. This is the contribution to the Geiger count-rate of photo-electric emission from the back wall of the counter at wavelengths for which the transmission of the gas filling is appreciable.

With regard to the other parameters of detection the typical recovery time of a Geiger counter ($\sim 10^{-4}$ secs)

is rather long for a counting detector (c.f. $\sim 10^{-5}$ sec for a proportional counter and $< 10^{-6}$ sec for a scintillation counter). Parratt (1950) has described a Geiger counter designed to overcome this problem. The gas avalanche in this counter was restricted to local regions of the anode wire by means of glass beads, and count rates up to 10^5 c.p.s. were achieved.

In X-ray astronomy the Geiger counter was the detector with which evidence was first obtained by the ASE - MIT Group for the existence of extra-solar x-radiation (Giacconi et al. 1962). Three geiger counters, each possessing a 20 sq.cm. mica window (two of 0.2 thou. thickness and one of 1.0 thou.), were carried on board an Aerobee sounding rocket with a view to checking experimentally a predicted flux of lunar fluorescent x-radiation. These predictions were not confirmed, but X-radiation was detected from the regions of the Galactic Centre, Cas A and Cyg A. Since that time, most of the observational results in the field below photon energies of 5 kev. have been obtained with Geiger counters. The NRL rocket survey flights have been responsible for much of this work. (See for example Bowyer et al 1965b and Friedman et al. 1967). The work was carried out with large area Geiger counters with windows of 6μ and 25μ Mylar (Melinex) in unstabilized rockets, the sky-scan being produced by spin and precession.

In the proportional mode, ideally the mean output pulse amplitude is proportional to the initial number of of ion pairs generated in the counter gas. The

amplitude distribution of the pulses about the mean value is defined by the statistics of ion-pair production and of the gas multiplication process. In practice, the distribution is approximately Poissonian and therefore approaches a normal (or Gaussian) profile for large initial numbers of ion pairs.

Under conditions in which the Fano Factor, the mean energy per ion pair and the gas multiplication factor are constant, then the profile f.w.h.m. may be expected to vary inversely as the square root of the energy initially dissipated in the counter gas. In return for this extra information, it is necessary to provide for the proportional counter system a well-stabilised EHT supply and a low noise pulse pre-amplifier (neither of which is necessary for geiger operation).

Like the Geiger counter the proportional counter is an established X-ray detector. The spectral variation of the photon detection efficiency again is governed basically by the transmissions of the window and gas filling. Some of the photons absorbed in the gas will form a subsidiary peak in the pulse height distribution following the escape of fluorescent radiation. This peak must be included when absolute flux determinations are being made with the counter, since this is necessary to make valid the assumption that all photons transmitted by the window and absorbed by the gas result in the registration of one count.

Caruso and Neupert (1965) claimed an accuracy of 10% for absolute flux measurements at 44 Å, using a flow proportional counter and a simple source of characteristic C_K radiation. Evidence was presented to illustrate the absence of any dead space behind the counter window.

In Chapters 3 and 4 of this thesis the experimental procedures and results of absolute flux determination using flow proportional counters are described. The purpose of this part of the work was to calibrate a series of satellite proportional counters for two solar experiments. Particular attention was paid to the spectral variations of mean charge output, energy resolution and photon detection efficiency of the counters, under normal operating conditions.

The stability, under extreme operating conditions of high count rates and count totals, of counters generally similar, but employing methane quench gas (instead of carbon dioxide), has been described by Sanford and Culhane (1967).

For proportional counters for non-solar X-ray astronomical experiments, extreme operating conditions must also be catered for. The count rates and count totals will be comparatively low but large collection areas and low counting backgrounds are required.

These requirements are conflicting in that a large area detector will usually possess a high cosmic background count rate as a result of a large active volume. Although the use of X-ray reflection optics

and a small volume detector can circumvent this problem, it is usually necessary to resort to low-background methods using either anti-coincidence techniques or pulse rise-time discrimination, or both (see for example Culhane et al. 1966).

The need for a large collection area also means that non-ideal counter geometries must be employed, since a cylindrically symmetrical design is wasteful of window space. The effect of this will be reflected mainly in the energy resolution of the counter.

Fig. 2.1. displays the energy resolutions reported for some proportional counters used in X-ray astronomical experiments. Also added for comparison, is the resolution of one of the monitor counters used in the laboratory work described in Chapters 3 and 4 and the ultimate resolution predicted for proportional counters in Chapter 4. With regard to the X-ray Astronomical counters, it is evident that considerable spread in performance exists. The time dependent changes present result from counter instability following gas seal-off. The resolution change from 28% to 70% at 5.9 Kev (Fe^{55} radiation) reported by Harries et al (1967) represents a particularly serious shift. A comparison with Fig. 2.4. will show that this resolution makes this counter inferior in performance to some scintillation detectors.

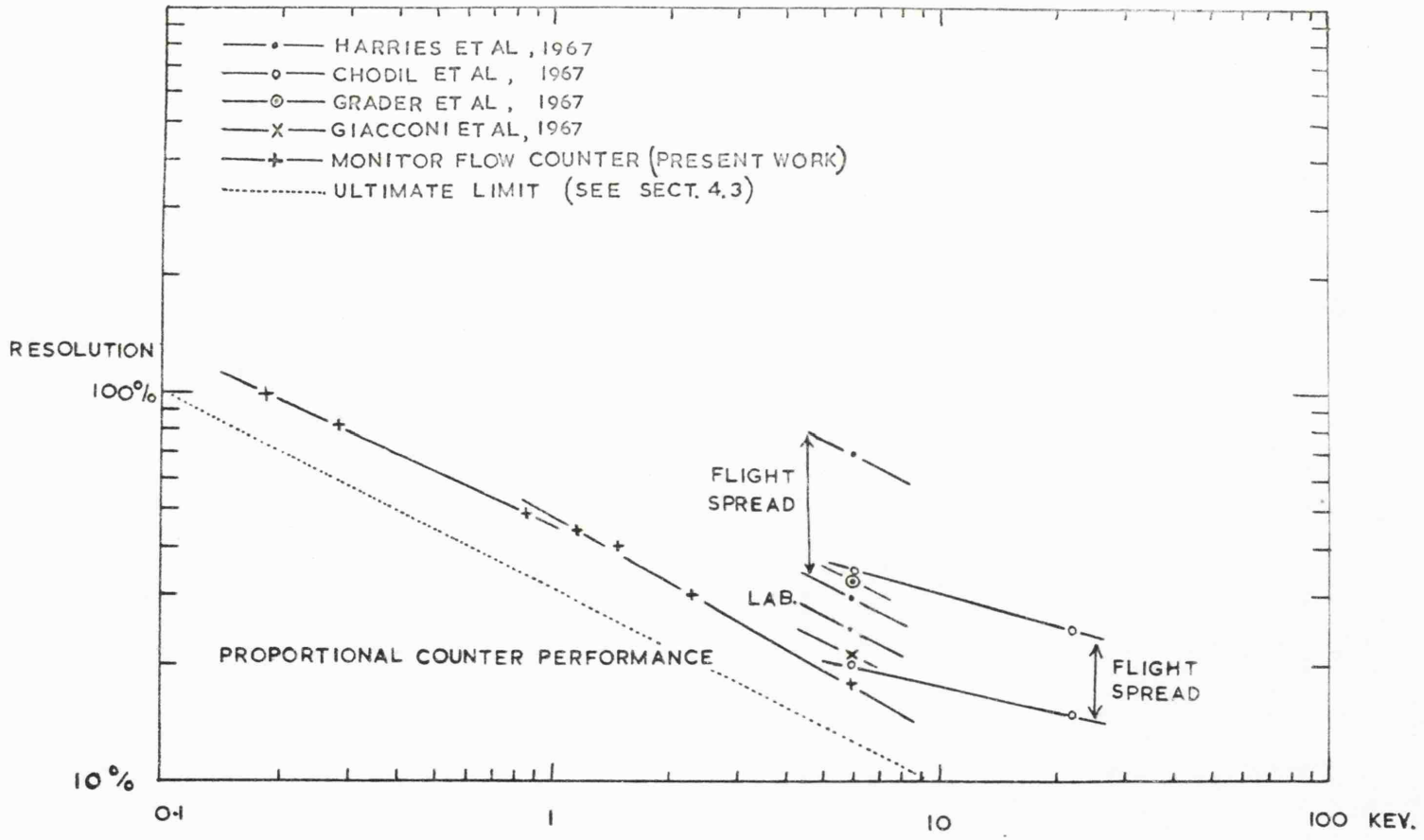
HARRIES ET AL , 1967
CHODIL ET AL , 1967
GRADER ET AL , 1967
GIACCONI ET AL, 1967
MONITOR FLOW COUNTER (PRESENT WORK)
ULTIMATE LIMIT (SEE SECT. 4.3)
RESOLUTION
100%
10 %
FLIGHT SPREAD
LAB.
PROPORTIONAL COUNTER PERFORMANCE
FLIGHT SPREAD
0·1
1
10
100 KEV.

FIG 2.1

2.2.4. Solid State Ionization Detectors

At high photon energies (> 20 KeV.) it becomes difficult to provide for the complete absorption of the radiation in a gas counter of normal dimensions and, for this reason alone, it is necessary to employ solid state detectors. At lower photon energies, however, the higher intrinsic energy resolution offered by the semi-conductor solid state detector also makes the device attractive. In general, the ionization products in the solid state material may be detected by means of the electronic registration of the initial electron-hole pairs, or by means of the secondary processes characteristic of the excited parent atoms. Into the second category falls the photographic process, the scintillation method and the thermo-luminescent detector.

Direct Electronic Registration

For the direct electronic detection of the initial ionization products it may be readily shown that, from shot noise considerations alone, very little leakage current is tolerable in thedetector. (See Appendix 4). Thus it is necessary either to decrease this current to an acceptably low value, or to multiply in some way the initial ionization product.

In the conventional photo-conductor the first requirement necessitates the use of high resistivity detector material. Zizzo and Platt (1949) obtained

single quantum registrations at photon energies of about 45 KeV with a Cadmium Sulphide crystal having carbon (dag) electrodes on opposite faces. No measurement of quantum efficiency was given, other than the estimate that only 1% of the X-ray photo current could be accounted for in pulse form above the counting threshold.

Frerichs (1950) did not consider the effects of single quanta but claimed that, in noise level, a Cadmium Sulphide crystal with dag electrodes compared well with a scintillation detector at a wavelength of 1.54 $\overset{o}{A}$. Henry and Cole (1959) compared a Cadmium Sulphide detector and a geiger counter at about the same wavelength. Comparable Spectra were recorded with both detectors but it was concluded that the Cadmium Sulphide detector did not compare at low intensity levels. Electrodes of Indium and Silver paste were used in this work. Much work has subsequently been reported on the γ - ray photo-conductivity of Cadmium Sulphide, (see for example Rompe and Schnürer (1960) and Franks (1961)), but the application of this material and other materials would seem to be limited to the field of dosimetry in which high γ - ray fluxes are detected with response times of seconds or minutes.

With the semi-conductor barrier detector, a low current is achieved by producing and reverse biassing a planar p - n junction in a piece of solid state material, usually Ge or Si. The radiation absorbed in

the depletion layer produces electron-hole pairs in a region otherwise relatively carrier-free and an electronic pulse is formed during carrier separation and collection by the reverse field.

In the soft X-ray region, there are two particularly severe problems associated with the use of these detectors for photon registration. The first is the need to absorb the X-ray photons in the depletion region, which will always be a certain minimum depth below the surface of the detector. The second is the fundamental electronic noise level of the detecting system. With regard to the second problem, the thermal noise of the detector may, in principle, be eliminated by operating at absolute zero temperature and the shot noise of the detector current may be reduced to zero by making the detector have infinite resistance. There will, however, always be a noise contribution from the pulse amplifier and this will then define the detection limit.

In Fig. 2.2. the intrinsic and extrinsic (or noise) contributions to the fractional standard deviation of the output pulse height distribution are plotted against photon energy E for a silicon and a germanium detector. The values assumed for the Fano Factor F are taken from Langmann and Meyer (1964) and Day et al (1966). Both F and ε, the mean energy per ion pair, have been assumed not to depend on photon energy. The curves represent the two terms of the function:

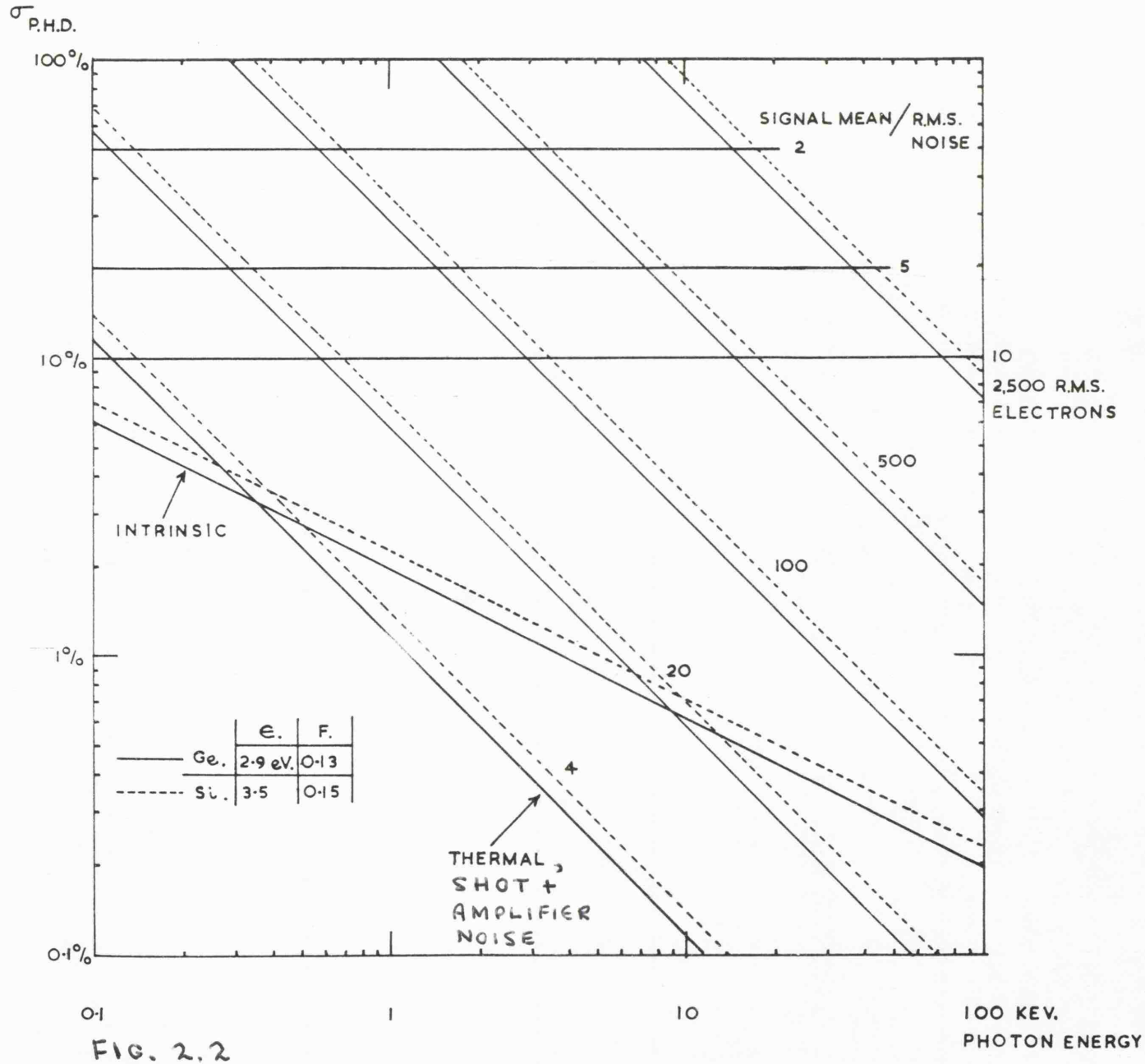
σ P.H.D.
100%
10%
1%
0·1%
SIGNAL MEAN / R.M.S. NOISE
2
5
10
2,500 R.M.S. ELECTRONS
500
100
20
4
INTRINSIC
THERMAL, SHOT + AMPLIFIER NOISE
ε. F.
Ge. 2·9 eV. 0·13
Si. 3·5 0·15
0·1
1
10
100 KEV.
PHOTON ENERGY

FIG. 2.2

$$\sigma = \left[\frac{F\varepsilon}{E} + \frac{\varepsilon^2 n^2}{E^2}\right]^{1/2}$$

Where n^2 (rms^2) is the quadratic total of all noise contributions following the formation of the initial electron-hole pairs, i.e. detector noise and amplifier noise. For σ = 100% the mean-signal/r.m.s.-noise ratio becomes unity by definition. The significance of this fact rests with the counting background level of the total electronic noise above the pulse discrimination level, because in practice this must be appreciably lower than the signal count rate. Fairstein (1962) has plotted out the noise count rate for different discrimination levels relative to the r.m.s. noise level, for both grid current shot noise contribution and the valve shot noise contribution. It is clear from these curves that the discrimination level must, for most purposes, be not less than a factor of 5 higher than the r.m.s. noise level.

In assessing the potential applications of this type of solid state detector to soft X-ray detection, it is obvious from Fig. 2.2. that amplifier noise is likely to be dominant. At present an amplifier noise level of 100 r.m.s. electrons is about the best that can be achieved, (See for example Radeka 1965), but care must be taken to achieve even a level of 2,500 r.m.s. electrons, particularly since all non-ideal detector-preamplifier systems possess a finite capacitance, which will greatly increase the lowest noise level attainable with all other factors constant.

At a <u>total</u> electronic noise level of 100 r.m.s. electrons the resolution of a solid state detector at 2.1. Å (5.9 Kev) would appear to approximately equal the best theoretically attainable with a proportional counter ($\sim$ 13% See Section 4.3.). To longer wavelengths, however, the proportional counter f.w.h.m. will increase only as the inverse square root of photon energy, since it is limited by the statistics of the gaseous photo-ionization process, whereas the f.w.h.m. of the solid state detector will increase as the inverse photon energy under amplifier noise limitation. Thus, at photon energies less than 10 KeV, normal solid state detectors would not appear to represent serious competition to the proportional counter on the grounds of energy resolution. Should total noise contributions as low as 4 r.m.s. electrons ever become attainable, however, it would appear that advantage could then be taken of the high intrinsic resolution of the solid state detector down to photon energies of the order of 0.1 KeV.

The problem of signal noise ratio will be further aggravated by the loss of carriers prior to collection. Zulliger and Aitken (1967) have investigated the linearity of the charge conversion function for cooled Li-drifted Silicon detectors in response to X-ray and low energy γ - ray excitation. The authors mention that this function would not be expected to remain constant for low energies and report experimental confirmation of this at photon energies in the range 5 - 75 KeV. The effect

is found to be worse at low values of detector bias (optimised for the best resolution) but still remains significant (2%) for an extrapolation to infinite collection field. It is shown that this loss is compatible with a dead layer content of photo-produced electrons and with additional losses produced by trapping behind the window.

Although there will not be the problem of the loss of compton scattered photons that exists at higher energies, the existence of any dead layer will place an upper limit on the photon detection efficiency for soft x-radiation. Fig. 2.3. gives the optical transmission factor of two thicknesses of Silicon 0.5μ and 1.0μ. ⁎ A similar graph for Germanium would show generally a lower transmission because of its greater atomic number. Drexler and Perzl (1967 a) report the attainment of a window thickness of less than 1μ of Germanium by making the detector face perpendicular to the plane of the depletion layer, thereby allowing the radiation to enter directly into the sensitive

---

⁎ The mass absorption co-efficients for Silicon were taken mostly from the data of Theisen and Vollath (1967) However, it is believed that these co-efficients have been subsequently withdrawn and therefore the curves should be considered to give only an indication of the transmission factors to be expected, particularly towards the longer wavelengths.

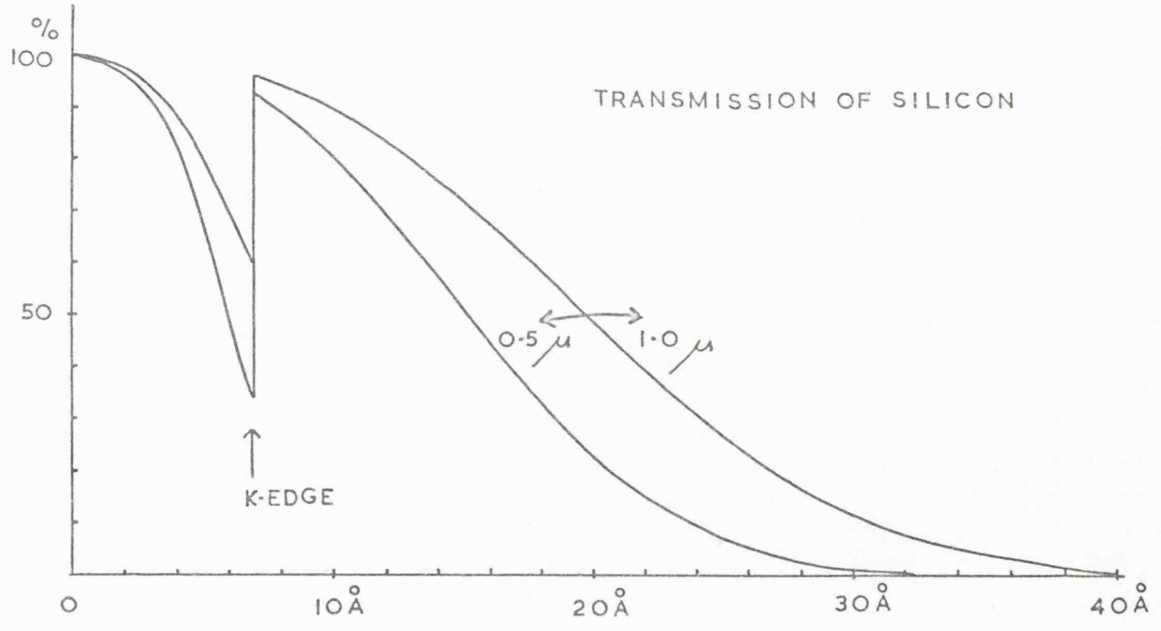
%
100
50
TRANSMISSION OF SILICON
0·5 μ
1·0 μ
K-EDGE
0
10Å
20Å
30Å
40Å

FIG. 2.3

region. Sample X-ray spectra obtained with such a detector are presented in a second paper (1967 b).

Assuming that the dead region of a detector may be made usefully thin for soft x-radiation, amplification of the initial ionization would seem to be a way of surmounting the problem of electrical noise. Devices employing this mode of operation become the solid state analogues of gas counters.

The development of solid state detectors employing internal charge multiplication has been reported by the GEC Space Sciences Group (Huth et al 1965, Huth 1966). It is understood that to date the experimental work on these devices, termed surface-contoured detectors, has been mainly in the Geiger Mode and that x-radiation in the region 1 - 20 Å can be detected (with a photon detection efficiency of about 90% at 2.1 Å). The pulses obtained are extremely fast and, using a tunnel diode type of pre-amplifier, 100 Mc. counting rates can be handled. In the proportional mode, resolutions (f.w.h.m.) of 30 - 40% at 2.1 Å and ~ 50% at 8 Å have also been obtained (Trice 1967).

Haitz and Smits (1966) have analysed theoretically the consequences of internal amplification in Silicon particle detectors. It is shown that, as a result of the statistical distribution of impurity (doping) centres in the detector material, there will be fluctuations of the local breakdown voltage in addition to the fluctuations to be expected in the multiplication factor.

The authors conclude that, in general, appreciable resolution increases can only be obtained at low particle energies (< 10 KeV) and, in the particular case of soft X-ray detection, the additional problem of window absorption means that, at photon energies below 1 KeV, it will probably be necessary to employ, instead of a p - n junction, a Schottky barrier fabricated at the detection surface with a thin layer of Beryllium or Aluminium. Also, to retain the optimum carrier multiplication conditions, it is shown that electrons will be required to be the majority carriers in the bulk material which must therefore be n-type.

Solid State barrier detectors do not appear to have been used yet in X-ray astronomy.

Indirect Registration

In addition to the photographic process the ionization produced in solid state material may be indirectly detected by thermo-luminescent methods or by scintillation counting. Since only scintillation counting can be expected to give single photon registration, this discussion will be limited to this method.

The application of scintillation techniques to X-ray detection is not new. Morgan (1942) and Marshall et al.(1947) used conventional sealed photo-tubes in conjunction with layers of scintillator wrapped round the outside of the tube and covered with black paper (to exclude visible light). Some of the most recent work into the low energy photon response of scintillators has been

carried out by the Stanford University Group. Aitken et al (1966) have reviewed previous work on the non-linear response of alkalihalide scintillation crystals and have presented comprehensive experimental measurements down to 3.3.Kev on Na I (Tl), Cs I (Na), Ca F_2 (Eu) and Cs I (Tl) (1967). Na I (Tl^1) is shown to possess the highest fluorescence output over the range of measurement (up to $\sim$ 1 Mev). Fine structure in both the fluorescence output and resolution spectral variations is evident, the latter showing discontinuities at the Iodine K and L edges. The authors comment that they believe this to be the first evidence of such edge effects. Another interesting feature of these results is the low energy increase in the fluorescence output per unit photon energy, which would indicate the possibility of a relative increase in sensitivity. The results presented for Cs I (Tl) show that it has the poorest performance of the four phosphors examined.

In X-ray astronomy, the best energy resolutions reported have also been obtained with Na I (Tl). This may be seen from the results of Matsuoka (1966) and of Hicks et al (1965) plotted on Fig. 2.4. Matsuoka also presents pulse output measurements which indicate a marked non-linearity in the scintillator response. The charge/KeV decreases towards low photon energies, however, and this is opposite to that displayed in the results of Aitken et al (1967).

Plastic Scintillators have also been examined at

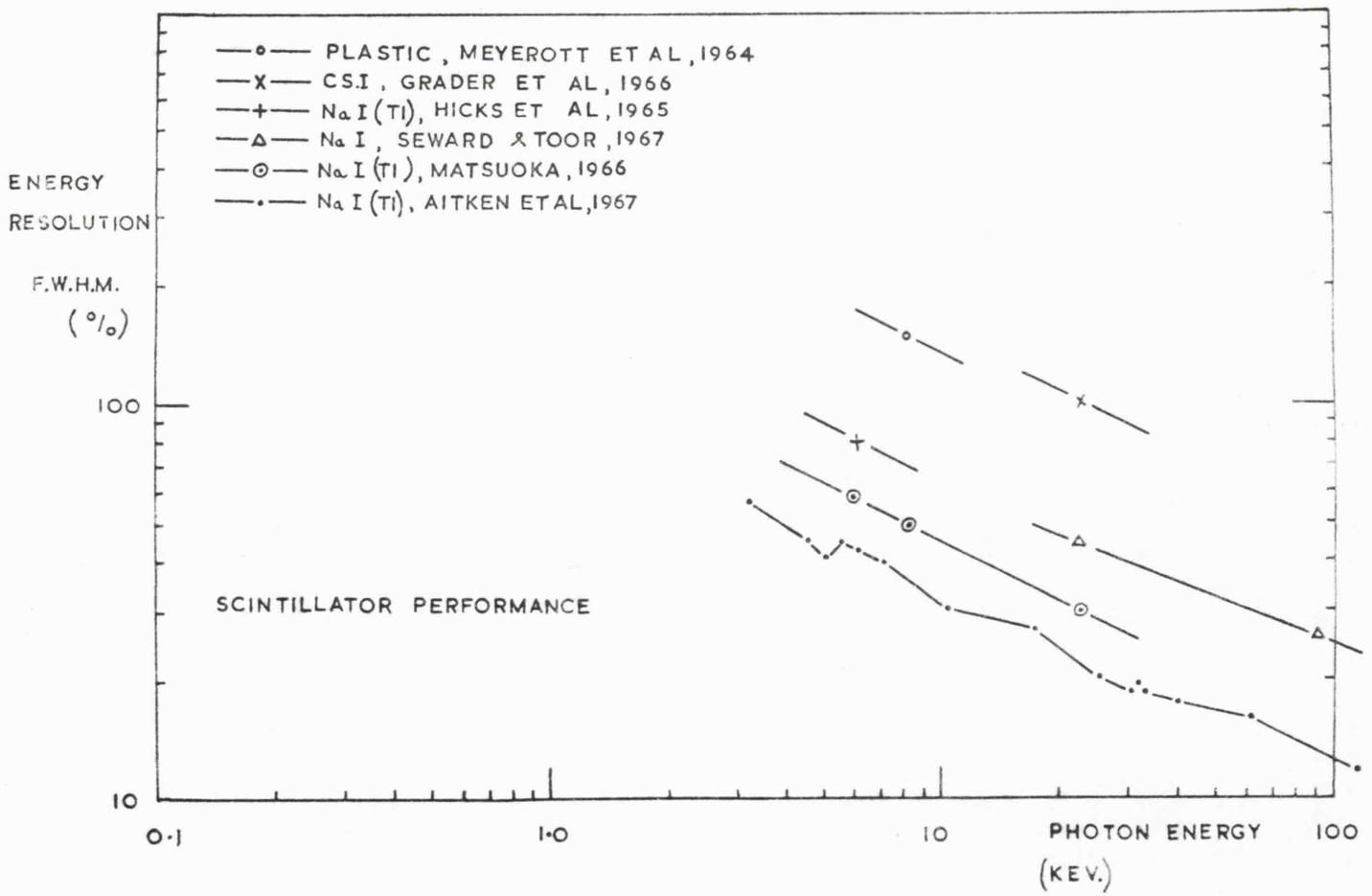
—o— PLASTIC, MEYEROTT ET AL, 1964
—x— CS.I, GRADER ET AL, 1966
—+— Na I (Tl), HICKS ET AL, 1965
—Δ— Na I, SEWARD & TOOR, 1967
—⊙— Na I (Tl), MATSUOKA, 1966
—•— Na I (Tl), AITKEN ET AL, 1967
ENERGY RESOLUTION F.W.H.M. (%)
100
10
SCINTILLATOR PERFORMANCE
0·1
1·0
10
100
PHOTON ENERGY (KEV.)

FIG 2.4

low photon energies. Ipatkin et al (1966) employed an air-filled ionization chamber to calibrate a 'solid solution of terphenyl in polystyrene with an admixture of popop' in the range 1 - 12 Å and Adlam and Burcham (1966) determined the relative conversion efficiency of an NE 102 A plastic scintillator in the range 1.8 — 4.5 KeV with a flow proportional counter. In both works explicit values of fluorescence yield (photons/photon) were not given and the significance of the works in these terms is not clear. Yield measurements were, however, given by Meyerott et al (1964) and were of the order of 0.1 - 0.4 electrons/KeV in the range 1 - 10 KeV. With conversion efficiences of this order, the plastic scintillator would appear to be markedly inferior to the phosphors investigated by Aitken et al. This is also borne out in the resolutions measured at 8.1 KeV ; Meyerott et al obtained ~ 150% and Aitken et al ~ 31%.

Plastic Scintillators have, however, found widespread use as guard detectors in X-ray astronomy. Grader et al (1966) employed a phosphor sandwich ("phoswich") detector in a rocket experiment in which the X-ray CsI Scintillator was completely surrounded by plastic scintillator, which then rejected cosmic ray background events by rise-time discrimination (The plastic scintillator gave a faster pulse than the CsI). Seward and Toor (1967) employed another double scintillator for background reduction in an X-ray telescope but used anticoincidence techniques.

With regard to the other parameters of scintillation detection, the most important of these are the photon

detection efficiency and background count rate. With the exception of the efficiency intercomparison of a scintillation counter and gas counters made by Metchnik (1964), there do not appear to be any experimental measurements of soft X-ray photon detection efficiency, it being usual to assume that the only efficiency limitation is that resulting from the optical transmission of the scintillator covering material (usually a thin layer of aluminium).

Matsuoka (1966) appears to have reported the lowest background level, as defined by the photomultiplier noise resulting from thermionic emission from the photocathode. At 15°C, above a pulse discrimination level equivalent to the peak of a 2.5. KeV pulse height distribution, the background level, for a detector area of 4.52 sq.cm., is approximately 1 c.p.s. This level compares well with what could be expected from the cosmic ray level of a properly operated proportional counter of the same window area. Towards lower photon energies, owing to the exponential rise in the photomultiplier noise spectrum, the scintillator would rapidly become inferior in background.

McIlraith (1962) tackled this problem in a laboratory spectrometer in the region of 50 Å by employing phase-sensitive detection. It was stated, however, that the sensitivity obtained was very low compared with that of a gas counter.

In summary it may be stated that, despite recent advances in the art, the scintillation method still does

not compare with a good proportional counter at low photon energies in either resolution or background. However, since it is a solid-state/sealed-vacuum device, it has the important advantage of high inherent stability and it is possible that this might outweigh the performance limitations in some X-ray astronomical applications. The scintillation method is important in X-ray image devices (q.v.).

2.2.5. Photo-electric Detectors

Photo-electric methods are attractive in that the problem of window opacity associated with the use of sealed gas counters and the electrical noise problem associated with the use of non-multiplying solid state detectors may, in principle, be simultaneously solved. As yet, photo-electric detectors have not seen extensive use at photon energies below 100 ev. This is probably a consequence of the fact that, for laboratory applications at least, it is usually possible to operate a flow gas counter instead and that, as yet, little is known about the spectral variation and stability of the external photo-electric yield in this region.

The process of X-ray photo-electric detection amounts in practice to the detection of the photo-produced electrons from the photo-cathode.

If the photo emission currents are high enough then measurements may be made with an electrometer. P.Lukirsky (1924 a. and b.) examined the retardation curves of the

photoemission from surfaces in the range 12 — 154 Å in this way, using a spherical capacitor arrangement. Richardson and Chalkin (1926) used an electrometer in conjunction with a copper photo-cathode and Rudberg (1928) used an electrometer andan omegatron type electron velocity analyser to investigate the energy distribution of the electrons ejected from Carbon, Copper, Silver and Aluminium by photons of energy less than 700 ev. The existence of two groups of electrons was evident. The first comprised more than 80% of the total and possessed energies below 20 ev. The second possessed a broad energy distribution up to a maximum of about 300 ev. This second group was not so sensitive as the first to the removal of gas from the photocathode surface. Absolute values of the emission yield (per photon) were not given.

For low photon fluxes counting techniques must be employed for electron detection. To-date, the commonest electron counting technique has been that of electron multiplication and the linear focussed dynode array, or Allen (1947), type of multiplier has seen most frequent use. Lifshits (1956) investigated the operation of Allen type multipliers with activated dynodes of Cu - Al - Mg, of Mg and of Ta at wavelengths in the range 0.07 - 0.25Å and beyond 2,000 Å. At the shorter wavelengths the spectral variation in photo-emission of a photocathode consisting of a series of parallel metal foils normal to the radiation was measured. It was shown that a large

number of thin foils had a greater photoelectric yield than a smaller number of correspondingly thicker foils. The main defect of the device was stated to be the poor collecting efficiency of the first dynode.

Tiutikov and Efremov (1958) discussed the particular need for photoelectric detectors for laboratory work in the wavelength range 20 - 600 Å and reported the successful application of Allen type electron multipliers to photon counting in the range 10 - 2,000 Å. Peaked pulse height distributions were measured at 44 Å and 113 Å and shown to be identical. By 1960 similar investigations were being reported in the U.S. Tomboulian presented results obtained with a Cu - Be photomultiplier in pulse mode and Jacob and Noble used an Allen type multiplier, in conjunction with an electrometer, in a laboratory grating spectrometer covering the range 160 - 450 Å.

In 1960 also appeared the first published reports of investigations into the X-ray external photo-effect by the X-ray Group at Leningrad State University. There can be no doubt that the subsequent programme of work of this group is the most comprehensive ever conducted into X-ray photoelectric phenomena, although it is clear that the physical processes involved are not yet well understood. In this work absolute measurements of X-ray photo-electric emission from metals and binary compounds have been made with Allen type electron multipliers and with electrometers. The photon flux measurements have been made with geiger and proportional

counters of established efficiencies. Much of this work has been directed at the determination of the laws governing the magnitude and spectral variation of the external photo-electric yields. * Measurements of the pulse yield X have been presented for the 1.39 - 13.3 Å range by Rumsh et al (1960 b.) and Lukirskii et al (1960 c.) and for the 23.6 - 113 Å range by Lukirskii et al (1960 b.) and Lukirskii et al (1964 b).

The problem of the interpretation of these results, and of others similarly obtained, has been discussed by Rumsh et al (1962 a. and b.), Savinov et al (1965) and Eliseenko et al (1965). Further analysis of the work, considered in conjunction with electrometer data, has been given by Denisov et al (1965) and Shchemelev et al (1965).

---

* This problem may be stated as the determination, for all n, of the probability per incident photon p(n) of ejecting n electrons from the photo-cathode.

In terms of the measured yields we have:

a). $\sum_{n=1}^{\infty} . p(n) = X$ Where X is the pulse (or counting) photo-electric yield.

(By Definition, $\sum_{n=0}^{\infty} . p(n) = 1$)

and b). $\sum_{n=0}^{\infty} p(n).n = \sum_{n=1}^{\infty} p(n).n = Y$ Where Y is the total yield (electrons/photon).

In summary, it may be said that limited success has been achieved in accounting for the observed photo-electric behaviour of different cathodes in terms of the optical, atomic and electronic constants of the cathode material and that reproducibility of certain of the measurements has been admitted to be limited. In the particular case of the determination of fluorescence yields from photo-emission discontinuities reported by Rumsh and Shchemelev (1962), the agreement with values obtained in other work was good. In a later paper (1963b) the authors discuss the considerable difficulties inherent in this method.

Other Russian work into the total yield Y has been reported recently (See for example Ganeev and Izrailev (1962) Nakhodkin and Mel'nik (1963 and 1964) and Izrailev (1963)). The last paper is particularly interesting in that the "forward" yield of a thin platinum foil was measured, in addition to the more usual "backward" yield. It is shown that, with the foil chosen, the forward yield was relatively small below 10 KeV. However, since this threshold will depend strongly on the foil thickness and mass absorption co-efficient, the effect would appear to have great potential importance in soft X-ray detection, especially in image devices (q.v.).

An independent attempt has been made by Ogier and Ellis (1965) to derive thick-target photo-electric yield formulae. In the model chosen in this work the electrons comprising the initial (or primary) yield of the photon are assumed to travel in straight lines for distances determined by an effective range-energy

relationship, or until they escape from the surface (This may be compared with the exponential electron attenuation function assumed by the Leningrad team). The predictions are shown to compare reasonably well with available Russian measurements at 1.54 Å.

Few independent measurements of external X-ray photo electric yields have been reported. Henke (1963) has stated that the Russian work was reproduced using both a Dumont Be-Cu Multiplier and a Bendix magnetic resistance strip multiplier. Values are presented which were obtained with the latter detector at 44 Å for W, BeCu, SrF_2 and CsI, in comparison with a geiger counter. No experimental details were given. Tomboulian (1964) presented efficiency calibrations for a Bendix photo-multiplier, at 2.1 Å, 113 Å, 180 Å and 305 Å, made with a geiger counter. The author commentedthat 2:1 variations in response were experienced and attributed these to photo-cathode and collection efficiency variations. With reference to the application of photo-electric instrumentation in X-ray Astronomy, Neupert (1965) reported the calibration of an entire solar satellite extreme ultra-violet grating spectrometer which employed a Bendix windowless photo-multiplier. The total coverage of the instrument was 10 - 400 Å and the calibration was made at 44 Å using a proportional counter of known photon detection efficiency. Since the detector efficiency was blended in with the unknown spectrometer constants in this calibration, no comparison with Tomboulian's results is possible.

Hinteregger et al (1964) employed a photo-electric detector with a Li F photo cathode in a similar type of spectrometer, but employed Leningrad data for the photo-electric efficiency of the Li F. The authors appear to have accepted order of magnitude accuracy for their total instrument calibration. Efremov et al (1962) have described a photo-electric detector used to study the solar X-ray flux which consisted of a Be O photo-cathode and a series of filters. No independent measurements of the photo-electric yield appear to have been made for the instrument.

Lastly, Giacconi and Gurksy (1965) described a novel photo-electric detector that was flown in a rocket experiment in 1964. The instrument possessed a curved alkali halide photo-cathode 40 cm^2 in area. The photo-produced electrons were electrostatically focused on to an electron multiplier.

The detector's response was claimed to extend beyond 44 Å, but no calibrations were reported. It is to be noted that, for the particular detector illustrated, the long wavelength limit could not have exceeded 18 Å since an aluminium window 6 μ in thickness was used.

Other Photo-electric Detectors

The electron multiplier does not represent the only way of detecting the photo-produced electrons. However, because of their generally low ejection velocities, it is usually otherwise necessary to accelerate the electrons

and then to dissipate their energy in a β-detector. Schumacher and Grodski (1965) have described a soft X-ray detector based on this principle. Photo-produced electrons from a foil photo-cathode assembly, of the sort used by Lifshits (1956), are accelerated to energies of around 20 KeV and counted with a scintillation detector. The detector is reported to have been operated in the range 5 - 3,000 Å and to possess only a low field-induced noise background, even at pressures as high as 10^{-4} Torr.

Chevalier (1967 a and b) has reported the use of a silicon solid state barrier layer detector in a similar role. The detector is located at the focus of an electron optical system, the object of which is a gold ultra-violet photo cathode. Accelerating voltages up to 35 KeV are employed and the peaks corresponding to photo-produced electron batches out to $\underline{n} = 4$ are shown to be well resolved.

This technique is similar to that being used for investigations into the statistics of transmission secondary electron emission at U.C.N.W., Bangor. Here, it is understood, peaks out to n = 14 are well resolved, with a negligibly low back-ground count rate at pulse amplitude levels less than that corresponding to n = 1 (Wilcock 1967). The method would seem to represent an extremely powerful technique for electron emission studies in general, and for soft X-ray photo electric investigations in particular.

Gas counters have also been used for post-

acceleration counting (See for exampleMehlhorn and Albridge (1964) and Charalambus and Theodossiou (1965)). Against the problems of the extra bulk of the detector and the need to support a thin window must be set the real advantages of the virtually noise-free gas amplification process and the reduction in back-scattering, as a result of the lower mean atomic number of the window material. Lane and Zaffarano (1954) have presented comprehensive electron transmission curves for the energy range 0 - 40 KeV for thin films suitable for gas counter windows. On the basis of this work there would appear to be no problem in making absolute electron counting measurements above 20 KeV.

2.3. Continuous Electron Multiplication.

Other than the crossed field multiplier the capillary(or tubular)channel multiplier has been most widely used.

The first space research application was reported by Evans (1965 a. and b.). In this work the channel multipliers were operated in pulse mode and attention was paid to the variations observed in the pulse height distribution. In particular the dependence of pulse height distribution and mean output charge on the operating voltage and pressure were investigated. The phenomenon of positive ion feedback in channel multiplication was discussed and the design of a curved channel put forward in which these effects were eliminated. The effects of pulse saturation in linear channels were described and a model for the mechanism proposed, in which the amplitude limitation was the result of axial field neutralization within the channel by the positive surface charge distribution resulting from the secondary emission events. Shortly afterwards an alternative explanation was put forward by Bryant and Johnstone (1965), in which the gain saturation was held to result from the effects of electron space charge within the channel during electron multiplication and a limiting charge density of 4.10^7 electrons per cm. was predicted. In 1965 also, the development of channel multiplier devices in the U.K. at the Mullard Research Laboratories was reported by Adams and Manley. Several

Erratum.

different kinds of channel multiplier, both linear and curved, were described together with their operating characteristics. In this work the effect of positive ion feedback was clearly demonstrated with the illustration of regular fine structure in the current pulse.

In 1966 investigations into the mechanism of channel multiplication were reported by Adams and Manley and by Schmidt and Hendee. Here attempts were made to produce models which would predict the amplitude and duration of the current pulse * of the channel multipliers it was concluded in both works that space charge saturation was responsible for gain limitation. The values predicted for the limiting charge density were in approximate agreement with that of Bryant and Johnstone.

With regard to the X-ray astronomical applications of channel multipliers there appear to be no experimental results reported as yet.

The development of other continuous electron multipliers has also been reported. Misso and Karpinski (1964) claimed to have demonstrated the feasibility of using a purely electrostatic single surface multiplier.

---

* The area of this pulse is equal to the charge output of the channel, which is equivalent to the gain of the device under conditions of single-electron excitation.

Of the various surfaces tried - gallium arsenide, magnesium oxide on gallium arsenide, tin oxide, nichrome and silicon - the last proved to be the most successful although the required electron multiplication factor was not achieved.

Spindt and Shoulders (1965) produced a strip multiplier using two parallel surfaces of alumina doped, during vacuum deposition, with molybdenum. Multiplication factors of 10^6 - 10^7 were achieved with the device which proved to be stable to both atmospheric storage and to 900°C vacuum bake-outs. The rectangular cross-sectional geometry of this detector would appear to be particularly suited to spectroscopic applications, since the radiation usually emerges from a slit which defines the beam cross-section. The possibility of stacking up alumina plates employing both front and rear surfaces for electron multiplication would also make the development attractive for one dimensional image dissection. A scheme for using such a device in the study of rare-earth X-ray emission line profiles has been put forward (Wilson 1966).

2.4. Special X-Ray Detectors

2.4.1. Imaging Detectors

Introduction

X-ray image detectors must record spatial distributions of photon flux density. In general these distributions will be 2-dimensional but 1-dimensional images do arise, particularly in dispersion spectroscopy.

Probably the photographic process is the simplest means of X-ray image detection. The use of film in X-ray astronomy has already been mentioned and this section will therefore be limited solely to photo-electronic image methods.

The operation of any image detector may be analyzed, in principle, in terms of the four operations: dissection, conversion, storage and read-out.

Image dissection does not usually exist as a separate process but is a function of conversion, storage and read-out. An exception arises in the case of channelled devices, such as the channel multiplier array, in which the image dissection may be considered to be a physical process. In all cases the final degree of dissection is given by the parameter 'spatial resolution'.

X-Ray Image Conversion

X-ray image conversion begins with the photo-electric interactions at the front end of the detector. Thus the first conversion will be to one of the following image forms:

a). A distribution of localised regions of ionization in either a gaseous or a solid material.

b). A distribution of visible or near visible scintillations from a phosphor.

Or c). A distribution in vacuum of photo produced electrons from a photo-cathode.

b). and c). are not suitable as final image forms and the images are therefore converted again, either directly or indirectly, into surface charge distributions. The facility of storage allowed by this conversion then allows the image information to be read-out, or extracted, serially without loss.

Electronic Read-out of Stored Images

Electron beam scanning under conditions of Cathode Potential Stabilisation is most commonly employed for this purpose. The image information is then transferred to the scanning beam (as in the Vidicon) or to the returned beam component, either during stabilisation (Image Isocon) or after stabilisation (Image Orthicon). Secondary electron multipliers are used to amplify the returned beam component in these last two devices.

Other read-out schemes have been devised. Waters (1964) outlined a digital method of direct read-out of an array of channel multipliers in which the output pulses from the individual channels are collected on electrically separate anodes and made to trigger bistable circuits (one circuit per channel). This system may be considered to possess storage, in that each bistable remains in the

triggered state until reset. However, no further information from a particular channel can meanwhile register and so, to prevent information loss, the read-out rate must be substantially greater than the image acquisition rate.

Weimer et al (1966) have reported actual development of another system not dissimilar to the last. The device consists of 180 x 180 solid state photo-conductor-diode elements, each of which produces analogue image information when digitally scanned. The device is likened to the Vidicon camera tube and it is claimed that promising results have been obtained with 2 -dimensional scanning.

Another scheme has been developed by the U.C.L. Space Research Group. With this device a stored 1 - dimensional image of an optical spectrum is scanned non-destructively with a vibrating reed maintained at a constant distance from the surface. The image information is then converted to charge displacements in the external circuit containing the reed gap.

Simultaneous Read-Out

The alternative to image storage, if no information loss can be tolerated, is the simultaneous electronic read-out of the initial X-ray ionization. To-date three systems appear to have been developed.

The first is based on the branching ratio of two components of the current pulse in a solid state detector. Analogue pulse arithmetic is employed to determine this ratio. The system is basically 1 - dimensional but an extension of the technique to 2 - dimensional dissection

has been reported (Owen and Awcock, 1967).

The second system achieves 2 - dimensional dissection again in a solid state detector but this time by the use of a multiplicity of electrodes and electronic gating. This is known as the 'Checker Board' Counter.

The third system is that dsscribed by Grennberg (1967) who has used a proportional counter with a conical anode wire. Here, the pulse ouput from the counter depends on the location along the wire of the absorbed photon. The device dissects in 1 - dimension but is severely chromatic since the pulse output is proportional to the photon energy at a given location.

With regard to soft X-ray images, it would seem unlikely that any of these methods could be used. The first two are based on solid-state detection and will therefore probably be limited to photon energies above 10^4 ev. The third is too severely chromatic and has limited resolution (Grennberg gives an estimation of 20 dissection channels available along the useful section of the anode wire).

It is shown in Appendix 3 that a modification of the first method will enable position sensitive techniques to be applied to the problem of simultaneous read-out in the case of a channel multiplier array of the type examined in the present work.

The Quantum Sensitivity attainable with a Scanning X-ray Image Detector.

As yet very little experimental work has been reported in the literature. The only X-ray image system that has seen appreciable use is the X-ray scintillation camera, which consists of the combination of a phosphor screen and a conventional camera tube (which is sometimes preceded by one or more image intensifier stages). Applications of the device to the fields of diagnostic X-rays, X-ray microscopy and X-ray scattering studies have been reported.

The scintillation camera is convenient in that the camera tube may be permanently vacuum sealed and in that fluorescence yields (photons/photon) in excess of unity can be achieved. In one respect, though, the device will be inferior to a straightforward X-ray photo-cathode system because the X-ray photocathode can have a high work function and therefore a lower thermionic noise current. However, further comparison of the two systems is not necessary since the performance estimate that follows will assume an X-ray conversion of 1 electron per photon which is reasonably typical of both systems. (This agrees roughly with Anderton's estimate of 1 → 2 electrons per photon for a Phosphor/C.P.S. Emitron system (1966) and with the photo-electric yields measured in the present work, see Chapter 4).

The results of Beyer et al (1966) enable an estimate to be made of the performance of the scanned X-ray image detector. In this work, evidence was presented to support

the claim that a point charge image on a SEC Target, corresponding to 150 electrons leaving the photo cathode, had been detected, by scanning, with a signal/noise ratio of 5. Further evidence given showed that the point image resulting from the integration of an electron flux of 1 electron per second for 10^3 seconds was also recorded with even higher signal/noise ratio. The spatial resolution of the read-out referred to the photo-cathode was about 90μ .

Under these conditions the brightest X-ray source SCO X-1 (Flux 2 — 8 Å approx. 20 photons/sq.cm./sec.) would be detectable over integration times of 100 secs with a telescope having an effective collection area of 0.5 sq.cm. Alternatively, the quiet solar disc (Flux 2 — 8 Å approx. 2,000 photons/sq.cm./sec.) could be dissected into 10 x 10 image points with the same instrument in the same time.

For weaker stellar sources an increase in collection area and/or integration time would be required. Likewise, in the case of a more active sun, an increase in the image resolution(spatial and/or time) could be made. Thus for an active sun (Flux 2 — 8 Å approx. 10^5 photons/sq.cm./sec.), the solar disc could be dissected into 100 x 100 image points with integration times of 200sec. The need to maintain the image point size to not less than 90μ at the photocathode will set a lower limit on the focal length of the telescope (Approx. 80 cm. in the second case).

2.4.2. X-Ray Polarimeters

The need for polarization measurements in X-ray astronomy was mentioned in Chapter 1.

The polarization sensitive X-ray interactions are the Borrmann Effect (anomalous X-ray transmission in a crystalline lattice), Thompson scattering and the Photo-electric Effect. Of these interactions the first two may be classed as polarization sensitive filtering. Neither process would appear to be suited to X-ray Astronomy polarimetry, since the Borrmann Effect takes place under conditions of Bragg-reflection (and the radiation is therefore limited to an extremely narrow angular range) and the Thompson Scattering cross section is swamped by the photo-electric cross section at photon energies much below 10 KeV.

The photo-electric effect enables, in principle, a measure of the plane of polarization to be made via the observation of the ejection direction of the photo-electron.

A polarimeter under development by the U.C.L. Space Research Group employs rise-time discrimination in a proportional counter to measure the orientation of the photo-electron tracks in the gas mixture.

An attempt to determine the dependence of the external photo electric yield on the X-ray polarization was reported by Rumsh and Shchemelev (1963c). For this work use was made of the partial polarization of an X-ray beam Bragg-reflected from a crystal.

No significant dependence was found.

Chapter 3. The Experimental Work - Apparatus and Procedure.

3.1 A Description of the Apparatus.

3.1.1. The X-ray spectrometer

The basic spectrometer

A curved crystal focusing X-ray spectrometer (Fig. 3.1) was used to provide monochromatic x-radiation in the present work. The mounting employed was of the Johann kind (1931); thus the locus of both the X-ray source and the slit assembly was a circle passing through the pole of the crystal, of diameter equal to the radius of curvature of the crystal. The source and slit assemblies were mounted on vertical taper located bearings on which they were free to rotate. The 2:1 angular relationship between the positions of the X-ray source and the crystal assembly with respect to the slit assembly was maintained with a gearing system external to the spectrometer which could, if necessary, be disengaged by means of a small clutch. The radial position of the X-ray source with respect to the spectrometer axis could be adjusted manually during operation.

The method employed to maintain the crystal illumination by the X-ray source and to keep the

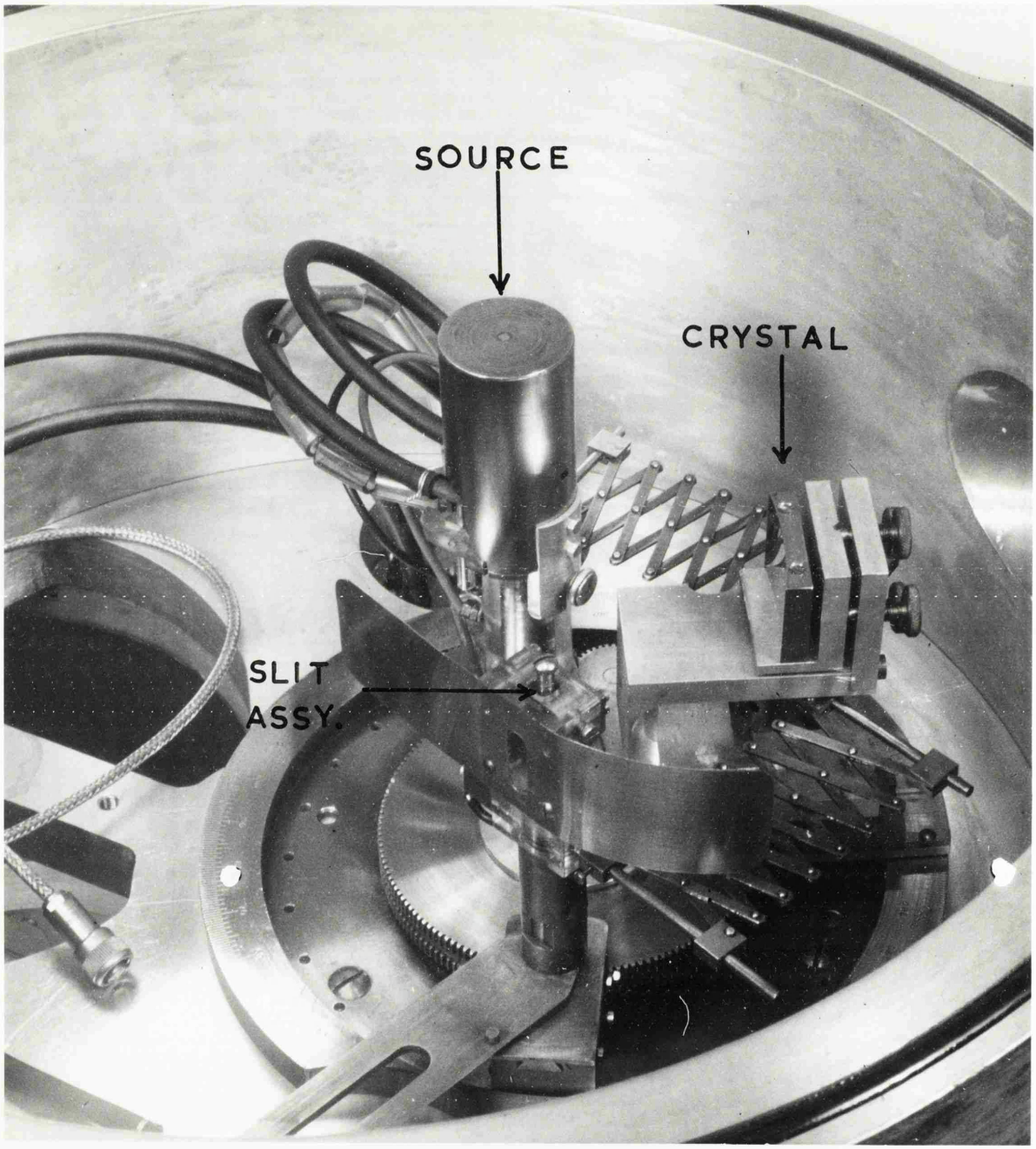

FIG 3.1

emergent X-ray beam normal to the plane of the slit is shown in Fig. 3.1. The 'lazy-tongs' elements maintained the two pairs of rods at the necessary angle, with respect to each other, once this had been determined for any one spectrometer position. The method of achieving this is described in Section 3.2.1. The crystal mounting could be used to support either a piece of mica sandwiched between two curved faces or a curved stainless steel blank, on which was deposited a crystal of copper barium stearate produced by the Langmuir-Blodgett process (1937) in this Department. In this way the spectrometer could be used to cover the first order wavelength ranges 7 - 17 Å and 35 - 85 Å.

The X-ray source is shown in more detail in Fig. 3.2. The electron source consisted of a small hairpin filament of thoriated tungsten wire (.005" dia.) which was mounted inside a small focusing aperture in the cathode assembly . This aperture was at the potential of one side of the filament. The positioning of the filament with respect to the aperture was not critical but was facilitated by adjusting the vertical positions of the two nickel rods, on to which the filament was spot welded. During the work, it became necessary for the X-ray source to be redesigned in its present form so that the cathode assembly was at, or near, earth potential instead of at negative E.H.T. as it had been

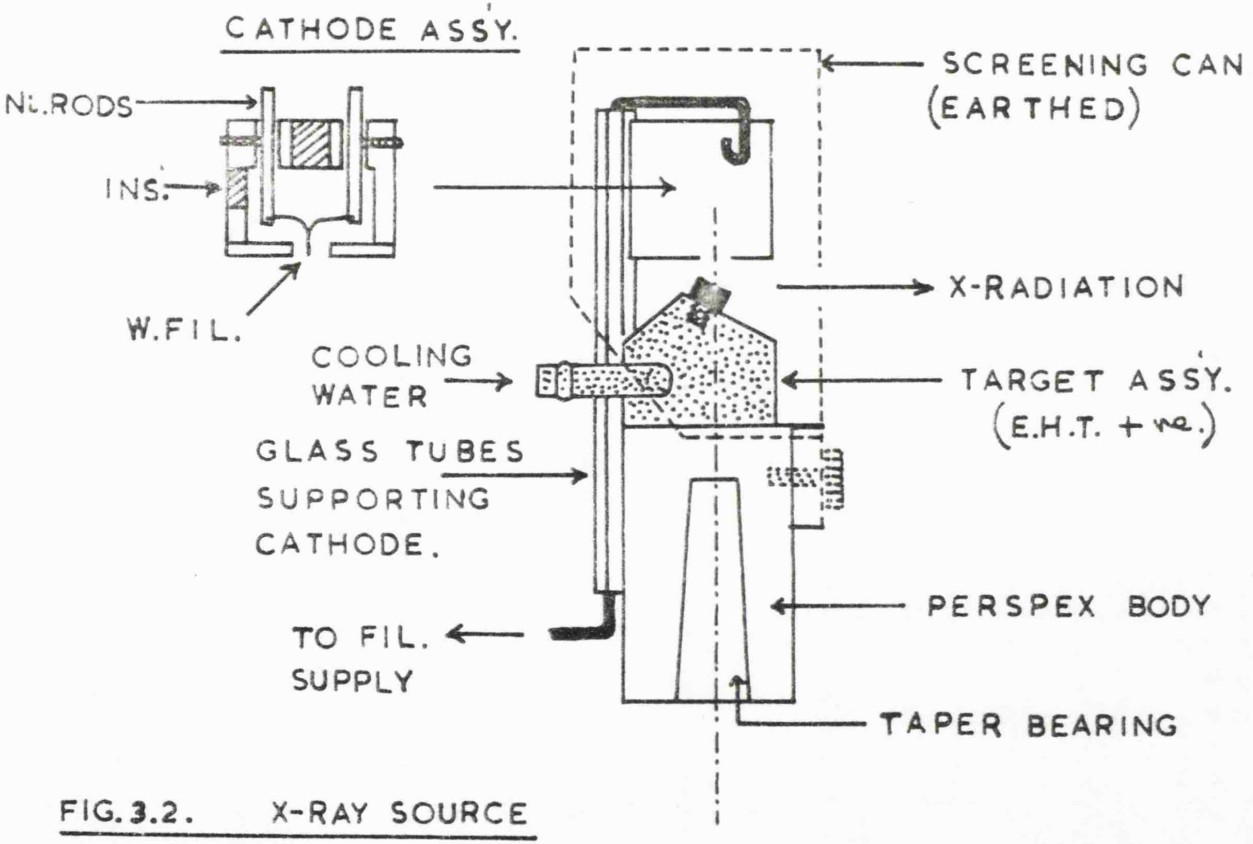

FIG. 3.2. X-RAY SOURCE

previously. This modification is described in Section 3.2.

Only X-ray line emissions were used for the work owing to the insufficient intensity of bremsstrahlung radiation available with the source at the wavelengths of interest. For this reason provision had to be made to change the material on the target according to the emission required. The physical nature of the target material for maximum intensity was found by experience to be different for different materials. Thus, nickel and molybdenum formed the most stable targets as pieces of thin sheet suitably shaped to fit closely to the target stud. The poor thermal contact existing between the two, which maintained the sheet at bright red heat, was thought to be the reason for this. Aluminium, copper, zinc and boron were best bombarded in powder form - the powder having been previously applied as a smooth paste (obtained by grinding with a little water, using an alumina mortar and pestle) to an aluminium target. Magnesium was found to be the only material in solid form which would provide a strong, stable source of characteristic radiation. Carbon K radiation could always be obtained very easily; this was undoubtedly due to the formation of a carbon layer on the target as a result of the high hydrocarbon concentration in the spectrometer.

The X-ray source was continuously water cooled during operation. Water was piped from the mains

supply to the anti-cathode assembly by means of flexible Neoprene tubing of the water resistant variety ($\frac{1}{8}$"" I.D. , $\frac{1}{4}$" O.D.). This tubing had been found by experiment to be superior in vacuum to P.V.C. tubing of a similar gauge, which was found to outgas at a high rate and to lose its flexibility quite rapidly. A warning lamp, operated by a microswitch flow meter device, gave an immediate indication of any loss of cooling resulting from water flow failure. The cooling water was conducted into the vacuum system through small brass tubes, sealed with an epoxy-resin into a Perspex port in the base of the spectrometer vacuum system. This port also contained several insulated terminals, which were used for the X-ray source power supply lines, and several other pairs of brass tubes for the Neoprene tubing conveying gas to the flow proportional counter in the vacuum system.

A small rotatable frame mounted on the crystal side of the adjustable slit assembly could be used either to measure the transmission coefficients of window material samples or to introduce filters into the X-ray beam.

The Vacuum System.

The spectrometer base plate, which was made of cold-rolled aluminium, also formed the base of the spectrometer vacuum system which consisted of a cast aluminium cylindrical wall section and a Perspex lid. (Two O-rings provided the main vacuum seals for the system) (Fig.3.4).

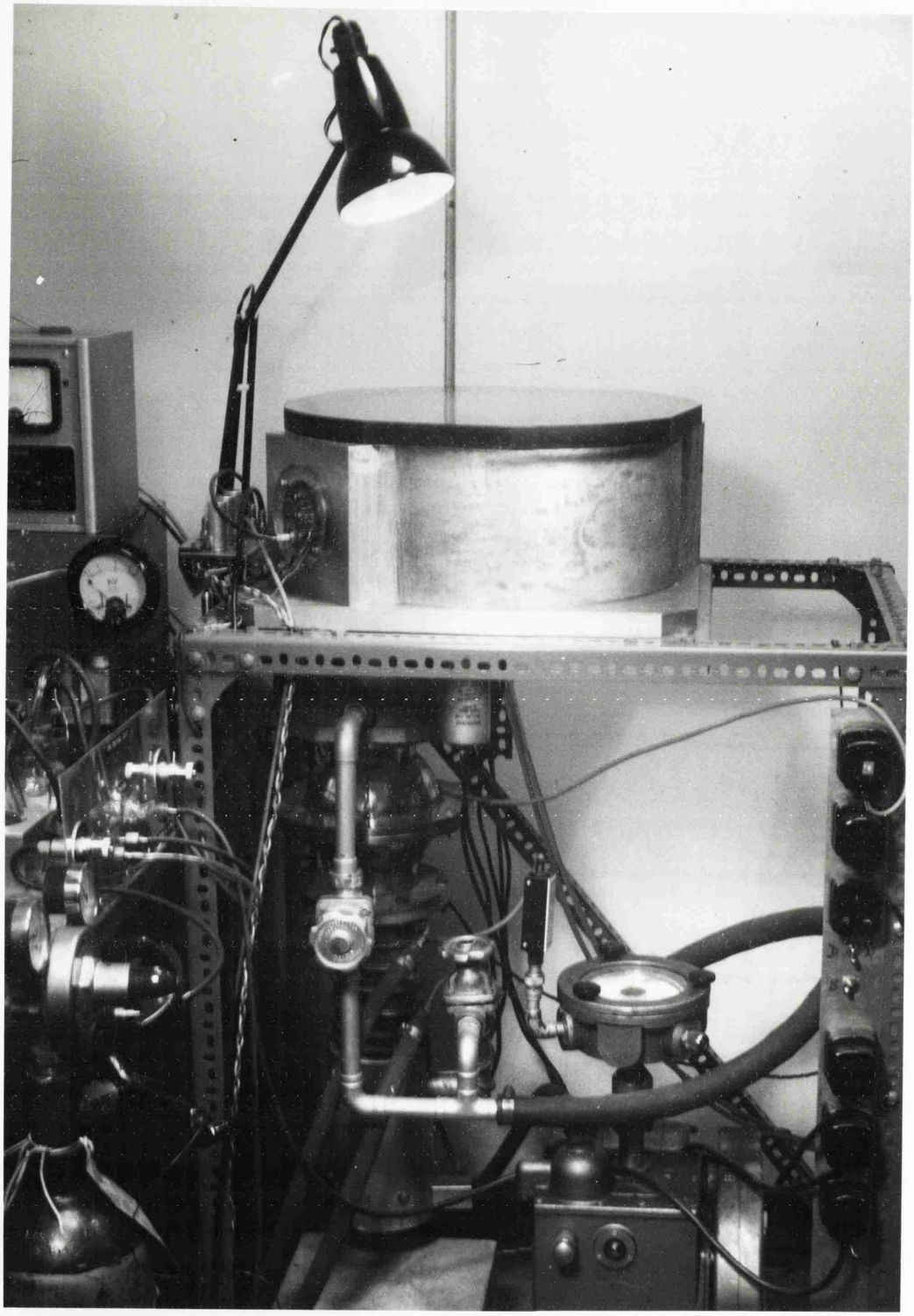

FIG 3.4

In addition to the main port in the base plate already mentioned, there were two similar ports in the wall section of the vacuum system. One of these was used for the mounting of three flexible drives and the other for a series of simple electrical terminals and three P.E.T. type coaxial lead-through connectors. (see Fig. 3.5) P.E.T. coaxial connectors had been found by experience to be very reliable for high voltage vacuum operation.

The vacuum chamber was pumped with a 4" Oil Diffusion Pump (Edwards 403 A) fitted with a liquid nitrogen spherical cold trap (Birvactype N.T.4). The normal operation pressure was 1.10^{-5} Torr but the lowest pressure attainable was approximately 3.10^{-6} Torr. A Penning Gauge, that had been previously calibrated against a Bayard-Alpert Type ionization gauge, was used for pressure measurement. It was found initially that heavy oil back-streaming resulted in a heavy liquid nitrogen consumption. A simple Chevron Baffle was constructed and fitted and was found to cure this, without apparent sacrifice of pumping speed. One filling then lasted for 10 hrs.

Spectrometer Ancillaries.

That part of the spectrometer external to the slits consisted of a horizontal machined beam fixed rigidly to the slit assembly perpendicular to the plane of the slits and approximately 2 c.m. from the base of the spectrometer. This may be seen in Fig. 3.1. On to this beam were

FIG 3.5

mounted the apparatus components that were required to be positioned in and out of the X-ray beam in the course of the investigations. The end of this beam remote from the slits was supported by a captive roller bearing, the height of which was adjusted by means of shims to allow the roller to lightly roll on the base of the spectrometer. This bearing relieved the taper bearing of the loading which would otherwise have arisen as a result of the weight of the apparatus mounted on the beam. Two units were designed and produced for the purpose of moving components in and out of the X-ray beam; these are described separately below.

1.First Unit (Proportional Counter Calibrations).

This unit is illustrated in Fig. 3.6 and was designed primarily for the testing and calibration of proportional counters. It consists basically of a carriage on which a vertical column may be moved continuously, horizontally and laterally, with respect to the X-ray beam by means of a dove-tailed slide. Another dove-tailed slide on this column allowed the platform assembly, on which one or more proportional counters could be mounted, to be moved continuously vertically with respect to the X-ray beam. Both lead screw mechanisms were operated manually via flexible drives. Two scales marked in cm. and mm., fitted with verniers and visible from outside the vacuum chamber, enabled horizontal and vertical positions to be recorded. The total scanning ranges available with the unit were 5 cms.

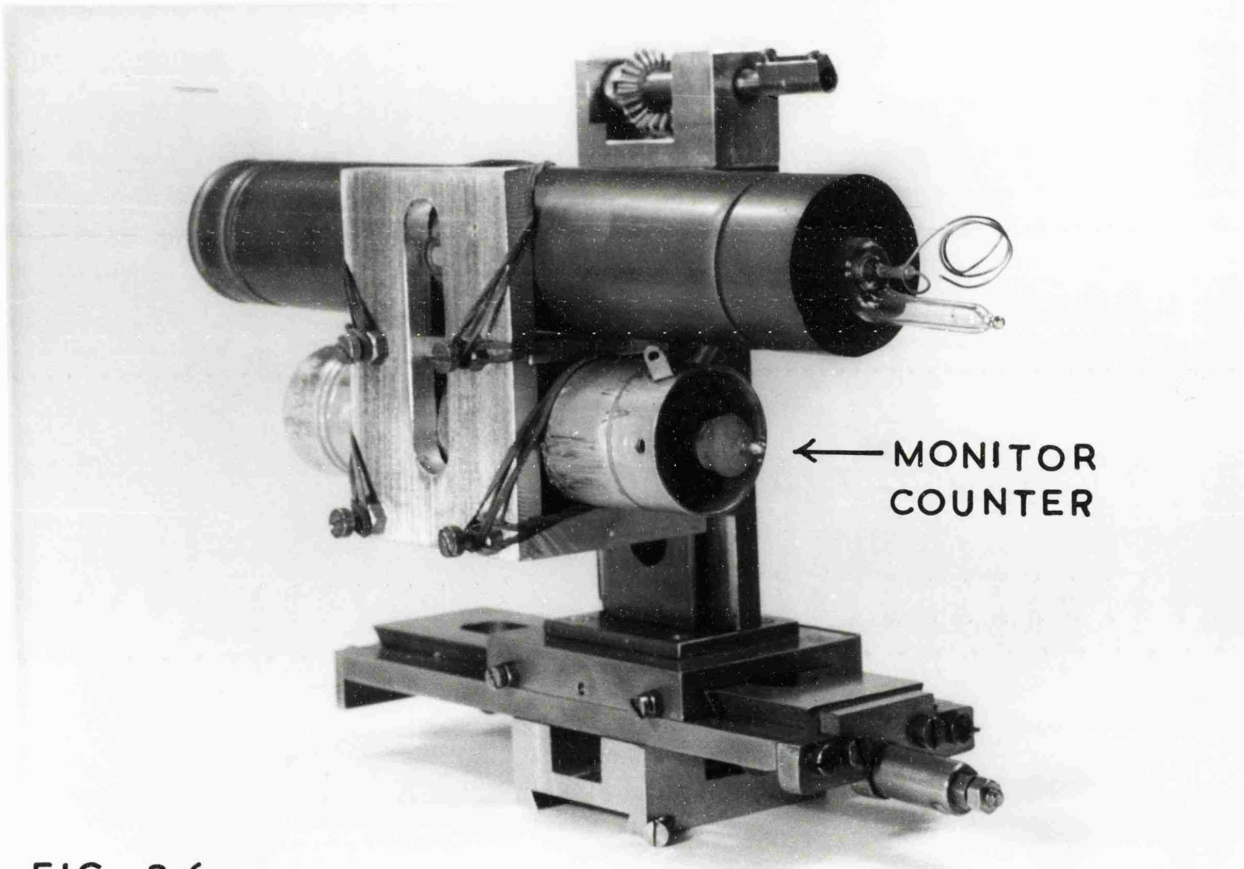

FIG 3.6

horizontally and 4 cms. vertically. In practice, however, scanning limits were imposed by the physical proximity of either the walls, lid or base of the vacuum system. The use of the unit in proportional counter investigations is described in section 3.2.4

2. Second Unit (Channel Multiplier Investigations).

The maximum depth of the apparatus on the platform assembly was insufficient to allow a channel multiplier specimen case to be suitably mounted with the necessary degrees of freedom and a second unit was therefore designed and constructed for this purpose. This unit is shown in Fig. 3.7. It consisted basically of a base assembly and a movable carriage. The carriage could be rotated about a vertical axis through O, which enabled either a proportional counter or the specimen case to be brought into the X-ray beam; the positions of both were indicated by graduations on the boss of the large gear wheel. No movement vertically was provided for, and so the height of the system was arranged so that the proportional counters and the spectrometer case were located in the middle of the X-ray beam.

The rotary movement about O was achieved with a gear-wheel system mounted on the carriage. The larger of the gear wheels was driven by the smaller one with which it was permanently meshed. A pin underneath the larger gear wheel, located in a machined slot in the base assembly, caused the carriage to rotate with a 'shaping-machine' action about O when the gear wheels revolved. (Fig. 3.8).

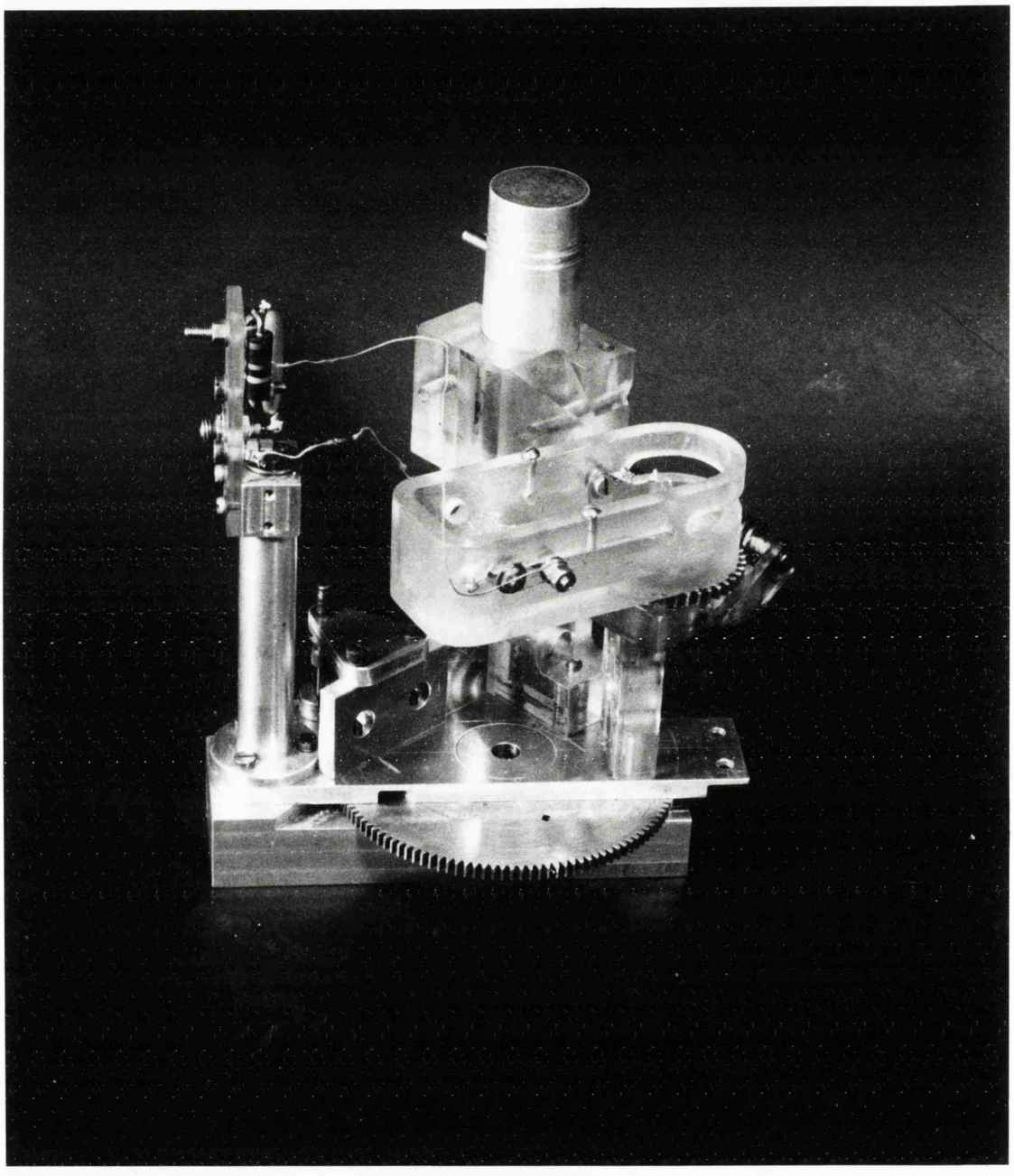

FIG 3.7

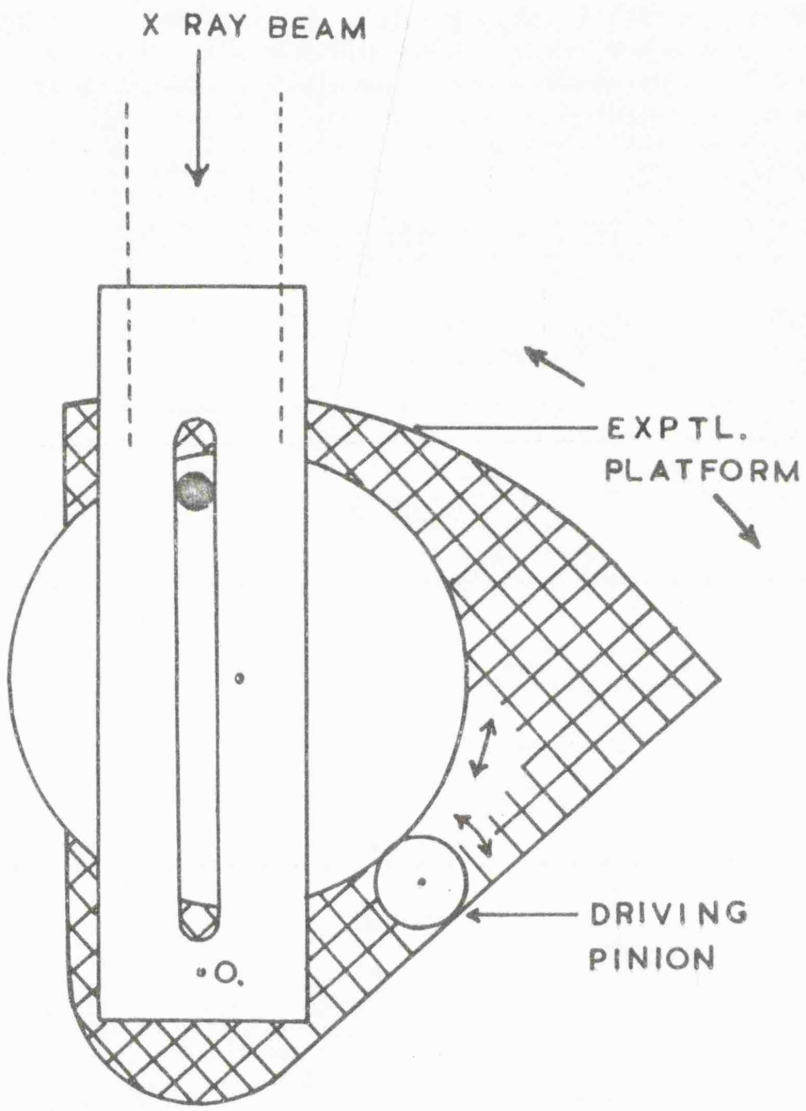

FIG. 3.8. CARRIAGE MOVEMENT

Initially a Leadex rotary solenoid was used to power the small gear wheel but it was soon rejected in favour of a manually operated flexible drive. The flexible drive was found to have several advantages over the solenoid in operation, the most important of which included a lack of vibration, a continuous bi-directional movement and a greatly reduced mass.

The proportional counter was mounted in a split cylindrical clamp made of Perspex which also provided insulation of the proportional counter from earth.

The specimen case was designed to provide a convenient mounting location for the channel multiplier device under investigation, which included both linear and curved single channel and matrix arrays of small linear channels. The case was machined out of Perspex for convenience, to enable high voltages to be supplied with a minimum risk of breakdown pulses arising. Terminal screws mounted in the walls of the case enabled connections to be made to the channel multiplier in the case which was supported by its terminal wires. The orientation of the case with respect to the X-ray beam could be varied continuously by means of a worm and worm-wheel rotated with a manually operated flexible drive. The axis of rotation was located by experiment and clearly marked on the specimen case, so that the device inside the case could be positioned with its aperture on this axis. This eliminated any translations of the device with respect to the X-ray beam during rotation of the specimen case. A small protractor fixed to the specimen case (not

shown in photograph) allowed the orientation of the case to be recorded.

Because of the proximity of the earthed worm driven pinion to the channel multiplier, a stainless steel screen was placed over the bottom of the front end of the specimen case. This screen was connected to the cathode terminal of the channel multiplier and prevented any lateral electric fields forming, in the event of the cathode not being at earth potential during any of the investigations.

3.1.2. The electronics systems.

System 1.

The electronics system was assembled to provide facilities for the amplification, display and amplitude analysis of the electrical pulse outputs of the X-ray detectors used in this work. The system is shown in schematic form in Fig. 3.9. With the exception of the pre-amplifier and the cathode follower the component units of the system were of commercial origin and are listed in Table 3.1. The replacement system was used in the latter stages of the work.

TABLE 3.1.

Unit	Type	Replacement Type
Wide Band Amplifier	I.D.L. 652	E.M.I. Wells Series Modules
Pulse Height Analyser	Dynatron N102	
Pre-Scaler	I.D.L.1850	
Timer-Counter/Scaler	Labgear D4107/4	
Ratemeter	I.D.L.	
Pen Recorder	Record, 6" per hr. Chart Speed	
Oscilloscope	Solartron CD1015	
E.H.T. Set (Proportional Counter)	I.D.L. 532	
E.H.T. (Channel Multiplier)	Brandenburg. S.0530.	

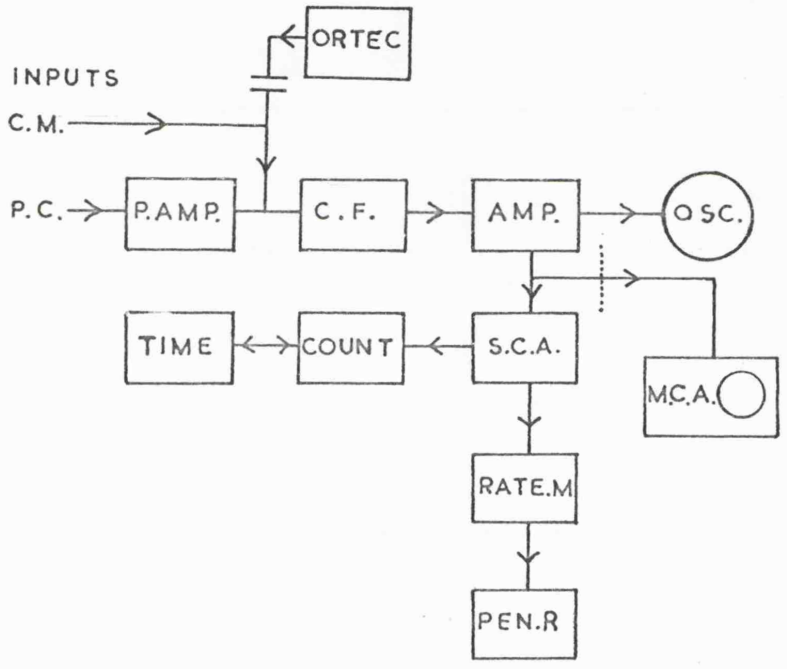

FIG. 3.9. ELECTRONICS SYSTEM I.

The Pre-Amplifier and Cathode Follower.

The pre-amplifier and cathode follower were contructed as one unit. Vacuum tubes were deliberately retained in the design because the frequency of occurrence of very large breakdown or discharge pulses, caused by accidental short circuits, was known to be relatively high. By reversing two connections on the chassis the proportional counter cathode could be kept either at earth potential or at negative E.H.T. For reasons discussed in Section 3.2.2. it was normally at earth potential.

The pre-amplifier first stage was operated in a charge sensitive mode. This resulted in a certain insensitivity of the circuit to the input capacitance and improved the stability of the stage. The second stage was a voltage amplifier with negative feed back applied via an un-bypassed cathode resistor. In operation the pre-amplifier was used in conjunction with the cathode follower. The cathode follower could also be used separately when necessary, by uncoupling the pre-amplifier from it. This facility was used whenever the input pulses would otherwise overload the pre-amplifier. ($\lesssim 10^{-12}$ Coulombs).

An Ortec precision pulser, in series with a 2pF. calibration capacitor, was used as the charge reference for all calibrations. This method of calibration is strictly accurate only for pre-amplifiers having very high capacitance ($\gg$ 2 pF.). However, as a result of the length of the input cable, the cathode follower input capacitance was about 60 pF which meant that the

calibrations were high by about 3%. The relative accuracy of the calibrations was set by the pulser and was much higher than this however.

System 2.

The apparatus in this second system, which is illustrated in Fig. 3.11., was assembled specifically for the purpose of making precision measurements on satellite proportional counters. The system comprised the units listed in Table 3.2.

TABLE 3.2.

Unit	Type
Low Noise Pre-Amplifier	Tennelec 100B
Multi-Channel Analyser	RIDL 34 - 12 with IBM Print-Out station
Precision Pulser	ORTEC 204
E.H.T. Supply	N.E. 5303
Digital Voltmeter	Solartron L.M. 1420.2 with internal standard cell calibration.

Voltage calibrations of the precision pulse generator and the E.H.T. supply were made with the digital volt meter which in turn was calibrated against an internal Weston Standard cell. At times, it was necessary to operate the system at high count rates to establish the behaviour of a proportional counter under conditions of high X-ray flux density. The pulse length at the output of the pre-amplifier was therefore reduced, by Double-RC-Clipping, to approximately 1μs. The absence of pulse pile-up in the multi-channel analyser then allowed

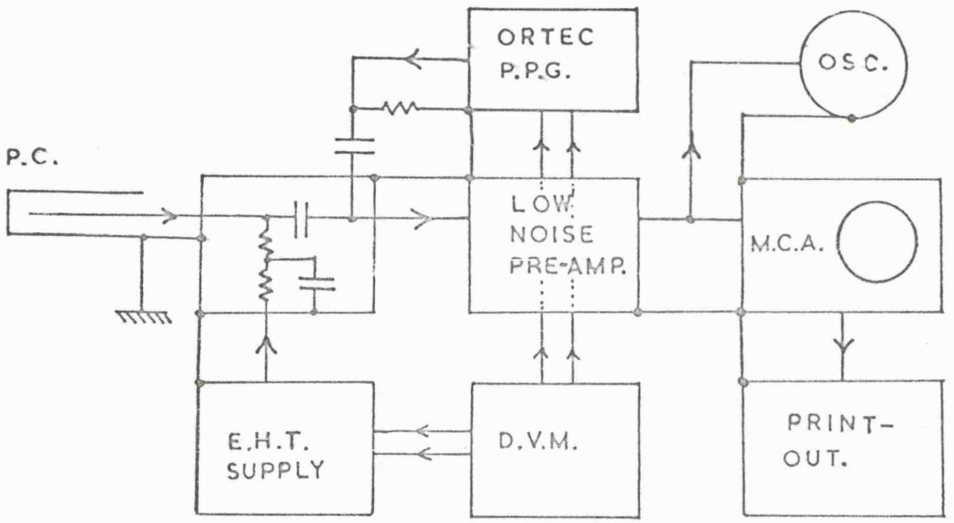

FIG. 3.11. ELECTRONICS SYSTEM 2

measurements to be made at count rates exceeding 10^5 c.p.s.

The X-Ray Source Power Supply.

The X-ray source in the spectrometer was operated by a filament-stabilised power supply system which is shown in Fig. 3.12. It consisted of the X-ray source voltage supply (A.P.T. 5705/2) and the feedback controlled filament supply (A.P.T. 6246/1) which kept the filament current at that value necessary to produce any selected emission current. This system was originally designed for operation with the source target at earth potential. This was found to lead to several difficulties in operating both proportional counters and channel multipliers in the spectrometer chamber, (see sections 3.2.2. and 3.2.3.), and so the cathode was made earthy by re-arranging the units. One problem created by this re-arrangment was that the target cooling water was now at a high voltage with respect to earth. However, it was found that the natural resistivity of tap water was adequate to support this potential difference across the Neoprene water supply tubing. A leakage current to earth of approximately 1 m A per k v. was measured to be present. As a result of the circuit arrangement, however, this current was not sensed by the filament stabiliser.

3.1.3. Other Apparatus.

The Ultra High Vacuum System.

At altitudes greater than 250 km. apparatus on board an orbiting satellite is likely to be operating under

conditions of ultra high vacuum. The X-ray spectrometer could not simulate these conditions and to enable U.H.V. testing of channel devices to be carried out a separate vacuum system was used. This system consisted basically of a 2 litre stainless steel chamber fitted with an electrode port, an ionization gauge of the Bayard-Alpert type and the necessary pumping components. Gold wire seals were used throughout. The system was mounted on a 'Syndanio' base-board and could be baked to 450^{0}C if necessary. At the commencement of each pumping cycle two molecular sieve sorption pumps were used to pre-pump the system for the Titanium Penning pump.

The vacuum evaporation unit.

This unit is shown in Fig. 3.13. The evaporation chamber was a 12" Bell Jar - electrode ring - baseplate system which could be evacuated to a pressure of the order of 10^{-5} Torr by means of a 2" Oil Diffusion Pump fitted with a liquid nitrogen cold trap . Tungsten wire evaporation spirals or Tantalum foil boats could be clamped, by means of stainless steel jaws, to two pairs of electrodes supplying A.C. power from a high current transformer. A manually operated shutter could be placed over the evaporation electrode system during the initial stages of evaporation to screen off out-gassing products from the substrate. During aluminium evaporations the plastic films were mounted in frames and positioned approximately 10" above the spirals.

A special mounting was constructed to support the channel multipliers in the system during photo-cathode

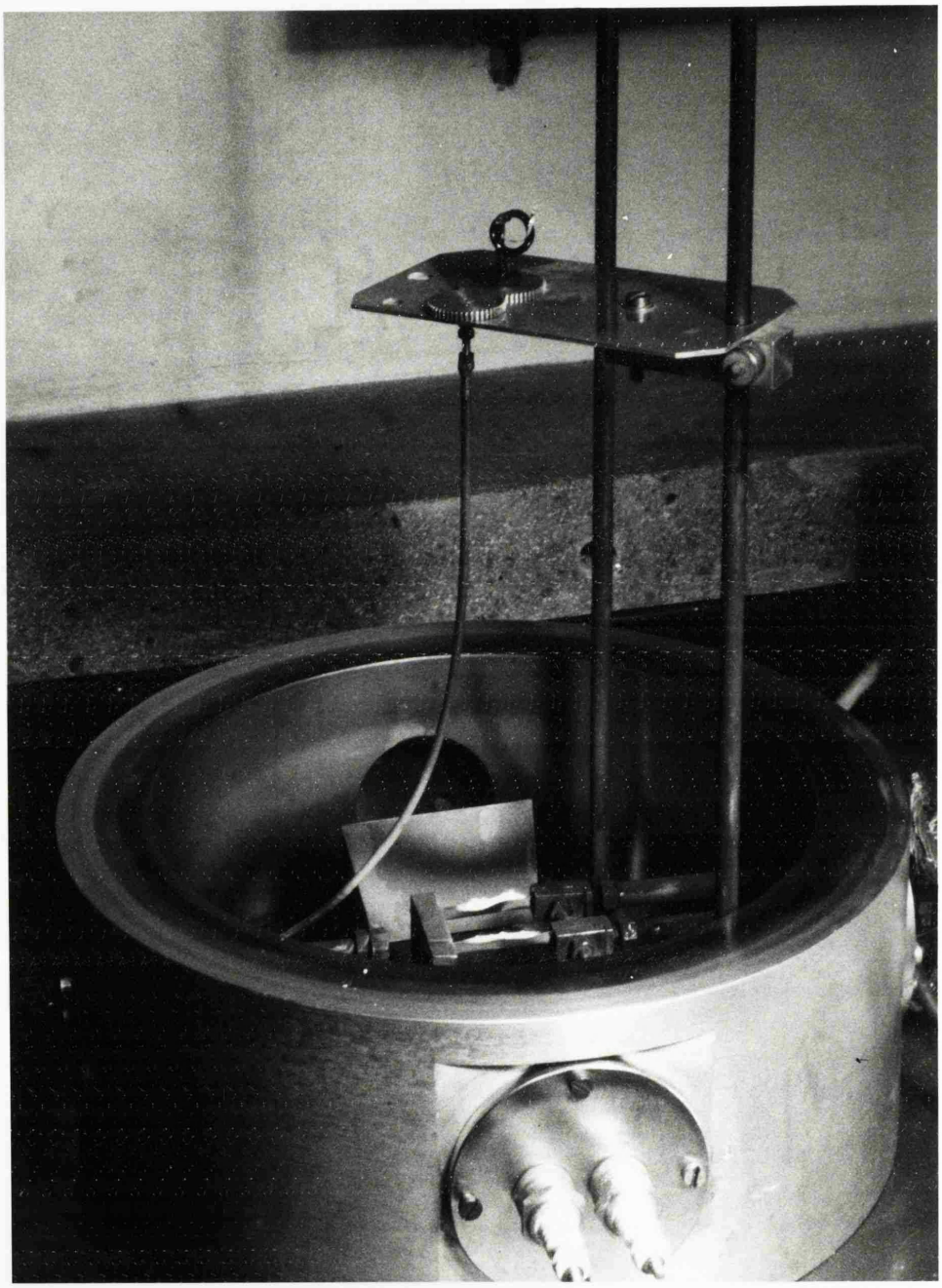

FIG 3.13

preparations. This is visible in Fig. 3 13. The mounting consisted of two permanently meshed gear wheels which could be rotated manually by means of a flexible drive. The second gear wheel supported the channel multiplier co-axially and in such a position above the tantalum boats that material was deposited around the inside surface of the channel multiplier. The underside of the aluminium plate on which the gear wheels were mounted served also to monitor the thickness of material deposited.

The counter gas pressure control unit

In the course of the work it became necessary to operate flow proportional counters in the X-ray spectrometer at reduced pressure. The apparatus assembled for this purpose is shown in Fig. 3.14. The gas pressure inside the proportional counter and the rate of gas flow through the counter could be set independently by suitably adjusting the two needle valves A and B. The operating pressure was measured with the mercury monometer and could be adjusted to remain constant for periods of thirty minutes or more without difficulty. A simple by-pass was provided for the silicone-oil bubble flow meter to prevent serious frothing during evacuation of the system.

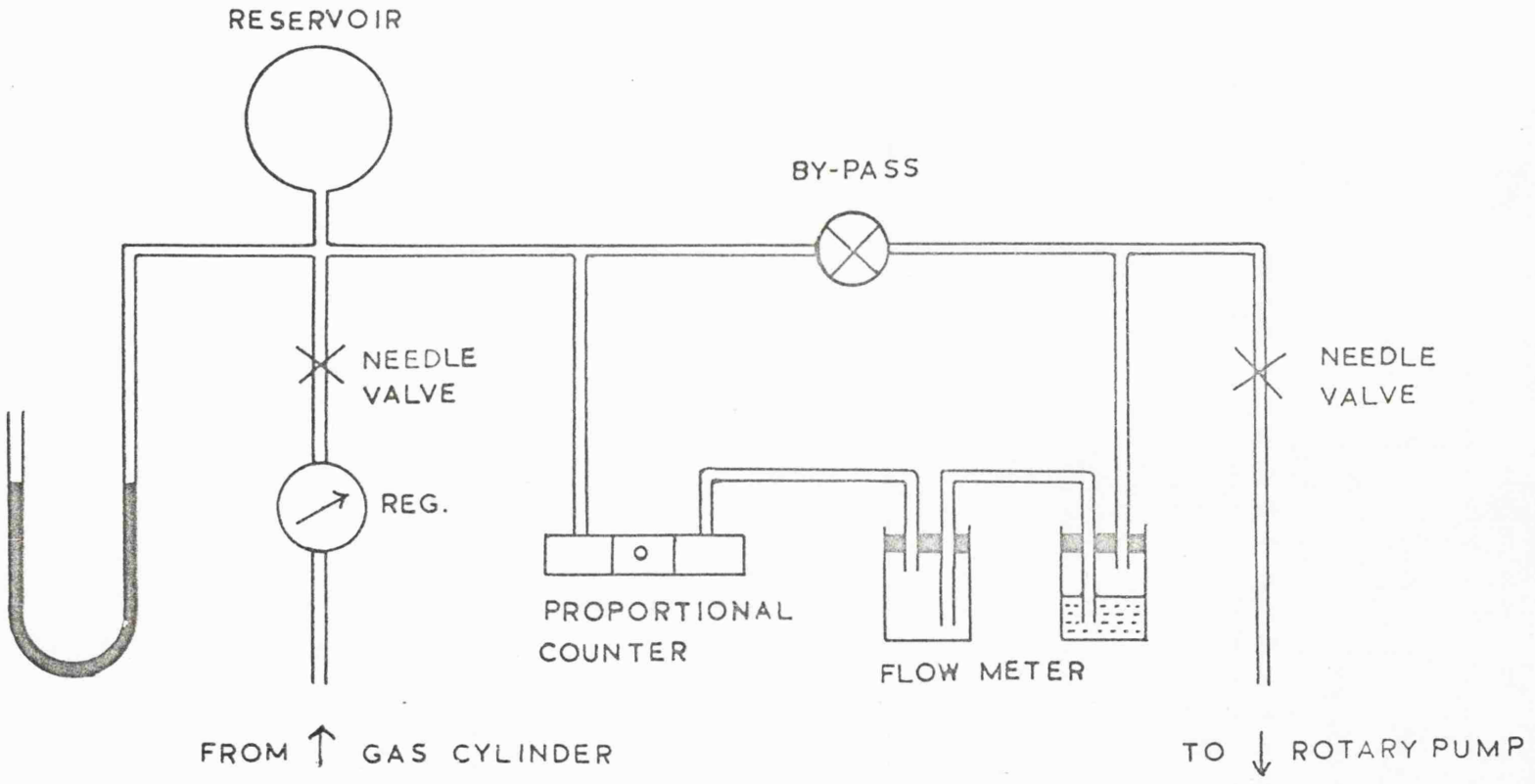

FIG. 3.14 GAS CONTROL UNIT.

3.2. The Measurement of Detector Characteristics.

3.2.1. The Alignment and Calibration of the spectrometer.

In the investigations it was required that the spectrometer produced a constant and uniform X-ray beam with sufficient wavelength resolution to separate characteristic emission lines from neighbouring continuum radiation. The first requirement was partly fulfilled by stabilising the X-ray source emission current, as described in section 3.1.2. ⁎

To meet the other requirements it was necessary for the spectrometer to possess a good crystal and to be correctly aligned geometrically.

Alignment.

The alignment was carried out in three stages:

1). The crystal was adjusted to be perpendicular both to the plane of the spectrometer and to the plane defined by

---

⁎ This technique does not produce complete X-ray emission stabilisation since variations in source efficiency remain uncompensated. Complete stabilisation is possible only if a controlling element sensitive to X-ray emission is used (see for example Tsukerman et al 1966).

the pole of the crystal and the axis of the spectrometer. This was achieved by putting the crystal in the 180^{0} position (i.e. diametrically opposite the slit assembly) and forming a focused image of the illuminated slits on the slit assembly by reflection at the crystal. By means of adjusting screws on the crystal mounting this image was centred in the two planes.

2).The radial distances of the crystal assembly and the slit assembly from the spectrometer axis were made equal to half the radius of curvature of the crystal. This was achieved by:

a. Measuring the radius of curvature of the crystal, by obtaining with calipers the distance between the crystal and slits.

b. Removing the slit assembly and adjusting the radial position of the crystal assembly so that the total translation of the pole of the crystal in going from the 90^{0} to the 270^{0} position was equal to the radius of curvature of the crystal. A travelling microscope was used for this measurement.

c. Replacing the slit assembly and adjusting with the calipers the distance between it and the pole of the crystal in the 180^{0} position to be equal to the radius of curvature of the crystal.

3). The positions of the two 'lazy-tongs' linkages on their respective rods were adjusted to allow firstly the x-radiation, emergent in operation from the exit hole in the X-ray source, to illuminate the crystal, and secondly to ensure

that the X-ray beam from the crystal passed normally through the slits. These adjustments were made with the help of a focusing lamp which was arranged to pass a fine collimated beam of light backwards through the system i.e. passing normally through the slits and falling on to the X-ray source target after reflection at the crystal.

A check on the alignment of the spectrometer could be made by illuminating a cigarette paper placed over the slits. A piece of white card attached to the target then displayed the ray pattern of the beam reflected from the crystal. In this way it was found that the focus point of the ray pattern, once set to be in the centre of the target at any spectrometer position, remained there at all spectrometer positions within the normal working range (Bragg Angles from 25^{o} to 85^{o}).

Calibration

The spectrometer was used to produce the characteristic X-ray emissions of several elements to provide a wavelength calibration, and hence to confirm that the instrument was properly set up. The results of this calibration are shown in Fig. 3.15.

Uniformity of the X-ray beam was checked both with photographic film and a scanning proportional counter with a small window. Some of the flux density distributions are shown in Fig. 3.16.

The stainless steel blank produced as a substrate for the fatty acid crystal was ground to the same radius of curvature as that of the mica crystal in use at the time.

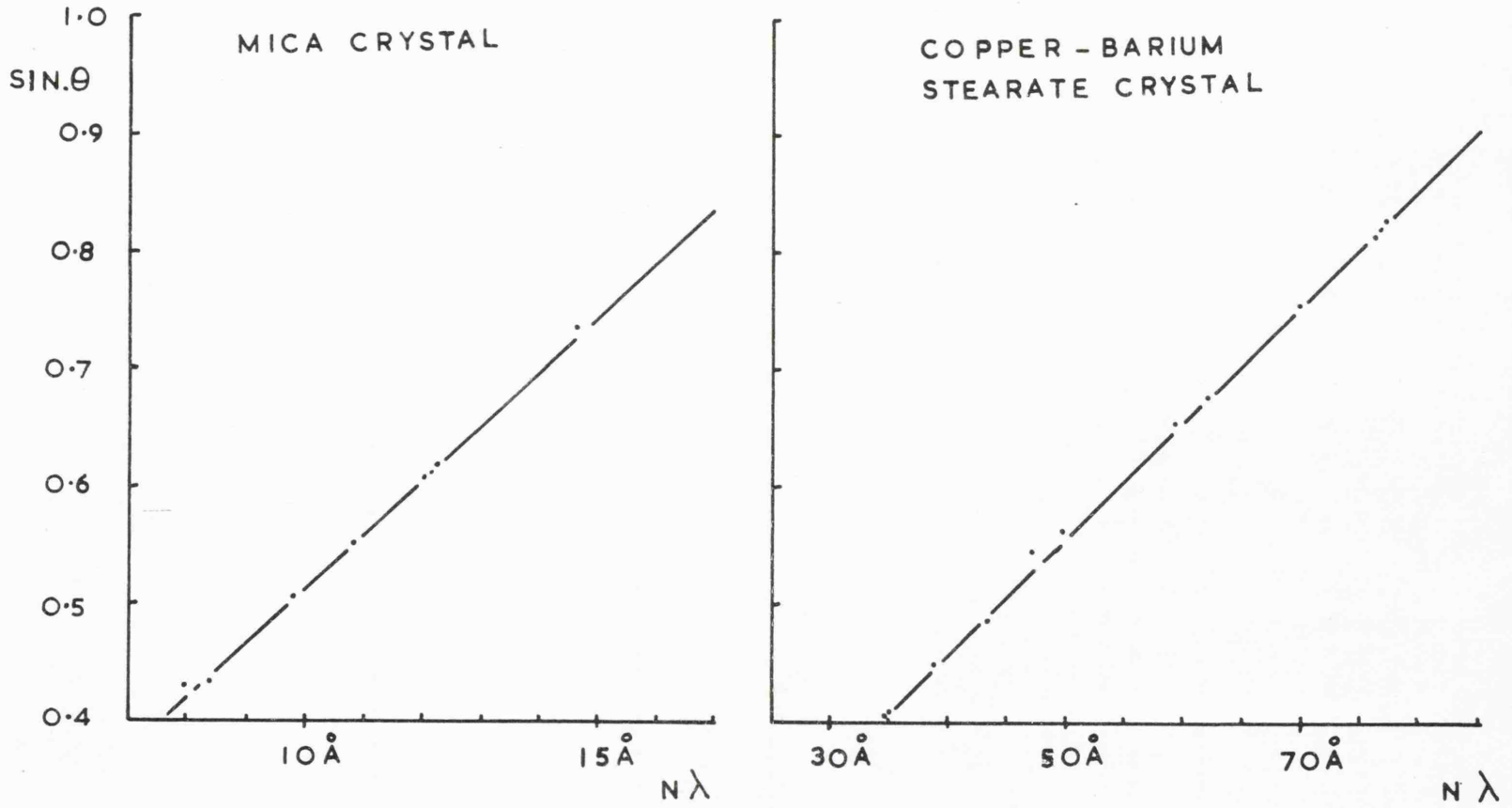
MICA CRYSTAL
SIN.θ
1·0
0·9
0·8
0·7
0·6
0·5
0·4
10Å
15Å
Nλ
COPPER - BARIUM
STEARATE CRYSTAL
30Å
50Å
70Å
Nλ

FIG. 3.15

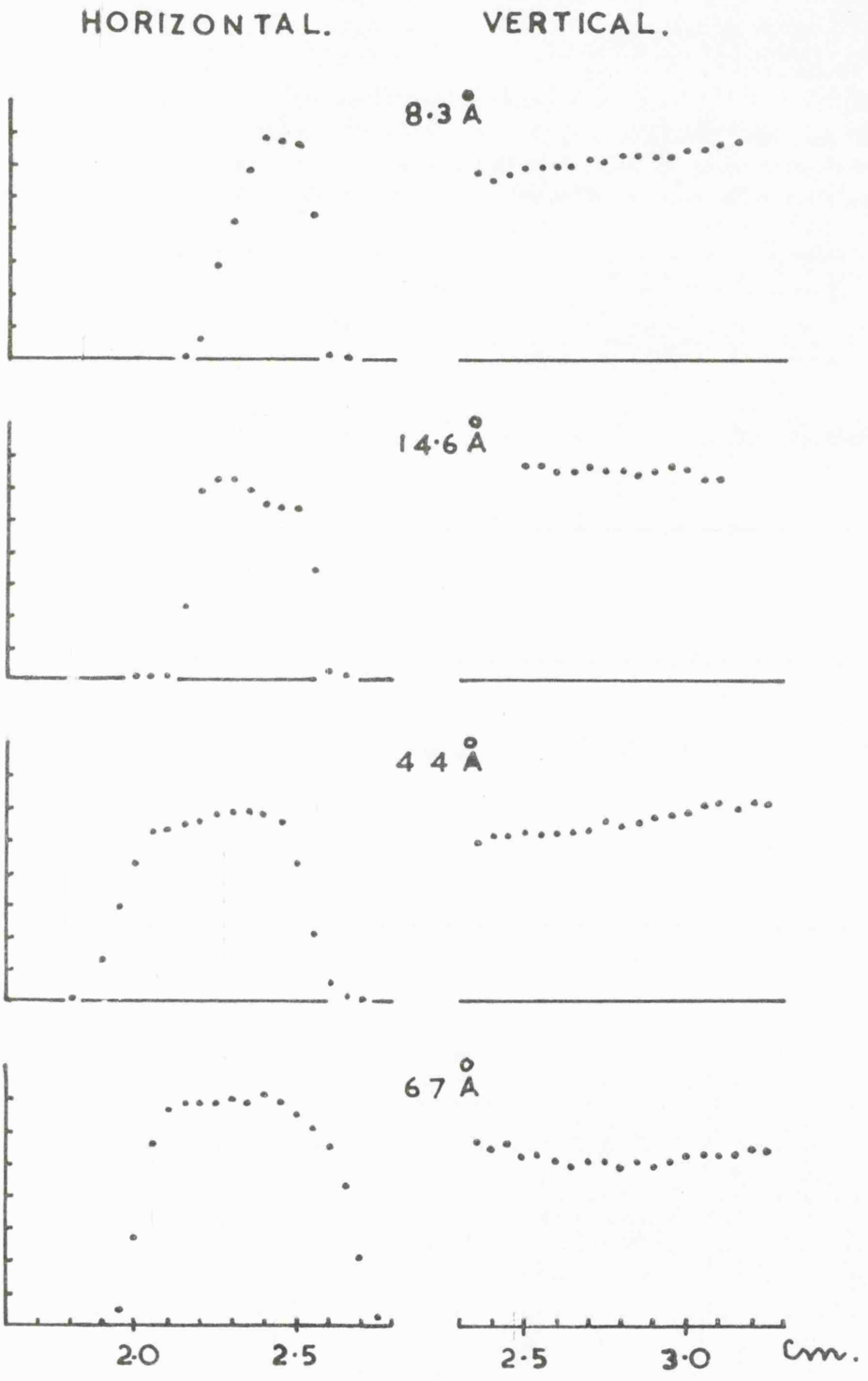

FIG. 3.16.

However, the mica crystal had later to be replaced owing to accidental damage. The new crystal was then found to have a slightly shorter radius of curvature and a separate alignment procedure was carried out for this crystal. The alignment settings for the two crystals were then recorded with scribed marks on the spectrometer.

3.2.2. The operation of proportional counters for absolute X-ray photometry.

Introduction

A detector of known photon detection efficiency was required in this work for the measurement of the flux density of the spectrometer radiation. A gas counter was selected for this role because, in principle, it is possible to establish the photon detection efficiency of such a counter at a given wavelength of operation, if the transmittance factors of the window and of the gas filling are known. In addition, it is necessary to be able to assume that every quantum absorbed in the counter gas is recorded as one pulse, or count, and that other counts do not arise. Thus there must not be any insensitive (or 'dead') volume in the counter, and the background noise level must be predictable.

Both the Geiger counter and the proportional counter have been used for absolute flux determination in the soft X-ray region.

e.g. Lukirskii et al	(1960 a.)	Geiger Counters (15 - 120 Å)
Lukirskii et al	(1963)	Proportional Counters (1 - 18 Å)
Tomboulian	(1964)	Geiger Counter (100 - 300 Å)
Metchnik	(1964)	Proportional Counters and Geiger Counters (1.54 Å)
Lukirskii and Brytov	(1965)	Proportional Counter (67 Å and 190.3 Å)

For the present work the proportional mode was chosen, because of the photon energy discrimination possible with the counter, and because of the short recovery time as compared with a Geiger counter.

The Proportional Counter

The counter used was a PX 28 K Type Proportional Counter ⁎ fitted with gas flow tubes and with a demountable side window assembly (Fig. 3.17.A). The window material used was thin Melinex ø approximately 1 μ thick.

The window was sealed to the counter body with a commercial rubber solution and gently clamped with the screwed plate. Melinex was chosen for the window material principally because its great strength enabled

⁎ 20th Century Electronics Ltd.

ø I.C.I. Trade name for Polyethylene terephthalate film (known as 'Terylene' in fibre form). This material was obtained in unstretched non-orientated form through the generosity of I.C.I. Ltd., and stretched as required.

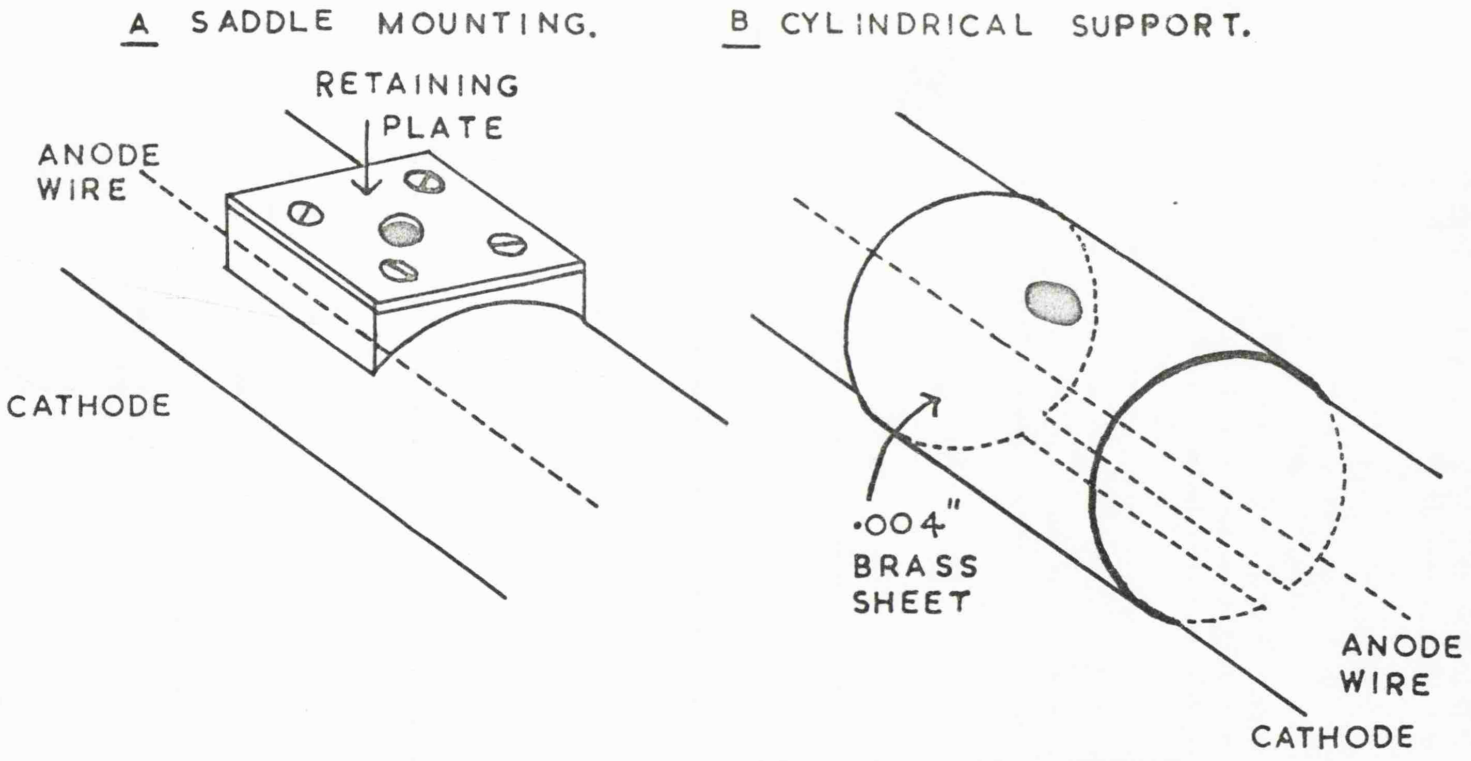

FIG.3.17. PROPORTIONAL COUNTER WINDOW DETAIL.

usefully large, transmissive windows to be produced which could withstand pressure differentials of the order of one atmosphere. These windows could also be made very uniform over the required areas in terms of the appearance of their interference colour pattern, which made the selection of a representative sample of the material for transmission measurements relatively straight-forward.

Initially, standard P.10 type gas mixture (90% Argon 10% Methane) was used in the counter. Good pulse height distributions were obtained at wavelengths in the range 2 - 15 Å and at 67 Å (Boron K Emission Line) but not at 44 Å (Carbon K Emission Line).

Operation at 44 Å

At 44 Å the counter pulse height distribution did not exhibit a well defined peak but appeared to include many extra smaller pulses between the expected position of the peak and zero pulse height. The total count rate, although fairly stable normally, could be greatly increased by lightly rubbing the Perspex lid of the vacuum system with a dry cloth or piece of paper. (This effect was found later not to be peculiar to the 44 Å spectrometer position, although the amplitude distribution of the extra pulses was similar to that of 44 Å radiation). The count rate could be reduced markedly by reversing the counter E.H.T. polarity and applying it to the counter cathode, and increased by reducing the operating pressure of the counter from atmospheric to a lower value.

It was obviously necessary to resolve these points

before attempting to make flux measurements.

At about the same time, Poen Sing Ong (1965) had reported similar effects to those described above with a proportional counter, used under similar conditions, and claimed that the pulse height distributions became less serious if the fraction of Argon in the gas mixture was reduced, although no mechanism of the effect was suggested. In view of this, the gas mixture was changed to that of 25% Argon 75% Methane. This required an increase in the operating voltage of the counter for the same output charge from about 2 kV. to 3 kV.

Some improvement in the 44 Å pulse height distribution at atmospheric pressure was obtained with this mixture but the pulse height distribution was still observed to slowly deteriorate during operation. It was found that good pulse height distributions could only be obtained after a) the window mount had been redesigned to locate the window much closer to the counter cathode (as shown in Fig. 3.17.B) and b) a partly conducting layer of aluminium had been deposited on the inside of the window. This layer was about 220 Å thick which was also the value, quoted by Sharpe (1955), citing Campion (1960), necessary for stable proportional counter operation.

The reason for the initially poor pulse height distributions was believed to be the extremely high absorption coefficient of the gas mixture at 44 Å. The significance of this is evident from Fig. 3.18. which gives, as a function of wavelength for the two mixtures,

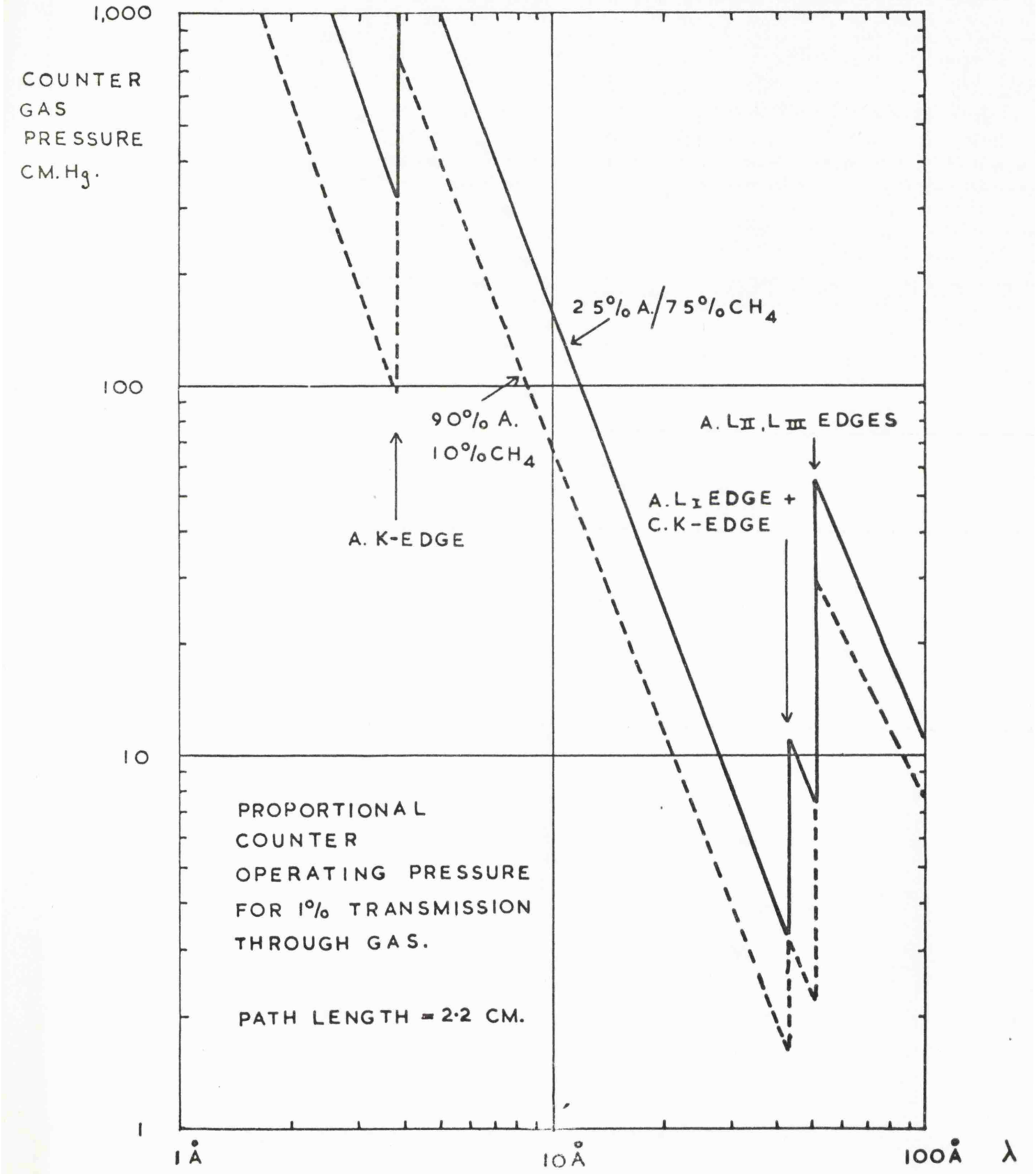
1,000
COUNTER GAS PRESSURE CM. Hg.
100
10
1
25% A./75% CH4
90% A.
10% CH4
A. K-EDGE
A. LII, LIII EDGES
A. LI EDGE +
C. K-EDGE
PROPORTIONAL COUNTER OPERATING PRESSURE FOR 1% TRANSMISSION THROUGH GAS.
PATH LENGTH = 2·2 CM.
1 Å
10 Å
100 Å
λ

FIG. 3.18.

the gas pressure necessary for the counter to transmit 1% of the flux. ✱ At 44 Å a pressure of only 3 cm. is required for the 90/10 Mixture, which would make the absorption path at 76 cm. a fraction of a millimetre, thus limiting the counter performance by the field conditions existing immediately behind the window. That this was so was confirmed by the greatly improved pulse height distributions obtained with the aluminized window even at atmospheric pressure (see Fig. 3.19).

Although some pressure dependence of count rate compatible with the existence of a dead volume was still observed to be present ϕ, the effect disappeared when the window was changed and was therefore attributed to window imperfections such as excessive curvature or a poor aluminium layer. For subsequent measurements, nevertheless, periodic low pressure checks (of count rate) were made; in fact for the 25/75 mixture the counter was also operated at reduced pressure for flux measurements, since the lower counter E.H.T. required decreased the risk of electrical breakdown pulses.

✱ Absorption data from Lukirskii et al (1964) Bearden (1959) and Henke et al (1957).

ϕ This dependence was of the form $e^{-\mu p \delta}$

where p = gas pressure
μ = absorption coefficient per unit pressure
and δ (= 0.12 mm.) = The equivalent depth of dead volume.

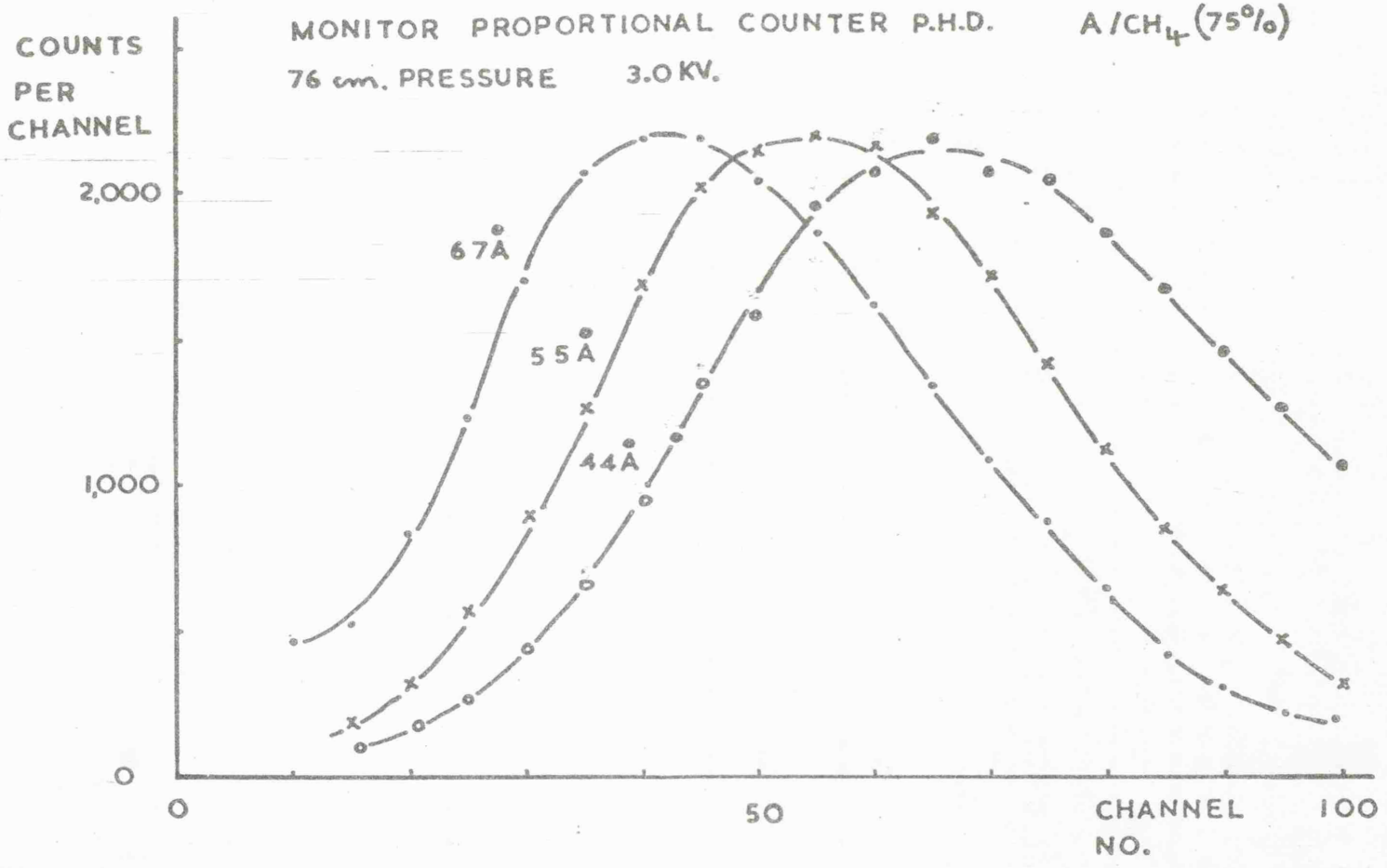
MONITOR PROPORTIONAL COUNTER P.H.D.
A/CH4 (75%)
76 cm. PRESSURE 3.0 KV.
COUNTS PER CHANNEL
2,000
1,000
0
67Å
55Å
44Å
0
50
100
CHANNEL NO.

FIG. 3.19

Other Count Rate Variations

Following the establishment of proper counter operations two sources of count rate variation remained.

The first took the form of a fluctuating 44 Å distribution associated with the accidental or deliberate brushing of the tank lid with a sleeve or piece of paper. Some effect, though weaker, was obtained even with the X-ray source off. An investigation indicated that the cause of this interference was the production of Carbon K fluorescence radiation in the Melinex counter window by electron bombardment via discharges between the charged Perspex lid and the spectrometer. The effect was illustrated in a controlled manner by bombarding the counter with electrons from the cathode assembly of the X-ray source. The pulse height distributions obtained for different bombarding voltages are shown in Fig. 3.20. and may be compared with the distributions obtained for monochromated 44 Å radiation from the same counter under similar conditions. An estimate of the efficiency of this process was made during the electron bombardment experiment by measuring the count rate from a channel multiplier next to the counter. On correcting this count rate for distance and aperture area, it was estimated that the proportional counter registered about 15% of the channel multiplier registrations for electrons of 5 keV. energy. For such electrons it may be assumed that the channel multiplier is about 60% efficient (Evans 1965); On this basis the counter efficiency would appear to be approximately 10% for these electrons.

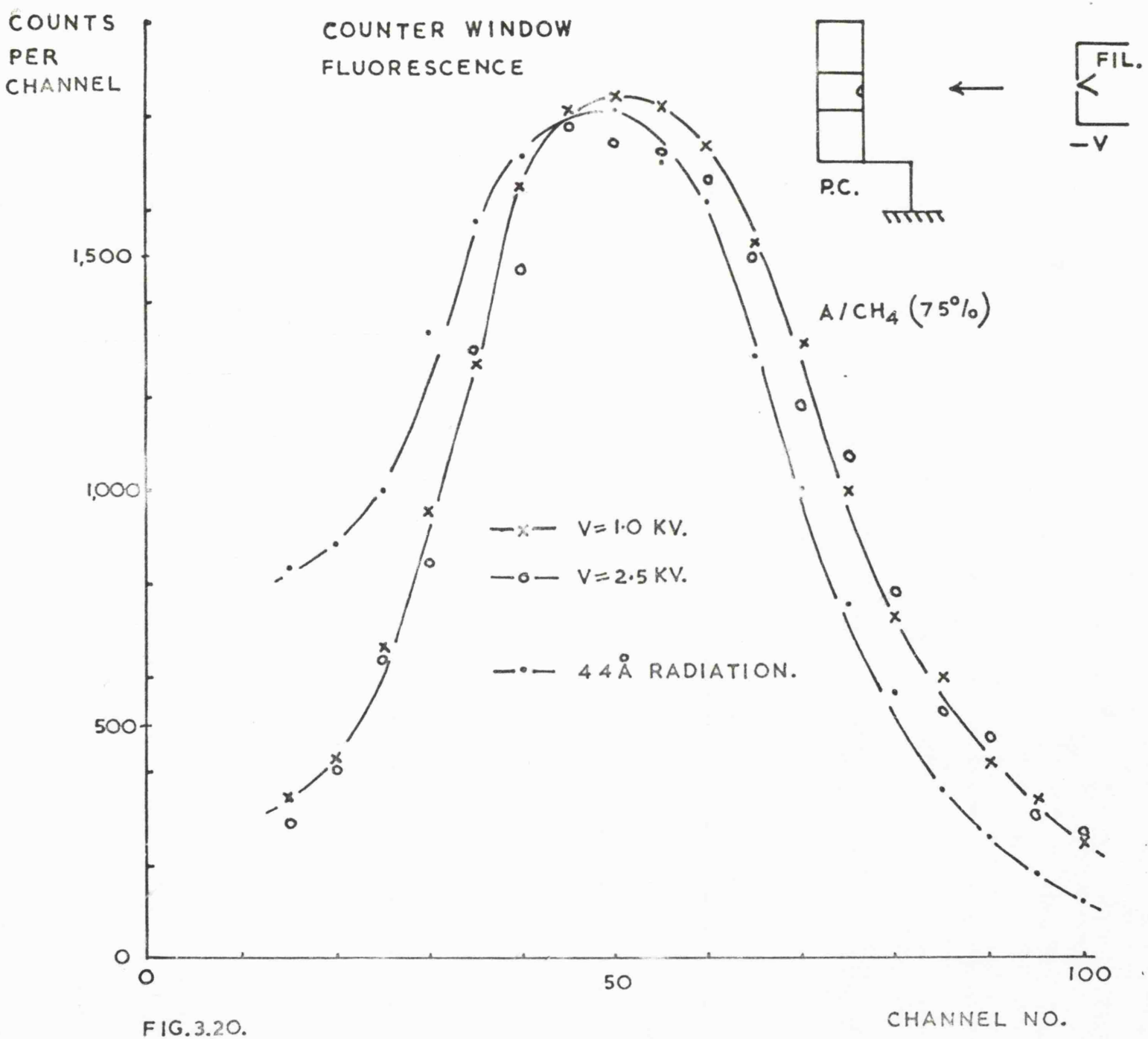
COUNTS PER CHANNEL
COUNTER WINDOW FLUORESCENCE
FIL.
-V
P.C.
A/CH4 (75%)
1,500
1,000
500
0
—x— V=1·0 KV.
—o— V=2·5 KV.
—•— 44Å RADIATION.
0
50
100
CHANNEL NO.

FIG. 3.20.

Thus the mechanism for the observed effect was found to be entirely spurious and not due to counter efficiency changes. Nevertheless care was taken during measurement not to frictionally excite the perspex lid. The effect was greatly reduced by the redesign of the X-ray source (see Section 3.2.2.) and later found to be further reduced if the underside of the lid was not cleaned with a solvent but just wiped with a tissue when necessary.

The second effect was apparent as a reduction in count rate following the establishment of a potential difference between the counter cathode and neighbouring bodies in the spectrometer. The effect was originally observed after switching on the channel multiplier positive E.H.T. supply to the specimen case next to the counter.

This time the control experiment devised to resolve the effect demonstrated that the counter efficiency was, in fact, changing. The experiment was carried out with an X-ray transmissive screen of aluminised melinex interposed between the counter and the spectrometer. Under conditions of steady X-ray flux a potential of + 2 kV. was applied to the screen. The subsequent variation of count rate is shown in Fig. 3.21.

The effect was reproducible from one window to another and could be reduced, though not eliminated, by operating the counter at lower pressures. The result of increasing the X-ray flux by a factor of two was to reduce the time constant of the variation by approximately the same amount.

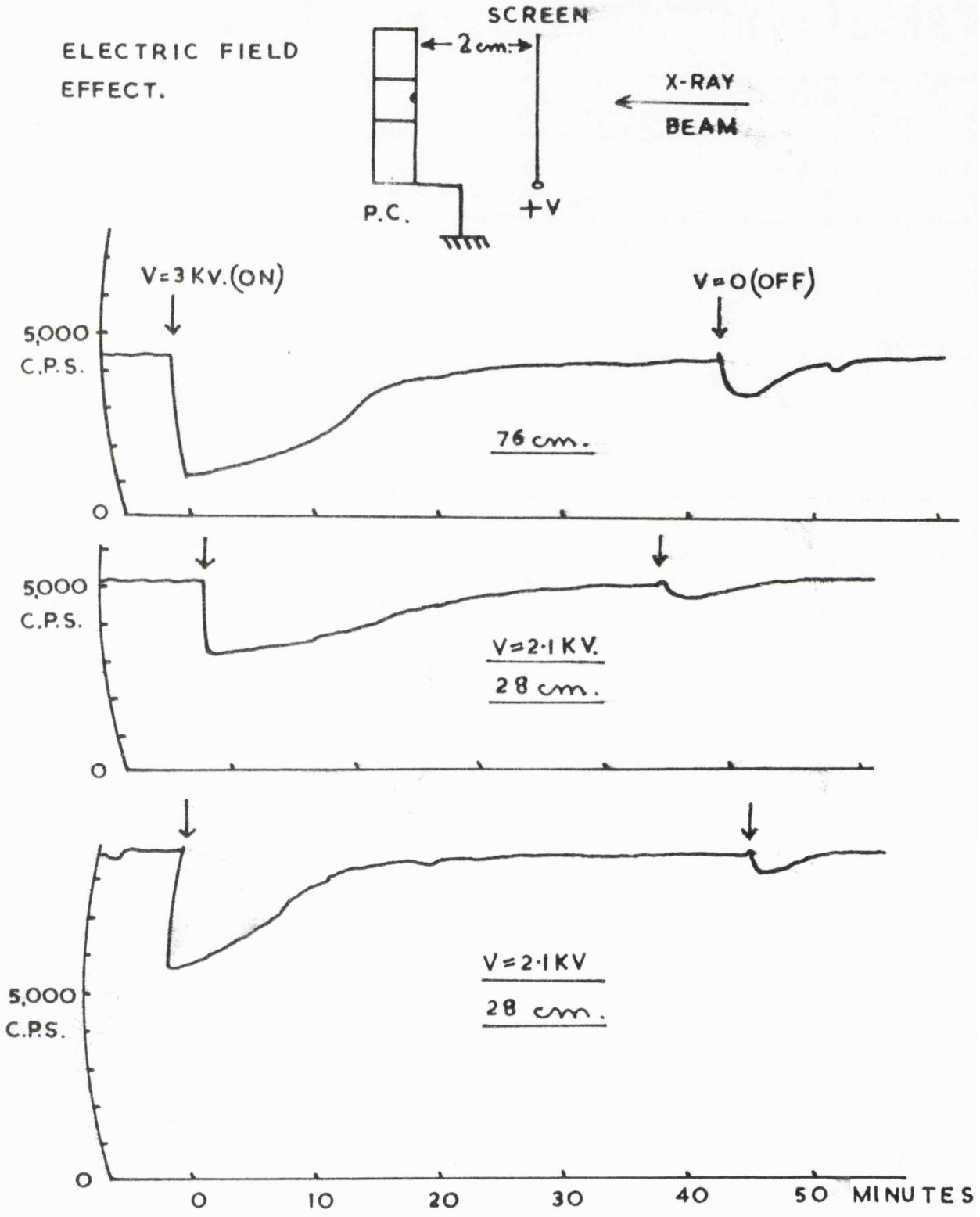
ELECTRIC FIELD
EFFECT.
SCREEN
2 cm.
X-RAY
BEAM
P.C.
+V
V=3 KV.(ON)
V=0(OFF)
5,000
C.P.S.
0
76 cm.
5,000
C.P.S.
0
V=2·1 KV.
28 cm.
5,000
C.P.S.
0
V=2·1 KV
28 cm.
0
10
20
30
40
50
MINUTES

FIG. 3.21

Negative potentials on the screen were found to have no effect.

The mechanism was therefore concluded to involve the charging, by dielectric displacement, and subsequent neutralisation of the inside surface of the window. It was thought probable that a thicker layer of aluminium on the inside would have eliminated this. This would, however, have seriously reduced the counter efficiency (see Fig.3.22). In practice, to eliminate the effect, the counter was operated in a field-free environment. This therefore precluded operation of the counter with its cathode at negative E.H.T. or in proximity to positive E.H.T. supplies.

Summary of Procedure.

As a result of the investigations described, a method of preparing, testing and operating proportional counters was developed. The counters possessed good pulse height distributions and were stable in operation at all wavelengths, provided that electron bombardment and electric field effects were absent.

Although not essential with a properly working counter, operation at reduced pressure was found to be convenient and also afforded a means of confirming the absence of dead-space behind the window.

Further measurements were made on the counters. These included the measurement of pulse height distribution at high count rates, which showed negligible changes up to 50,000 c.p.s. and of the counter noise background which was less than 1.c.p.s

At wavelengths in the range 2 - 12 Å the 90% counter gas mixture was used. As can be seen from Fig. 3.18 a correction

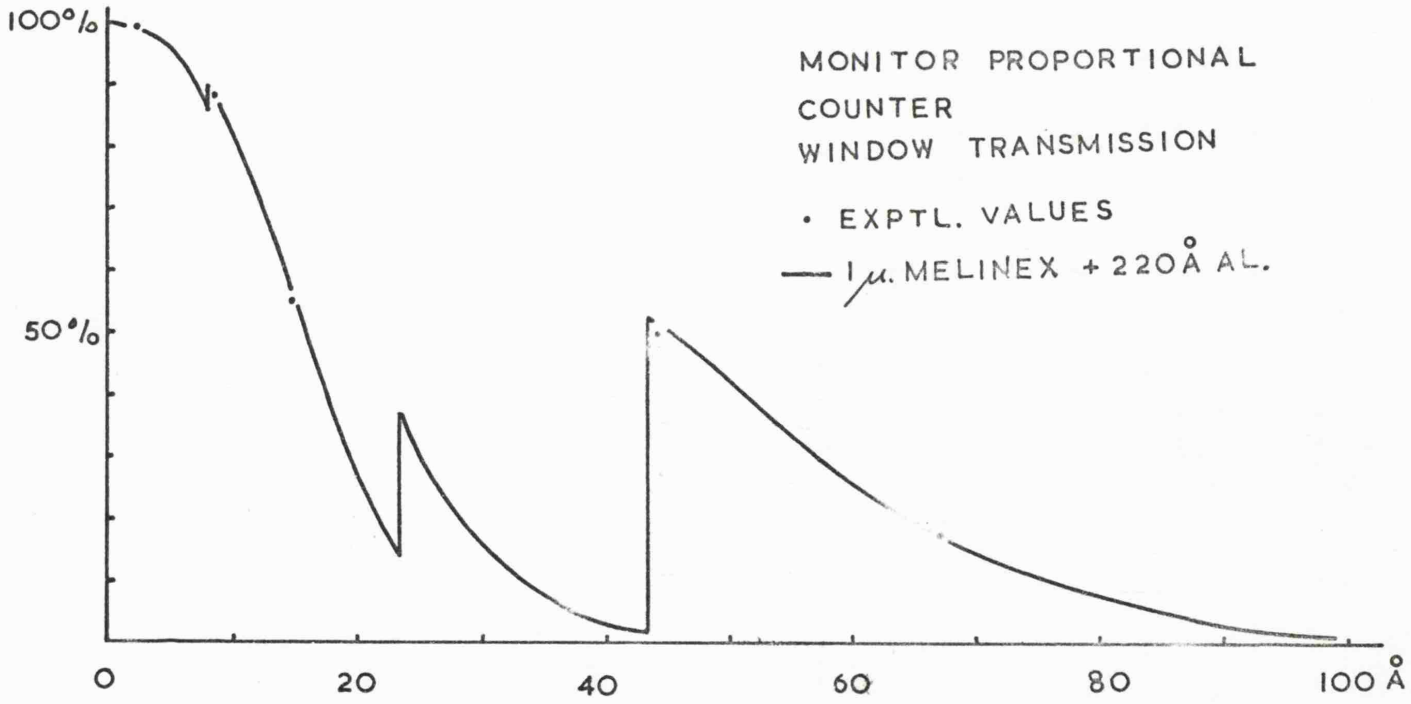
100%
50%
MONITOR PROPORTIONAL
COUNTER
WINDOW TRANSMISSION
• EXPTL. VALUES
— 1 μ. MELINEX + 220Å AL.
0
20
40
60
80
100 Å

FIG. 3.22

for the transmittance of the gas was necessary below 10 Å and the correction factor was obtained from this graph. A single check was made at 5.4 Å (2nd. order MoL Emission) to confirm the accuracy of this procedure. At this wavelength krypton has an absorption factor in excess of 99% over the path length of the counter (2.2 cm.). The check consisted of determining the count rate change resulting from the change of gas mixture from A/CH_4 (90/10) to Kr/CH_4 (90/10) at a constant X-ray flux. Multichannel analysis was used to separate the 5.4 Å line from the 10.8 Å 1st order continuum. (see Fig. 3.24). The argon absorption factor was measured to be 0.66, this was in good agreement with the value predicted by Fig. 3.18 (0.65). At 2.1 Å the argon fluorescence escape peak was present in the counter pulse height distribution. Care was taken to include this peak when making flux measurements at this wavelength. To facilitate the measurement of small X-ray fluxes in a reasonable time, the monitor counter window used for the channel multiplier work was quite large (5.41 sq.mm.). A correction to take into account the curvature of this window in absolute flux measurements was made. (see Appendix 1).

3.2.3. The Operation of Channel Multipliers for the detection of X-radiation.

The isolation of the X-ray response.

For an investigation into the use of channel multipliers for the detection of X-radiation it was

obviously necessary to ensure that the measured response of the device was that resulting only from the incidence of X-radiation, and further, that the radiation was monochromatic and from a given direction. In this work it was expected from the nature of the device, and found, that there were very many other sources of channel multiplier counts. These included:

a). Positive and negative ion production by the X-ray source and Penning Gauge.

b). E.U.V. radiation produced by the X-ray source reaching the multiplier by reflection from the crystal and reflection, or scattering, from the spectrometer walls.

c). Photo-electric emission in the vicinity of the channel cathode by X-radiation.

d). Noise from the channel background and from electrical interference.

Because of the relative independence of pulse distribution on the nature of the original excitation, the procedure for isolating the X-ray response was essentially a negative one. Thus all other mechanisms were either eliminated, or known to be present to a predictable extent.

Ionic interference from the pressure gauge was eliminated by keeping the gauge switched off during measurements. That due to the X-ray source was reduced in two stages by a) reducing the production rate and b) reducing the sensitivity of the channel multiplier to the ions.

The production rate was greatly decreased by

redesigning the X-ray source so that the cathode assembly was at earth potential instead of at negative E.H.T. (Fig. 3.2.). This reduced the electron flux streaming from the source into the vacuum chamber, evidence of which was previously obtained both by operating the source at a higher pressure than normal, when a violet glow surrounding the source was clearly visible, and by measuring the current collected at a positively charged point probe in the spectrometer system.

The sensitivity of the channel multiplier to the ions was much reduced by operating the channel multiplier with its cathode end at earth potential (as shown in Fig. 3.23). Positive ions were thus not encouraged to enter the channel multiplier aperture.

With this mode of operation, however, it was necessary to provide both a high voltage coupling capacitor and extra decoupling for the E.H.T. supply to reduce the ripple content well below the signal level.

One adverse result of this arrangement of channel voltage was noticed in the case of the matrix array of channel multipliers described in Section 4.2. It was necessary to use a fine slit assembly close to the matrix to define the X-ray beam (44 Å) and trouble was experienced with a high background level resulting from photo-electric emission from the edges of the slit. A bias of +500 v. on the slit assembly was found to suppress this background. Care was also taken to earth all spectrometer components in the vicinity of the matrix.

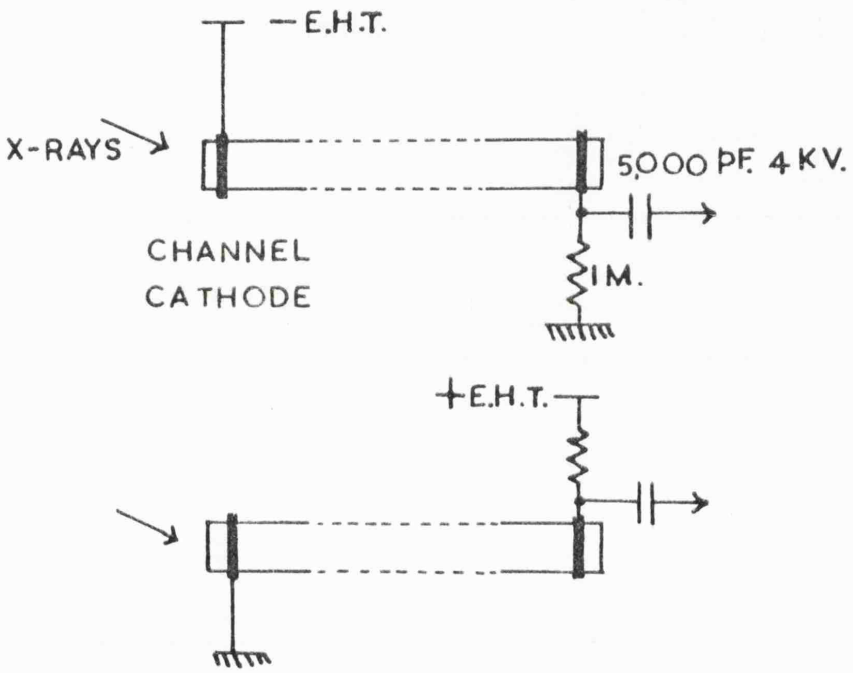

FIG. 3.23

Background illumination of the channel multiplier by X-ray source radiation was prevented with suitable screens extending laterally from the X-ray slit assembly. In front of the slit assembly could be placed a filter which was opaque to ultra-violet radiation from the X-ray source. This filter was, in fact, a representative sample of the proportional counter window material and therefore served to compensate for window absorption losses in the proportional counter during measurements of photon detection efficiency.

The inherent noise level of the channel multipliers was very low and represented only a small fraction of the background normally present during measurements. Knowledge of this noise was important, however, for other reasons and its magnitude and origin are discussed in section 4.17.

The electrical noise level was usually defined by pick-up and E.H.T. smoothing. The use of co-axial cable for signal leads and the provision of adequate decoupling ensured that this was lower than the inherent noise level of the channel multiplier.

The procedure adopted for the measurement of the X-ray response included the use of X-ray line emissions Although this was necessary for the attainment of adequate flux intensities, the procedure was valuable for another reason. By measuring the count rate of the channel multiplier and the proportional counter alternately, both at the peak of the emission line and at spectrometer positions to the high and low wavelength sides of the line,

it was possible to completely eliminate by subtraction the total background of the channel multiplier. This was typically 5 - 10% of the total count rate. Thus the net proportional counter count rate yielded a measure of the extra flux density in the emission line over the continuum radiation, and the net channel multiplier count rate represented the response of the channel multiplier to this extra flux. The accuracy of the method of measurement is discussed in Chapter 5.

For measurements at 2.1 Å an Fe^{55} source was used. This was mounted in front of the spectrometer slit together with a metal filter of aluminium or beryllium, to stop the electron emission from the source reaching the channel multiplier and monitor counter. In principle, the correction for counter window absorption level had still to be made, but since this was measured to be 0.996 at this wavelength, it could safely be neglected.

Second order emission lines were found to have too low an intensity, relative to the level of background radiation and generated ions, to allow proper measurements to be made.

3.2.4. The calibration of satellite proportional counters.

This part of the work was carried out as part of the programme of preparation for the two Leicester/University College London solar X-ray spectrometers for the OSO -D and ESRO II satellites. The object

of the work was to produce counters of known spectral characteristics stable over the operating life of the experiments ($\sim$ 1 year).

This involved the measurement, as a function of wavelength, of the modal output charge $\underline{q}$, the energy resolution $\underline{R}$ (% f.w.h.m.) and the photon detection efficiency $\underline{\mathfrak{Z}}$ (counts per incident 100 photons). The procedure adopted was to examine the counters at different wavelengths using X-ray line emissions, isolated by the X-ray spectrometer, and then to interpolate and extrapolate the characteristics to other wavelengths.

Owing to the severe stability specification imposed by satellite operation and the need to unfold the maximum solar information from the pulse height spectra obtained in orbit, measurements to better than 2% were arrived at in the measurement of output charge and resolution. Electronics system 2 described in Chapter 3 possessed adequate stability but further precautions were necessary. These involved:

a). Using the same charge calibration capacitor for all measurements.

b). Making careful charge calibration cross-checks in the event of having to use a different multi-channel analyser for any of the measurements.

c). Calibrating at flux density levels producing count rates < 500 c.p.s. to isolate the results from high count rate distortions, the extents of which were evaluated separately .

d). Keeping the incident radiation normal to the counter windows.

The X-ray fluxes were standardised with a proportional counter, prepared and operated as described in Chapter 3; the window material was aluminised thin Melinex again. (Area = 0.578 sq.mm.)

For the first measurements of charge output and resolution it was required only that the counters be illuminated with monochromatic radiation; therefore these could be made while the X-ray source was settling down. Pulse height distributions were recorded at the specified counter voltage, calibrated with the precision pulser and printed-out for permanent storage.

The measurements of photon detection efficiency were made only after the X-ray emission had become constant. The procedure adopted was to a) measure the flux density at a certain point in the X-ray beam with the thin window monitor counter

b) record the count rate from the satellite counter when placed at the same position in the beam with an aperture of known area over its window

and c) repeat the monitor counter measurement. If the two monitor readings differed by more than 3% the measurements were repeated.

The count rates were corrected for background and dead-time, if these corrections were fractionally significant. The absorption in the monitor counter window was compensated by placing a sample of the window material

in the X-ray beam during the satellite counter measurements.

For measurements at 5.4 Å (2nd. order MoL - emission) a refinement of the procedure outlined above was necessary. This involved the measurement and subtraction of the 10.8 Å 1st order component of the continuum radiation. This correction was made by graphically separating and integrating the two wavelength components from the counter multi-channel pulse height spectra. Fig. 3.24 shows typical pulse height distributions for the monitor counter and for one of the satellite counters (only those with 5 μ Aluminium windows were sensitive to 10.8 Å radiation). Because of the day to day changes in the state of the molybdenum target, the magnitude of this correction had to be re-measured periodically.

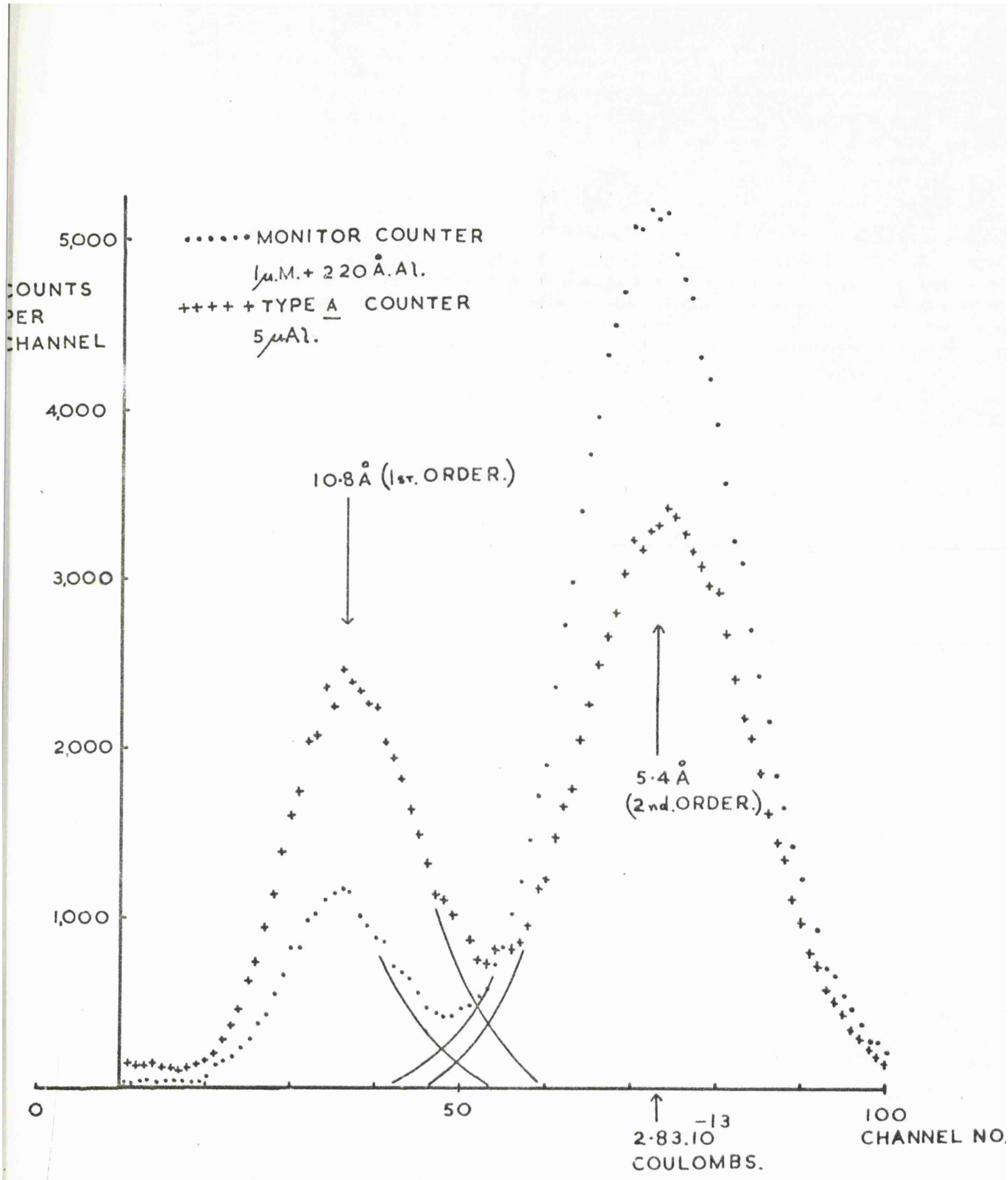
5,000
4,000
3,000
2,000
1,000
COUNTS PER CHANNEL
•••••• MONITOR COUNTER
1μ.M. + 220 Å. Al.
++++ + TYPE A COUNTER
5μAl.
10·8 Å (1st. ORDER.)
5·4 Å (2nd. ORDER.)
0
50
100
CHANNEL NO.
2·83.10⁻¹³ COULOMBS.

FIG. 3.24.

Chapter 4. The Experimental Results and their Analysis.

4.1. The Investigation of Single Channel Multipliers

4.1.1. The pulse height distribution from channel multipliers.

The multipliers examined in this work were produced by Mullard Research Laboratories and were of Vanadium Glass construction. The two classes of multiplier are illustrated in Fig. 4.1. and their physical details are given in Table 4.1.

TABLE 4.1.

Multiplier Class No.	D.C.Resistance	Channel length.	I.D.
A).B 400 A	$1.4 \times 10^{10}\ \Omega$	7.5 cm.	0.22cm.
B).B 400 B (Special)	$2.2 \times 10^{10}\ \Omega$	11.5 cm.	0.24cm.

To establish proper definitions and values of photon detection efficiency and noise for any radiation detector it is necessary to state unambiguously the conditions of measurement of these quantities. For a counting detector these conditions may be summarized by describing the amplitude distribution of the output pulses (pulse height distribution) and the counting amplitude thresholds (lower and upper discrimination levels).

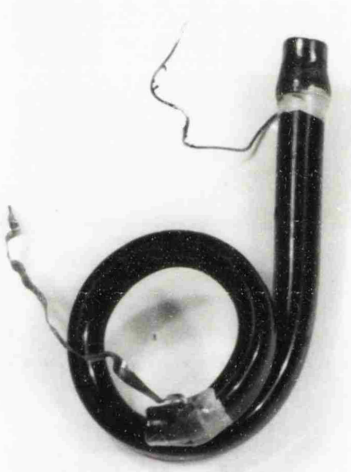

TYPE A

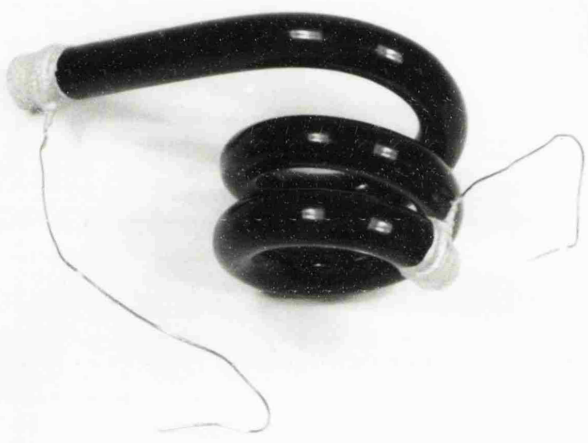

TYPE B

FIG 4.1

In the case of the channel multiplier, it was discovered in this work that considerable differences in pulse height distribution existed according to the conditions of operation, and this was therefore investigated prior to the measurement of the X-ray response. Fig. 4.2 shows the change of pulse height distribution with increasing channel voltage at a constant count rate. These distributions were obtained for curved channel multipliers, although similar variations were found with linear channels (see, for example, the sample distributions shown in the first report of this work, Smith 1966).

Owing to positive ion feed-back, linear channel multipliers are gain sensitive to gas pressure (this is shown in Fig. 4.3.A), which may be compared with the relative invariance of gain with pressure for a channel curved to eliminate positive ion feed-back (Fig. 4.3.B).

Typical variations of mean gain with count rate are shown in Fig. 4.4. for channel multipliers having three different values of D.C. resistance. (The dotted lines indicate for each case the pulse current limitation imposed by the value of the standing wall current of the multiplier). Similar effects have been reported by Adams and Manley (1966) and attributed to field distortion in the channel. This effect is discussed further in Section 4.1.9.

The relative insensitivity of the channel multiplier to the character of the exciting radiation is shown in Fig. 4.5. A.

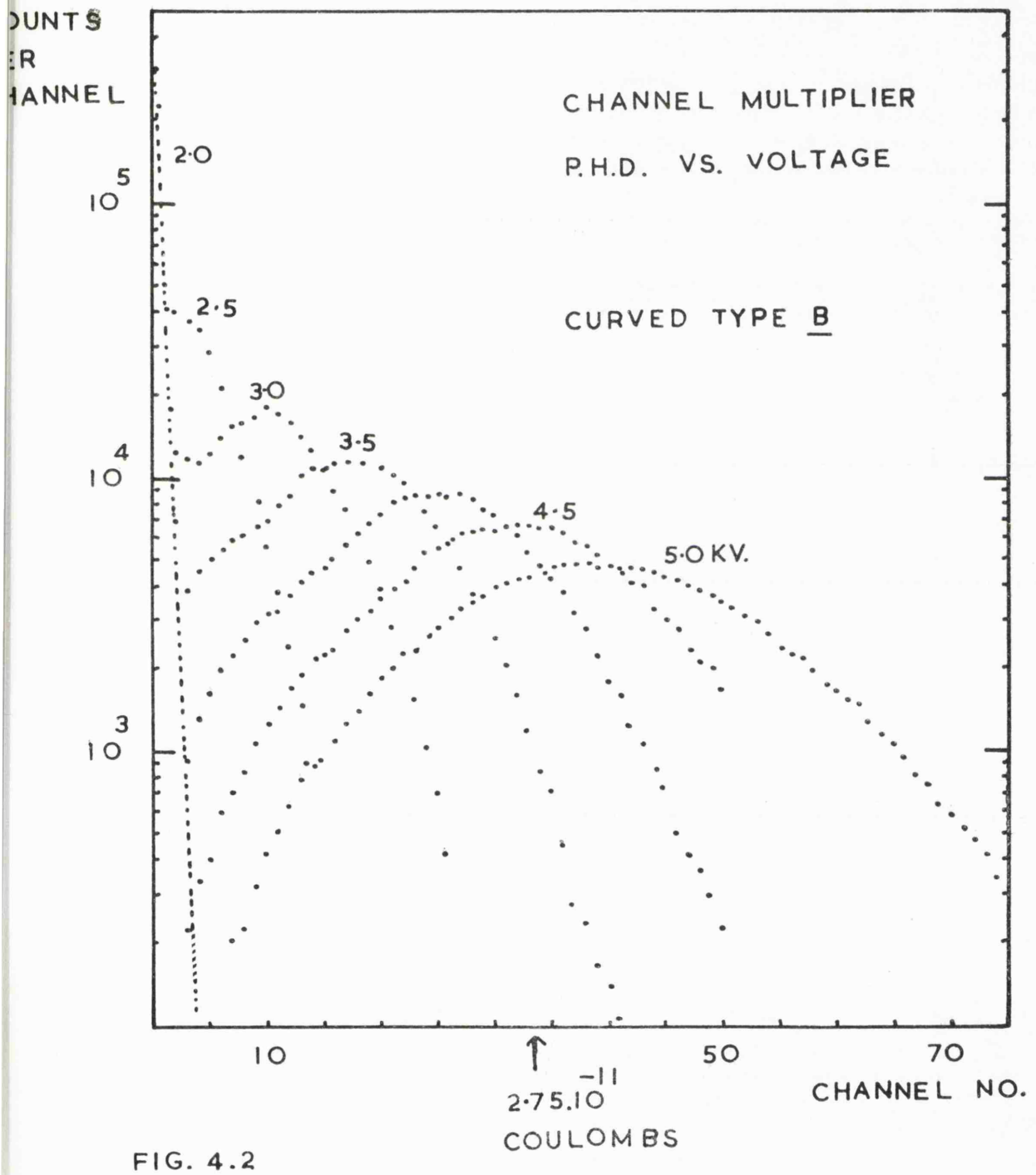
OUNTS
ER
HANNEL
CHANNEL MULTIPLIER
P.H.D. VS. VOLTAGE
CURVED TYPE B
2·0
2·5
3·0
3·5
4·5
5·0 KV.
10^5
10^4
10^3
10
50
70
CHANNEL NO.
2·75.10^-11
COULOMBS

FIG. 4.2

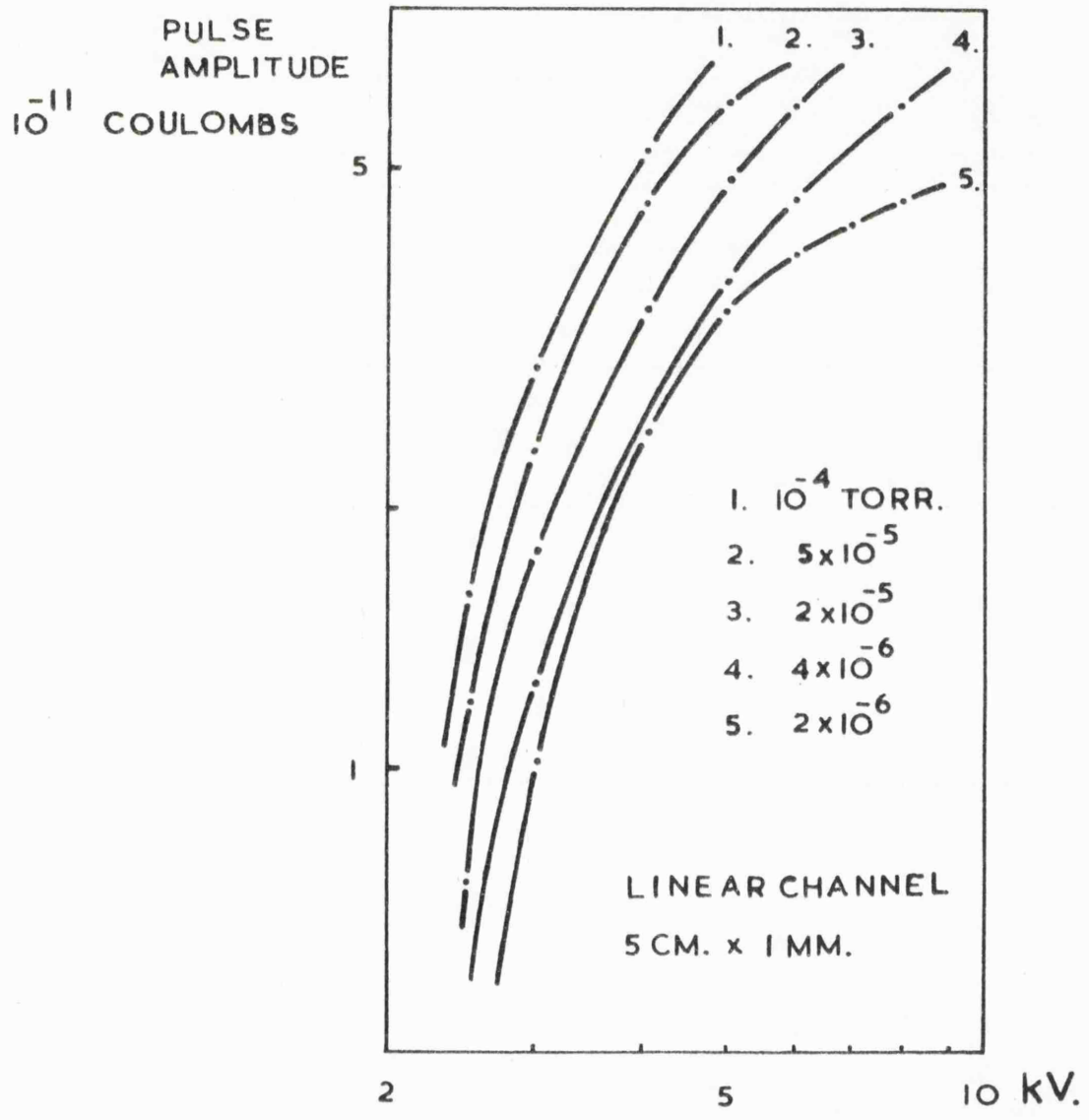
PULSE
AMPLITUDE
10^{-11} COULOMBS
5
1
1. 2. 3. 4. 5.
1. 10^{-4} TORR.
2. 5×10^{-5}
3. 2×10^{-5}
4. 4×10^{-6}
5. 2×10^{-6}
LINEAR CHANNEL
5 CM. x 1 MM.
2
5
10 kV.

FIG. 4.3.A.

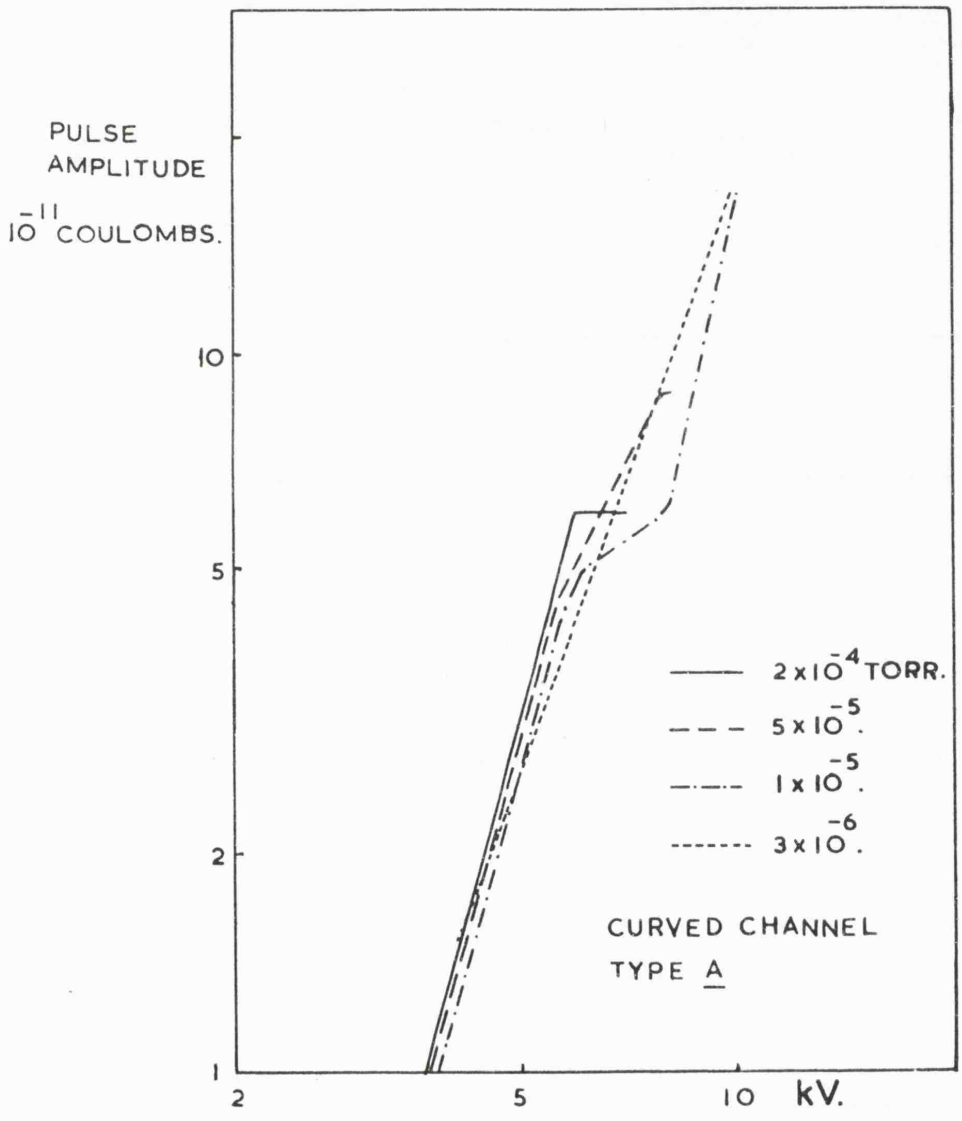
PULSE
AMPLITUDE
10^{-11} COULOMBS.
10
5
2
1
2
5
10 kV.
2×10^{-4} TORR.
5×10^{-5}.
1×10^{-5}.
3×10^{-6}.
CURVED CHANNEL
TYPE A

FIG. 4.3.B.

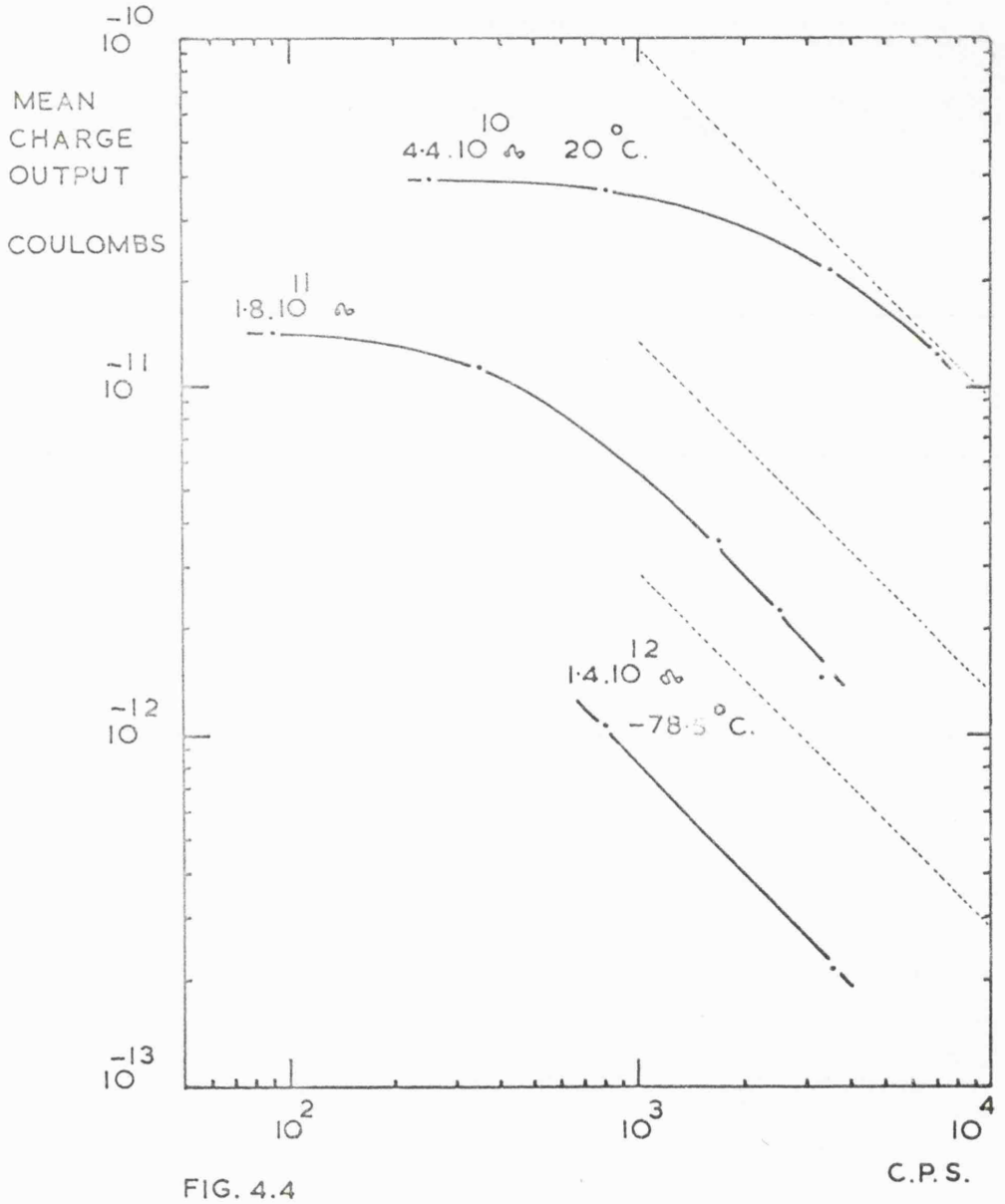
-10
10
MEAN
CHARGE
OUTPUT
COULOMBS
10
4·4.10 Ω 20 °C.
11
1·8.10 Ω
-11
10
12
1·4.10 Ω
-78·5 °C.
-12
10
-13
10
10^2
10^3
10^4
C.P.S.

FIG. 4.4

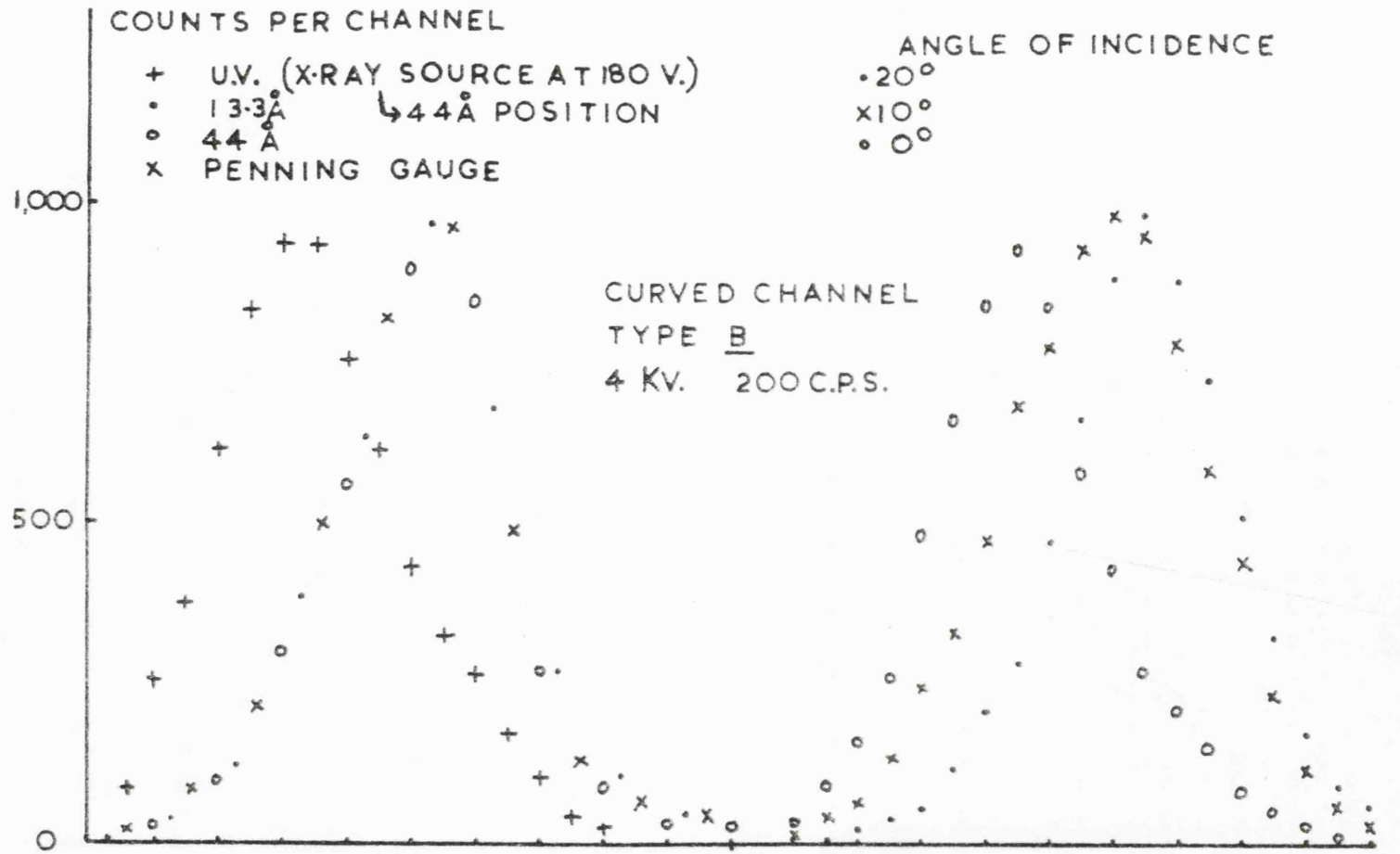
COUNTS PER CHANNEL
+ U.V. (X-RAY SOURCE AT 180 V.)
• 13·3Å ↳44Å POSITION
o 44 Å
× PENNING GAUGE
ANGLE OF INCIDENCE
•20°
×10°
o 0°
CURVED CHANNEL
TYPE B
4 KV. 200 C.P.S.
1,000
500
0
0
50
100/0
50
100
CHANNEL NO.

FIGS. 4.5.A. 4.5.B.

The ions were generated in the Penning type vacuum gauge and the ultra-violet light in the X-ray source. In the second case, the spectrometer was at the 44 Å position but the tube voltage was reduced to 180 V. Thus the radiation incident on the multiplier had, probably, a broad photon energy distribution in the region of 90 e V.

This independence is in keeping with what is to be expected from the operation of the device, since the only variable can be the initial number of electrons ejected at the primary particle interaction on the channel inside surface. This variation would be reflected in the pulse height distribution under conditions of proportional amplification by the electron multiplication process in the channel. Any multiplication saturation or fluctuations, however, would tend to smooth out the distribution and thereby make the channel output independent of the nature of the excitation.

Fig. 4.5.B. shows the change in pulse height distribution obtained for different angles of incidence of x-radiation (wavelength and count rate kept constant). The most significant change evident is at zero angle of incidence, i.e. for radiation parallel to the axis of the channel, although the distribution is still saturated under these conditions. Such a change almost certainly reflects the fact that the radiation is impinging further down the channel. These pulse height distributions show that more than 99% of the channel multiplier pulses have amplitudes greater than the counting threshold, which was

usually set to between 5 and 10% of the mean pulse height.

Under these conditions no pulse loss occurs during changes of angle of incidence or of count rate for channels of D.C. resistance of the order of $10^{10}\ \Omega$ at count rates less than 7.000 c.p.s. However, a constant watch was kept on the pulse height distributions during the investigations.

4.1.2. The X-ray response of the bare channel multiplier.

Using the methods described in Chapter 3, the X-ray response of several channel multipliers without special preparation were investigated. The operating voltage was set at 4 k V. for the present investigations, which was felt to be the maximum convenient for the generation and supply in the OAO - C satellite experiment, described in Chapter 5. The pulse height distribution was as shown in Fig. 4.2., which indicated that at this voltage the multiplier was operating into saturation and made complete pulse registration straightforward.

The variation of the X-ray response with angle of incidence at several wavelengths is shown in Fig. 4.7.A and 4.7.B. The ordinate scales are normalised to give photon detection efficiency η as defined by

$$\eta = \frac{n}{N \pi r^2}$$

where n = channel multiplier count rate

N = flux density of beam (measured as described in Chapter 3).

r = radius of channel aperture.

For convenience, no correction is made for the cosine reduction of aperture area normal to the X-ray beam; this

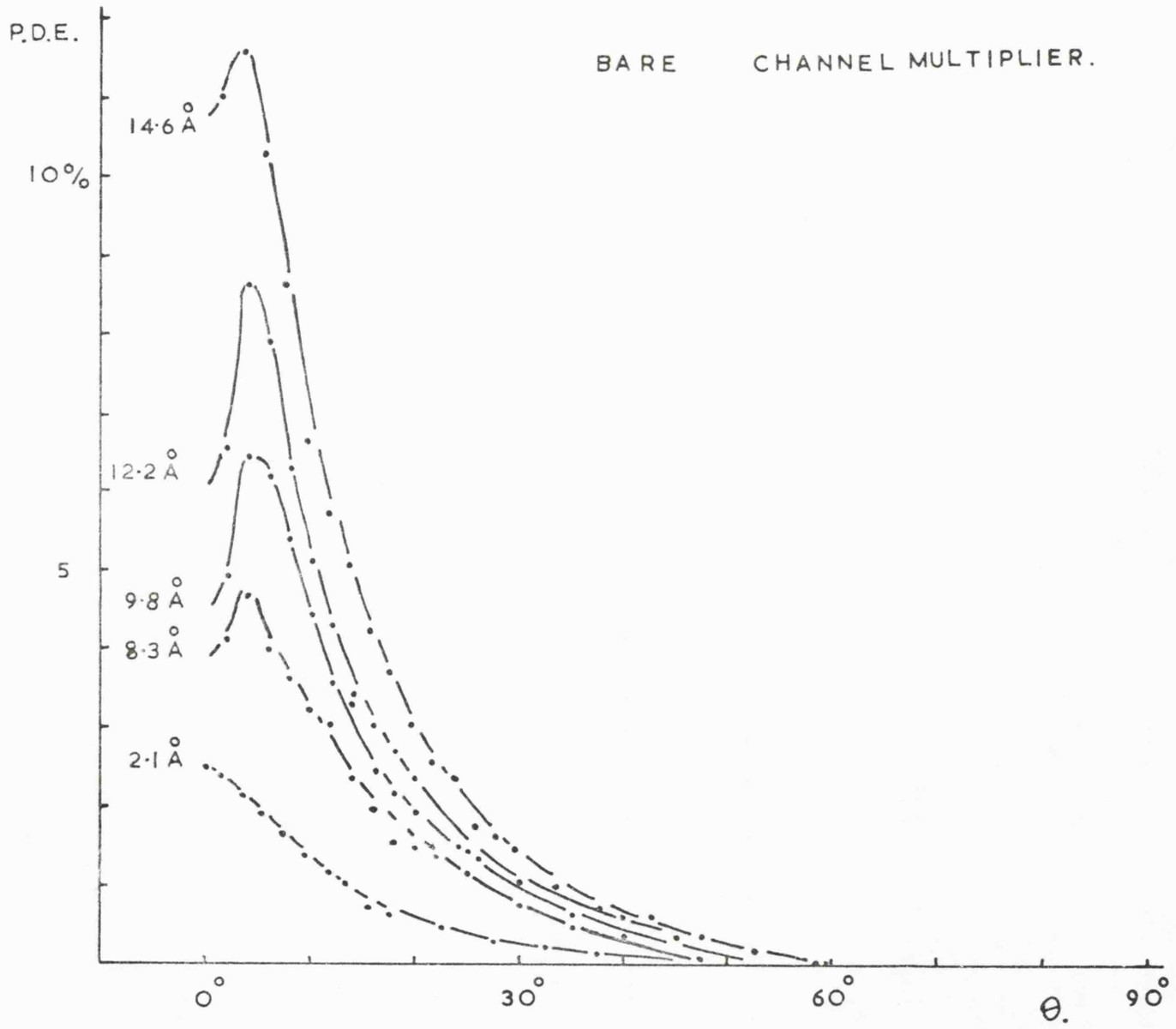
P.D.E.
BARE CHANNEL MULTIPLIER.
14·6 Å
10%
12·2 Å
5
9·8 Å
8·3 Å
2·1 Å
0°
30°
60°
θ.
90°

FIG. 4.7.A

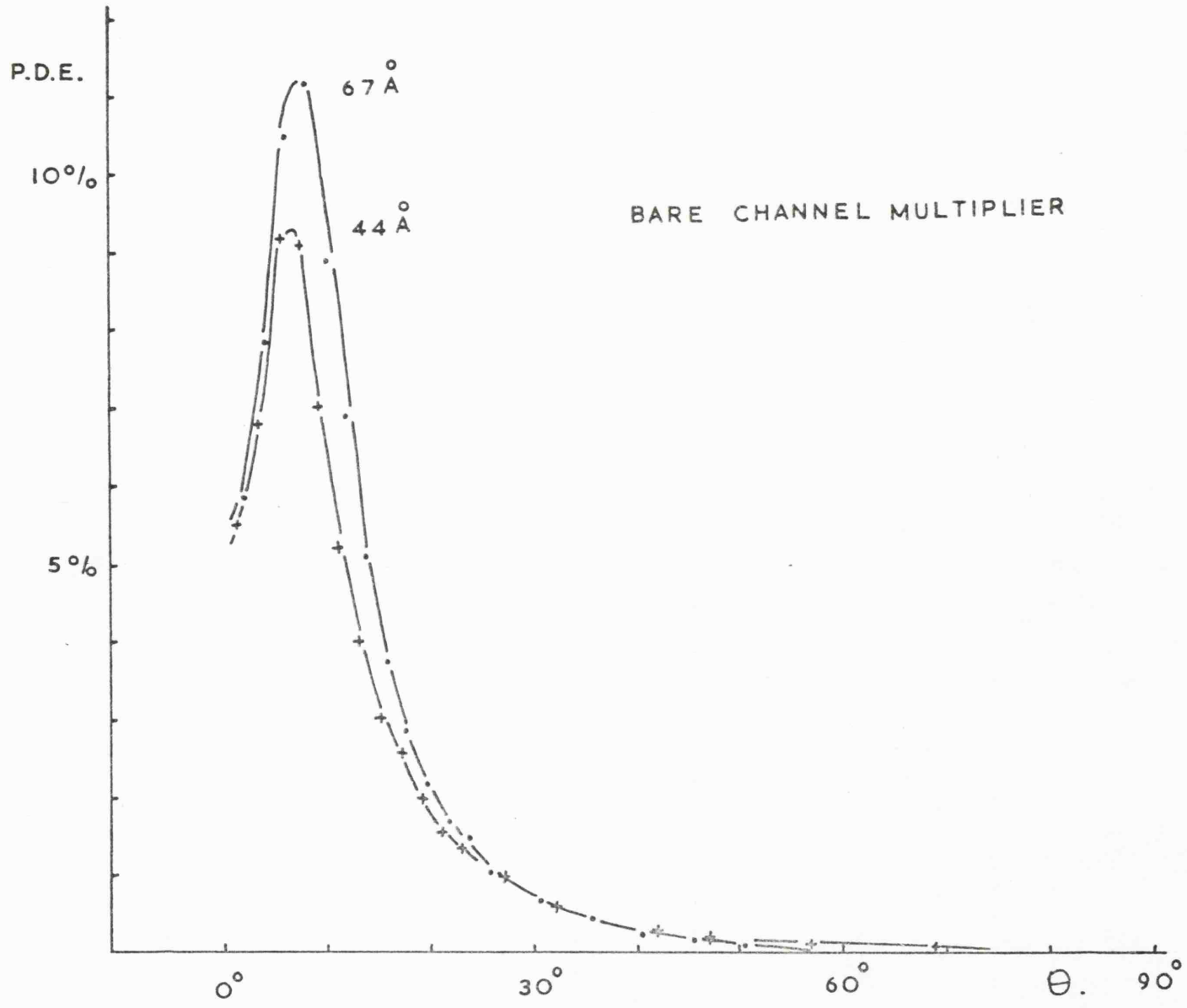

FIG. 4.7. B

factor is included in the theoretical analysis instead (see Section 4.1.4.).

4.1.3. The X-ray response of channel multipliers with specially prepared photo-emissive cathode surfaces.

Three channel multipliers of the A type were used for this section of the investigation. At 4 k v. the pulse height distributions were not as saturated as those of the B channels but, by increasing the electronic amplification used, the counting threshold could be exceeded by 99% of the pulses, without interference from secondary pulse overshoots.

In an attempt to obtain higher photon detection efficiencies, several materials known to have high external photo-emission yields were deposited by evaporation on to the channel inside surface at the cathode end of several multipliers. The materials were NaBr, CaF_2, CsI, SrF_2, LiF and MgF_2. To get the material deposited evenly and sufficiently far along the channel it was necessary to evaporate at a small angle (4^o) to the channel axis with the multiplier slowly rotating about this axis. The approximate thickness of material deposited could be determined by observing the fringe colour changes on the underside of the assembly supporting the rotating channel multiplier and was of the order of 1,000 Å normal to the channel multiplier surface (1,500 Å for MgF_2 and 1,700 Å for Li F).

The prepared multipliers were examined initially for

stability of photon detection efficiency, measurements being made shortly after preparation and at subsequent intervals. Since the detection efficiencies exhibited a strong angular dependence these comparison measurements were made at the reponse maxima. Thus the measurements were independent of small deviations in the directional location of the multiplier with respect to the specimen case.

Figs. 4.8 A and B show the relative changes in photon detection efficiency measured subsequently to evaporation for NaBr, CaF_2, CsI, SrF_2, LiF and MgF_2. (absolute values of p.d.e.are given for the last two compounds). Of these materials MgF_2 was found to be the most stable and was therefore examined over the longest period,with a view to establishing the stability to be expected under conditions of laboratory storage. Of more practical significance is the stability of efficiency under conditions of operation (i.e. in ultra-high vacuum for a satellite). Direct measurement of this was not feasible,however,and it was therefore considered that the storage stability would give a pessimistic indication of the operating stability since, in operation,there would be an absence of the most likely source of surface changes i.e. contamination from dust and occluded atmospheric gas molecules. Figs. 4.9 A and B display the variations of p.d.e. with the angle of incidence. The measurements were background corrected by subtracting the 90° count rate from each reading. This correction was usually of the order of 5 - 10%. After this

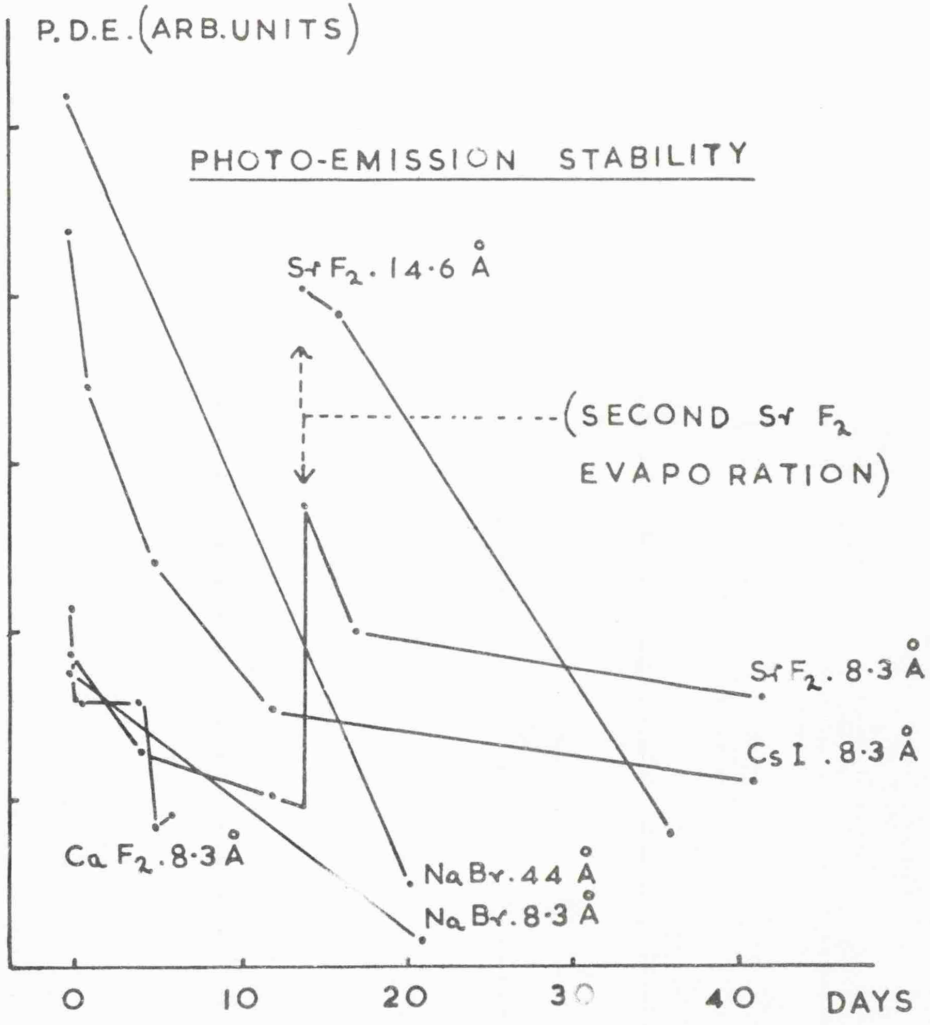
P.D.E.(ARB.UNITS)
PHOTO-EMISSION STABILITY
Sr F2 . 14·6 Å
(SECOND Sr F2
EVAPORATION)
Sr F2 . 8·3 Å
Cs I . 8·3 Å
Ca F2 . 8·3 Å
Na Br . 44 Å
Na Br . 8·3 Å
0
10
20
30
40
DAYS

FIG. 4.8.A

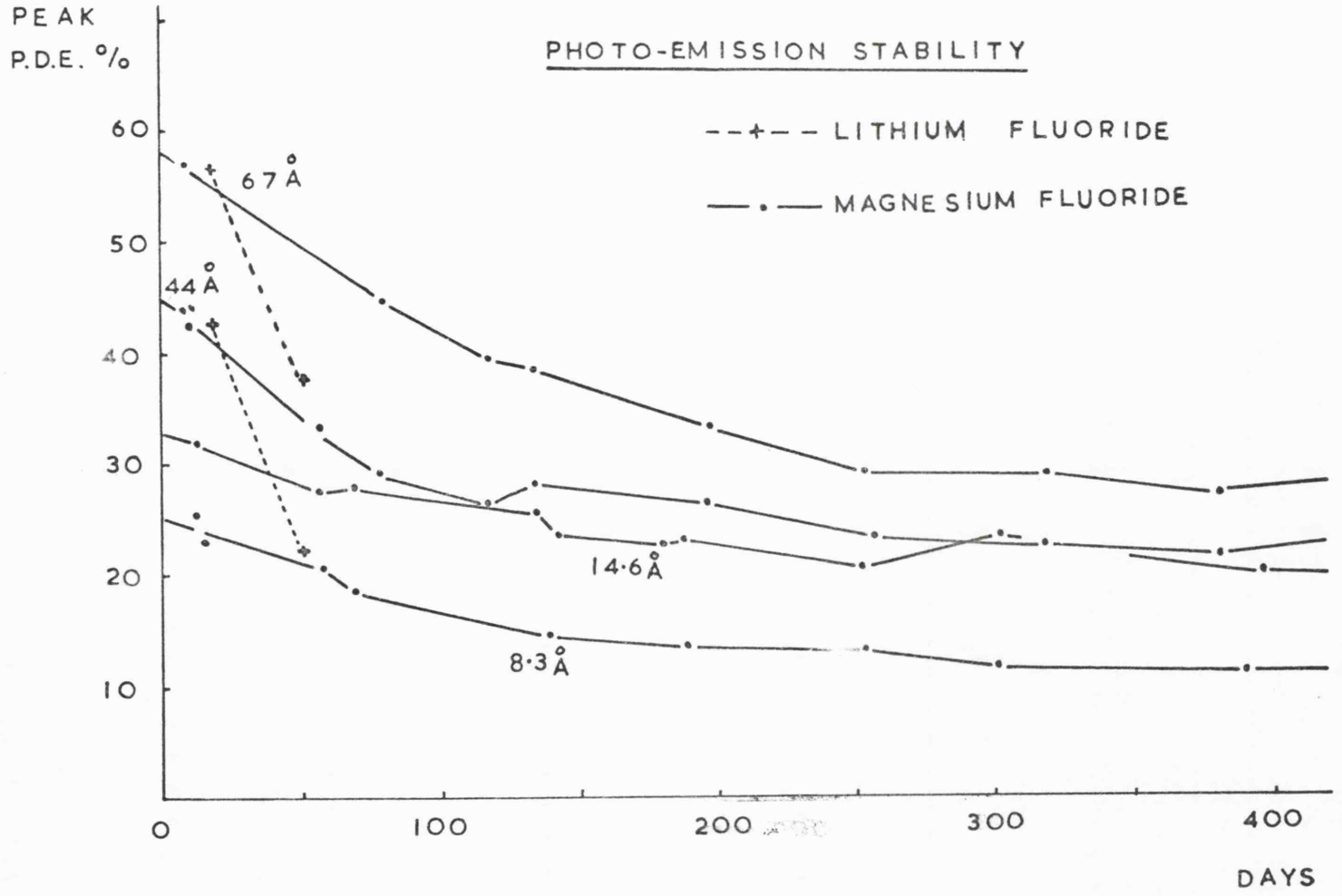
PEAK
P.D.E. %
PHOTO-EMISSION STABILITY
LITHIUM FLUORIDE
MAGNESIUM FLUORIDE
67 Å
44 Å
14·6 Å
8·3 Å
60
50
40
30
20
10
0
100
200
300
400
DAYS

FIG. 4.8.B.

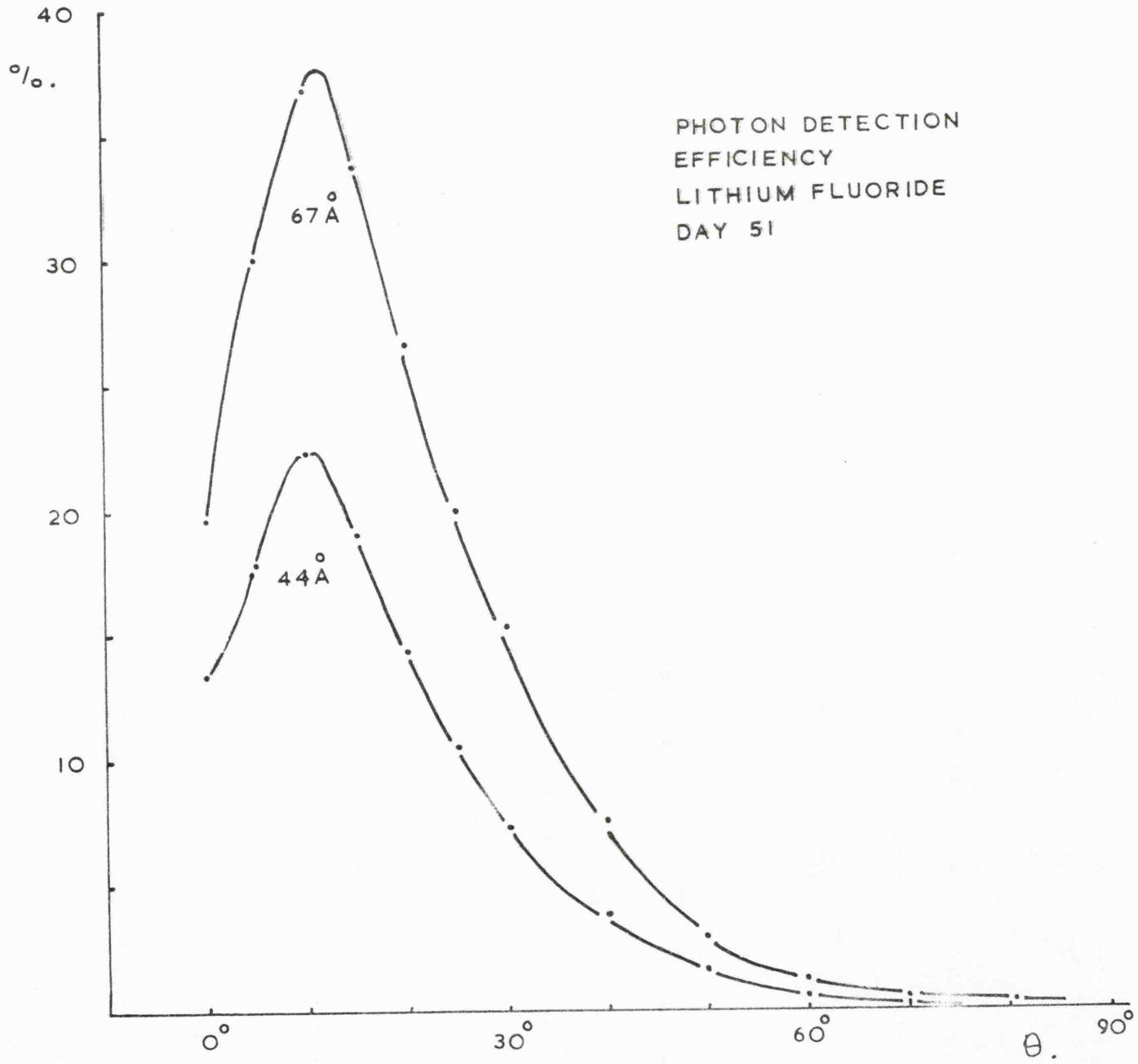
40
%.
30
20
10
67 Å
44 Å
PHOTON DETECTION
EFFICIENCY
LITHIUM FLUORIDE
DAY 51
0°
30°
60°
90°
θ.

FIG. 4.9.A

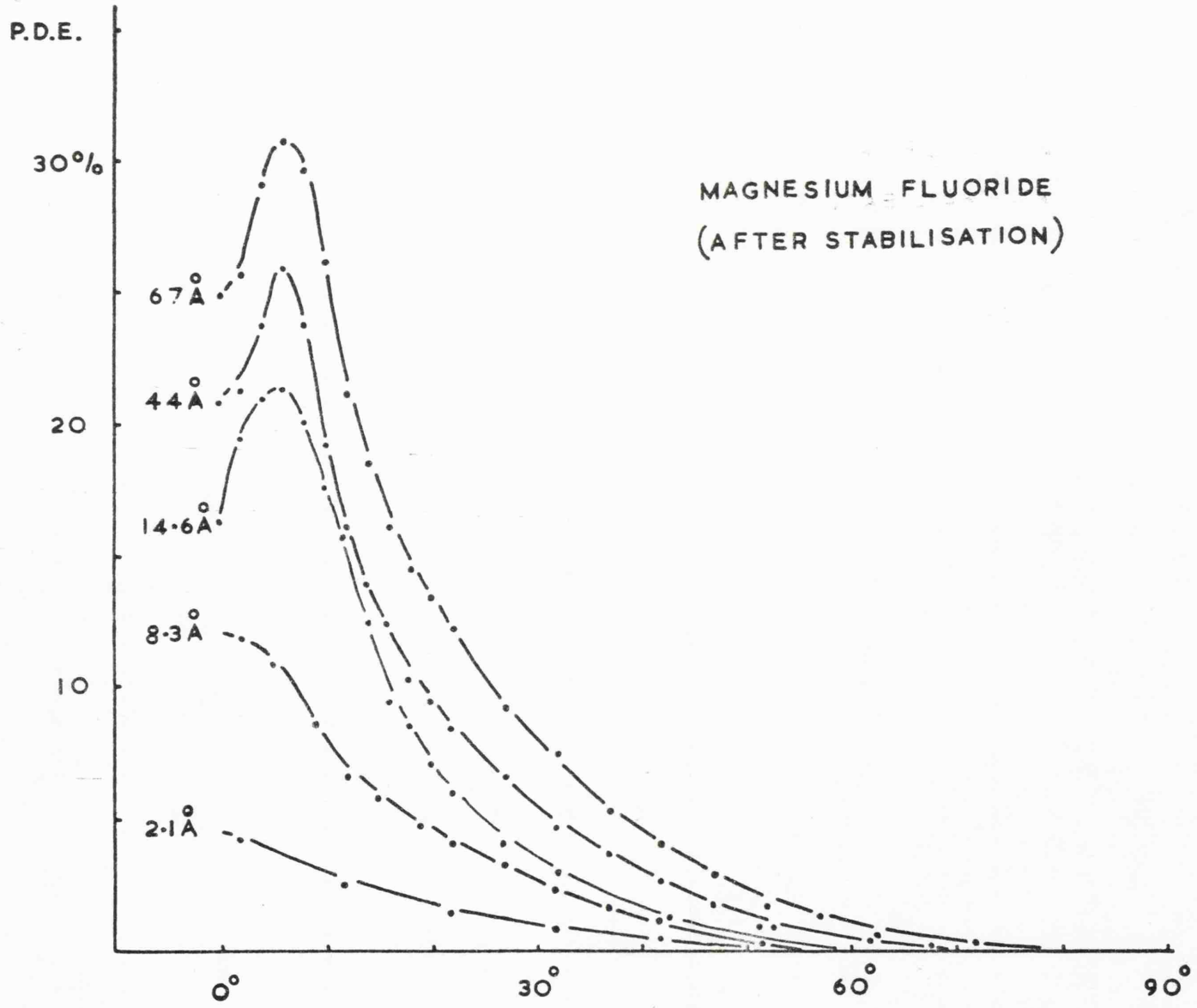
P.D.E.
30%
20
10
6·7Å
4·4Å
1·4·6Å
8·3Å
2·1Å
0°
30°
60°
90°
MAGNESIUM FLUORIDE
(AFTER STABILISATION)

FIG. 4.9.B.

the curves were normalised using the peak efficiencies measured as described in Chapter 3.

4.1.4. Analysis of channel multiplier X-ray response

The X-ray response of the channel multiplier is defined basically by the photo electric properties of that portion of the channel intercepting x-radiation i.e. the photo cathode of the device viewed as a photo multiplier.

If it is assumed that none of the electrons arising from the photo-emission processes are lost prior to multiplication and registration, then the X-ray response at any angle of incidence may be predicted wholly in terms of the effective external photo-electric yield* of the surface material. Because of the angular variation of this quantity however, and the spread in angle of incidence resulting from the geometry of the multiplier, it was necessary in this work to consider the channel as a composite photo-cathode consisting of an infinite number of plane incremental strips and to sum the photo-electric contributions of these strips.

This analysis is carried out in Appendix 2 . It is shown that, in the absence of X-ray reflection from the surface of the channel, the variation of count rate with angle of incidence may be expected to vary as Cot θ if

---

* Defined as the probability per incident photon of the emission of a group (or batch) of one or more electrons.

the dependence of photo-electric yield on angle follows a cosecant law [x] .

In particular that $n = N.4r^2.\chi_{\pi/2}.\ \mathrm{Cot}\ \theta$

Thus $\delta = \frac{n}{N.\pi.r^2} = \frac{4.}{\pi}\ \chi_{\pi/2}\ \mathrm{Cot}\ \theta$

Where N = Flux density

n = Channel multiplier count rate

r = radius of channel

and $\chi_{\pi/2}$ = photoelectric yield at normal incidence.

The effect of reflection at the surface of the channel multiplier has been estimated by assuming that the reflection is complete below a certain idealised critical angle of incidence (θ_c) and that the reflected photons do not subsequently register. The result of this is the introduction of the factor

$$\left[1 - \frac{\mathrm{Sin}^2 \theta_c}{\mathrm{Sin}^2\ \theta} \right]^{1/2}$$

in the expression for n.

---

x Evidence of such a variation has been reported by Rumsh et al.(1960b)for W, Ni and Be (1.39 — 13.3 Å) and by Heroux et al. (1965) for W (304 Å). Also, after taking refraction of the radiation at the surface into account, by Savinov et al. (1965) for Al. and Au (23.6 — 113 Å) and by Stanford et al. (1966) for Au and Pt (300 — 1200 Å). Evidence may also be obtained from the results of Lukirskii et al. (1964b)for LiF, MgF_2, and other compounds (23.6 — 113Å) See Figs.4.11. A and B.

This factor represents a progressive falling-off of γ from the Cot θ variation at small angles of incidence and therefore predicts a maximum value of the angular response function and a minimum of zero(at $\theta = \theta_c$) .

To test the support offered by the experimental results for this analysis, the values of γ obtained for the bare multiplier and for the multipliers coated with LiF and MgF_2 were replotted against Cot θ (see Figs. 4.9.C, D, and E.)

Of the displayed variations of γ with Cot θ there are several that directly support the analysis, these indicating a linear relationship at angles away from those at which reflection plays a significant part. Under these conditions, the intercept of these curves at Cot θ =1 gives the value of $(\frac{4}{\pi} \cdot \chi_{\pi/2})$ for the material of the surface at the wavelength of measurement. For the other curves it is evident that the fall-off of γ towards large angles of incidence is steeper than that predicted by the analysis. This fall-off is attributed to a loss of counts and is discussed below. Values of $\chi_{\pi/2}$ taken from lines drawn through the plotted points at 45° are presented in Table 4.2 and plotted out in Figures 4.10. A, B and C.

TABLE 4.2

Bare Multiplier

$\mathring{A}$	2.1	8.3	9.8	12.25	14.6	44	67
$\chi_{\pi/2}$%	0.189	0.472	0.621	0.715	0.927	0.895	1.18

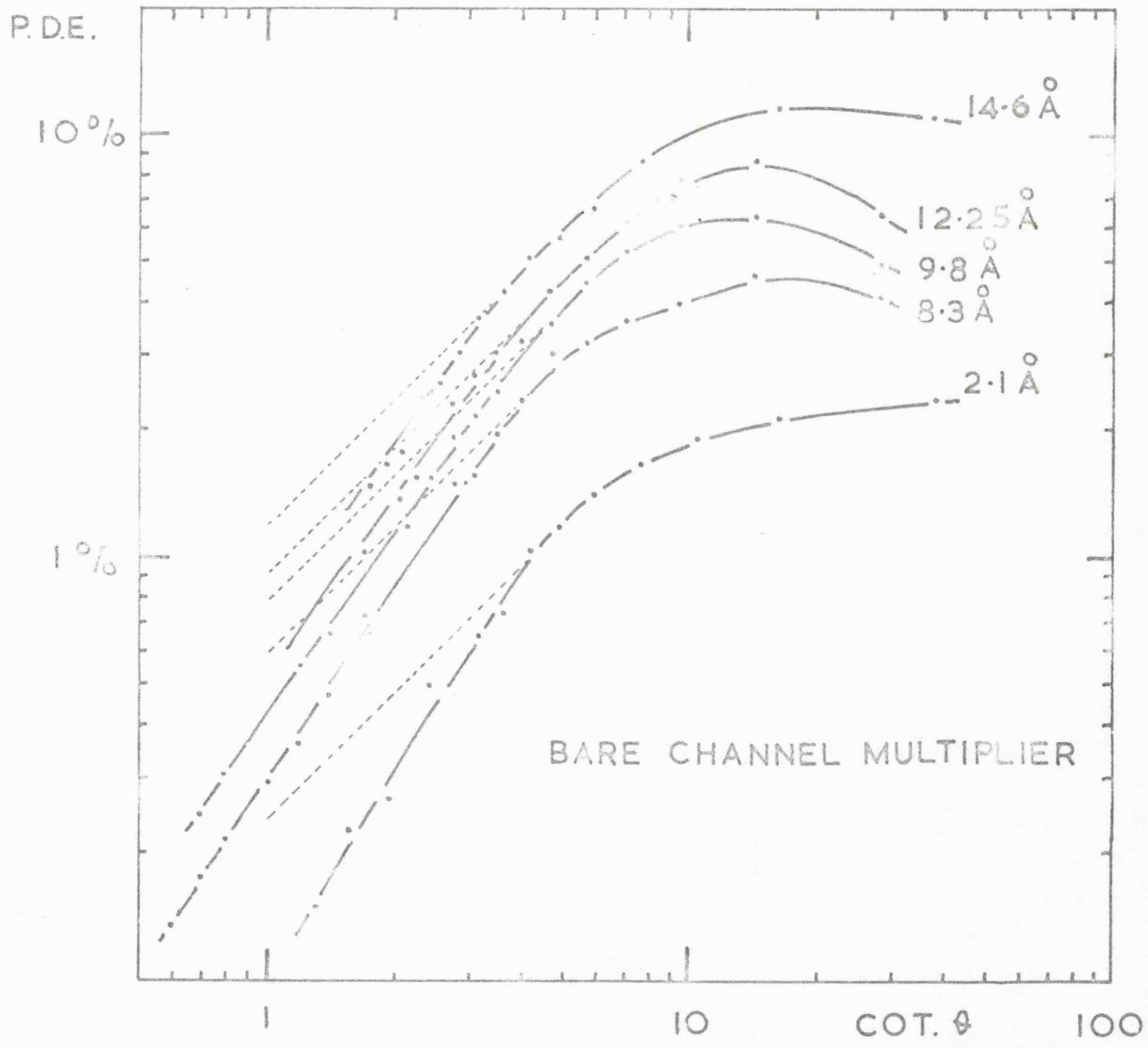
P.D.E.
10%
1%
14·6 Å
12·25 Å
9·8 Å
8·3 Å
2·1 Å
BARE CHANNEL MULTIPLIER
1
10
COT. θ
100

FIG. 4.9.C.(A)

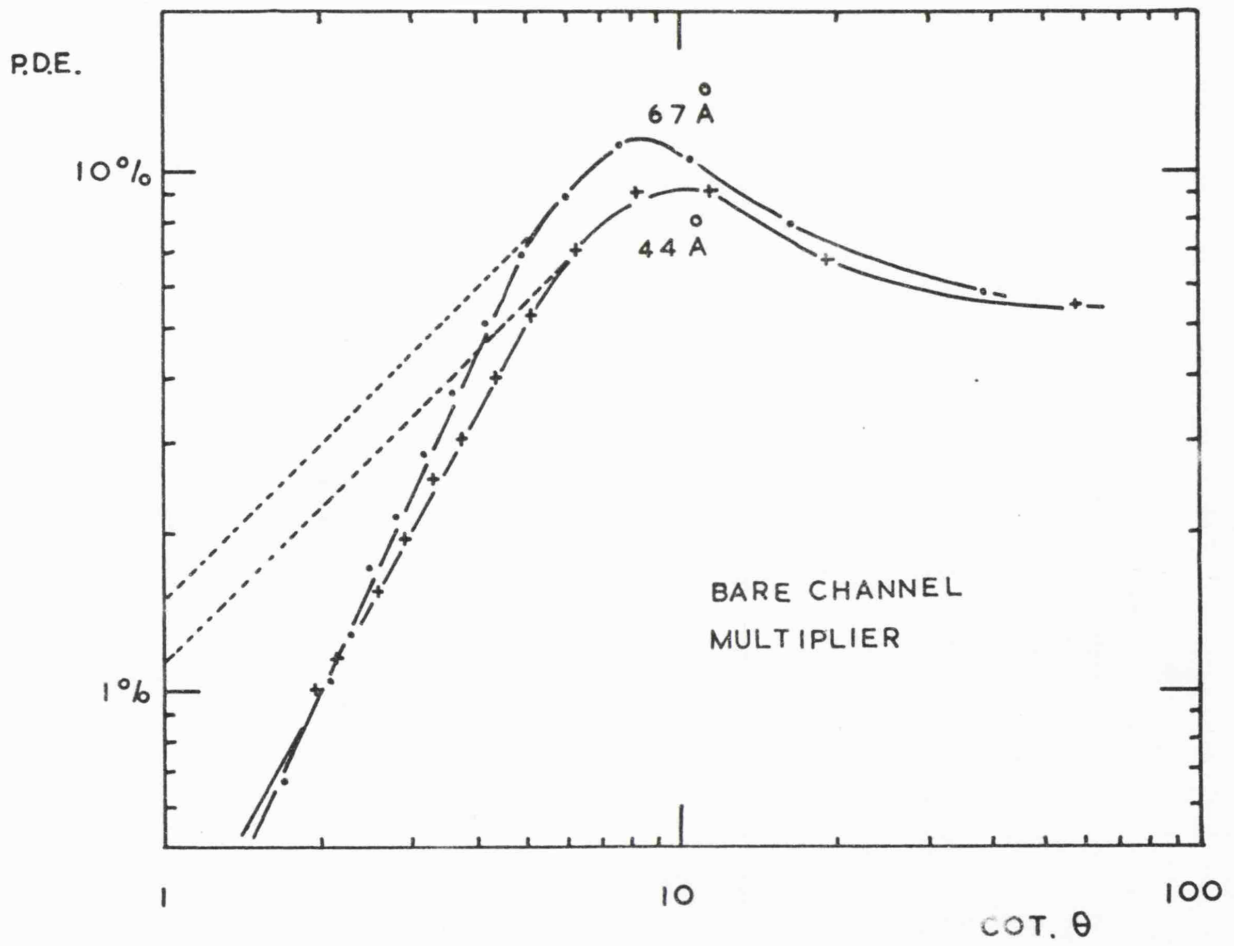

FIG. 4.9.C(B)

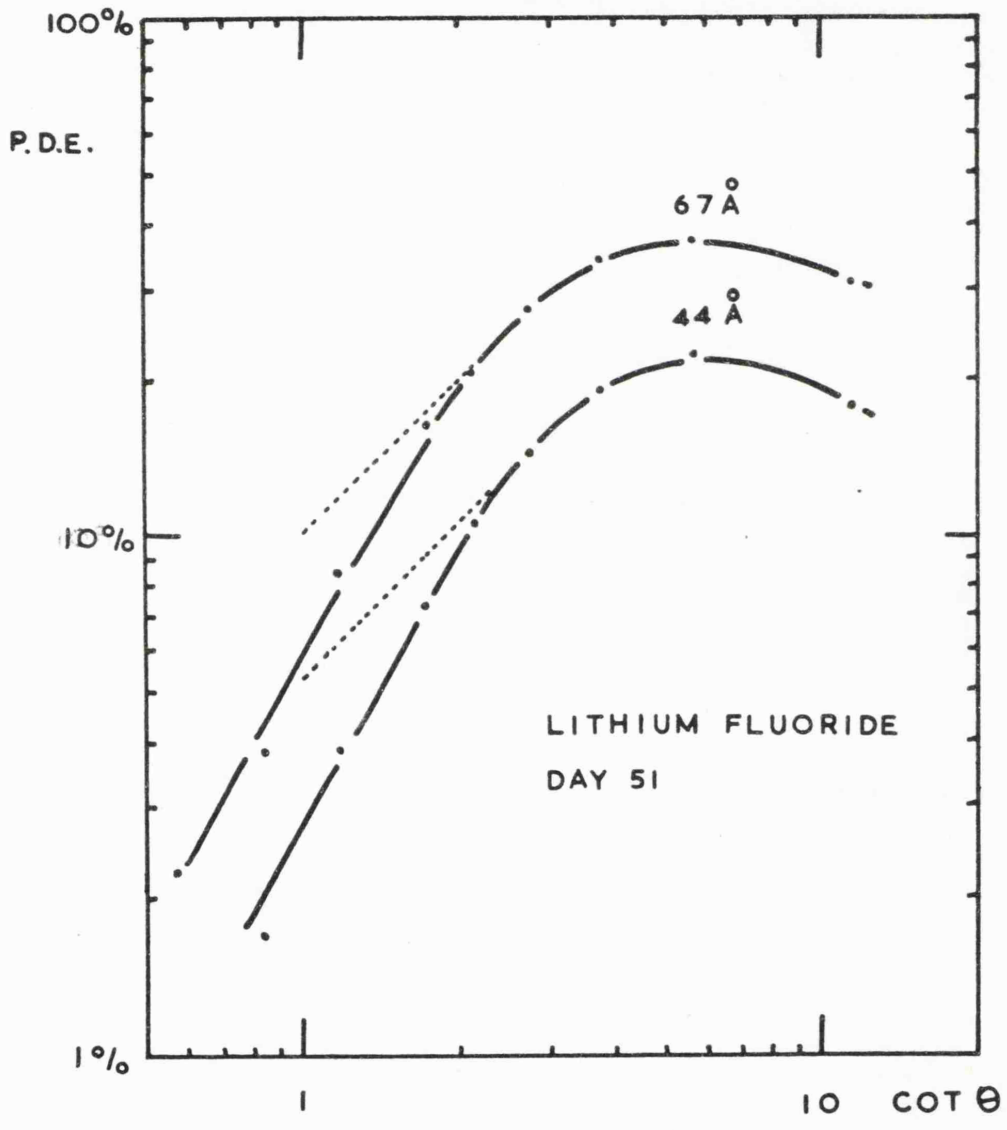

FIG. 4.9.D.

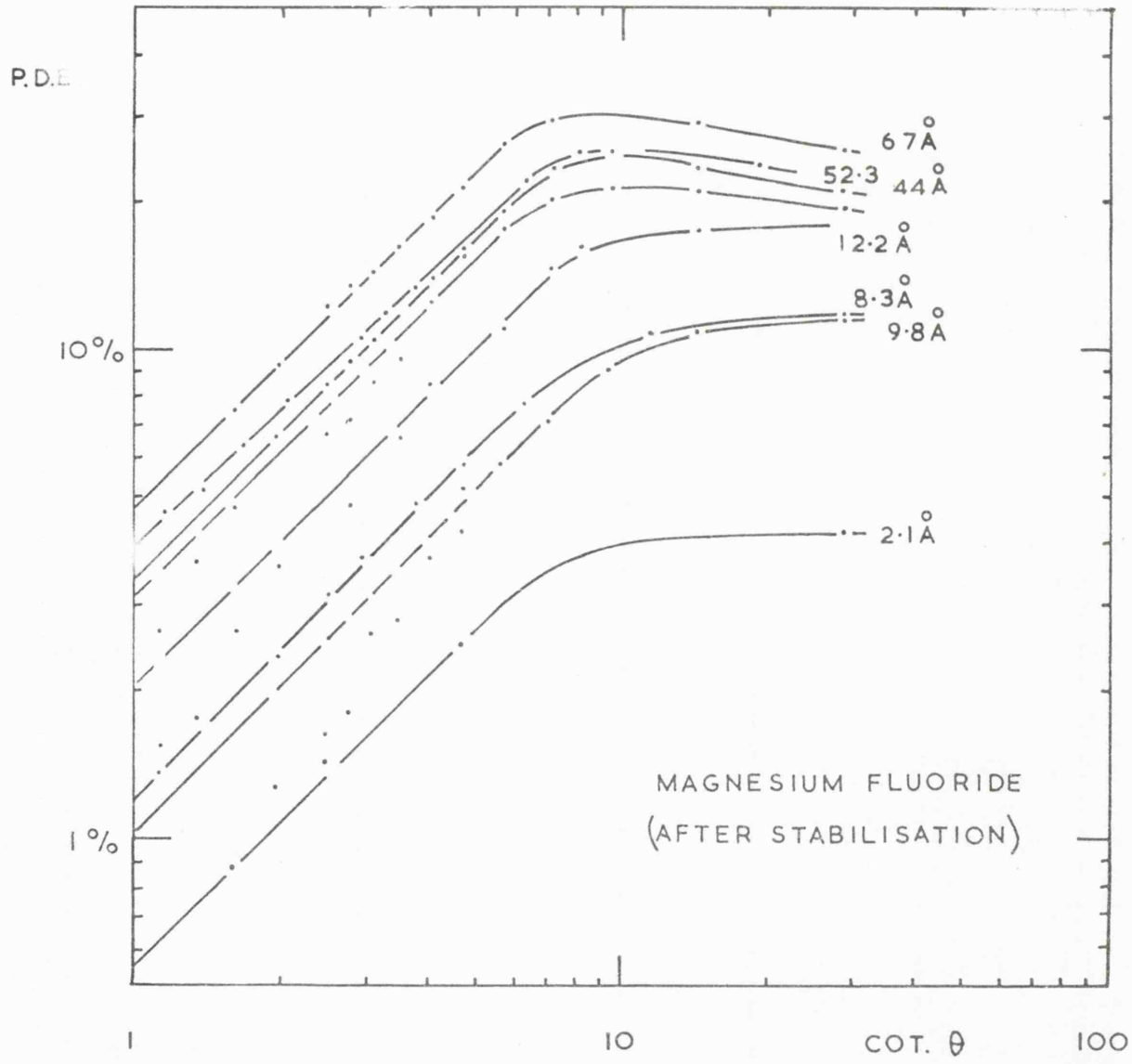
P.D.E.
10%
1%
6·7Å
52·3
44Å
12·2Å
8·3Å
9·8Å
2·1Å
MAGNESIUM FLUORIDE
(AFTER STABILISATION)
1
10
COT. θ
100

FIG. 4.9.E.

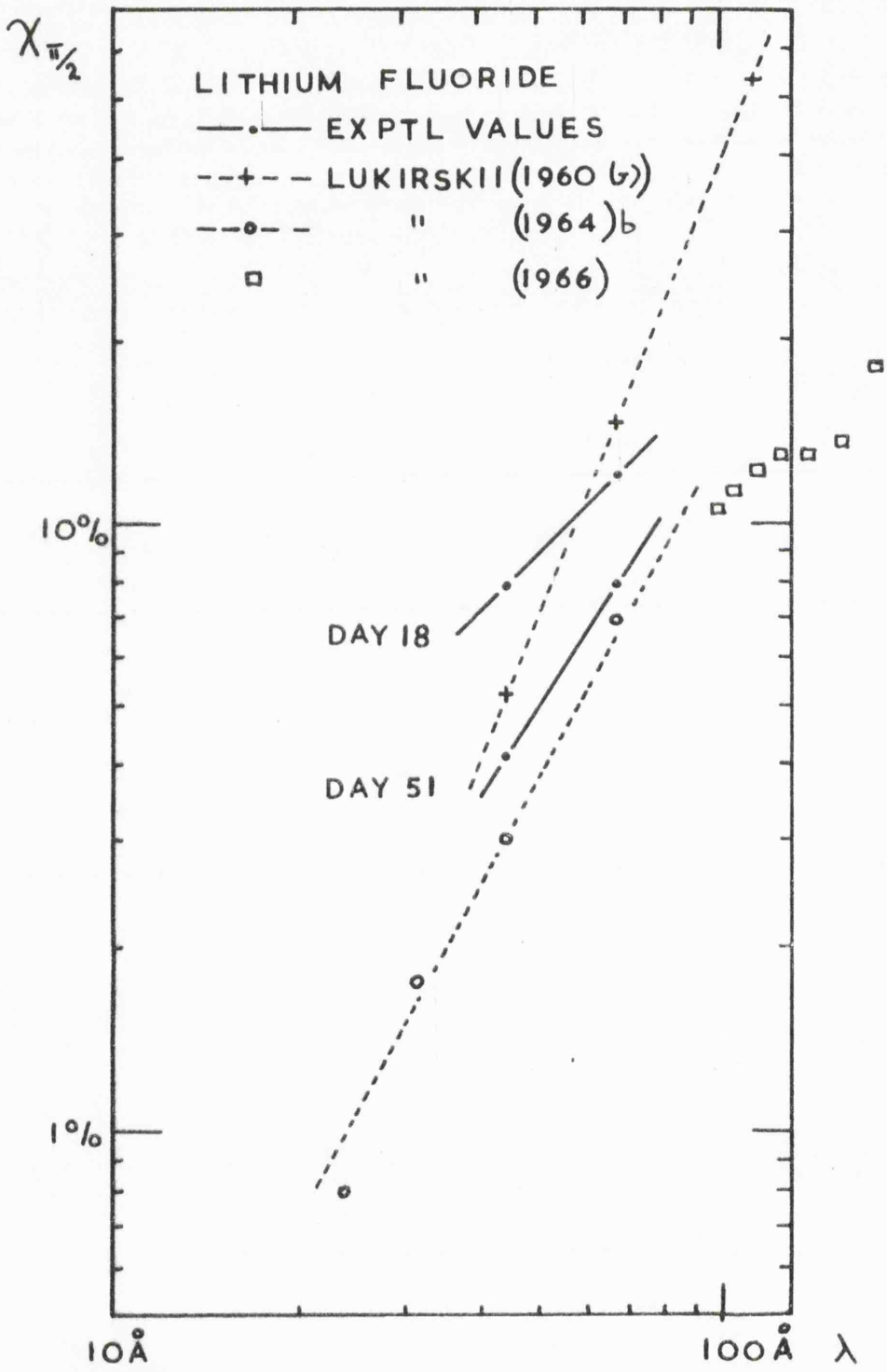
$\chi_{\pi/2}$
LITHIUM FLUORIDE
EXPTL VALUES
LUKIRSKII (1960 b)
" (1964) b
" (1966)
10%
1%
DAY 18
DAY 51
10Å
100Å
λ

FIG. 4.10.A.

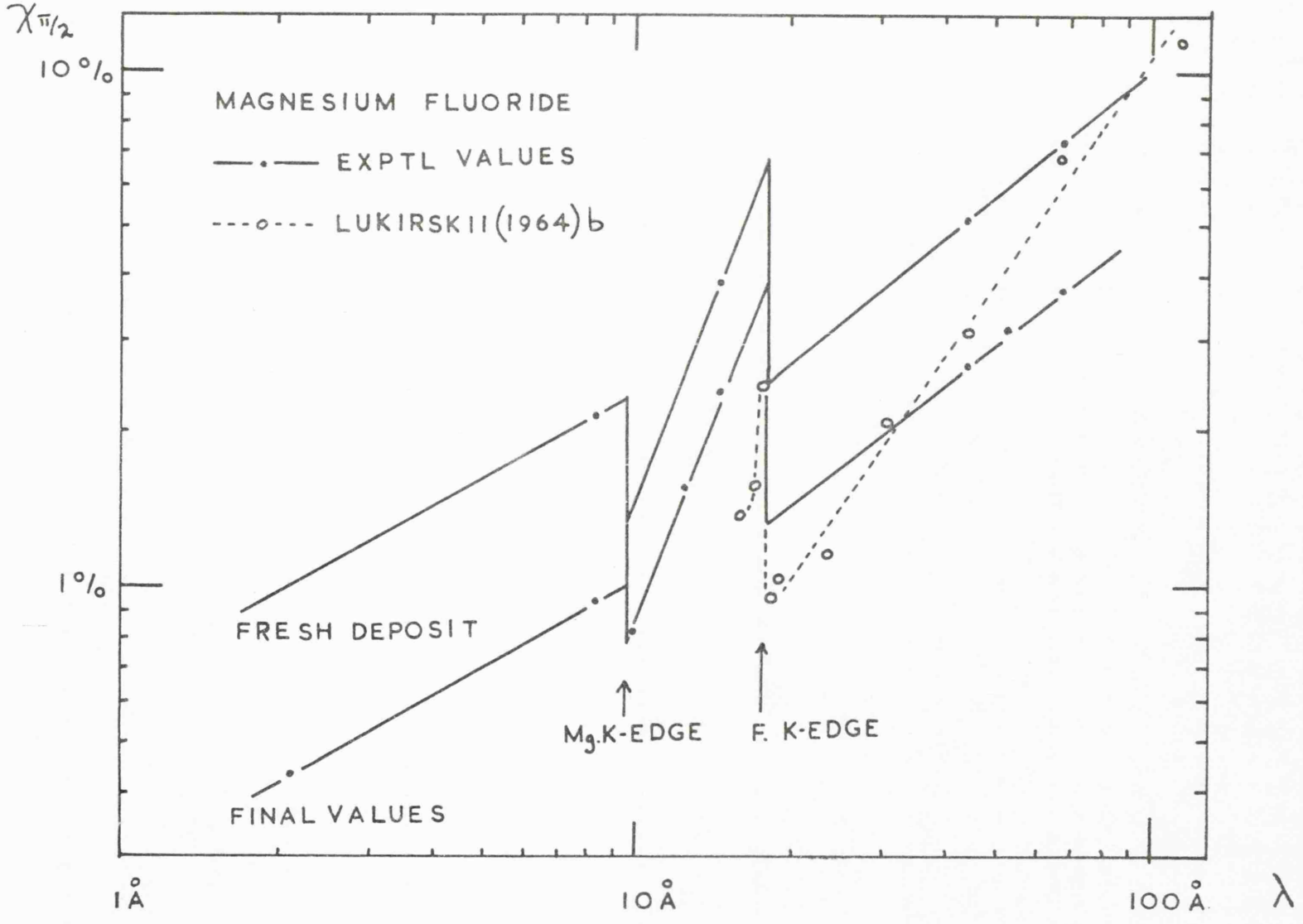
$\chi_{\pi/2}$
10 %
1 %
MAGNESIUM FLUORIDE
EXPTL VALUES
LUKIRSKII (1964) b
FRESH DEPOSIT
FINAL VALUES
Mg.K-EDGE
F. K-EDGE
1 Å
10 Å
100 Å
λ

FIG. 4.10.B.

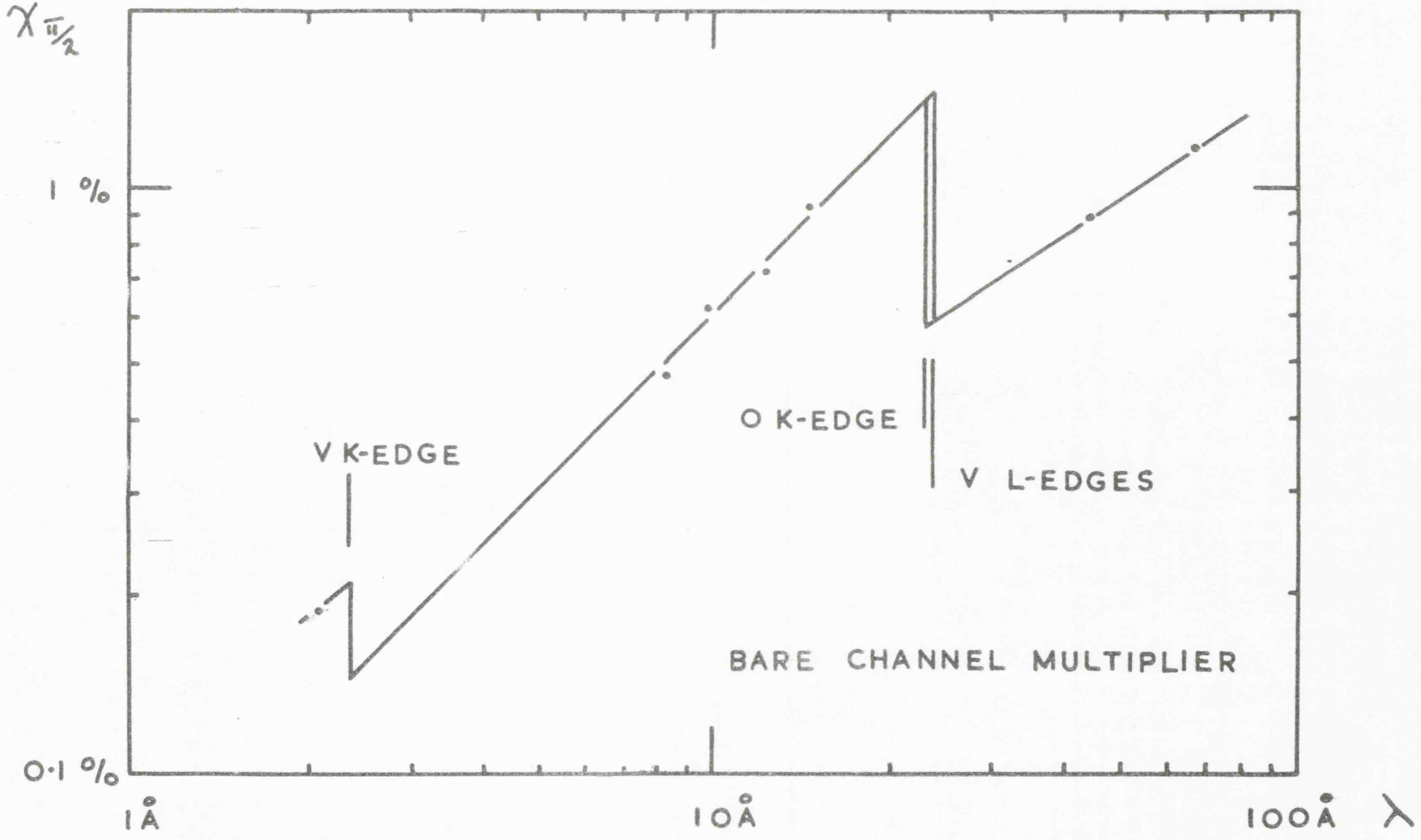
$\chi_{\pi/2}$
1 %
0·1 %
V K-EDGE
O K-EDGE
V L-EDGES
BARE CHANNEL MULTIPLIER
1Å
10Å
100Å
λ

FIG. 4.10.C

TABLE 4.2 (cont.)

LiF Coated Multiplier

Å		44	67
$\chi_{\bar{\nu}/2}$ %	Day 18	7.9	12.0
	Day 51	4.14	7.9

MgF_2 Coated Multiplier

Å		2.1	8.3	9.8	12.25	14.6	44	52.3	67
$\chi_{\bar{\nu}/2}$ %	Fresh		2.145			3.90	5.1		7.30
	Final	0.432	0.940	0.818	1.18	2.45	2.67	3.142	3.73

Discussion of the shape of the channel multiplier X-ray response curves.

Towards low angles of incidence the responses are in qualitative agreement with that predicted by the theory of Appendix 2, based on X-ray reflection from the wall of the multiplier. Values of θ_c may be obtained from the curves * and, for long wavelengths, these may be compared with published reflection measurements (Lukirskii et al. 1964 c).

---

* At the angle of incidence θ, for which the response deficiency = 0.5

$\sin\theta_c = 0.866 \sin\theta$

	λ	θ_c Channel Multiplier	θ_c Lukirskii
LiF	44 Å	6° 8'	5° 12'
	67 Å	7° 2'	7° 20'
MgF_2	44 Å	3° 33'	4° 11'
	67 Å	3° 54'	5° 40'

The fact that the response never becomes zero at small angles may be explained in terms of the inadequate reflection model chosen, the divergence of the X-ray beam from the spectrometer and the subsequent registration of reflected photons.

Towards large angles of incidence, it was found that the response slope was partly dependent on the cylindrical uniformity of the channel. Thus, measurements of the MgF_2 responses with the multiplier rotated through 90° produced a slight steepening of the response slope away from the Cot θ line, although the peak efficiencies were unaltered within the limits of reproducibility (± 5%). In addition to geometrical effects, however, a steepening of the response towards large angles of incidence would be expected, as the result of a loss of photo produced electrons from the channel/aperture and, in the case of deposited photo cathode layers, of the decreasing optical depth of the layers. (The second effect would result in the photo-electric yield of the surface becoming increasingly dependent on the yield of the substrate material.)

4.1.5. Comparison of results with other published measurements.

Plotted on Figures 4.10 A and B are also values of $\chi_{\pi/2}$ taken from efficiency measurements made earlier in the life of the coatings and values of $\chi_{\pi/2}$ taken from the results of Lukirskii (1964b) (replotted as shown in Figs. 4.11 * A and B). Also for Li F are values of $\chi_{\pi/2}$ taken from the ~~earlier~~ papers of Lukirskii et al. (1960 b. and 1966)

It should be noted that the ~~se~~ 1960 results are questioned by the authors in the ~~later~~ 1964 paper on the grounds that all of the electron multiplier pulses might not have been recorded as a result of the insensitivity of the electronics system.

For Li F the plotted points indicate that the results of the present work might be expected to compare well with those of Lukirskii (1964b) some time after Day 51, both in magnitude and spectral slope. This would infer that either the coating in the present work gave initially a particularly high X-ray response for some reason or that Lukirskii's measurements were made on

---

* The figure for Li F at 113 Å is omitted since, although the curve is linear for large angles of incidence, it does not tend towards the origin. In view of the unlikelihood of a systematic 10% error in Lukirskii's published results, there would appear to be no obvious explanation of this anomaly.

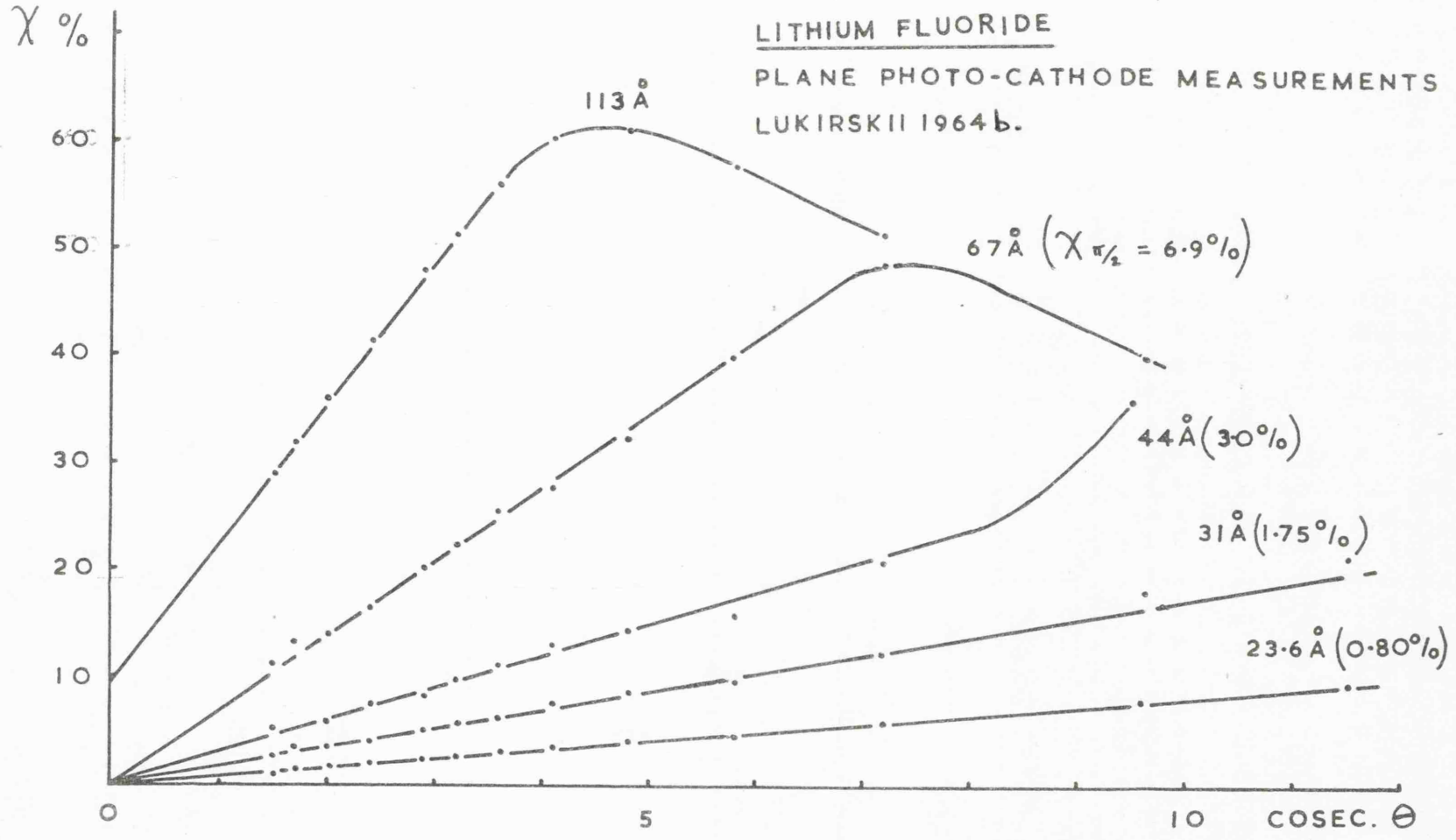
χ %
60
50
40
30
20
10
0
5
10
COSEC. θ
LITHIUM FLUORIDE
PLANE PHOTO-CATHODE MEASUREMENTS
LUKIRSKII 1964b.
113 Å
67 Å (χ π/2 = 6·9%)
44 Å (3·0%)
31 Å (1·75%)
23·6 Å (0·80%)

FIG. 4.11.A.

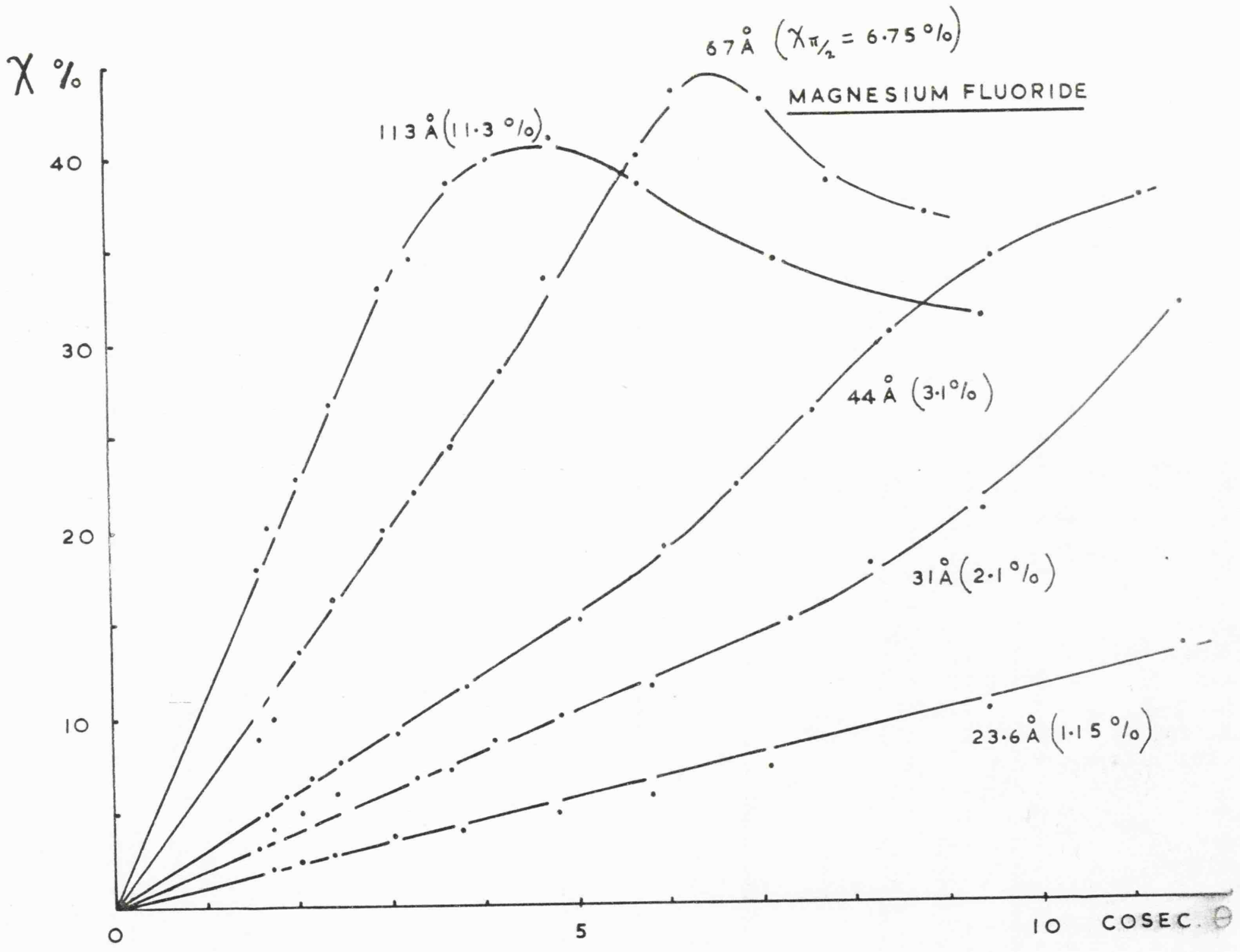
χ %
40
30
20
10
0
5
10 COSEC. θ
MAGNESIUM FLUORIDE
67 Å (χπ/2 = 6·75 %)
113 Å (11·3 %)
44 Å (3·1 %)
31 Å (2·1 %)
23·6 Å (1·15 %)

FIG. 4.11.B.

an aged photo-cathode.(Referring to the question of stability the authors only state that their photo-cathodes were not poisoned in air and that their results were reproducible to within 15% with different electron multipliers).

In this respect,but without attaching over-significance to the differences between the results presented in the two papers,it is interesting to note that the earlier figures of Lukirskii intersect the extrapolated results of the present work as a consequence of the difference in spectral slope, thus showing partial agreement.

For the $Mg F_2$ coating,analysis of the experimental results is rather more difficult owing to the effects of the Magnesium K and Fluorine K absorption edges which produce discontinuities dividing the covered wavelength range (2.1 Å - 67 Å) into three intervals. A power law extrapolation of $\chi_{\pi/2}$ with λ has been assumed for each of these intervals. A comparison with the results of Lukirskii (1964b)shows partial agreement above 18 Å for different wavelengths at different times, again a consequence of difference in spectral slopes. Between 16 Å and 18 Å there is apparent disagreement of the order of 2:1 even after the channel multiplier coating had stabilised. After allowing for the total experimental error margins, (- 15% for Lukirskii and + 10% for the present work), there is still a difference of 1.55 : 1 outstanding.

In the case of the results obtained for the bare multiplier there are no published works with which they can be compared. In view of the modest success of the X-ray analysis model used, it may be claimed that the values of $\chi_{n/2}$ are characteristic of the channel multiplier material. These are plotted out in Fig. 4.10.C together with simple power law variations between the absorption edges of vanadium and oxygen. The results support the existence of such edges in the response variation, although there might well be others present (e.g. Silicon K - edge at 7 Å). The slope of the response in the region of 2.1 Å has been assumed.

4.1.6. Discussion of photo cathode stability.

Although MgF_2 appeared to form the most stable photo cathode, some variation of photo-electric efficiency took place after evaporation. A possible reason for this is thought to be the likely inferior quality of the deposited layer resulting from the necessarily small evaporation angle. Holland (1956) states that post-evaporation baking and burnishing improve the quality and durability of deposited MgF_2 films - this was not possible in the present work owing to the nature of the substrate. For Li F Holland mentions that layers $< 2\mu$ in thickness are porous. With regard to the possibility of surface contamination, measurements reported by Rudberg (1928) at 44 Å, by Walker et al. (1955) in the range 1400 - 473 Å and by Dawber (1960) in the range 200 - 300 Å, indicate

higher photo electric yields for metallic cathodes before outgassing. Izrailev (1963) mentions, on the basis of Walker's results, that the yield for soft X-rays may be expected to depend weakly on the cleanliness of the photo cathode surface and reports reproducibility of measurement to within 60% for metallic photo cathodes from 0.42 - 18 Å. Rumsh and Shchemelev (1963 a and b) report poor reproducibility of measurements on metallic photocathodes at 1.54 Å and attribute this to abrasive contamination, filament evaporation (during preparation of the cathode) and the production of fluffy non-mirror-like surfaces. (It is also suggested that binary compounds might not be so liable to this trouble, since lower evaporation temperatures are generally required).

In assessing the relevance of these reported results to the question of the stability of a channel multiplier soft X-ray detector, it is to be noted that prepared photo cathode reproducibility need not necessarily be a good indication of the subsequent stability. The sensitivity of a photo-cathode after preparation may be expected to strongly depend on the composition and microstructural details of the photo-cathode layer contributing to the external photo-electric yield, whereas the subsequent photo-electric stability will depend on the changes of this layer with time. This will be dependent on the interaction between the surfaces and the gaseous atmosphere above it since the layer is very

thin. (see for example Nakhodkin and Mel'nik (1963)).

In addition, the published work mentioned was carried out electrometrically and this might be expected to give rise to variations in photo-electric yield greater than those observed in pulse measurements, since an electrometer would be sensitive to the total electron content of the emitted batches, whereas one-electron batches would still be likely to give photon registration in pulse measurements.

4.1.7. The background level of the channel multiplier

The background level of the channel multiplier viewed as an X-ray detecting element is defined as the count rate present, under the conditions of operation, as the result of mechanisms other than the photo-effect of x-radiation entering the channel aperture. This level may, in principle, be divided into three parts:- that due to electron emission within the channel, e.g. thermionic emission, photo emission, field emission or β- emission , that resulting from the interaction with the channel of penetrating radiation e.g. cosmic rays and radio active contamination in the channel and in the operating environment ,and that resulting from electrical noise .

Measurements of background level were made on several multipliers and the results are presented in Table 4.3. The noise contribution due to the electronic system had previously been measured to be much lower. * Also

* For this measurement the noise was determined in the usual way but with the channel multiplier removed.

tabulated are values of the expected total cosmic ray flux in a downward direction at sea-level intercepted by the longitudinal cross sectional area of each channel multiplier, assuming a level of 1 per sq. cm. per min. (Wolfendale 1963)

TABLE 4.3

Specimen	1	2	3	4	5	6	7
Longitudinal Cross-sectional area.	5cm. X0.10 cm.	7.5 cm. X0.30cm.		11.5 cm. X0.35 cm.			
Mean Noise Level at 4 K.v.(sec per count).	1,000	360	90	125	40	36	80
Cosmic Ray Level (sec per interception).	120	80		15.			

These results indicate a general increase in the background level with size of multiplier, which would be in keeping with a cosmic ray origin. However, for this mechanism to be responsible, it would seem that a rather high detection efficiency to cosmic ray events would be required, even if the whole channel was assumed to be sensitive to such events. (This is not the case, since there is a minimum length of channel required to provide sufficient electron multiplication for pulse registration). Further, it would not be clear how the wide differences observed in the background levels of different channels

of the same physical size could be accounted for. Even so, the measured levels per unit active volume compare reasonably well with that typical for a good proportional counter under conditions of cosmic ray limitation. Thus a counter of active volume 20 cc with a background of 0.5 cps would indicate a level of about 1 count in 400 sec for a channel of active volume of 0.1 cc.

With regard to the electrical noise content, extra pulses could only arise, with the multiplier connected, as a consequence of the channel conduction current. Since the channel surface exhibited conduction behaviour, at least partly characteristic of a semiconductor (see next section), additional noise might be expected. However, excess "1/f" (or current) noise normally becomes dominant only below a few kilocycles (See Chapter 11, D.A. Bell (1960) for example) and pulses arising would be well outside the bandwidth of the electronics system, which had a fall-time constant of 10 μs.

In the case of low-noise conventional photo-multiplier tubes, the β component of the radioactive decay of K^{40} in the glass envelope may determine the tube dark current once the thermionic content has been sufficiently reduced. However, it is difficult to assess the

probability of this being the background mechanism in channel multipliers, in the absence of information concerning the potassium content of the channel material.

Of the possible mechanisms remaining, field emission would be expected to arise as a likely result of the presence of thin insulating films on the inside surface of the channel. An idea of the surface charge density required to produce a given electric field normal to the surface may be obtained using Gauss's Law. If the relative dielectric constant of the layer material is taken as unity to enable a lower limit of the necessary charge density to be estimated, then 10^{-9} coulombs per sq.mm. may be seen to be necessary to establish a field of 10^{6} volts per cm. Since the maximum charge output from a channel multiplier is only of the order of 10^{-11} coulombs, it would appear that field emission cannot represent a likely mechanism for the background level. However, the multipliers were examined for evidence of after-pulsing under conditions of normal and high count rates, since field emission might be expected to produce such effects, but none was observed.

An estimate of the thermionic contribution may be obtained using the Richardson-Dushman equation.

$N.e = 120\ T^{2}.\ e^{-\Phi/KT}$ Amperes/sq.cm

For $\Phi = 1.0$ev. $N = 4 \times 10^{8}$ electrons/sq cm/sec

For $\Phi = 1.5$ev. $N = 1.0$ " ($T=293\ ^{o}K$)

For $\Phi = 2.0$ev. $N = 2.5 \times 10^{-9}$ "

The magnitude of this contribution is clearly critically dependent on the work function of the surface, which was not known for the multiplier. Hunter (1962) has reported a long wavelength reduction in the e.u.v. photoelectric response of some Bendix channel multipliers * similar to that of tungsten, which offers support for a photo-electric work function of the order of 4 e.v. However the surface material in this case was stated to be an oxide of some metal (since believed to be tin).

In the present case therefore, a work function of about 1.5 ev would give a thermionic background of the observed order of magnitude. However, the surface would then also be likely to be photo-emissive at visible wavelengths and no direct evidence for such a sensitivity was obtained in the course of the work.

Summarizing, it would seem that the background does not obviously result from any one mechanism. The levels observed could be produced by the known cosmic ray level of the laboratory but more uniformity in the results would normally be expected, even allowing for poor measurement statistics. β - emission from the glass represents a possible mechanism, the probability of occurrence of which is difficult to assess. Normal thermionic emission would appear to be ruled out by the apparent absence of photo-emission by visible light, and field emission would seem to be prohibited by the

* Trade named "Channeltrons".

magnitude of the minimum surface charge densities required.

4.1.8. The results of extended life testing of channel multipliers in U.H.V.

This investigation was carried out principally to determine the long-term behaviour of channel multipliers operating remotely in conditions of ultra-high vacuum, as in an orbiting satellite. The general procedure adopted was to continuously operate the channel multipliers in the ultra-high vacuum system described in Chapter 3, at the channel voltage chosen for the OAO experiment (4 KV). The results of these tests have been reported in a published research note, Smith (1967).

4.1.9. The operation of channel multipliers at low temperatures.

Although the OAO vehicle and experiment may be considered broadly to represent the likely operating conditions for detectors in future X-ray telescopes, it is not likely that the environmental (package) temperature will necessarily always be as high ($\sim -20^{\circ}C$), particularly if large open structures are employed, when the power dissipated by the electronics will be sufficient to balance thermal losses only at low temperatures. An investigation into the operation of a channel multiplier at reduced temperatures was therefore carried out. The multiplier examined was operated in the U.H.V. system with a tritium source and cooled radiatively by surrounding the vacuum chamber with dry ice, thereby

reducing the wall temperature to - 78.5°C.

The change of D.C. resistance of the channel multiplier measured with a megohmeter (at 500v) over one cooling (and thawing) cycle is shown in Fig. 4.12. The multiplier evidently attained a steady temperature after 1 hour.

In this state the pulse height distributions a) and b) in Fig. 4.13 were measured. These may be compared with curves c) and d) - the distributions measured at room temperature. A considerable change of mean gain is seen to result from the decreased operating temperature, this being lower by factors of approximately 15 and 65 at 800 c.p.s. and 3000 c.p.s. respectively. (Also evident are changes in pulse height distributions, which no longer indicate pulse amplitude saturation - although a comparison with those measured at room temperature at lower voltages (Fig. 4.2) shows that the distributions are in accordance with what would be expected at the reduced gain levels.)

The reason for the reduced multiplier gain is evident from Fig. 4.4 in which the variation of mean gain with count rate is plotted for the present multiplier at 20°C and -78.5°C and for a second multiplier having an intermediate value of channel resistance.

Also plotted are the boundaries set by the channel wall currents. * The tendency in each case for the pulse

* For the purpose of calculating the standing wall current twice the value of resistance has been used since the outer surface of the channel is in parallel with that of the inside.

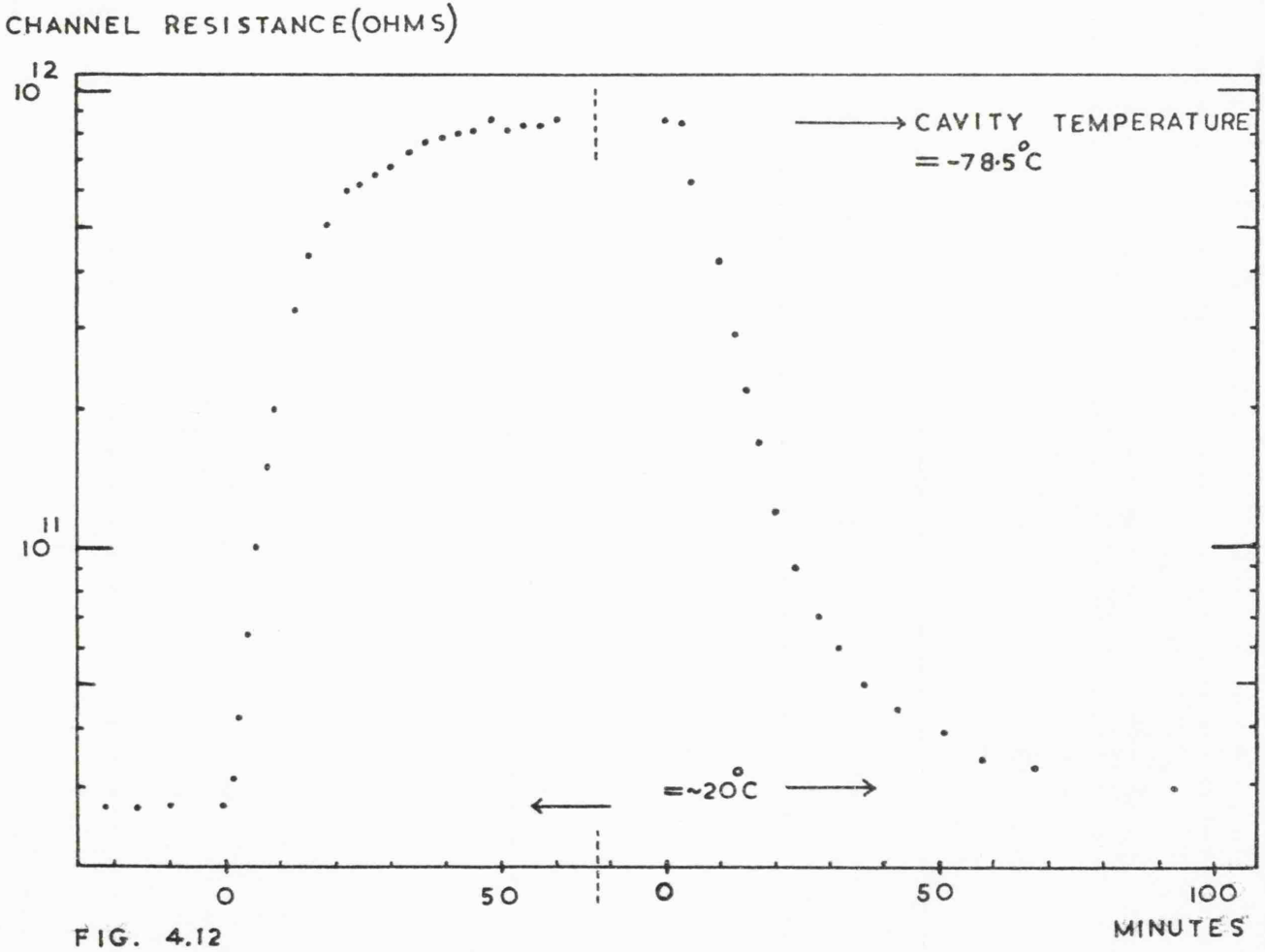
CHANNEL RESISTANCE (OHMS)
10^{12}
10^{11}
CAVITY TEMPERATURE
= -78·5°C
= ~20°C
0
50
0
50
100
MINUTES

FIG. 4.12

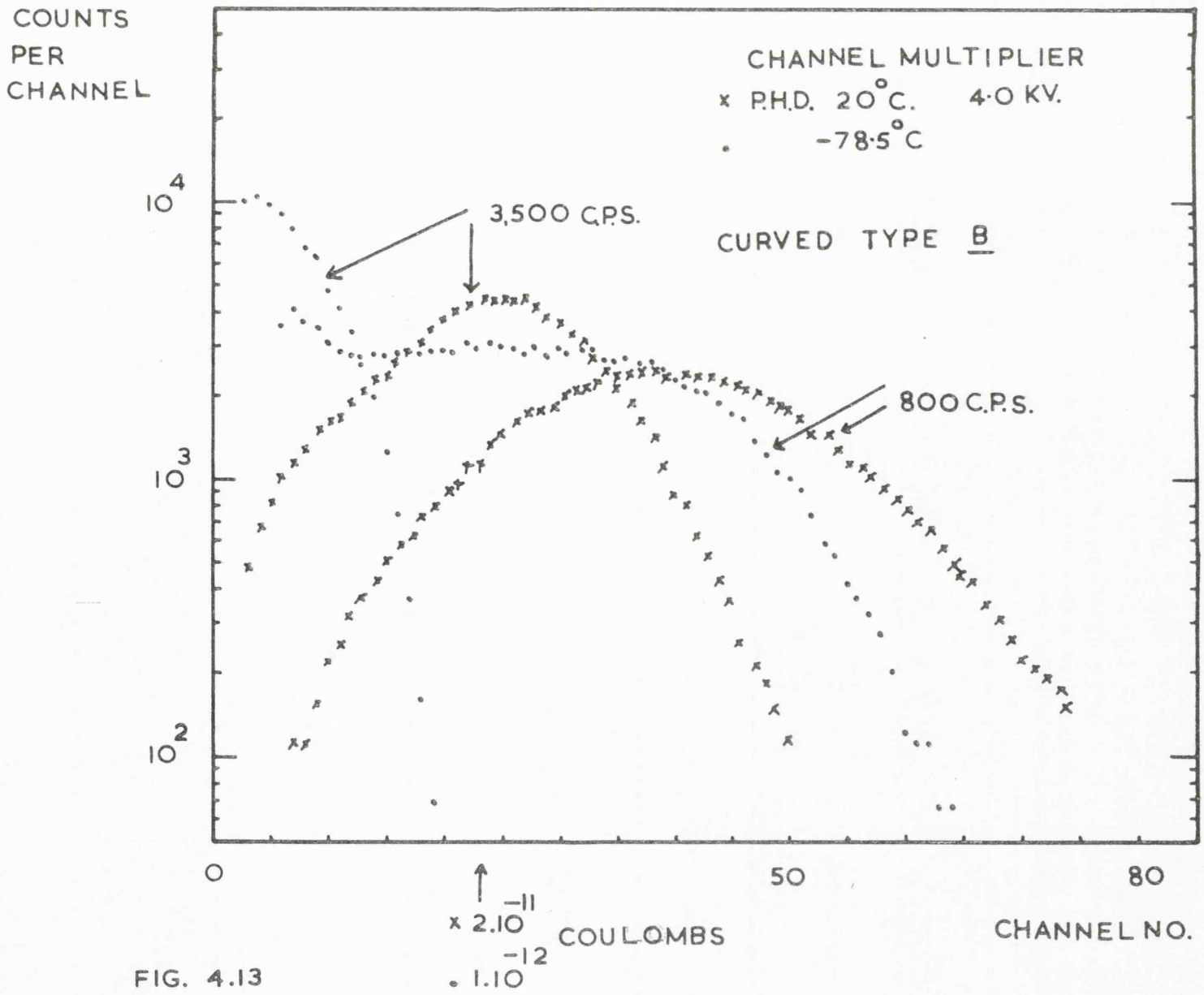
COUNTS
PER
CHANNEL
CHANNEL MULTIPLIER
x P.H.D. 20°C. 4·0 KV.
. −78·5°C
10^4
3,500 C.P.S.
CURVED TYPE B
800 C.P.S.
10^3
10^2
0
50
80
x 2.10^{-11}
. 1.10^{-12}
COULOMBS
CHANNEL NO.

FIG. 4.13

current to approach a fraction of the channel wall current clearly indicates the presence of pulse current limitation. That this is so much more severe at low temperatures arises as a result of the greatly increased channel resistance.

The practical significance of this effect is the need to provide adequate margins of amplifier gain and overload protection so that no X-ray information arises below the counting discrimination level. This will become increasingly difficult to achieve towards high count rates.

It is perhaps interesting to note that the measured temperature variation of channel resistance reflects the solid state properties of the channel wall material.

Fig. 4.15.A) gives the logarithmic plot of channel resistance (normalised to R 20°C) with temperature. The points are well represented by the relationship

$R = R_o\, e^{-T/T_c}$ where $T_c = 28.6\ C^o$, although the significance of this function is not obvious. Further analysis is possible, however, if the readings are replotted against I/T in the conventional manner as shown in curve B). The variation may now be approximately represented by the two sections of the form

$$R = A\, e^{\Phi/KT}$$

1. For $I/T < 4.10^{-3}\ ^oK^{-1}$ $\Phi = 0.307$ eV

and the section is characteristic of the intrinsic conductivity of a simple band model having this value of energy gap.

2. For $I/T > 4.10^{-3}\ ^oK^{-1}$ $\Phi = 0.130$ eV

which may be considered to indicate an extrinsic

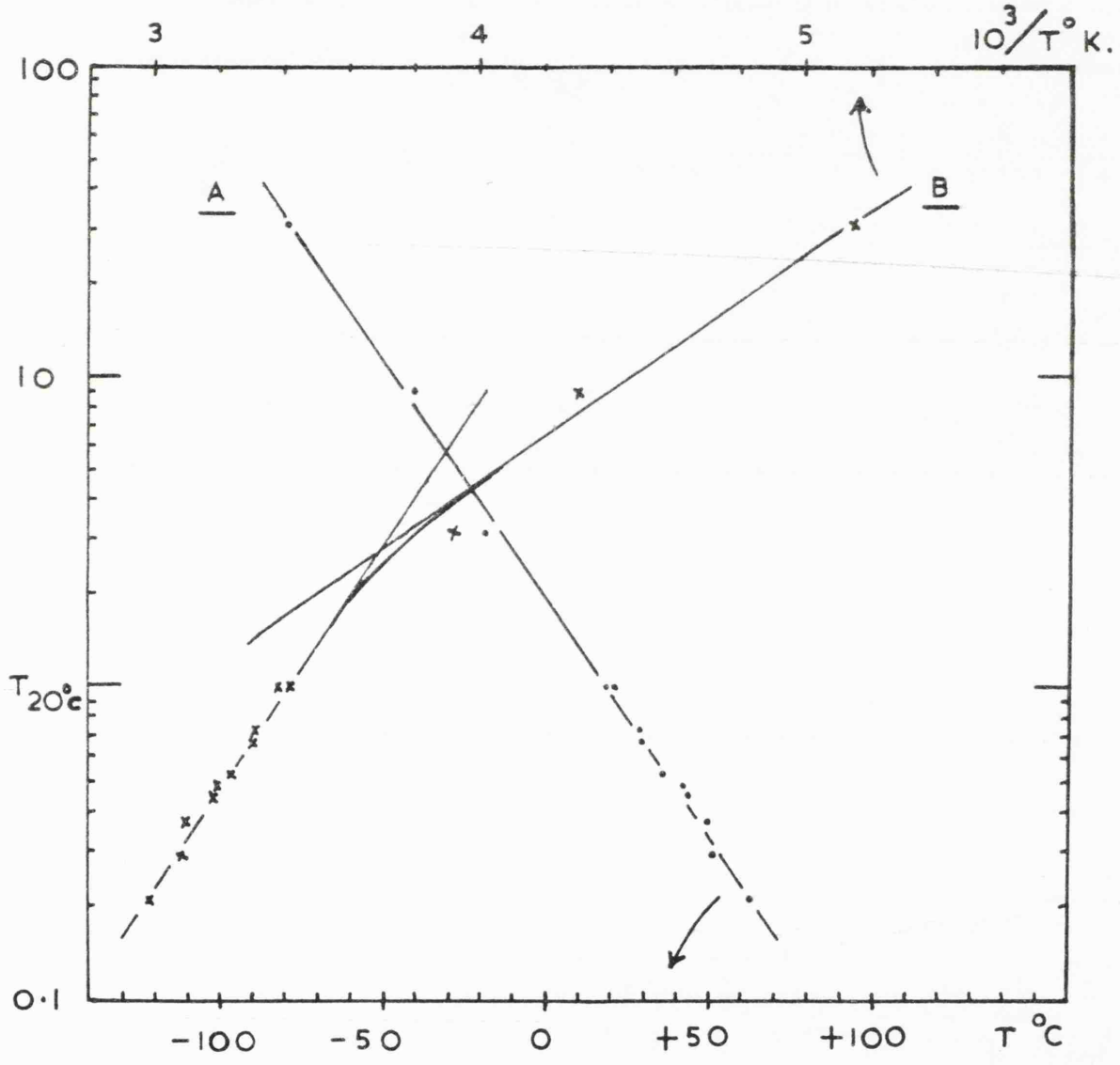

FIG. 4.15.

component of conductivity resulting from, and characteristic of, the inter-gap band structure.

It was evident from the lack of channel photoconductivity that the conduction mechanisms could not be well represented by a simple band model. This fact was checked by means of megohmeter measurements made in the dark and under strong visible illumination.

4.2. The Investigation of the Operation and X-ray Response of Channel Matrix Arrays.

4.2.1. Introduction.

The two matrices examined in this work, the details of which are shown in table 4.4, were produced and kindly loaned by Mullard Research Laboratories.

TABLE 4.4

	Matrix A	Matrix B
Material	Lead Glass	Soda Glass
Size of Matrix	Hexagonal 1.4 cm. sides.	0.75 cm. square
Channel Bore	200 μ.	25 μ.
" Pitch	267 μ.	40 μ.
" Length	1 cm.	4 mm.
Channels per cm.^{2}	1.620	6.25×10^4
Mean resistance per channel	$4 \times 10^{10}\Omega$ (20°C)	$7 \times 10^{17}\Omega$ (20°C) *
% Aperture Area	51 %	36 %

(* Quoted by manufacturer.)

The investigation was carried out in two stages:

1). A determination of the operating characteristics of the matrices so that X-ray detection efficiency could be defined and measured.

2). A study of the response of a matrix to a narrow

rectangular beam of x-radiation with a view to determining the spatial resolution of the device when used as an image dissector.

4.2.2. Apparatus modification

The apparatus was basically that described in Chapter 3 with the following modifications.

1. To achieve the necessary flux density the spectrometer was locked in the straight through position, so that x-radiation from the X-ray source illuminated the mounted matrix directly, instead of via the crystal. Filters of aluminium and Melinex were placed as required in the X-ray beam to provide some isolation of 8.3 and 44 Å radiation, the intensity of which was measured with the monitor proportional counter in the usual way.

2. The X-ray specimen case was removed and replaced by a calibrated lead screw mechanism which, when operated by a flexible drive, enabled the matrix assembly to be traversed across the X-ray beam defined by an adjustable razor blade slit.

The matrix assembly is shown in Fig. 4.16.A. The matrix was mounted behind the X-ray slit together with one of two collector assemblies as shown in Figs. B and C. These guarded collectors defined regions on the matrix under investigation from which pulses were extracted and recorded.

The circuit evolved for the investigation is shown in Fig. 4.17. The potential divider R_1 R_2 was arranged

FIG. 4.16.A.

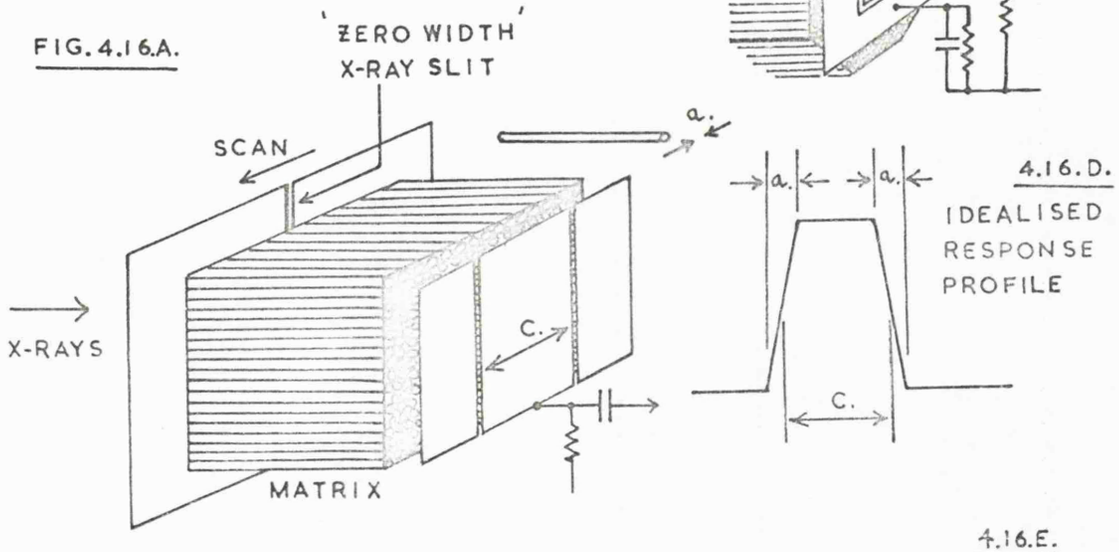

4.16.B.

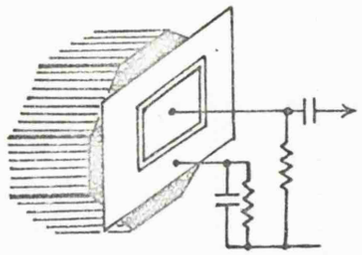

4.16.D.

IDEALISED RESPONSE PROFILE

4.16.C.

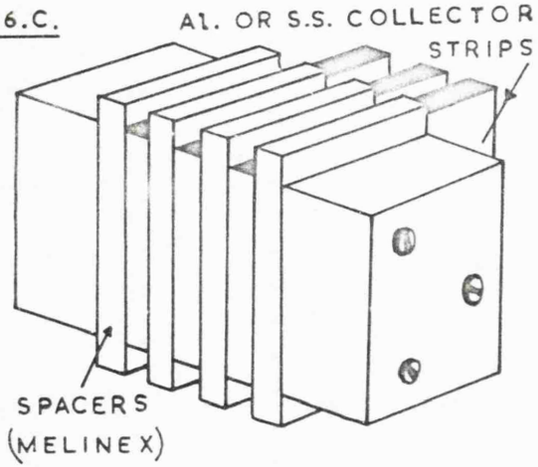

4.16.E.

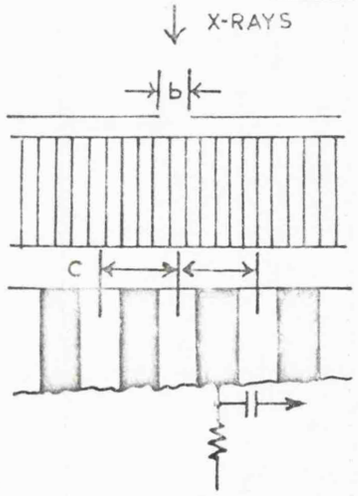

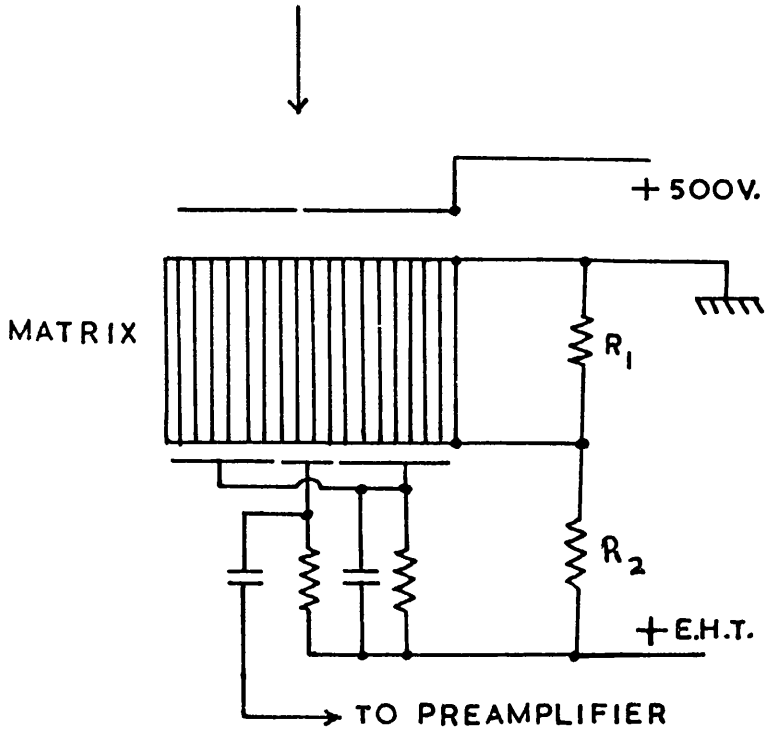

FIG. 4.17.

to give a collector bias of ~ 60 v at 2.6 kv. (This was known not to be critical). The bias (+500 v) on the X-ray slit and, in the case of the strip collectors, the decoupling on the guard collectors, were found to be necessary for the quiet operation of the matrix. The slit bias simply prevented, by retardation, the photo electrons ejected at the slit from reaching the matrix, and the decoupling reduced the effects of pulse capacitive cross-coupling between the collectors to a sufficiently low level.

4.2.3. Determination of the operating characteristics of the matrix arrays.

Matrix A was examined at 44 Å with the rectangular collector assembly mounted ~ 0.5 mm. distant. The polar response was found to be similar to that measured for single channels and the matrix was subsequently set at one of the response maxima.

The pulse height distribution of the matrix was measured using electronics system 2. The variations of pulse height distribution with channel voltage at constant count rate and with count rate at constant channel voltage are shown in Figs. 4.18 A and B. It is evident that the distributions are sensitive to both voltage and count rate but may be approximately represented by the sum of the two experimental sections each of the form:

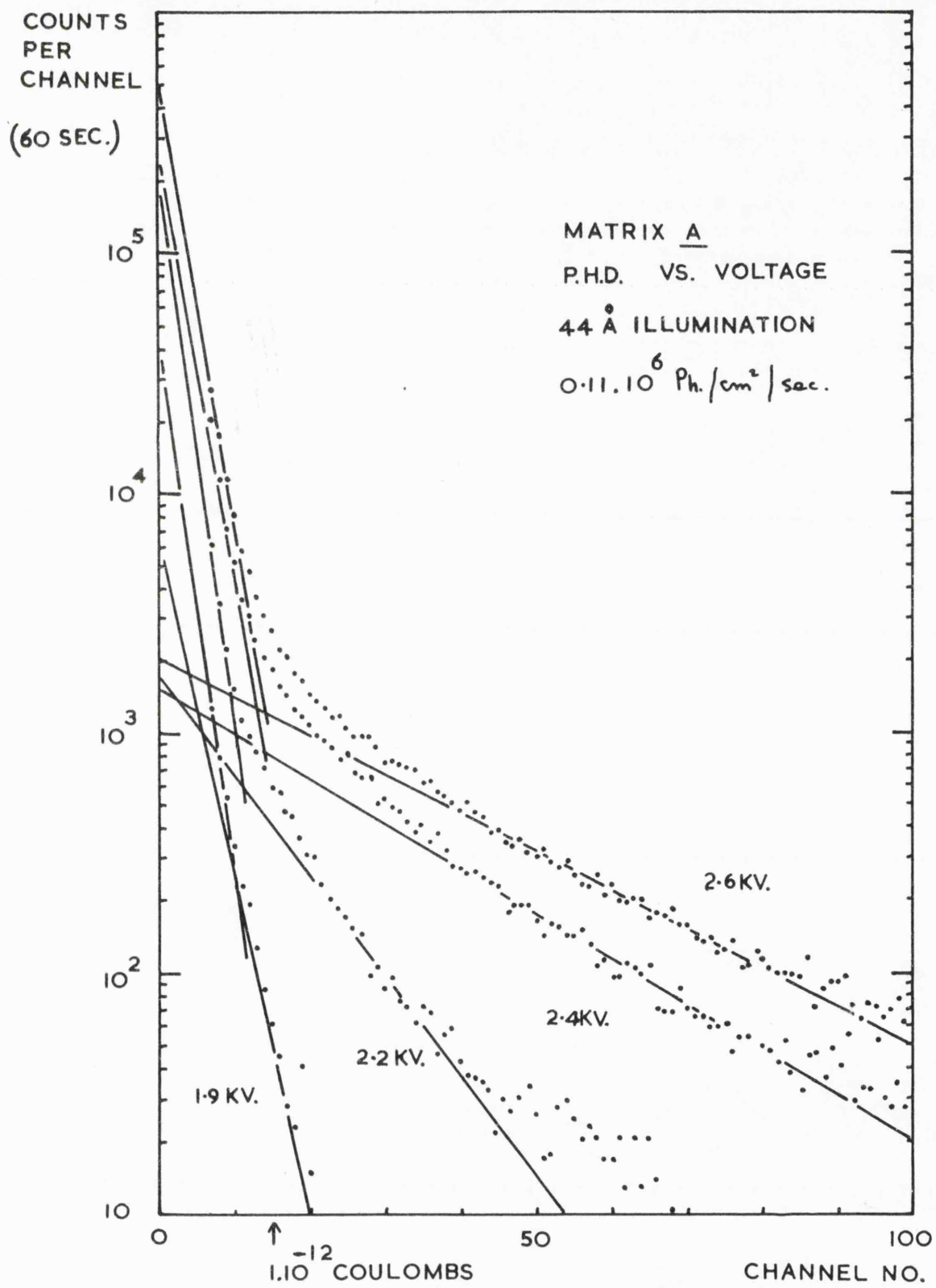
COUNTS
PER
CHANNEL
(60 SEC.)
MATRIX A
P.H.D. VS. VOLTAGE
44 Å ILLUMINATION
0·11.10^6 Ph./cm²/sec.
10^5
10^4
10^3
10^2
10
2·6KV.
2·4KV.
2·2 KV.
1·9 KV.
0
50
100
1.10^-12 COULOMBS
CHANNEL NO.

FIG. 4.18. A

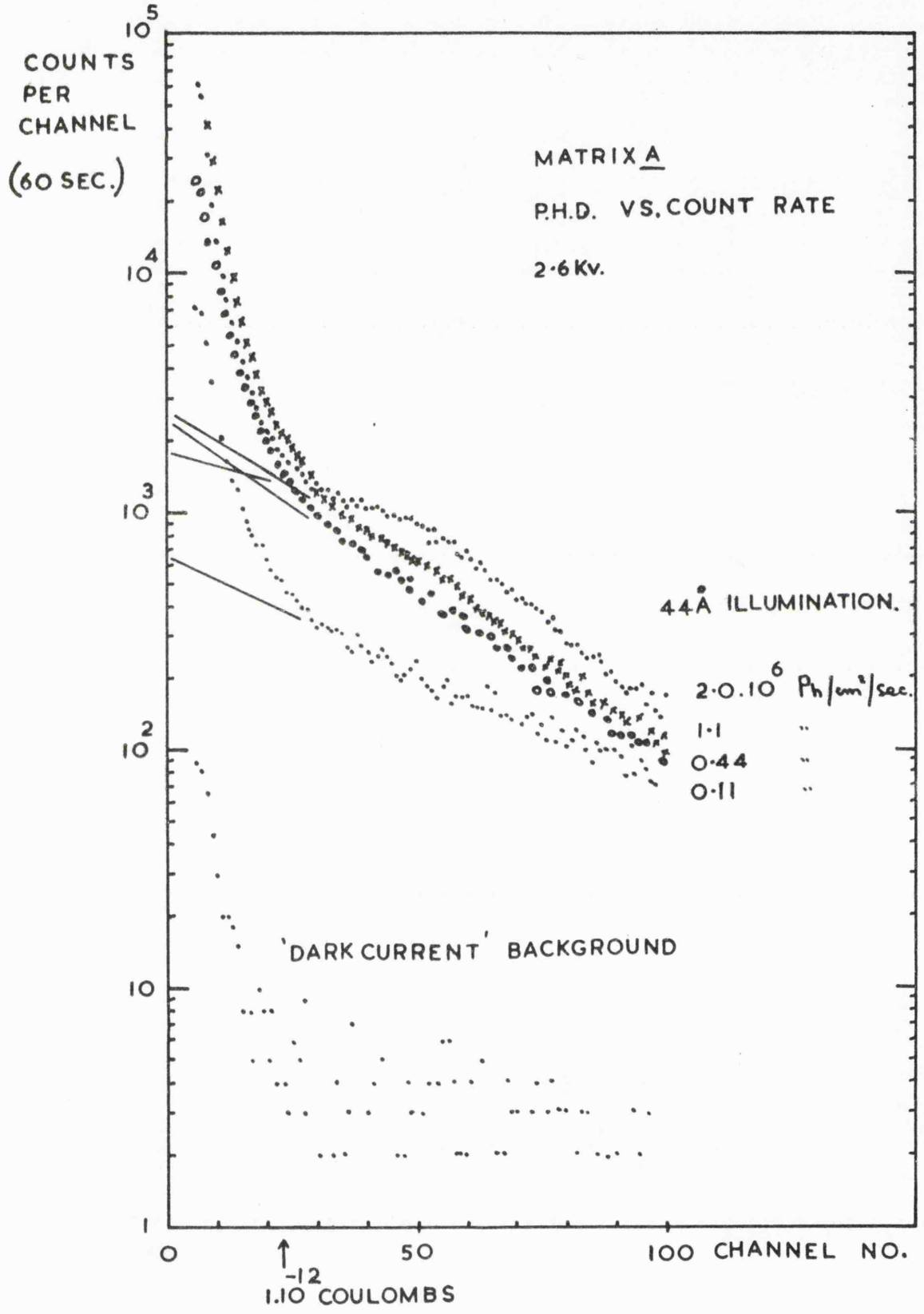
COUNTS PER CHANNEL (60 SEC.)
10^5
10^4
10^3
10^2
10
1
MATRIX A
P.H.D. VS. COUNT RATE
2·6 Kv.
44Å ILLUMINATION.
$2{\cdot}0.10^6$ Ph/cm²/sec.
1·1 "
0·44 "
0·11 "
'DARK CURRENT' BACKGROUND
0
50
100 CHANNEL NO.
1.10^{-12} COULOMBS

FIG. 4.18.B

$N = N_0 e^{-q/\bar{q}}$ where N = Counts per channel at q

N_0= Counts in channel at q = 0

$\bar{q}$ = Mean charge amplitude of distribution.

As will be evident from the efficiency measurements, there are many more pulses in the pulse height distribution than there were photons incident. Similar effects have been experienced in the course of electron amplification measurements (Adams 1967) and it is believed that the phenomenon is characteristic of this type of matrix. Although some ionic feedback would be expected from the linear channels in the matrix the rise time of the electronics system would be inadequate to resolve the individual feedback components, these having separations of the order of 0.05 μs or less (Adams and Manley 1966). Thus the extra pulses must be quite separate events (secondary, tertiary, quaternary etc.). Since the x-radiation was incident within a few diameters of the end of the channel, it would be expected that the primary pulses would arise after electron multiplication along the whole channel length. Because of this, it is assumed that the upper exponential section of the pulse height distribution consists of these primary pulses. The variation with applied voltage of mean charge output of this distribution is shown in Fig. 4.19 C.

If the photon detection efficiency of the matrix is now defined as the probability per photon passing through

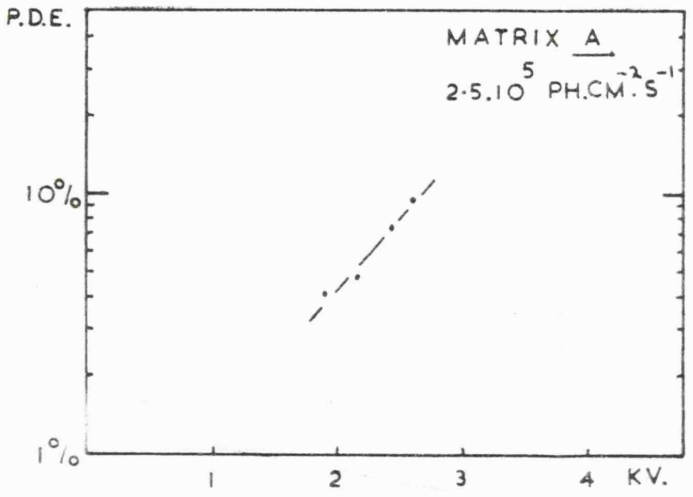

FIG. 4.19.A.

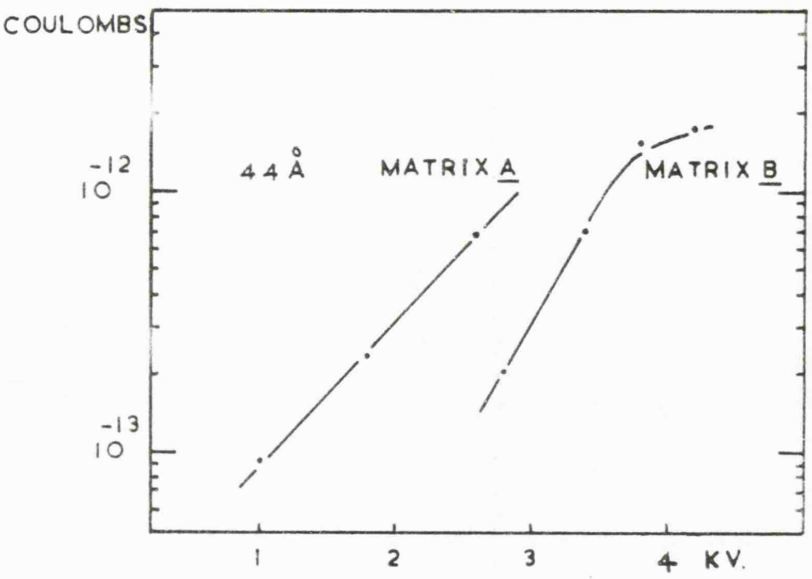

FIG. 4.19.C.

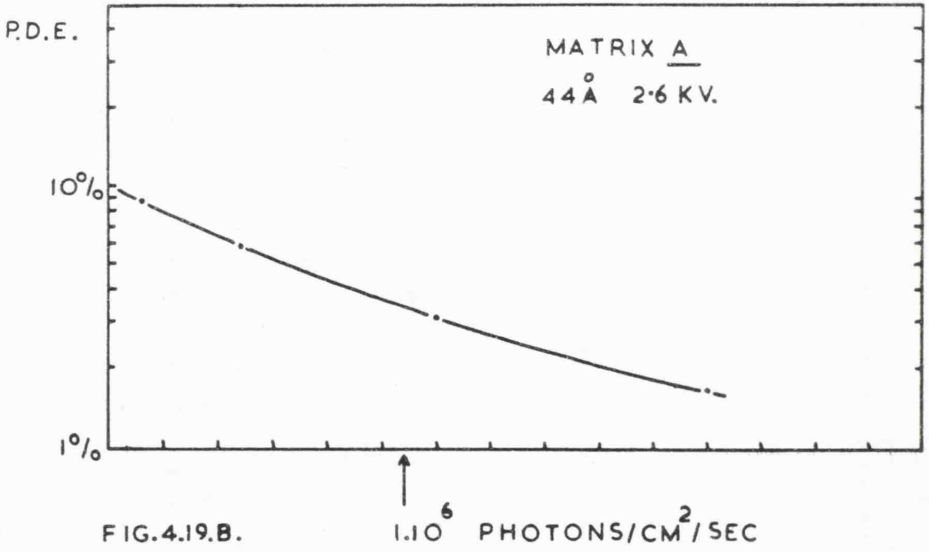

FIG.4.19.B.

a channel aperture * of the production of one primary pulse, then the variation of photon detection efficiency with operating conditions may be obtained from Figs. 4.18 A and B.

Figs. 4.19 A and B show how the 44 Å photon detection efficiency varies with channel voltage and with X-ray flux density (i.e. count rate). The maximum value of photon detection efficiency is about the same as that measured for the bare single channel multiplier at 44 Å, although agreement would not necessarily be expected since the channel materials are different.

Although the photon detection efficiency increases with channel voltage, it was not possible to take advantage of this owing to the rapid increase in noise level that occurred above 2.6 kv.

The reason for the decrease of photon detection efficiency with count rate appears to be a saturating mechanism in the matrix which progressively removes pulses from the upper section of the pulse height distribution. The likelihood of wall current limitation was thought to be very small since inspection of the mean pulse current per channel shows that it is at least two

* If continuous electron multiplication also takes place along the outside surfaces of the channels in the interstitial regions of the matrix, then the sensitive area of the matrix will be greater than that of the apertures alone.

orders of magnitude less than the standing current defined by the quotient of channel voltage and channel resistance.

According to Bryant and Johnstone (1965), the effects of electronic space charge should limit the maximum pulse obtainable from this size of channel to ~~1.3~~ 4.8 x 10^{-12} coulombs. It is evident that this prediction is not borne out by the present results since at 2.6 kv most of the pulses in the upper section of the pulse height distribution are much greater than this value.

The possibility does remain, however, that the effects of space charge, while not apparently producing a peaked pulse height distribution, might enhance the effects of wall current limitation which by itself would seem inadequate to account for the observed changes.

The dynamic range of the matrix.

This is defined by the interval between the dark current noise level of the matrix and the useful maximum count rate set by the fall-off of photon detection efficiency (p.d.e.). If the 44 Å efficiency is taken as typical for the soft X-ray region this interval extends from a noise level equivalent to 1 x 10^{3} photons/sq.cm./sec. to a maximum flux of 1 x 10^{6} photons/sq.cm./sec., at which level the p.d.e. has decreased to 35% of its zero-count-rate value. Little significance may be attached to the background level of the matrix since its value was very strongly dependent on the operating

voltage. A full investigation into this dependence would be necessary for the intrinsic component of the background to be isolated and its source of origin established.

4.2.4. The linear X-ray resolution of a matrix array.

For this investigation the finer of the two channel matrices (B) was used. The matrix was mounted in the apparatus with wire connections attached with fine silver paste. The sandwich collector assembly was located approximately 25 μ. distant from the matrix anode by means of melinex spacers of this thickness. The necessary alignment between the collector strip and the X-ray slits was achieved by observing the slits, visibly illuminated, through the melinex spacers of the sandwich assembly. This could be carried out both with and without the matrix in position since the latter possessed high optical transmission.

The matrix was operated at 3.5 kv which was the maximum compatible with low background noise level. The p.h.d. was observed to be quite flat with a mean value of approximately $6.\ 10^{-13}$ coulombs. As in the case of matrix A this mean charge output greatly exceeded the Bryant and Johnstone space charge maximum which amounted to 6.10^{-14} coulombs for this size of channel. Erratum.

The effect of the high channel resistance soon became evident in that, on first illuminating the matrix at 44 Å, a burst of counting took place which then decreased over

a period of one or two seconds to a much lower value ($\sim$ 200 c.p.s.). Alternatively, if the X-ray flux was slowly increased from zero, the count-rate was discovered to reach a flat maximum of about 200 c.p.s., which represented 1 count per sec. for each channel illuminated by the X-ray beam. That this was most probably a result of current limitation in the matrix became evident on calculating the standing current per channel at the channel voltage of operation, which was found to be approximately twenty times lower than the mean pulse current. This result was considered to indicate that the resistance figure given by the manufacturer was too high but this could not be confirmed since the total matrix was found to measure only $10^9 \Omega$ as a result of leakage currents.

The significance of the effect described was a dead time of about 1 sec. per channel.

The variation of matrix response with distance across the X-ray beam on two occasions is shown in Fig.4.20.

The p.d.e. of the matrix at the peak position was measured with the monitor proportional counter to be 24.0% after correcting for the 5 ms. dead time. This value seemed rather high and therefore a measurement of p.d.e. was also made at 8.3 Å. The value obtained was 11.8%. Thus at both wavelengths the p.d.e. was measured to be approximately twice that obtained for a bare single channel multiplier. The possibility of the presence of extra pulses did exist but the pulse height

distribution was observed to be without a low amplitude tail of the sort given by the matrix A. It was concluded therefore that the measured p.d.e.'s were characteristic of the matrix material within the uncertainty introduced by the large dead-time corrections.

The shape of the X-ray response profiles affords, in principle, a measure of the linear or spatial resolution of the matrix, since each edge of the rectangular X-ray beam may be considered as a unit or step input function to the system.

The response profile is potentially a function of the following quantities.

1. The width of the X-ray beam (including the effect of diffraction at the slit defining the beam).
2. The lateral spread of photo-produced electrons across the front face of the matrix.
3. The mean internal diameter of the matrix channels.
4. The degree of parallelism of the channels in the matrix.
5. The lateral spreading of the output electrons before collection.
6. The width of the collector.
7. The mutual alignment accuracy of the X-ray beam and the collector.

Under ideal conditions, i.e. zero contributions from 1,2,4,5 and 7, the profile will be defined solely by the internal diameter a of the individual channels and the width of the collector. Thus under these conditions and

for a random distribution of channels in the matrix the response profile will take the form of an approximately linear ramp of length a at each collector edge (see Fig. 4.16.D). For the present work conditions were non-ideal in that an X-ray beam, of finite width b was used. The effect of this may be taken into account however since the ramp length will now be a + b (25μ + 43μ). The full width at half maximum (f.w.h.m.) of the profile should be given by the effective collector width c which in this case consisted of the width of the metal collector strip plus twice the semi-thickness of the spacers (41μ + 30μ). See Fig. 4.16.E.

The comparison of the experimental profiles with that expected on the basis of the above analysis is also shown on Fig. 4.20.

If the accuracy of measurement of distance and width is taken into account ($\pm$ 5%), it may be concluded that the mean f.w.h.m. is not more than 20% in excess of c.

The profiles are wider than predicted at their bases. This is to be expected generally as the sum of the contributions of quantities 2,4,5 and 7 but may also be partly accounted for by the effects of Fresnel Diffraction at the jaws of the slit. The extent of the diffraction broadening will be several times the distance of the first maximum, which is given by $\sqrt{d\lambda}$ where d is the distance between the slit and the matrix. For

$d = 0.2$ cm. and $\lambda \sim 44$ Å $\qquad \sqrt{d\lambda} = 3\mu$.

Apart from the base broadening, it is evident that the profile of the matrix is controlled by the finite size of the individual channels and that this quantity may therefore be taken as an indication of the resolution available for X-ray dissection.

Dynamic range of Matrix B.

At 3.5 kv. the equivalent noise level at 44 Å was approximately 4.10^2 photons/sq.cm./sec. The upper limit was taken to be that flux for which a 100% dead-time correction was necessary; this was 4.10^5 photon/sq.cm./sec.

Thus, although the maximum count rate per unit area was five times lower, the dynamic range of Matrix B was about the same as that of Matrix A. This resulted from a higher photon detection efficiency and a lower noise level.

4.3. The Calibration of Satellite Proportional Counters.

4.3.1. The experimental results.

Using the method described in Section 3.2.4. measurements of Modal output charge (q) Resolution (R) and Photon detection efficiency ($\mathfrak{Z}$) were made on several counters of each type (A,B,C,D,E,F and G). The measured values are presented in Tables 4.6.1. → 4.6.6. together with the gas filling pressure, the measured window area, and the reference charge output given at the calibration window of each counter.

Typical spectral variations of q, R and $\mathfrak{Z}$ are shown in Fig. 4.23 A. and B. Simple power-law variations have been assumed,

i.e. $q = A\,\lambda^{-\alpha}$ where $\alpha \simeq 1$

and $R = \dfrac{2.36\ k}{E^m}$ where $m \simeq 0.5$ and E = Photon energy (Kev)

Values of α, K and m, obtained graphically in this way are given in the tables for each counter examined at two or more wavelengths. The experimental values of $\mathfrak{Z}$ are plotted out in Figs. 4.24 A.→ F. together with the nearest spectral variations calculated from the counter diameters (i.e. absorption path lengths), and selected window thicknesses using published mass absorption data.*

* Mean values taken from compiled figures from the works of:- Henke et al (1957), Cooke and Stewardson (1964) and Bearden (1966).

TABLE 4.6.1.

Type A Counters								
REF. NO.	q Charge Output 10^{-13} Coulombs							α
Area mm^2	R Resolution % f.w.h.m.							K
Pressure cm.	3 Photon Detection Efficiency %							m
	Solar Window						Cal.	
	2.1Å	5.4	8.3	9.8	12.2	14.6	2.1	
1093	7.50	2.83	1.80		1.19	1.00	2.00	1.034
0.581	18.1	32.3	40.8		50.3	56.0	19.8	0.181
61	7.12	8.19	53.0		22.3	8.13	-	0.620
1095	7.40	2.76	1.77	1.48	1.17	1.01	1.97	1.043
0.587	21.6	33.3	40.2	46.0	50.7	54.3	18.7	0.215
61	7.74	8.18	52.1	40.6	22.6	9.06	-	0.500
1094	7.79			1.56		1.07	1.92	1.023
0.605	21.8			45.5		55.1	18.8	0.227
67	-			49.5		11.8	-	0.476
189	5.04			1.00		0.674	1.36	1.037
0.196	19.5			43.0		52.2	18.6	0.197
70	-			51.0		11.8	-	0.510
1365	7.48			1.52		1.02	1.78	1.027
0.605	20.7			43.7		54.1	21.0	0.210
	-					12.7	-	0.500
1364	6.56					0.874	1.71	
0.100	21.0					54.3	20.5	
	-					11.0	6	

TABLE 4.6.2.

Type B Counters						
REF.NO.	q Charge Output 10^{-13} Coulombs					α
Area mm^2	R Resolution % f.w.h.m.					K
Pressure cm.	3 Photon Detection Efficiency %					m
	Solar Window				Cal.	
	2.1Å	5.4	8.3		2.1	
1338	4.50	1.62	1.02		1.62	1.077
54.0	19.6	33.3	38.1		26.0	0.194
59	11.3	41.9	6.19		-	0.516
277	3.64	1.35	0.869		1.71	1.044
45.8	21.4	32.6	39.1		21.1	0.232
57	10.4	34.4	-		-	0.443
1337	—	2.43	1.56		-	—
45.7	—	33.1	38.4		-	—
58	11.6	35.8	7.57		—	-
220	3.68	1.40	0.906		1.73	1.012
39.6	19.6	31.1	38.2		23.4	0.206
57	10.5	34.5	5.23		-	0.485

Type B Counters (cont.)						
1336	3.90	1.47	0.915		1.60	1.038
54.2	19.0	31.1	39.8		21.4	0.191
60	11.73	39.0	7.81		-	0.531
208	4.32	1.66	1.05		1.93	1.029
39.2	21.0	30.8	40.5		21.0	0.203
	-	41.6	8.50		-	0.500
206		1.70				
67.0		31.2				
	11.20	43.3	-		-	
N.N.	4.19	-	1.04		1.89	1.009
40.2	19.3	-	39.4		21.0	0.199
	-	-	6.15		-	0.517.

TABLE 4.6.3.

Type C Counters						
REF.NO.	q Charge Output 10^{-13} Coulombs					
Area mm^2	R Resolution % f.w.h.m.					
Pressure cm.	3 Photon tection Efficiency %					
	Solar Window				Cal.	
	2.1Å	5.4	8.3		2.1	
1096	3.81	1.43	-		1.64	1.045
3.05	19.3	30.8	-		19.1	0.200
52	10.03	19.0	0.620		-	0.490
1097	3.66	1.40	—		1.67	1.023
2.63	19.3	30.0	-		19.4	0.206
52	12.05	27.9	-		-	0.464
191	5.65	2.17	-		2.47	1.000
2.93	20.6	32.5	-		22.1	0.215
54	10.29	22.4	0.716		-	0.483
192	-	2.66	-		-	—
2.71	—	32.3	-		—	—
53.5	10.09	28.2	-		—	—
190	6.83	2.58	-		2.55	1.034
2.82	21.2	31.8	-		22.0	0.232
52	9.94	19.8	-		-	0.425
1098	4.04	1.56	—		1.67	1.000
2.46	21.3	31.0	-		20.4	0.239
52	10.86	20.5	-		-	0.393

TABLE 4.6.4.

Type D Counters.			
REF.NO.	q Charge Output 10^{-13} Coulombs		
Area mm^2 Pressure cm.	R Resolution % f.w.h.m. η Photon Detection Efficiency %		
	Solar Window	Cal.	
	2.1Å	2.1Å	
1334	1.90 ± 10% over window	6.4	
705	21 ± 10% over window	27.6	
55	26.7	-	
1335	1.85 ± 10% over window	3.08	
685	23 ± 10%. over window	21.6	
59	30.9	-	

TABLE 4.6.5.

Type E Counters.					
REF.NO.	q Charge Output 10^{-13} Coulombs				α
Area mm^2	R Resolution % f.w.h.m.				K
Pressure cm.	3 Photon Detection Efficiency %				m
	Solar Window			Cal.	
	2.1Å	5.4		2.1	
1099	2.72	1.09		2.10	0.970
37.7	19.7	26.8		23.6	0.245
61	45.2	0.798		-	0.315
1100	2.88	1.06		2.60	1.041
40.2	19.1	26.6		19.8	0.222
61	46.2	0.945		-	0.343
1102	2.45	0.960		2.11	1.000
-	18.1	27.7		19.2	0.197
61	44.8	0.768		-	0.440
1103	-	0.926		-	-
45.3/38.2*	-	27.7		-	-
61	42.6	0.752		-	-

* Aperture Fitted.

Type E Counters (cont.)	2.1 Å	
1101	2.48	2.31
45.3	17.7	19.8
61	40.5	-
1362	1.88	1.70
40.4	17.3	20.6
	45.2	-
N.N.	1.76	1.49
44.4	17.9	21.1
	45.3	-
1363	2.36	1.72
58.8	18.7	18.0
	42.8	-

TABLE 4.6.6.

Types F and G Counters			
REF.NO. Area mm^2 E.H.T. Kv.	q Charge Output 10^{-13} Coulombs R Resolution % f.w.h.m. ε Photon Detection Efficiency %		
	Solar Window		Cal.
	2.1Å	44	2.1
G 1359	-	1.72	1.30
0.0935	-	≫100	25.4
1.28	-	-	-
G.1361	-	1.45	1.28
0.196	-	≫100	22.1
1.28	-	-	-
G 185	-	0.39	2.35
-	-	111	24.3
1.30	-	8.42	-
F N.N.	-	-	-
0.169	-	-	-
1.30	-	2.22	-
F 183	-	1.71	1.79
0.176	-	139	22.0
1.30	-	2.64	-
F 184	-	2.49	2.53
0.197	-	185	25.4
1.30	-	2.37	-

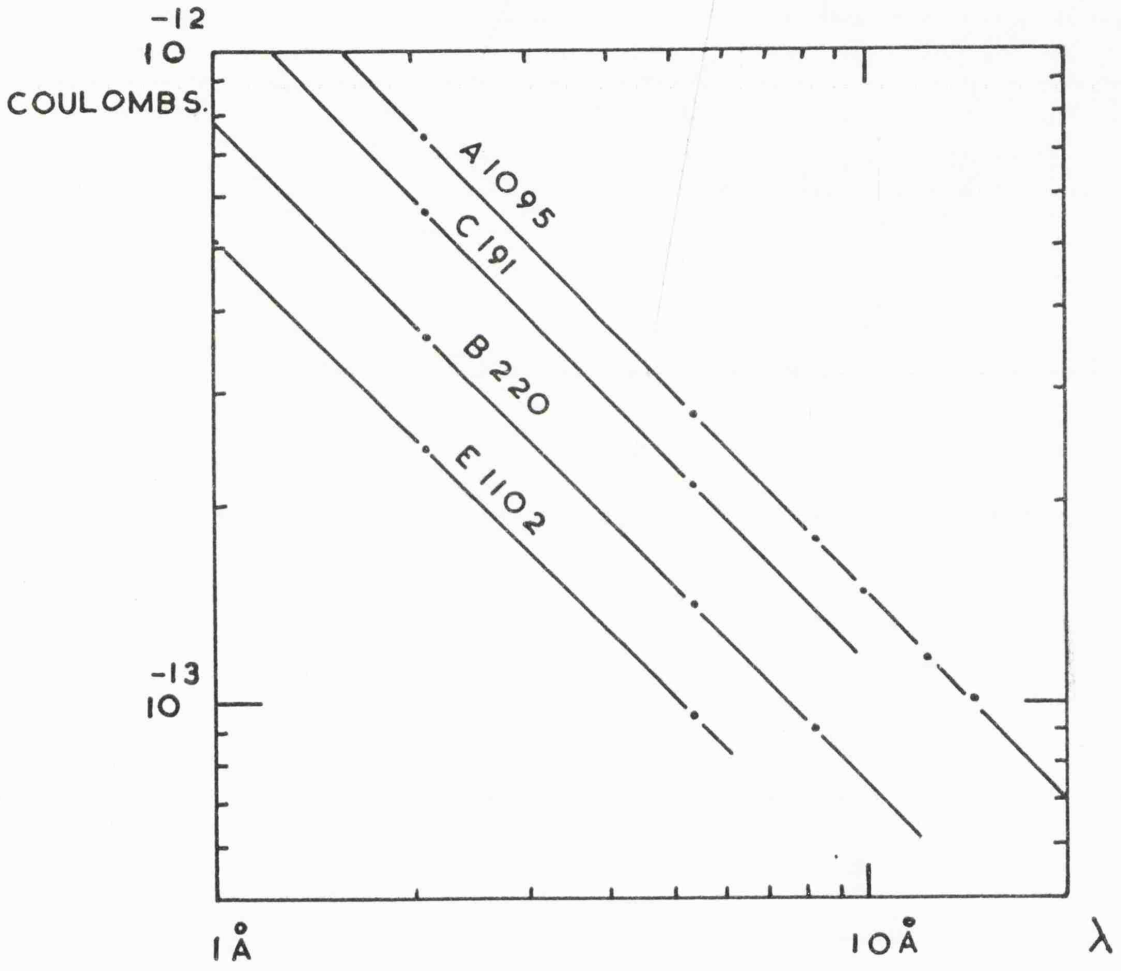

FIG. 4.23.A PROPORTIONAL COUNTER OUTPUT.

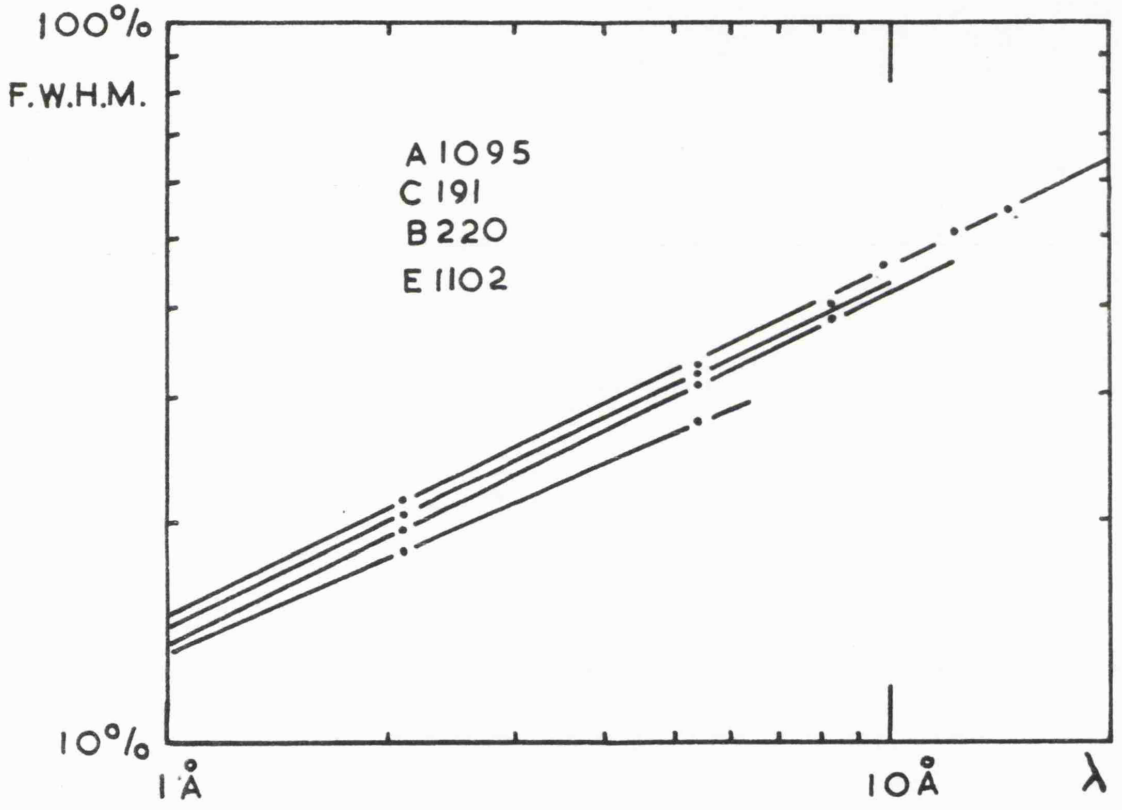

FIG. 4.23.B PROPORTIONAL COUNTER RESOLUTION.

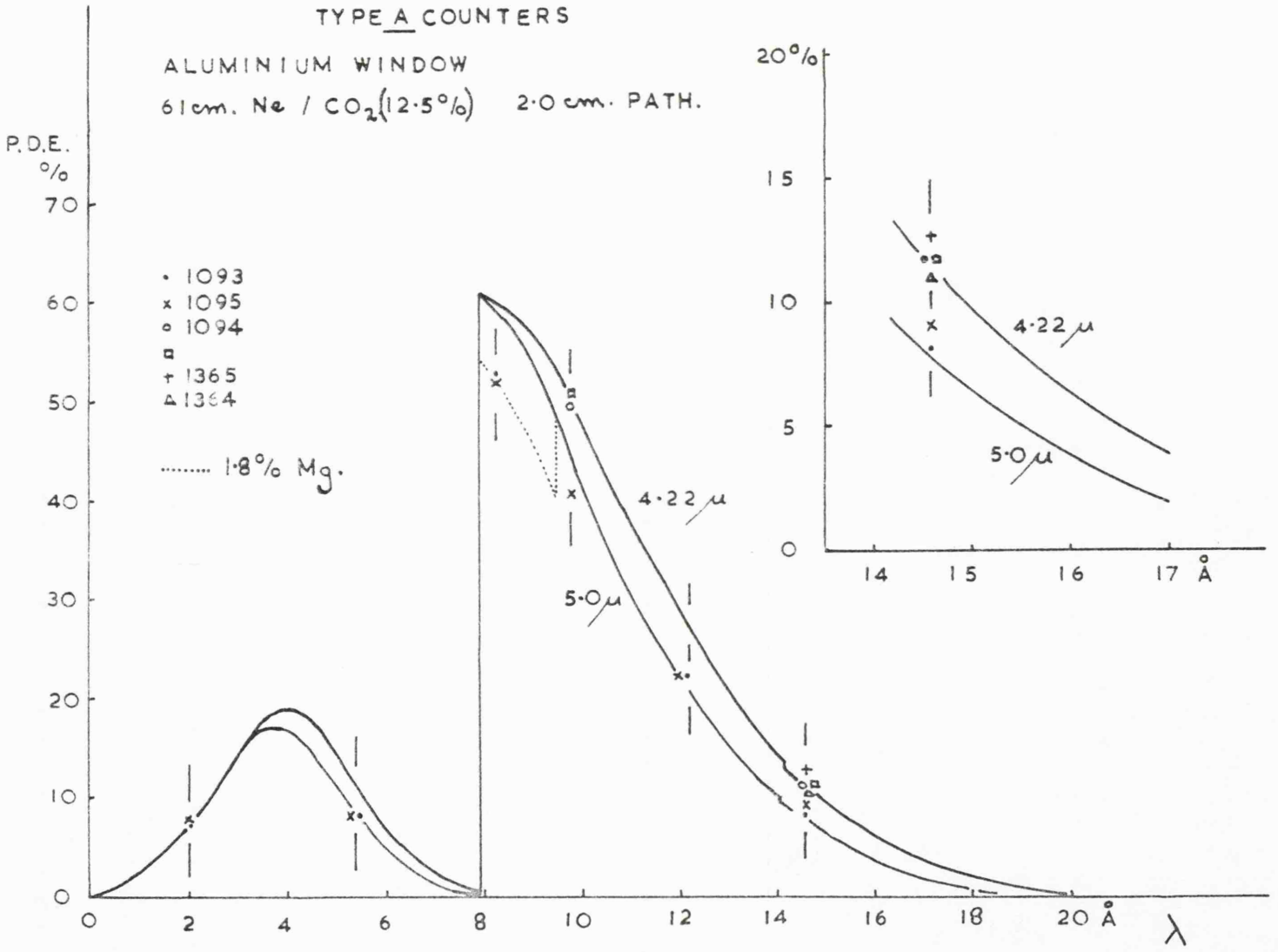
TYPE A COUNTERS
ALUMINIUM WINDOW
61cm. Ne / CO2(12·5%) 2·0 cm. PATH.
P.D.E. %
70
60
50
40
30
20
10
0
• 1093
x 1095
o 1094
□
+ 1365
△ 1364
..... 1·8% Mg.
4·22 μ
5·0 μ
0
2
4
6
8
10
12
14
16
18
20 Å
λ
20%
15
10
5
0
4·22 μ
5·0 μ
14
15
16
17 Å

FIG. 4.24.A

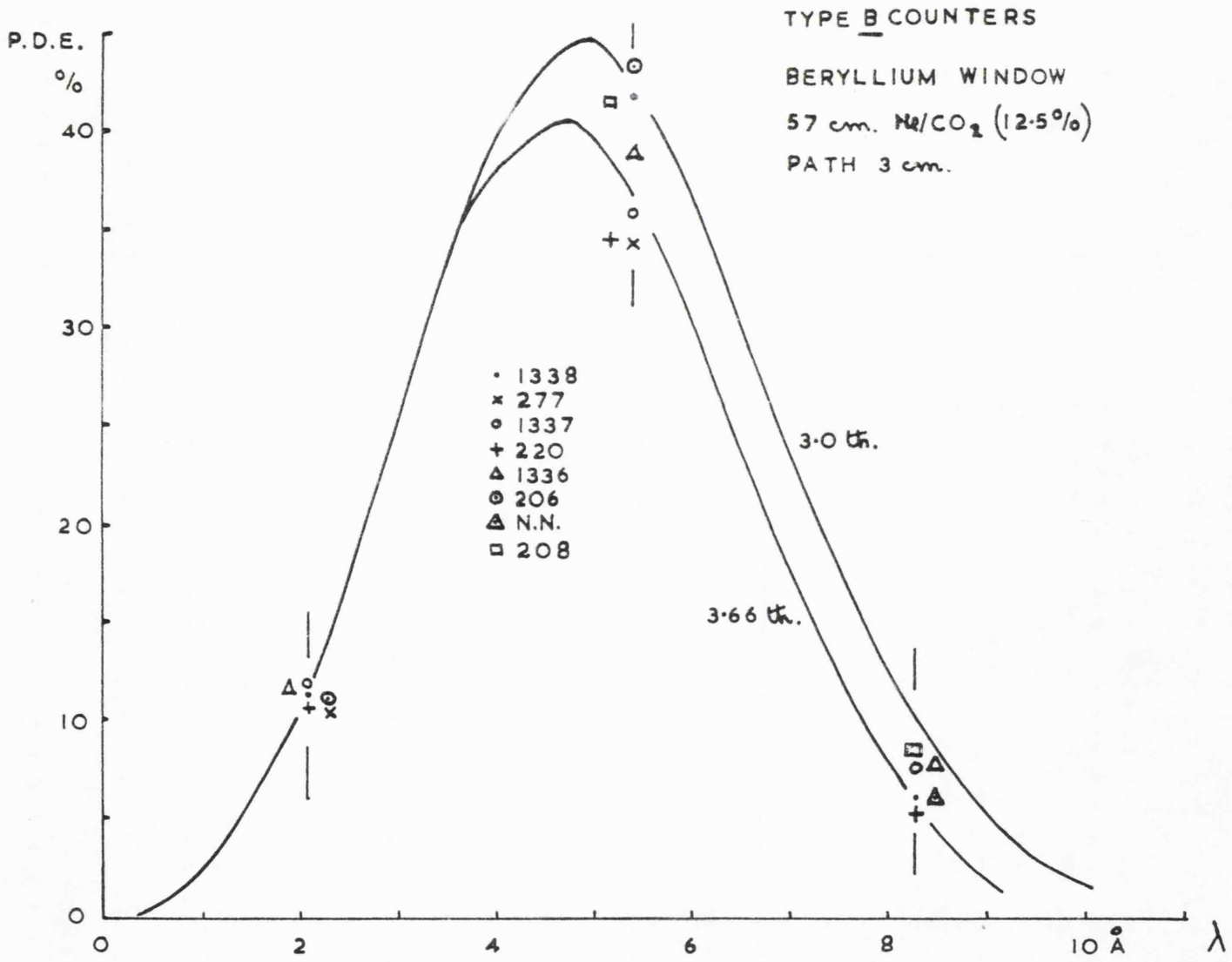
TYPE B COUNTERS
BERYLLIUM WINDOW
57 cm. Ne/CO2 (12·5%)
PATH 3 cm.
P.D.E.
%
40
30
20
10
0
0
2
4
6
8
10 Å
λ
· 1338
× 277
○ 1337
+ 220
△ 1336
⊙ 206
△ N.N.
□ 208
3·0 th.
3·66 th.

FIG 4.24. B

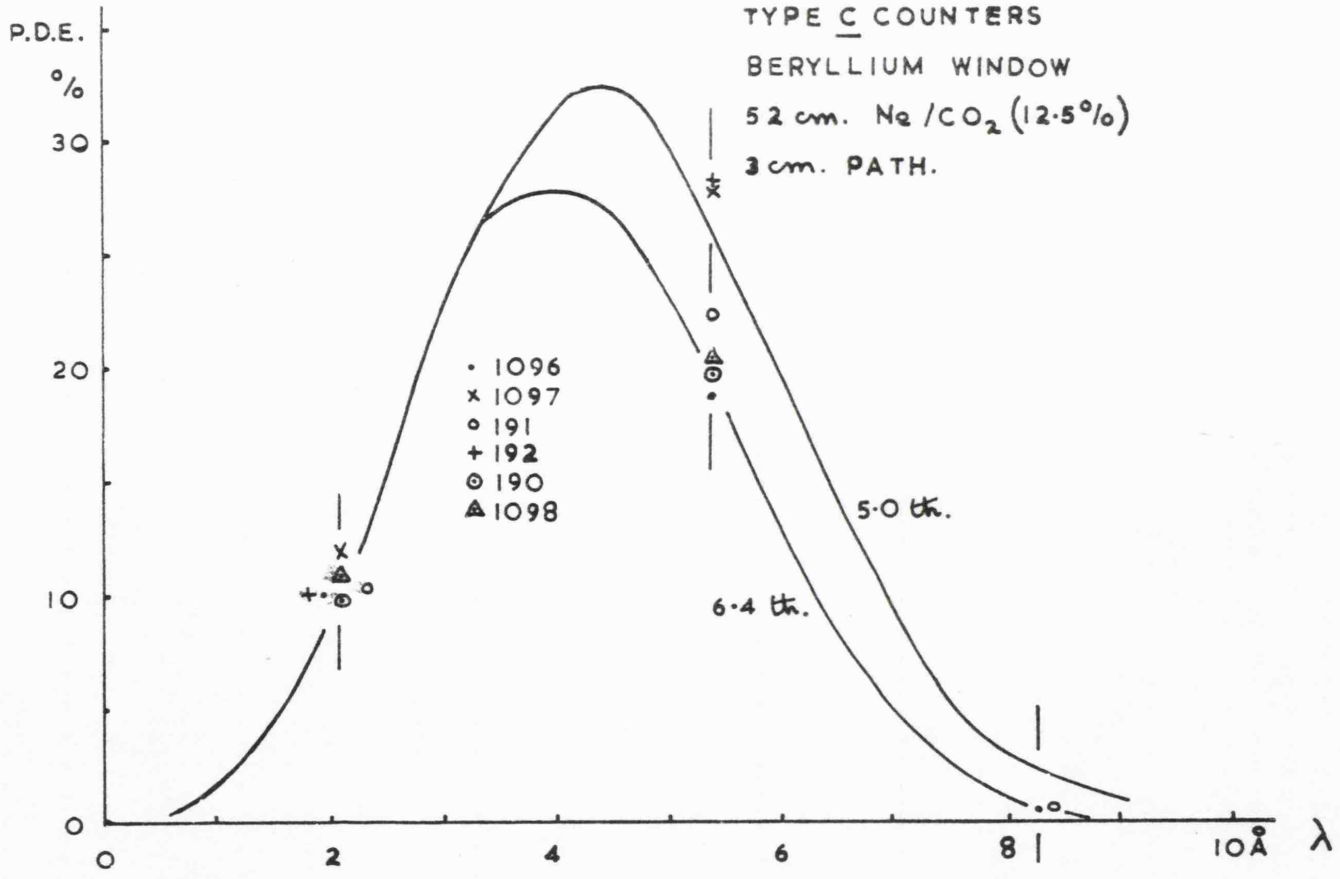
P.D.E.
%
30
20
10
0
TYPE C COUNTERS
BERYLLIUM WINDOW
52 cm. Ne/CO2 (12·5%)
3 cm. PATH.
· 1096
× 1097
○ 191
+ 192
⊙ 190
△ 1098
5·0 th.
6·4 th.
0
2
4
6
8
10Å
λ

FIG. 4.24.C.

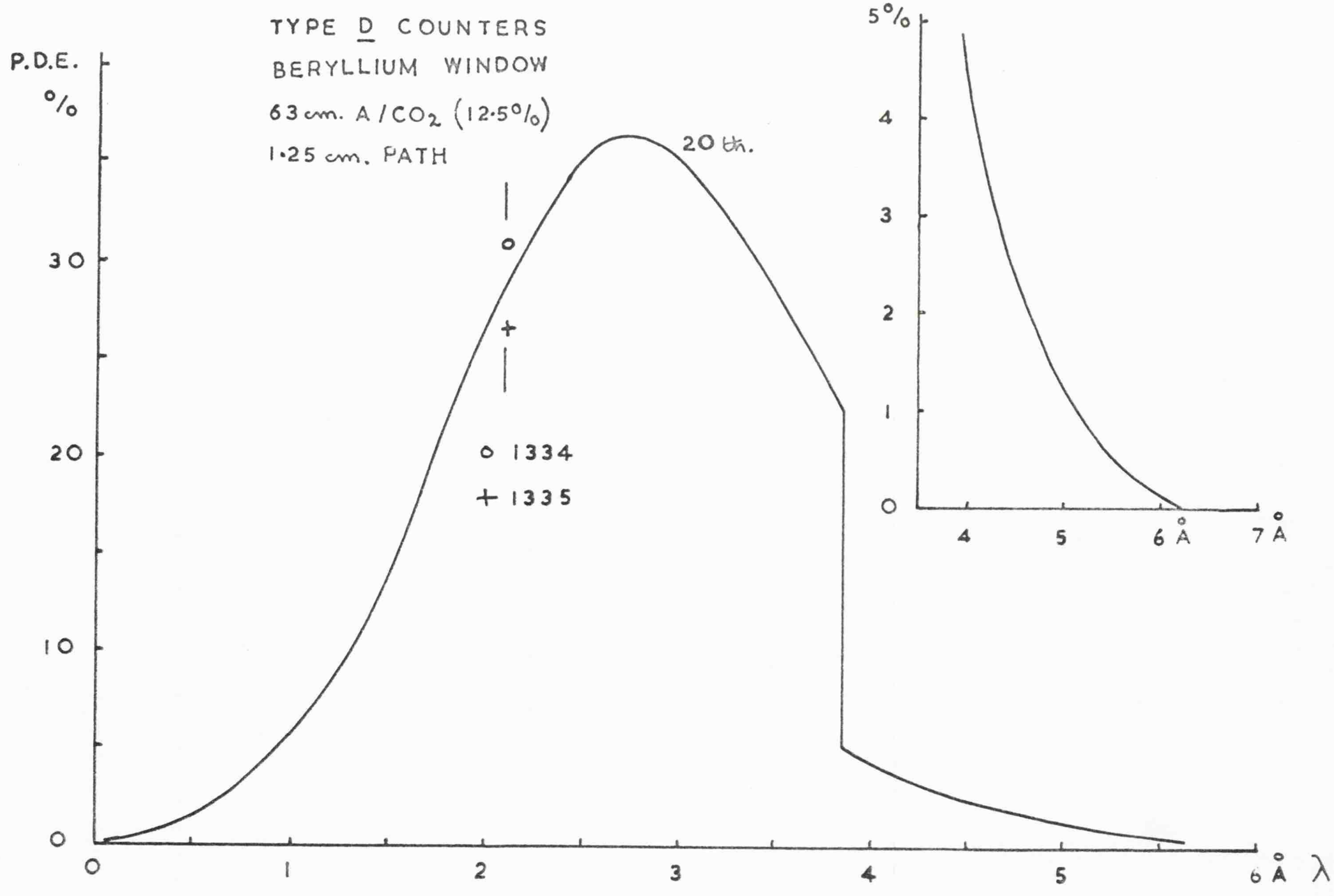
TYPE D COUNTERS
BERYLLIUM WINDOW
63 cm. A/CO2 (12·5%)
1·25 cm. PATH
P.D.E. %
30
20
10
0
20 th.
o 1334
+ 1335
0
1
2
3
4
5
6 Å
λ
5%
4
3
2
1
0
4
5
6 Å
7 Å

FIG. 4.24.D.

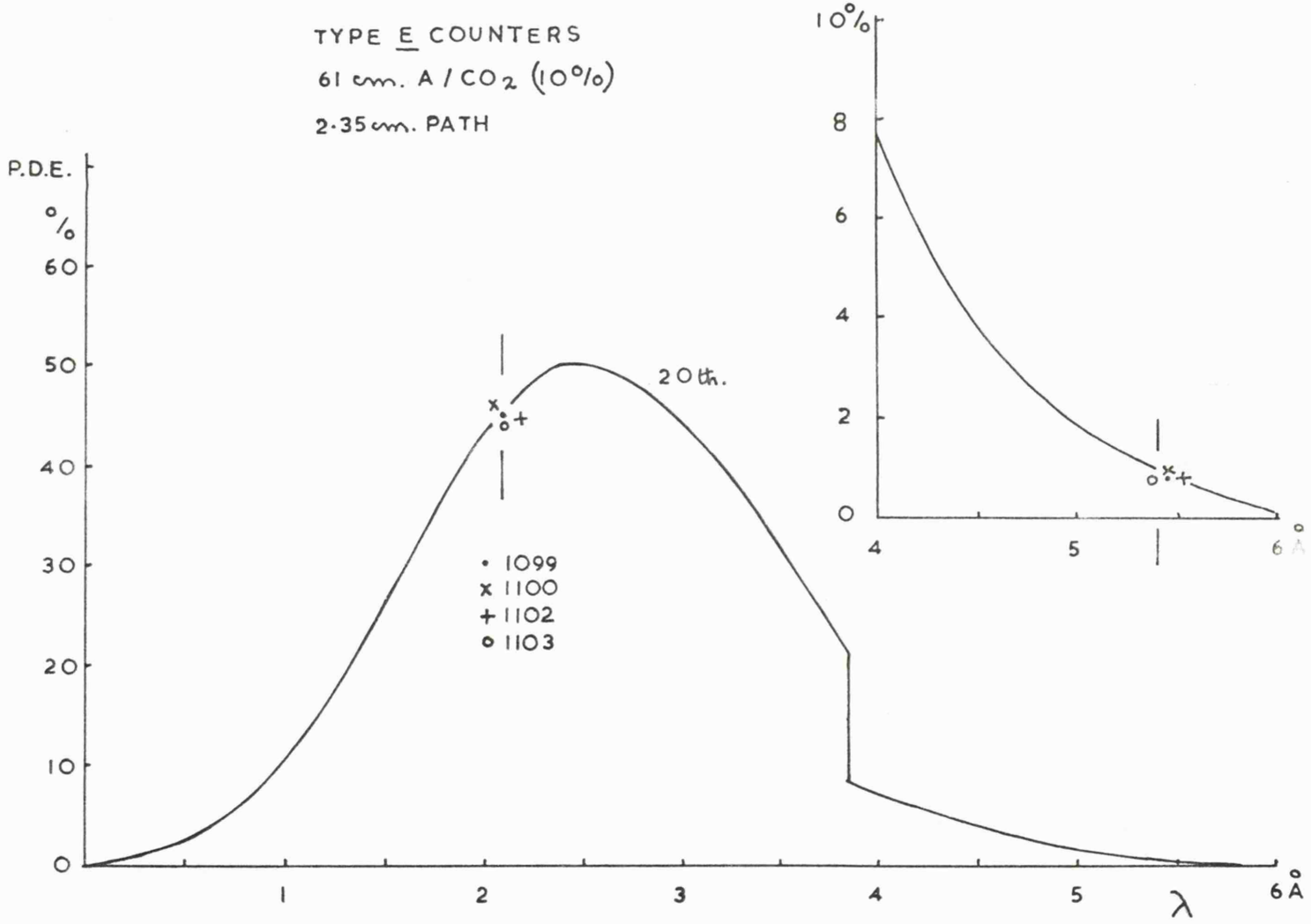
TYPE E COUNTERS
61 cm. A / CO2 (10%)
2·35 cm. PATH
P.D.E.
%
60
50
40
30
20
10
0
20th.
• 1099
x 1100
+ 1102
o 1103
1
2
3
4
5
6Å
λ
10%
8
6
4
2
0
4
5
6Å

FIG. 4.24.E.

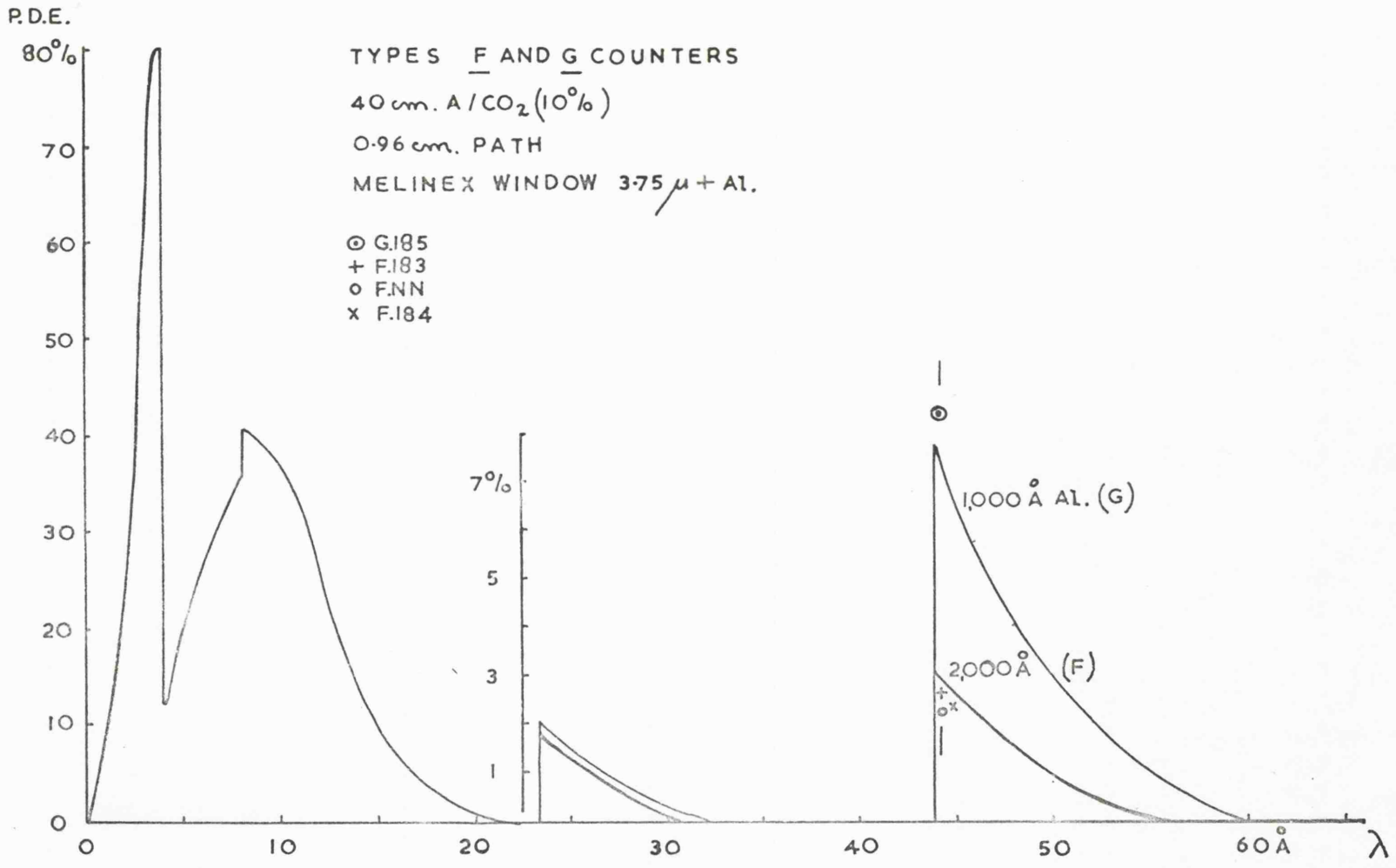
P.D.E.
80%
70
60
50
40
30
20
10
0
TYPES F AND G COUNTERS
40 cm. A/CO2 (10%)
0·96 cm. PATH
MELINEX WINDOW 3·75 μ + Al.
⊙ G.185
+ F.183
o F.NN
x F.184
7%
5
3
1
1,000 Å Al. (G)
2,000 Å (F)
0
10
20
30
40
50
60 Å
λ

FIG. 4.24.F.

4.3.2. Discussion of the results.

Photon Detection Efficiency.

In general the curves drawn out fit the experimental points fairly well and represent the spectral variations of photon detection efficiency for the counters within the limits of experimental error. Several differences exist, however, and of these the most systematic are the values for Type A counters 1093 and 1095. At 8.3 Å the p.d.e. is lower than would be expected in the light of measurements at other wavelengths by about 11%. This is greater than the error of measurement and indicates extra absorption in the window. If it is assumed that a single contaminant is responsible then, to account for the decreased effect at longer wavelengths, it must have an absorption edge between 8.3. and 12.2 Å. In view of its position in the periodic table, Magnesium is the most likely candidate and the modification to the p.d.e. curve that would result from a 1.8% mass fraction is indicated.

The other outstanding disagreement is that existing for B 1338. For this counter the efficiency at 5.4 Å is compatible with a 0.00300" Be window, whereas that at 8.3 Å indicates a thickness of 0.00366". In this case almost any contaminant free of absorption edges in this spectral region could be responsible. Traces of Iron, Fluorine, Magnesium and Oxygen are known to be present in commercial beryllium. However, oxygen is the only element likely to be abundant enough to give the measured

reduction of 60% at 8.3 Å. For this a mass fraction of 3.75% of Be O would be required, which is not greatly in excess of that specified by one manufacturer, Péchiney (10,000 ppm).

Proportionality

The index α relating charge output to photon energy is, in general, greater than unity with a mean excess for counter types A,B,C and E of 3.3, 3.5, 2.0 and 0.4% respectively. As departures from strict proportionality, these deviations are not severe but, on the basis of the accuracy (2%) and statistics of measurement, the effects are significant. There would appear to be three possible sources of origin: asymmetry in the pulse height distributions, a supra-linear increase in the mean ionization towards shorter wavelengths (i.e. a decrease in the mean energy per ion-pair) or a wavelength dependence of counter gas-gain.

The first possibility can only be rejected with complete confidence after a full computer analysis of the pulse height distributions has been carried out. However no signs of asymmetry were apparent during measurement on the screen of the multi-channel analyzer (and it would be expected that small separations of the mean and the mode could only arise with large distortions of the distributions wings).

Evidence mentioned in the next section makes it seem unlikely that the second possibility can be responsible and it must be concluded therefore that gas

gain variations are present. Such variation might be expected to arise, for example, if the quenching action of the CO_2 was reduced for large electron avalanches. This mechanism might also be expected to give rise to the observed spread in α for different counters of the same design.

Resolution:

The fractional r.m.s. of the output pulse height distribution of a proportional counter is given by:

$$\sigma = \left[\frac{F}{n_o} + \frac{\sigma_m^2}{n_o}\right]^{1/2}$$

Where:-

$\frac{F}{n_o}$ = Variance of the n_o initial ion pairs.

and

σ_m^2 = Variance of the multiplication process "single" electron" pulse height distribution.

This may be re-written as:

$$\sigma = \left[\frac{F\varepsilon}{E} + \frac{\varepsilon\sigma_m^2}{E}\right]^{1/2} \quad \text{——— 1.}$$

Where:-

F = Fanc factor of medium ionized.

ε = Mean energy per ion-pair

E = Photon energy.

Thus if $\sigma = kE^{-1/2}$

then $k = \left[\varepsilon(F+\sigma_m^2)\right]^{1/2}$ ——— 2.

For multiplication factors $\gg 1$, σ_m^2 has been estimated and measured to be 0.666 and 0.696 respectively by Curran (1949) and theoretically restricted by Byrne (1962) to the range: $0.61 \leqslant \sigma_m^2 \leqslant 1.0$

On the basis of equation (2) it is clear that, for a properly operating counter, variations in $\underline{K}$ and $\underline{m}$ can result only from a photon energy dependence of $\underline{\varepsilon}$ and/or $\underline{F}$. Should this be the case, however, then the variations would become characteristic of the gas mixture and not subject to fluctuations from counter to counter, as is evident from the results. Further, since $\underline{\varepsilon}$ has been shown to be constant for Argon-Methane and Nitrogen between 0.5 — 50 Kev (Curran et al 1949) it would be necessary for $\underline{F}$ to control the values of $\underline{K}$ and $\underline{m}$. That this cannot be the case is evident from Fig. 4.25 which displays equation (3) for two values of σ_m^2, Curran's mean value (0.681) and Byrne's lower limit (0.610). For $\underline{\varepsilon}$ = 26.5 eV (Argon CO_2 (20%) - Melton et al 1954) it is clear that Fano Factors of $\sim$0.8 are required to give even the lowest of the measured values of $\underline{K}$. (Assuming $\underline{\varepsilon}$Neon/CO_2 = 26.5 eV also).

Although Fano (1947) suggested limits for gases of $0.33 \leqslant F \leqslant 0.50$., recent measurements by Alkhazov et al (1967) confirming more refined calculations give much lower values for gas mixtures not very different to those used in the counters. For Argon-Methane (0.8%) F = 0.19 and for Argon-Acetylene F = 0.09. On this evidence, it must be concluded that Fano Factors of the magnitude implied by the measurements are unacceptable and that therefore the counter parameters are not gas-controlled.

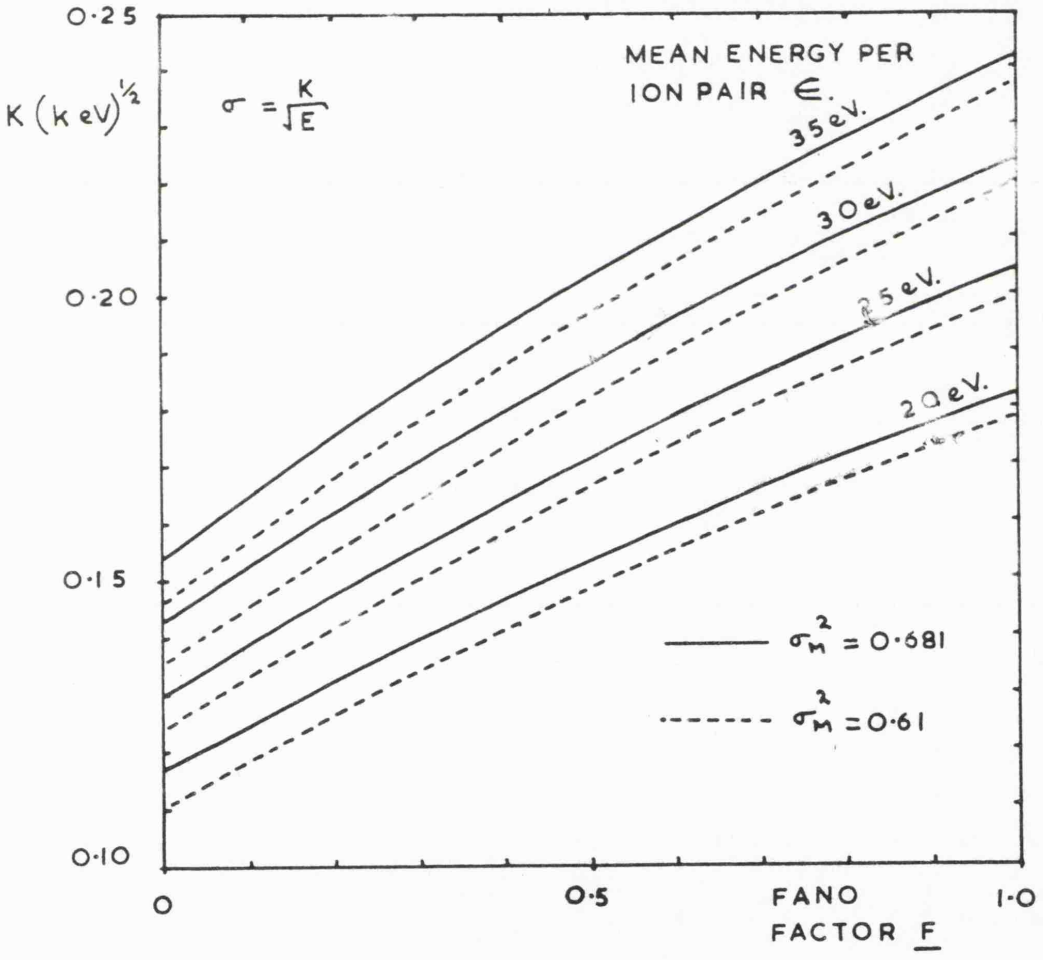
0·25
0·20
0·15
0·10
K (k eV)^½
σ = K/√E
MEAN ENERGY PER
ION PAIR ∈.
35eV.
30eV.
25eV.
20eV.
σ_M² = 0·681
σ_M² = 0·61
0
0·5
1·0
FANO
FACTOR F

FIG. 4.25.

The most likely alternative mechanism is the existence of a gas gain spread in the counter. This would be expected to arise as the result of variations in cathode geometry (particularly in the vicinity of the window) and/or imperfections in the anode wire. Recent work in this Department has indicated that the second factor is particularly important and that greatly improved resolutions may be obtained with highly uniform anode wires (Charles 1967).

Further support for the existence of geometrical distortion may be found in the results for the E-Type counters. Although the E-counter has the same cathode for the solar and calibration sections and a common anode wire, there are appreciable differences existing in the measured values of charge output and resolution. These variations are broadly consistent from counter to counter and must arise mainly from the differing window geometries in the two sections. Anode wire imperfections on the other hand will produce random fluctuations in counter performance and are most probably responsible for the spread in the measured counter parameters for all counter types. Commercial tungsten wire, unless specially cleaned, usually contains a coating of carbon fragments, which dates from the use of this element as a lubricant at the drawing stage of manufacture.

Fig. 4.25 may also be used to provide an estimate of the inherent resolution of the gas mixtures used in the counters; i.e. the resolution that could be obtained, in

principle, under conditions of zero geometrical distortion. Taking ε = 26.5eV, F = 0.1 and σ_m^2 = 0.61 gives K = 0.135 $(Kev)^{\frac{1}{2}}$. At 2.1 Å this would represent, if attainable in practice, a resolution of 13.1% f.w.h.m. This would be a most useful improvement over the resolutions typical of the present counters.

High Count Rate Performance.

The changes arising in the counter pulse height distributions at high X-ray flux densities were measured for several counters of each type. Sources of 2.1 Å (Fe^{55}) and 8.3 Å (AlK) radiation were used for these measurements. The second source was a small X-ray tube with an Aluminium target . The double-RC-clipped electronics system was cross checked against a double-delay-line pulse shaped system and found not to contribute appreciably to the pulse amplitude shifts below 10^5 c.p.s.

The shifts were found to be approximately linear with count rate. The values at 10^5 c.p.s. are displayed in Table 4.7.

TABLE 4.7

High Count Rate Performance

Counter	Wavelength	Solar Window 1.6 kv.	
		q_o Coulombs	q_{10^5}/q_o
A 1095	8.3 Å	$1.77.10^{-13}$	0.78
A 1093	8.3	1.80	0.78
B N.N.	2.1	4.9	0.73
B 1337	8.3	1.56	0.64
B 1338	8.3	1.02	0.78
B 1336	8.3	0.915	0.78
B 220	8.3	0.906	0.78
B 277	8.3	0.869	0.78
C 190	8.3	1.63	0.815
C 1098	8.3	1.00	0.834
E 1100	2.1	2.88	0.92
E 1099	2.1	2.72	0.92
E 1101	2.1	2.48	0.92
E 1362	2.1	1.88	0.92
E 1363	2.1	2.36	0.92.

It is evident that very little pattern is apparent in the behaviour of the counters as a whole although, for each type of counter, there is some mutual consistency in the results. For one C type counter and one B type counter there is an indication that the decrease at 10^5 cps is greater for increased values of q_o. Another B type counter indicates the opposite however.

Spielberg (1966) and Culhane et al (1966) reported a count-rate amplitude shift dependence on pulse amplitude and the former also showed that an increase in

anode wire diameter from 0.002" to 0.005" greatly reduced the extent of the shift, thus supporting a positive ion space-charge mechanism for the phenomenon.

Burkhalter et al (1966), however, reported considerable shifts with 0.010" anode wires but without any photon energy dependence apparent. On the basis of other evidence concerning the reproducibiliy of measurement, the authors suggest that anode wire contamination is responsible for the counter behaviour but mention that cleaning procedures (ultrasonic cleaning in acetone and heating in air) failed to produce a significant improvement. The rather modest energy resolution displayed by the authors (24% f.w.h.m. at 1.66 Å with A/CH_4 (10%)) would certainly support their suggestion.

The lack of success of the cleaning procedure would not be unexpected if the anode wire was physically non-uniform or contained high melting point fragments on the surface (and attached to it).

In the present measurements of amplitude shift the counters all possessed anode wires, adjacent to the windows illuminated, of 0.002" dia. It therefore seems that space charge limitation is the most likely primary mechanism for the measured shifts. Within the limitations imposed by the poor statistics, this is supported by the measured values.

It should be noted that, for a given space charge density, the size of the counter window will determine

the count rate at which the pulse amplitude reaches a given level. In addition, the window size and X-ray beam divergence will define the extent of geometrical contributions to the high-count-rate pulse height distributions.

Chapter 5. The Significance of the Experimental Work

5.1. The accuracy of the measurements

X-ray flux density

With the method of flux measurement adopted, the X-ray flux density at any wavelength is given by the expression:

$$N = \frac{S}{A(1+\tau S)T} \quad \text{photons/sq.cm./sec.}$$

Where S = The proportional counter count rate

A = " " " window area

τ = The counting dead-time

T = The photon detection efficiency.

The uncertainty in S was kept to be less than 1% by the accumulation of at least 10^4 counts, usually in five batches to reduce the possibility of spurious counts arising undetected.

The window area A was measured by obtaining the mean diameter with a travelling microscope. For the two monitor counters used, the diameters were approximately 2.5 mm. and 1.0 mm. Thus, for a vernier accuracy of $\pm$ .02 mm. at both ends of a diameter, and taking the mean of four diamters, the uncertainties in A were about $\pm$ 0.5 % and $\pm$ 2% respectively.

The counting dead-time correction was known to a much higher degree of accuracy, since the product τ.S did not usually exceed 2% (τ = 4μs. and S = 5,000 cps.): it can therefore be ignored here.

The uncertainty in T is set by the unknown difference between the mass thicknesses of the window and of the

sample used in the compensating frame at the spectrometer slits. The thicknesses visibly gave the same interference colour in reflection (green), in the same order, and therefore a worstcase estimate of the difference may be made by taking the thickness variation necessary to produce the colour red in one of the two pieces of material. This amounts to approximately 20%, assuming the green wavelength to be 5,300 Å and the red to be 6,300 Å. Since both pieces were green, half this difference is considered to be the maximum that could have existed. The X-ray transmission variation caused by a ± 10% thickness variation will be given by $\pm 10\sqrt{T}$, this amounts to

$\pm$ 3% for T = 80%

$\pm$ 7% for T = 50%

and $\pm$15% for T = 20%

The uncertainty is therefore strongly dependent on wavelength. An experimental estimate of the total measuring accuracy at 44 Å was made by measuring the flux density of the same X-ray beam with both counters in turn. The results differed by 4%, after correcting for the curvature present in the larger window (See Appendix 1). In view of this, it was concluded that the window samples were much closer than 10% to the actual window thicknesses (which would have given a discrepancy of 7% for both counters)

The calibration accuracy in the wavelength range 12 - 67 Å is therefore estimated to be better than $\pm$ 10%, since T was approximately 20% at 67 Å (See Fig. 3.22). For the 2 - 12 Å region, T is greater than 50% and the counter

calibration will be higher. However, since the X-ray beam profiles are both less uniform and narrower, it is unlikely that the overall accuracy will have improved very much, and $\pm$ 10% may be taken to be the calibration accuracy for the total spectral range.

Photo-electric yield

The effective plane photo cathode yields, reduced from the channel multiplier photon detection efficiencies, will be lower than the true photo-electric yields by a factor defined by the probability that an electron batch from the photo-emissive surface will fail to register as one count. This probability will depend both on the secondary emission coefficient of the channel multiplier surface and the number of electrons per batch. In the absence of definite information on these quantities, a worst case estimate may be made by assuming a secondary emission coefficient of 1.1, say, for the surface. The probability per primary electron of producing zero secondary electrons would then be $e^{-1.1}$ (= 0.33), assuming a Poissonian distribution of secondaries. For a primary batch of two electrons, this would decrease to 0.33^2 (= 0.11) and for three electrons to 0.33^3 (= 0.036).

The calibration of the flight proportional counters

Since most of these counters were calibrated at more than one wavelength, the net uncertainty of measurement will be lower than that estimated for each measurement. In the

case of photon detection efficiency, the window sample uncertainty will still limit the accuracy of the method to ± 5%, although it is probable that the actual error is less than this.

For the measurement of pulse height and resolution, the uncertainties are determined mainly by the statistical errors present as the result of counting pulse height analyzer channels. These amount to ± 2% and ± 3% for the mean and f.w.h.m. respectively. Should a proper numerical reduction of the pulse height spectra be made, it will be possible to reduce these uncertainties until the intrinsic stability of the electronics system becomes dominant. In the equipment used, the stability of the counter E.H.T. supply was calibrated only to ± 1 V. For the counters examined, this would produce a pulse-height uncertainty of about ± 1% , which is an order of magnitude greater than that resulting from the pulser instability.

5.2. The Channel Multiplier Detector in the OAO - C Experiment.

Introduction.

The UCL - Leicester soft X-ray telescope on the OAO - C satellite consists of three photon counters, each located at the focus of a paraboloidal grazing incidence reflector, and a fourth counter used without a reflector. Proportional counters have been specified for the reflectors covering the wavelength ranges 3 - 9 Å and 8 - 18 Å and also for the fourth range, 1 - 3 Å, (for which no useful increase in collecting area can be obtained with grazing incidence optics). The third reflector is to be used for wavelengths beyond 18 Å and a single channel multiplier has been specified for the detector.

The focussed radiation has axial symmetry and is incident on the inside surface of the channel at grazing angles in the range $7^{\circ}46'$ — $10^{\circ}48'$, as defined by the dimensions and focal length of the reflector. The multiplier is mounted and potted in a compartment adjacent to the E.H.T. converter supplying the channel voltage (4 KV). Fig. 5.5. shows the converter assembly with the prototype multiplier temporarily in place.

In orbit, the detector has to operate over a period in excess of 100 days, maintaining both a high photon detection efficiency and a low background counting level. The ambient temperature inside the telescope package is expected to remain within the limits, $-45^{\circ}C \rightarrow -15^{\circ}C$.

The Spectral Sensitivity of the Long Wavelength Telescope

Since magnesium fluoride was found to give the most stable photo-emissive surface, it will be used for the telescope channel multiplier. Using the stabilised values of $\chi_{\pi/2}$ given in Fig. 4.10. B, the mean photon detection efficiency of the detector over the angular range in the telescope has been determined. For this purpose a cosec. variation of χ_{θ} was assumed and the mean value of cosec θ obtained graphically. (The effect of X-ray reflection from the surface was considered to be too small to warrant inclusion). The spectral variation of photon detection efficiency is shown in Fig. 5.1.

To increase the energy resolution of this detector, a series of filters was designed. The four filters considered to provide the best spectral dissection in combination with both ease of manufacture and high self-support strength were:

A. 0.75 μ Teflon + 500 Å Aluminium.

B. 2.61 μ Aluminium.

C. 5,500 Å Aluminium.

D. 1.14 μ Polypropylene + 500 Å Aluminium.

Fig. 5.2. displays the calculated transmission characteristics of these filters.

The filters are intended to be used one at a time but in balanced pairs. The spectral dissection attainable in this way is shown in Figs. 5.3. and 5.4. in which values of the product of net photon detection efficiency and mirror reflection coefficient are plotted against wavelength.

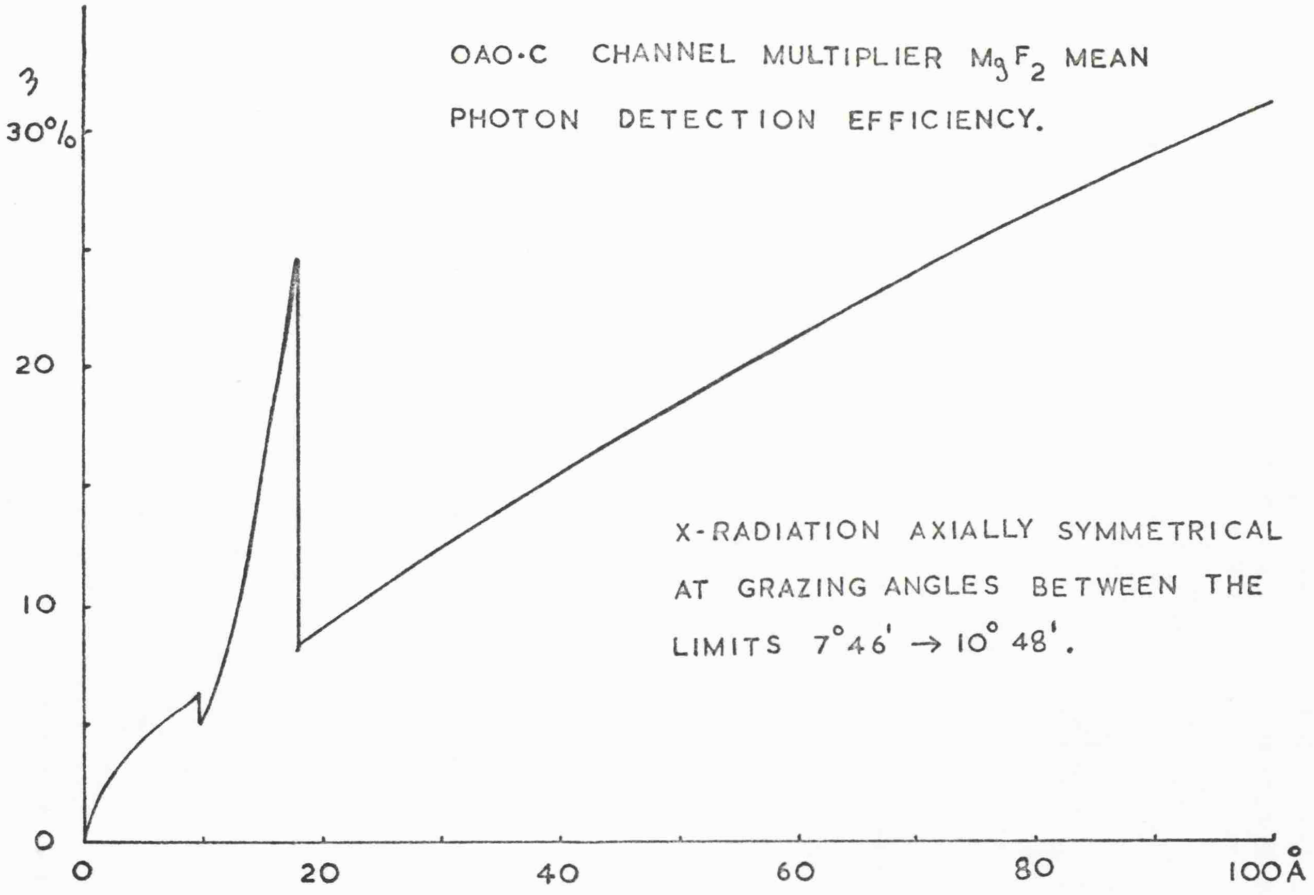
OAO-C CHANNEL MULTIPLIER MgF_2 MEAN
PHOTON DETECTION EFFICIENCY.
X-RADIATION AXIALLY SYMMETRICAL
AT GRAZING ANGLES BETWEEN THE
LIMITS 7°46' → 10° 48'.
30%
20
10
0
0
20
40
60
80
100Å

FIG 5.1

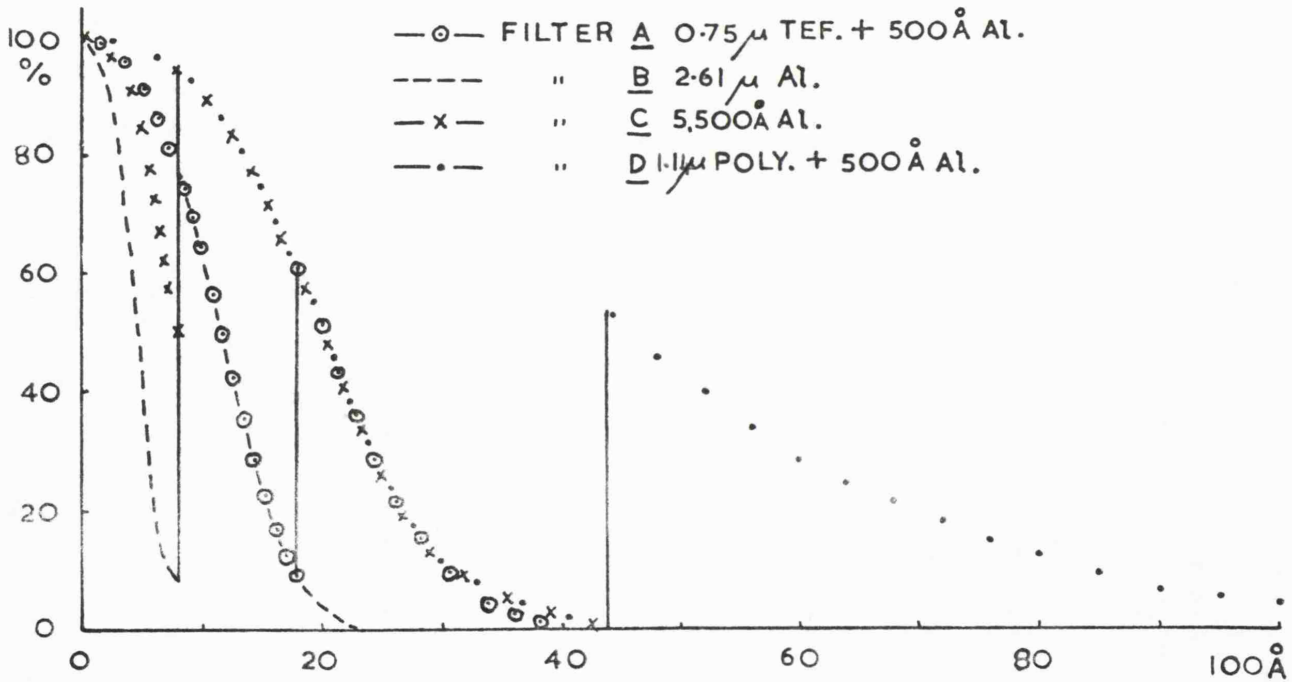

FIG 5.2 OAO-C C.M. FILTER CHARACTERISTICS

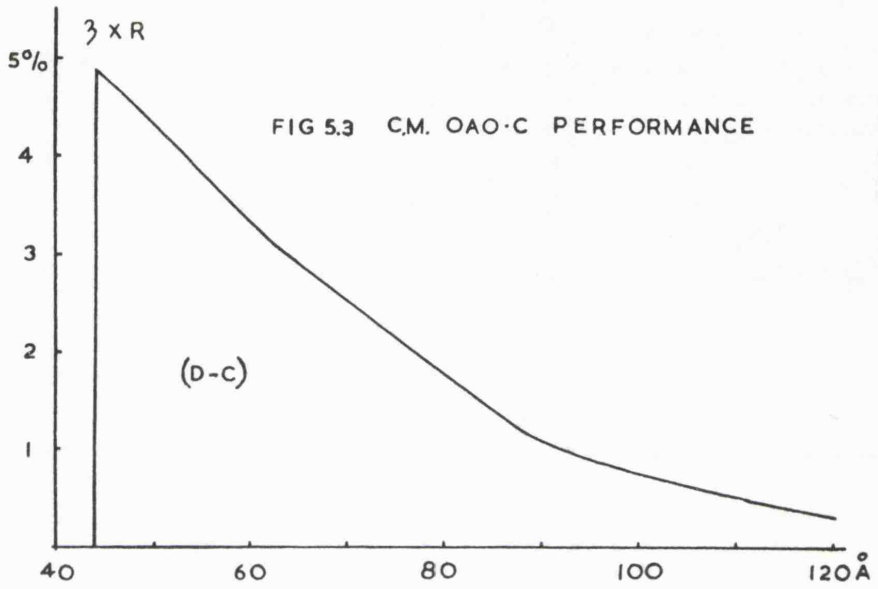

FIG 5.3 C.M. OAO·C PERFORMANCE

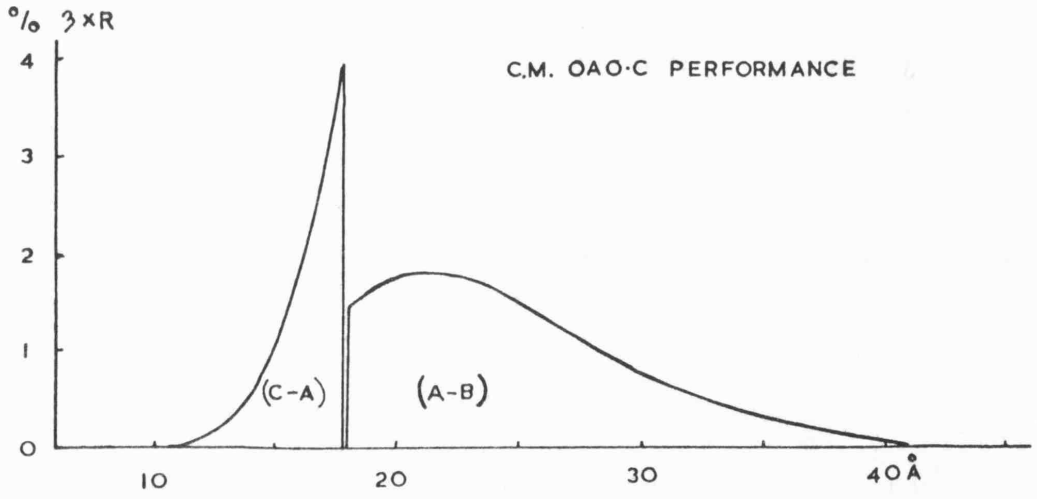

C.M. OAO·C PERFORMANCE

FIG 5·4

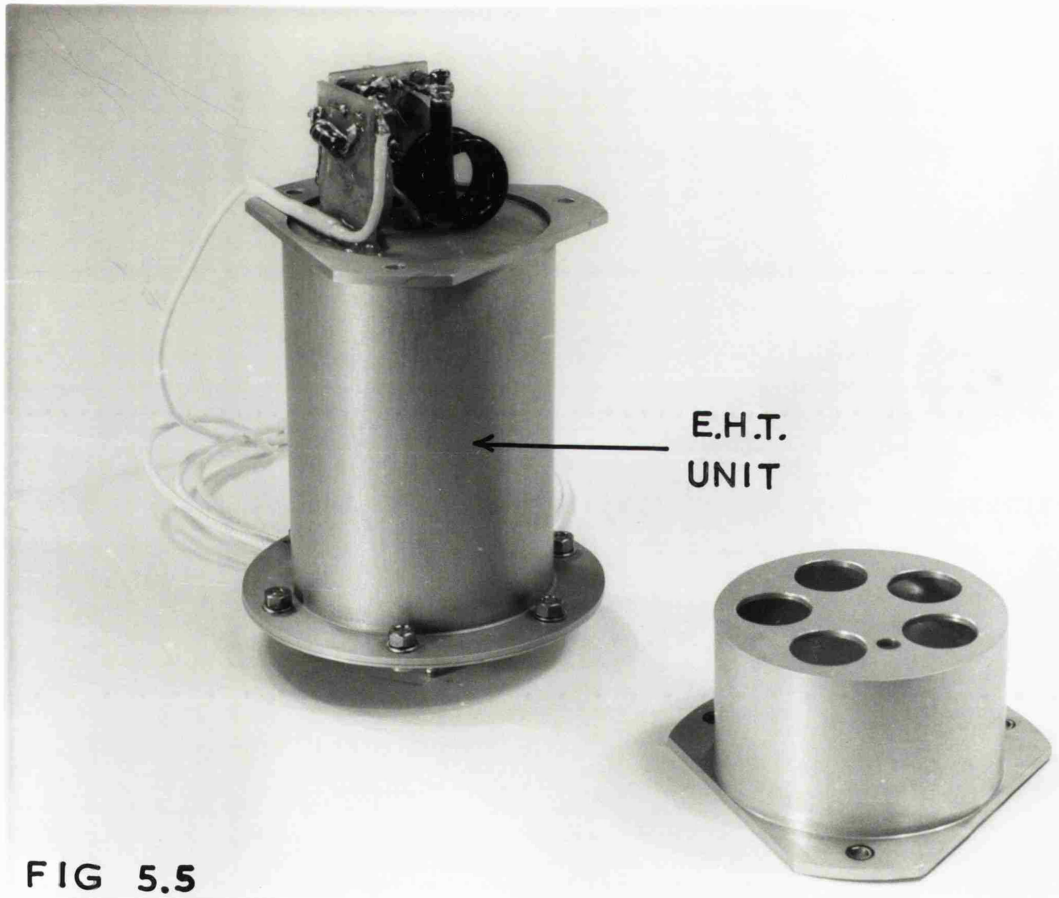

FIG 5.5

The reflection coefficients were based on measurements made on Nickel at 4^{o} at shorter wavelengths (Evatt, 1967). No allowance has been made for the Ni L absorption edge at 14 Å, because of the absence of precise information. The effect of this edge will be a reduced reflection coefficient in the 10 - 14 Å region, which will modify the (C - A) curve.

The plastic filters A and D have been designed, each with a 500 Å layer of aluminium. The purpose of this layer is two-fold; firstly to maintain the filter surface facing the channel multiplier at earth potential, by preventing electrostatic charging, and secondly, to assist in the exclusion of ultra-violet light from the channel multiplier, in the event of appreciable transmission through the plastic. The principal contribution is from resonantly scattered Hydrogen Lyman-Alpha(1216 Å) from the solar corona (see for example Kupperian et al, 1959) but auroral contributions can also be expected (see for example Murcray, . 1966). Normally, the absorption of the much thicker plastic will dominate in this region, but this might not be the case should there be thin flaw regions in the filters. On the basis of the data of Hunter (1964), the optical transmission of 500 Å of aluminium may be estimated at about 1% in the 1,000 – 2,000 Å region. A slightly thicker layer would give a much greater rejection should this be required.

It is to be noted that Nakhodkin and Mel'nik (1964) reported difficulty in using a 5μ filter of aluminium

directly in front of an electron multiplier, owing to the occurrence of exo-electronic emission, even in the absence of X-radiation. This effect was looked for in the present work. Pieces of pure aluminium and of anodised aluminium were placed in turn next to a channel multiplier and subjected to ultra-violet illumination. No signs of afterpulsing, following the cessation of illumination, were obtained. However, since the electron emission is likely to be strongly dependent on the state of the surface of the aluminium, it is clearly desirable that the absence of the effect be confirmed with the integrated experiment.

Shea et al (1967) have reported that the low energy electron interference present in a channel multiplier experiment (measurement of low energy auroral particles) was eliminated by operating the channel apertures at - 55v. with respect to the space-craft structure.

The operating performance of the complete OAO - C experiment.

The performance of the long wavelength channel multiplier telescope is best given in comparison with that of the other telescopes in the experiment. The most efficient way summarising and displaying this information was considered to be the spectral variation of the Noise Equivalent Photon Energy Flux Density. This parameter is the X-ray energy flux density required, at a given wavelength, to produce a count rate equal to the background level of

the appropriate detector (i.e. unity signal to noise ratio).

The counting background level was assumed to be 10^{-2} cps. for all detectors except the 1 - 3 Å counter for which 10^{-1} cps. was assumed. The channel multiplier background level is based on the present work. The proportional counter backgrounds are taken from work carried out at UCL (Sanford and Culhane 1967 and Sanford 1967). An allowance for the reduction in noise attainable from pulse height analysis was made by multiplying each level by the mean fractional pulse height resolution obtainable with the counter. These were taken to be 0.2, 0.33 and 0.5 for the 1 - 3 Å, 3 - 9 Å and 8 - 18 Å counters respectively.

The performance of a proportional counter for the long wavelength telescope was also evaluated for comparison with the channel multiplier detector. The mean pulse height resolution was assumed to be unity in this case.

The extra reflection coefficients for the 3 - 9 Å and 8 - 18 Å reflectors were taken from computed data (ASE, 1967), assuming mean grazing angles of 50' and 70' respectively.

Fig. 5.6. displays the spectral variation of Noise Equivalent Photon Energy Flux Density for the complete experiment.

For the channel multiplier response curve it has been assumed that a single aluminium filter, 500 Å in thickness,

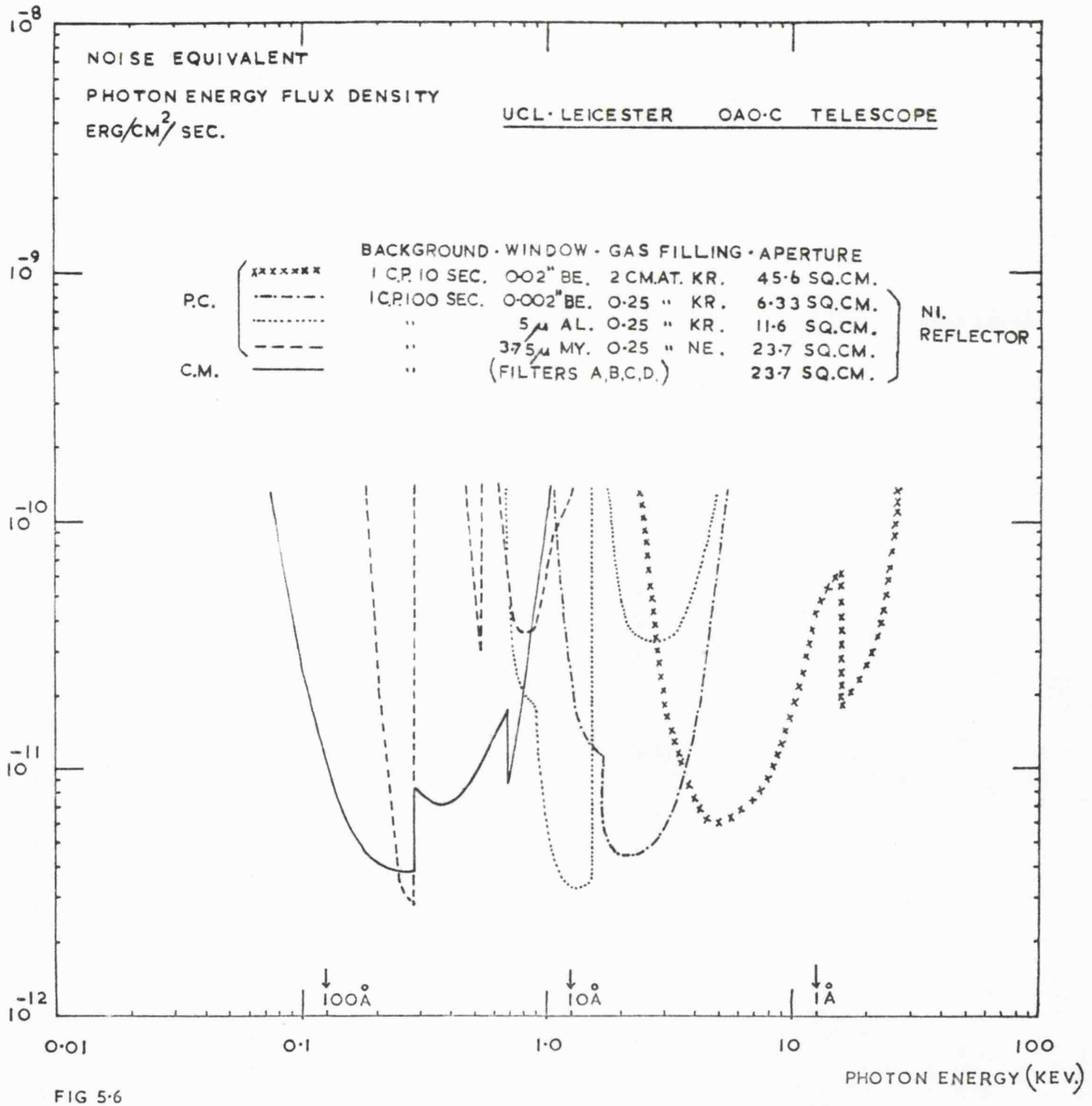
NOISE EQUIVALENT
PHOTON ENERGY FLUX DENSITY
ERG/CM²/SEC.
UCL · LEICESTER OAO·C TELESCOPE
BACKGROUND · WINDOW · GAS FILLING · APERTURE
P.C.
C.M.
1 C.P. 10 SEC. 0·002" BE. 2 CM.AT. KR. 45·6 SQ.CM.
1 C.P. 100 SEC. 0·002" BE. 0·25 " KR. 6·33 SQ.CM.
" 5μ AL. 0·25 " KR. 11·6 SQ.CM.
" 3·75μ MY. 0·25 " NE. 23·7 SQ.CM.
" (FILTERS A,B,C,D.) 23·7 SQ.CM.
NI. REFLECTOR
10⁻⁸
10⁻⁹
10⁻¹⁰
10⁻¹¹
10⁻¹²
100Å
10Å
1Å
0·01
0·1
1·0
10
100
PHOTON ENERGY (KEV.)

FIG 5·6

has been used. This gives the envelope of ultimate sensitivity within which spectral dissection may be carried out with the listed filters, A, B, C and D.

It is seen that, although the peak response of the long wavelength proportional counter is higher in the 44 - 60 Å region, the mean response from 15 - 120 Å is much lower. This becomes clear if the integrated noise levels of the five detectors are determined from Fig. 5.6. For this determination a 'flat' X-ray spectrum has been assumed, i.e. one with a constant photon flux per unit energy interval. This assumption will not be unreasonable over the limited spectral pass-band of each detector taken in turn. The integrated noise levels are given in the third column of Table 5.1.

TABLE 5.1.

Detector	Mean KeV	Noise level- erg/sq.cm/ sec/KeV.	SCO X-1		Source X	
			c.p.s	S/N	c.p.s.	S/N.
1-3Å P.C.	6	7.5×10^{-12}	540	5,400	12.8	128
3-9Å P.C.	2.5	1.1×10^{-11}	100	10,000	0.36	36
8-18Å P.C.	1.2	1.7×10^{-11}	75	7,500	0.11	11
18 Å→P.C.	0.25	8.5×10^{-11}	19*	1,900*	0.05	5.0
18 Å→C.M.	0.30	1.3×10^{-11}	120*	12,000*	0.37	37.

(* 'Flat' spectrum assumed below 1 KeV).

The significance of these noise levels may be examined by considering the response of the experiment to the X-ray source SCO X-1, which has established itself as a reference source in X-ray astronomy. The signal to noise ratio and count rate for each detector have been evaluated

using the compiled data of Gould (1967) and are presented in the fourth and fifth columns of Table 5.1. With the present uncertainty over the nature of the low energy spectrum of SCO X-1, the spectrum has been assumed to be 'flat' below 1 KeV.

Clearly the experiment possesses a useful signal to noise ratio with all the detectors. The channel multiplier complements the proportional counters particularly well and contributes a worthwhile improvement, in comparison with the alternative proportional counter detector for the long wavelength telescope.

The last two columns of Table 5.1. display the operating performance of the telescope for a hypothetical 'Source X', having a flat spectral density of 0.1 photons/sq.cm./sec./KeV. Clearly the signal to noise ratio is still good for the $1 \rightarrow 18$ Å region and for the long wavelength telescope with the channel multiplier detector. The long integration times available with the satellite will enable the signal contrast to be improved at the expense of time resolution (which would only be important in the case of extremely rapid brightness fluctuations).

Diffuse Sources

In the case of non-discrete sources, the performance of the experiment requires a more exact definition, since the X-ray flux collected by the telescope may be partly defined by the field of view of the telescope. The normal fields

of view for the experiment are given in Table 5.2. In the case of the short wavelength proportional counter the field is restricted by means of a collimator in front of the window.

TABLE 5.2.

Detector	Field of view		Diffuse Flux	
	Diameter	Ster.	S/N	N^{-1}
1-3 Å	1°	2.4×10^{-4}	3×10^{-1}	2.5
3-9 Å	10'	6.7×10^{-6}	7×10^{-3}	3.0
8-18 Å	10'	6.7×10^{-6}	6×10^{-3}	3.7
18 Å→P.C.	10'	6.7×10^{-6}	3×10^{-4}*	70*
C.M.	10'	6.7×10^{-6}	2.5×10^{-3}*	9* (Deg.^{2})

(* Diffuse spectrum assumed to be 'flat' below 1 KeV).

The field of view for each detector has been used in conjunction with the data compiled by Gould, for the so-called Diffuse Cosmic X-ray Flux, to predict the signal to noise ratios to be expected from the experiment. These are given in the fourth column of Table 5.2., and show without doubt that the experiment would not be sensitive to such a flux.

However, if the flux is not truly diffuse, i.e. results from a finite number of discrete sources, then these ratios are meaningless.

The performance parameter now chosen for these conditions is N, the maximum sky density of discrete sources, measurable as such, with unity signal to noise, by the telescope. It is assumed that the sources are similar, although these

conditions are unlikely to exist in reality.

Values of N^{-1}, in units of square degrees per source, are given in the fifth column of Table 5.2.; these have been calculated from the integrated noise levels in Table 5.1. and from Gould's compiled data. The values show that the OAO experiment can make a significant contribution to the study of the Diffuse Flux since, regardless of the precise nature of the distribution of the contributing sources (if these exist), the telescopes are sensitive to lesser degree of anisotropy than that detectable by current rocket experiments, which possess fields of view of the order of 100 sq.deg. (See for example Matsuoka, 1966 and Seward et al, 1967).

5.3. The channel multiplier matrix array and a proposed solar emission-line profile spectrometer.

Introduction

A design for a solar X-ray emission-line profile spectrometer has been proposed by the Leicester group. Fig. 5.7. is taken from the proposal submitted to NASA for consideration for the OSO - H Satellite.

The instrument employs an array of planar symmetrical parabolic mirrors plus what is basically a Johansson mounting crystal spectrometer. The detector is essentially a high resolution one-dimensional image dissector, based on a matrix array of channel multipliers. Provision is made for twenty image points (strips in this case), each provided with its own electronics channel.

The primary mode of operation of the instrument is the measurement of the spectral profile of pre-selected emission lines originating in the solar disc. The field of view is restricted to 40 arc, secs. square, to increase the likelihood that the solar region under observation at any one time is homogeneous. This condition is desirable from the point of view of interpreting the results in terms of emission mechanisms.

The minimum wavelength resolution of the instrument is designed to be not less than 3,300. This performance is achieved with a detector channel 20μ in width and a Rowland Circle diameter of 25 cm.

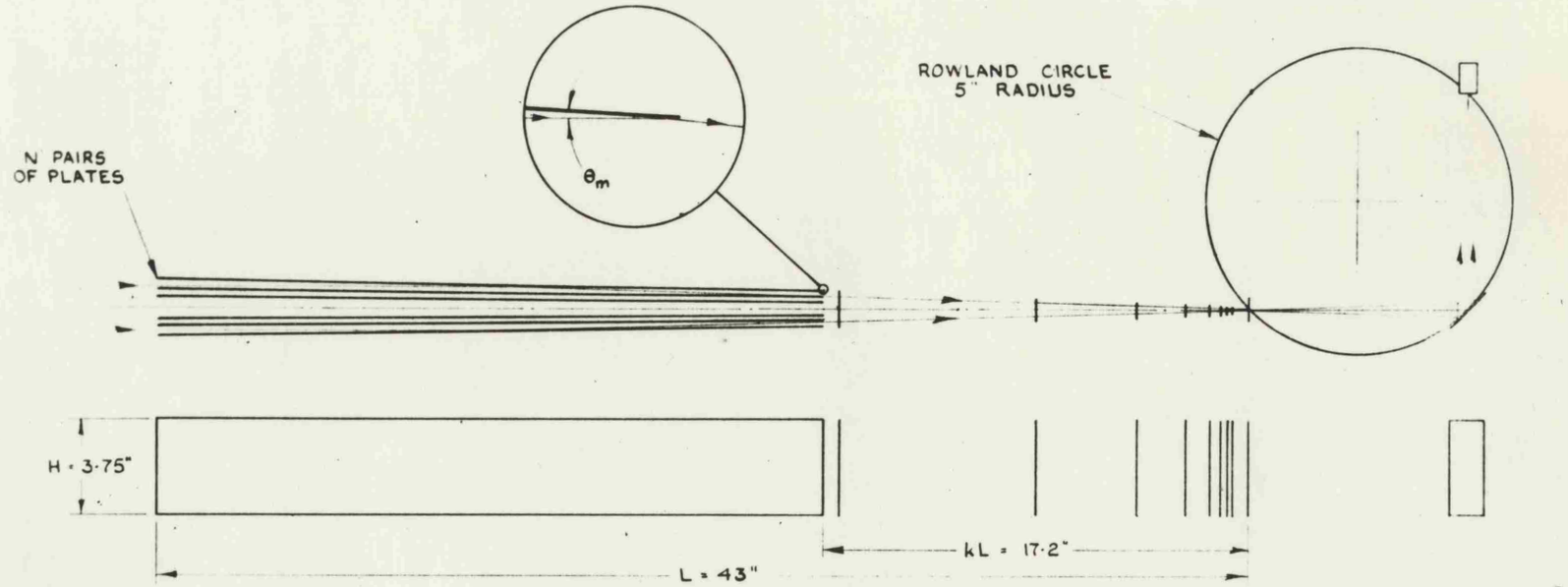
N PAIRS
OF PLATES
θ_m
ROWLAND CIRCLE
5" RADIUS
H = 3·75"
kL = 17·2"
L = 43"

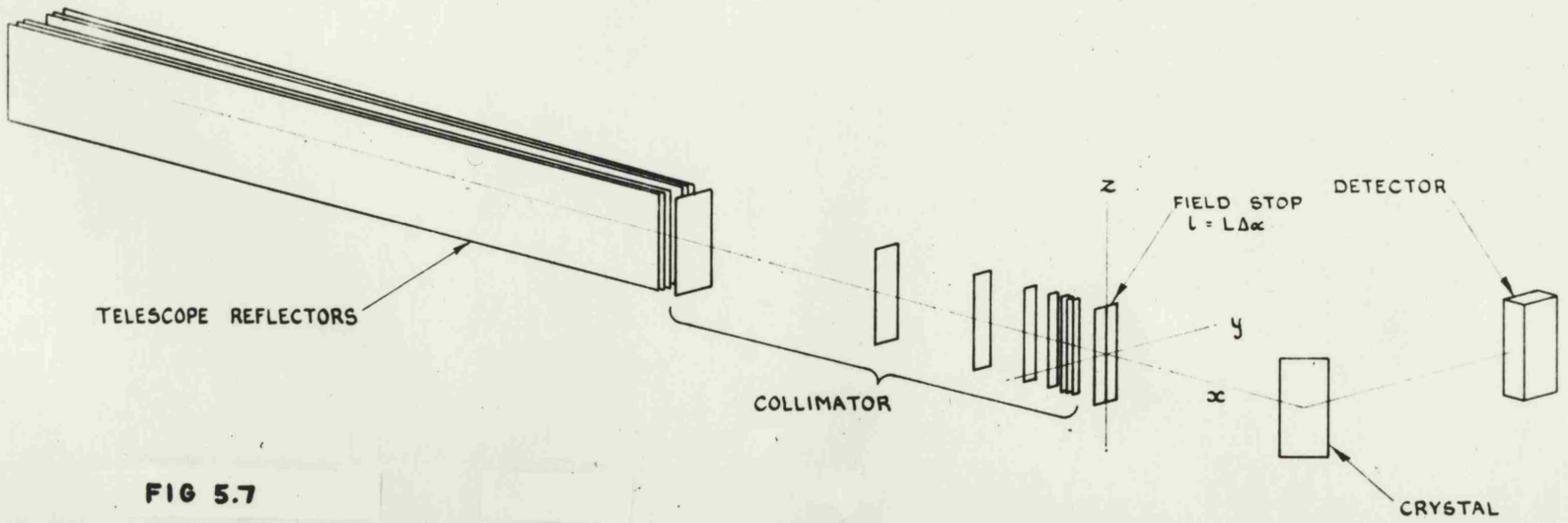
TELESCOPE REFLECTORS
COLLIMATOR
z
FIELD STOP
$l = L\Delta\alpha$
DETECTOR
y
x
CRYSTAL

FIG 5.7

The detector resolution attainable

It was concluded in Section 4.2. that the increase in f.w.h.m. in the linear response profile of Matrix B resulting from factors degrading the intrinsic resolution of the matrix channels, was about 20%. If it is assumed that this degradation does not increase in the case of finer matrices used with narrower collector strips, then 15 μ channels, if available, would be expected to give a resolution of 18 μ . This resolution would just meet the demands of the experiment.

The detector noise level

The background level of Matrix B was measured to be about 50 cps. per sq.cm. (This was equivalent to a flux of 200 44 Å photons per second per sq.cm. at a photon detection efficiency of 24%).

At this level, one detector channel in the line profile spectrometer would have a background of approximately 1 cps. since it occupies an area of 0.02 sq.cm. (10 cm x 20 μ). In terms of equivalent emission line energy, an estimate may be made by assuming reasonable values for the other parameters of the spectrometer. For a total collecting area of 10 sq.cm., a mean mirror reflection coefficient of 10%, a mean crystal reflection coefficient of 10% and a matrix detection efficiency of 5%, the equivalent noise level at 7.5 Å say, amounts to 5×10^{-7} erg/sq.cm./sec. per detector channel. This noise level

would permit the dissection into five channels of an emission line with intensity 10^{-5} erg/sq.cm./sec. at a mean signal to noise ratio of four. Lines of this strength would be expected, on the basis of the measurement at longer wavelengths of Evans and Pounds (1968).

For the observed emission line to be displaced or broadened to twice an intrumental resolution of 3×10^{-4}, it may be seen from Fig. 1.3. that the solar region responsible would need to produce bulk transport velocities of 200 km/sec. or ion temperatures of the order of 2×10^{6}M (where M is the mass of the ion giving the emission line).

Clearly, the limitations imposed by the resolution available in the experiment greatly exceed those due to the intrinsic widths of the emission lines, as discussed in Chapter 1.

In principle, if the transfer function for the spectrometer can be accurately measured, it will be possible to analyse emission lines possessing widths or displacements less than 3.10^{-4}. However, much greater observation times would be necessary for the accumulation of information sufficient to allow spectral 'unfolding' under these conditions.

The accuracy of the intensity calibration of the spectrometer will depend on the method adopted for its measurement. With inaccuracies of $\pm$ 5% in the measurement of the detector efficiency and the crystal and mirror reflection coefficients, it might be

expected that ± 15% could be achieved. However this method would assume a perfect integration of the component parts of the instrument, which is unlikely in view of the sophisticated nature of the experiment. A better calibration could be made by illuminating the instrument with monitored laboratory radiation. In this way, an accuracy of ± 5% could be achieved and integration uncertainties would be included in the measurement. However, the production of a parallel, unpolarised and uniform beam of monochromatic radiation, over even a fraction of the aperture area, will present difficulties. The accuracy with which neighbouring lines can be compared will be much higher, of course since, relatively, the spectrometer parameters will be slowly varying with wavelength. Under these conditions, only anomalous fluctuations in the parameters will degrade intensity comparisons.

5.4. Conclusion to Thesis

This work has shown that the operating characteristics of apparatus for X-ray astronomical experiments can be satisfactorily evaluated in the laboratory with the use of a crystal spectrometer and a proportional counter. If precautions are taken in the preparation and use of thin windows in the counter, it is possible to achieve flux calibrations to better than 10% out to a wavelength of 67 Å.

On the basis of the tests carried out, the channel multiplier appears to be eminently suitable for soft X-ray detection, provided that care is taken to exclude stray particles and radiation. The X-ray response can be explained in terms of a composite photocathode model and the established angular variation of photoelectric yield. Where possible, the reduced normal incidence yields have been compared with those measured for the same materials by other methods and shown to be in reasonable agreement.

The channel multiplier detector developed for the OAO - C experiment compares favourably with the nearest equivalent proportional counter in terms of noise and spectral sensitivity. (This counter must possess a window equivalent to a maximum of 3.75 μ Melinex to achieve the necessary sensitivity). On the basis of the present work, the channel multiplier detector has a greater operating stability than has been established for such a proportional counter under satellite-like conditions.

A brief analysis of the operating performance of the complete OAO - C experiment has demonstrated that useful X-ray astronomical investigations can be carried out. Compared with current experiments, the OAO - C experiment will allow greatly increased observation times in the case of rockets, and an improved signal to noise ratio in the case of conventional large-area detectors in both rockets and satellites.

With regard to the X-ray use of channel multiplier arrays, it has been shown that high detection efficiencies and good spatial resolution can be obtained in the pulse mode of operation.

In the case of a proposed design for a solar X-ray spectrometer, it has been shown that the intrinsic widths of the solar emission lines are small, compared with the spectral design resolution of the instrument. The measured noise levels of two channel multiplier arrays show that the proposed spectrometer will have adequate photon detection efficiency. If channel multipliers sufficiently small can be manufactured and set up to give the required detector resolution, then the instrument will enable important advances to be made in the fields of solar and plasma physics. Tousey (1967), in commenting on the need to observe solar regions of the same type, has remarked that 'great instruments must be assembled in orbit'. This spectrometer design shows that the instruments can be quite small in the X-ray region.

With regard to the continuation of this work three topics stand-out in particular.

1. It is recommended that future flux measurements be made with a counter of the type described in Chapter 3, but modified with a demountable window assembly to obviate the need for the use of a window sample.
2. A thorough investigation of the dependence of the X-ray photo-electric yield on surface conditions is required to allow the long-term stability of a photo-cathode to be determined under conditions of atmospheric storage followed by U.H.V. operation, as in the case of a satellite experiment.
3. There is a need for an investigation into the after-pulsing in arrays of channel multipliers. Such an investigation could be undertaken, for example, with either a pulsed source of X-rays or an amplifier having a controllable and accurately known dead-time.

Appendix 1. The correction for the curvature in the channel multiplier monitor proportional counter window.

Because of appreciable curvature, the compensation given by the flat window material sample will be inadequate.

For the purpose of estimating the necessary correction, the window has been assumed to be spherical of radius r, as shown in Fig. AP. 1. The window transmission factor for radiation parallel to, and at a distance y from, the window axis is given by: $e^{-\mu t_y}$.

Where t_y is the window thickness parallel to the axis.

This may be re-written as

$$e^{-\mu t_w \cos\theta^{-1}}$$

$$= e^{-\mu t_w (1-y^2/r^2)^{1/2}}$$

Where t_w is the actual window thickness.

Thus, the total flux transmitted by the whole window of radius a is proportional to

$$\int_0^a e^{-\mu t_w (1-y^2/r^2)^{-1/2}} . y . dy \qquad (1)$$

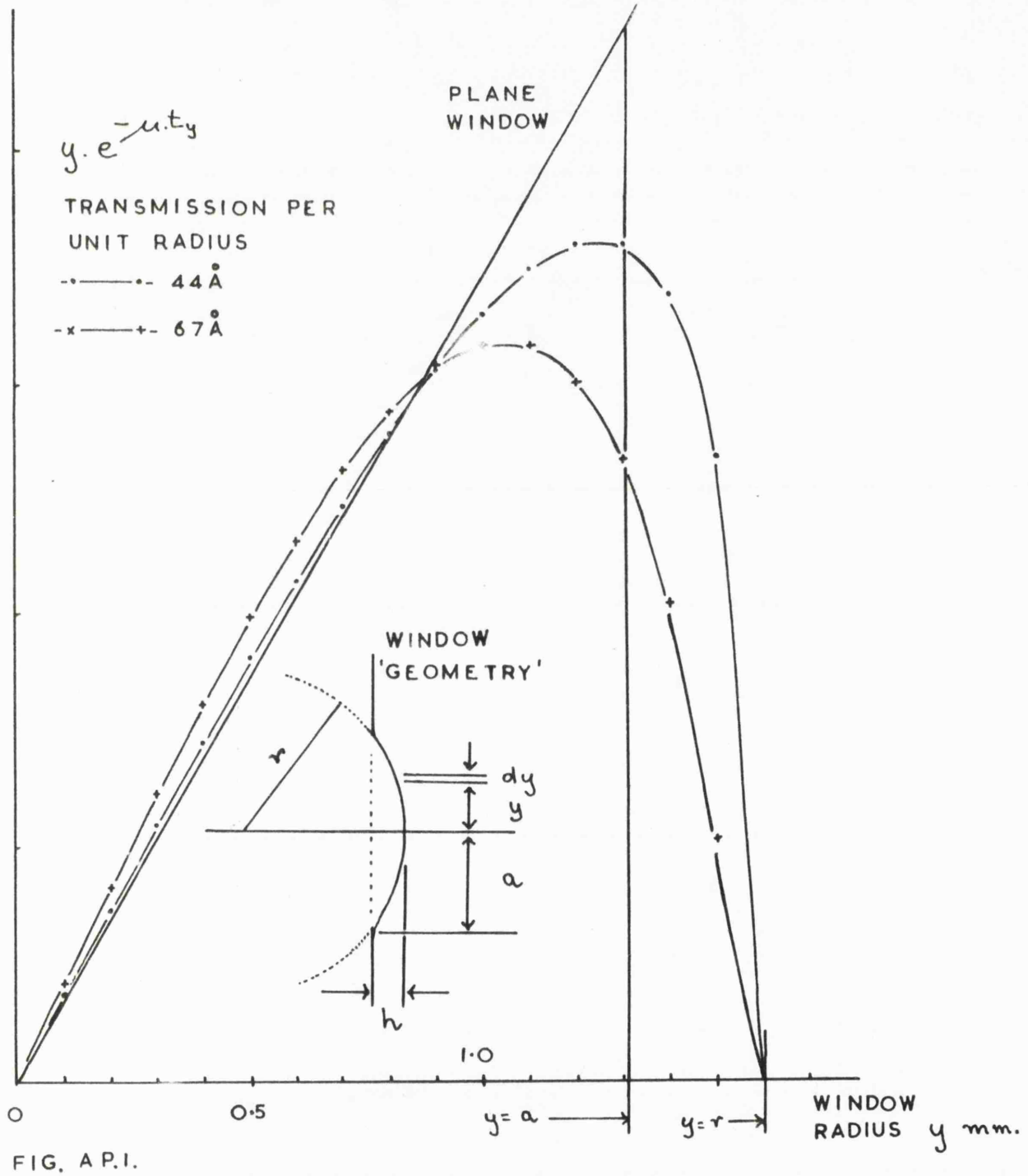
$y.e^{-\mu.t_y}$
TRANSMISSION PER
UNIT RADIUS
44Å
67Å
PLANE
WINDOW
WINDOW
'GEOMETRY'
r
dy
y
a
h
1·0
0
0·5
y = a
y = r
WINDOW
RADIUS y mm.

FIG. A P.I.

The equivalent expression for the plane sample is simply

$$\int_0^a e^{-\mu t_s} \cdot y \cdot dy \qquad (2)$$

Where t_s is now the actual thickness of the sample.

The ratio t_s/t_w is set by the extent to which the window has increased its area during stretching. This was estimated to be 0.577, on the assumption that, during stretching, the volume of the window material remained constant.

From measurements with a travelling microscope it was found that h = 0.68 mm. and a = 1.31 mm. (whence r = 1.60 mm.)

The window correction is given by the ratio of quantities (1) and (2) integrated out to y = a (= 1.31 mm.)

This is the ratio of the areas of the sample curves plotted out in Fig. AP. 1. for 44 Å ($e^{-\mu t_s} = 0.50$) and for 67 Å ($e^{-\mu t_s} = 0.18$.)

The corrections are as follows:

67 Å	6%
44 Å	3%
14.6 Å	3%
< 10 Å	< 1%

i.e. The monitor counter counted low by these amounts as a result of the curvature in the window.

Appendix 2. The X-ray photo-electric response of a cylindrical channel multiplier.

In this analysis the X-ray beam incident on the channel is assumed to be uniform and parallel with a flux density N. photons/sq.cm./sec. (In practice there was a divergence of approximately $\pm 2^{o}$ across the aperture of the channel multiplier).

At a given angle of incidence, θ , the illuminated portion of the inside surface of the channel is assumed to become the X-ray photo cathode.

The (grazing) angle of incidence, α , of the radiation on the photocathode varies over a range $o \rightarrow \theta$ (See Fig. AP. 2). To sum the contributions of the different photocathode regions, the channel is divided up into paraxial strips each making an angle ψ with, and subtending an angle $d\psi$ at, the channel axis.

The area of each strip is given by:

$$dA = r.d\psi.2r.\cos\psi/\tan\theta \qquad (1)$$

Where $2r$ is the bore of the channel.

The count-rate from each strip is given by:

$$dn = N.dA.\sin\alpha.\chi_{\alpha} \qquad (2)$$

Where χ_{α} is the external photoelectric yield at angle α .

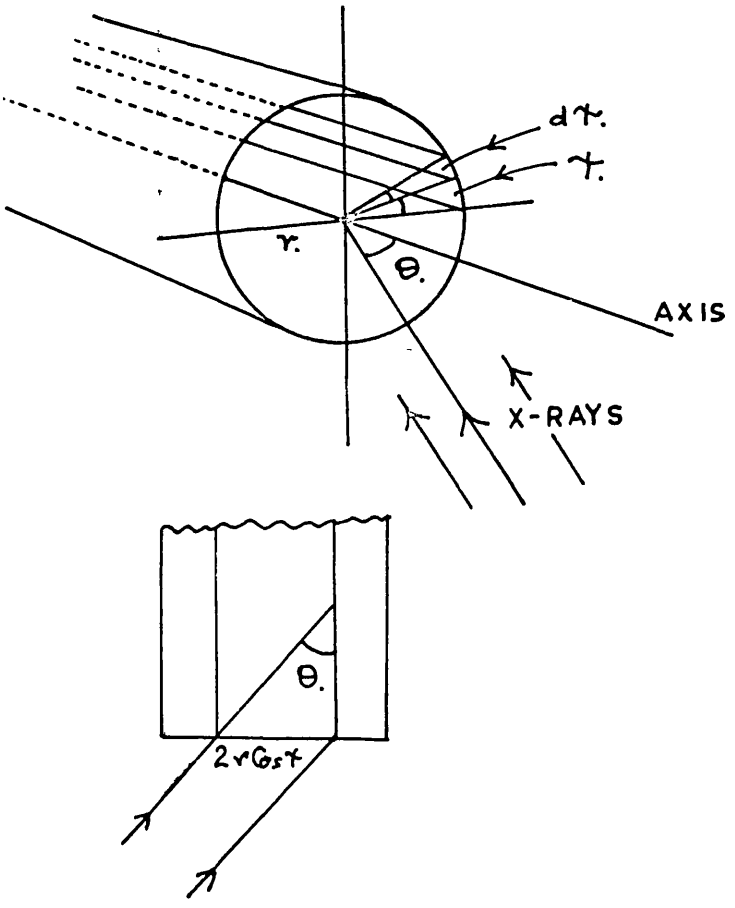

FIG. AP.2.

The total count-rate for the whole channel is given by:

$$n = \int_{-\psi_{max}}^{+\psi_{max}} .dn = 2\int_{o}^{\psi_{max}} .dn \qquad (3)$$

Where, at ψ_{max}, reflection losses reduce dn to zero. It is therefore assumed that this occurs for $\alpha = \theta_c$, the critical-angle at the X-ray wavelength of operation.

(The X-ray reflection coefficient is assumed to be zero for $\alpha > \theta_c$ and unity for $\alpha < \theta_c$).

From (1), (2) and (3):

$$n = N.4r^2.\cot\theta.\int_{o}^{\psi_{max}} \chi_\alpha.\sin\alpha.\cos\psi.d\psi$$

If the variable is now changed from ψ to α this expression becomes, using $\cos\psi = \sin\alpha/\sin\theta$,

$$n = N.4r^2.\frac{\cot\theta}{\sin\theta}.\int_{\theta_c}^{\theta} \frac{\chi_\alpha.\sin^2\alpha.\cos\alpha.d\alpha}{\sqrt{\sin^2\theta - \sin^2\alpha}}$$

Further reduction of this expression is only possible if the variation of χ_α with α is known. For the case in which $\chi_\alpha = \chi_{\pi/2}.\operatorname{cosec}\alpha$ we have:

$$n = \frac{N.4r^2.\chi_{\pi/2}}{\tan\theta.\sin\theta}.\int_{\theta_c}^{\theta} \frac{\sin\alpha.\cos\alpha.d\alpha}{\sqrt{\sin^2\theta - \sin^2\alpha}}$$

Whence

$$n = N.4r^2.\chi_{\pi/2}.\cot\theta.\left[1-\sin^2\theta_c/\sin^2\theta\right]^{1/2}$$

Appendix 3. A method for the (simultaneous) extraction of the image information from a channel multiplier array.

In the case of the emission line-profile spectrometer outlined in Chapter 5, it was possible to employ a separate pulse amplification and counting system for each channel of dissection, since there were only 20 of these present. In general however, the cost of doing this will be prohibitively high and an alternative method for extracting the information must be used.

There are several ways of achieving this via image conversion, storage and electron-beam scanning.

However, every stage of conversion will result in degradations in the image signal/noise ratios and, in this respect alone, there would seem to be an advantage in detecting the channel multiplier electron pulses directly.

In the method outlined below, which is believed to be original in the form described, the pulses are detected electronically without image conversion.

The method employs analogue pulse division to amplitude-code the output pulses according to their dissection channel of origin.

The dissection channels from n = 1 to n = N-1 are capacitively coupled, as shown in Fig. AP.3.1., either

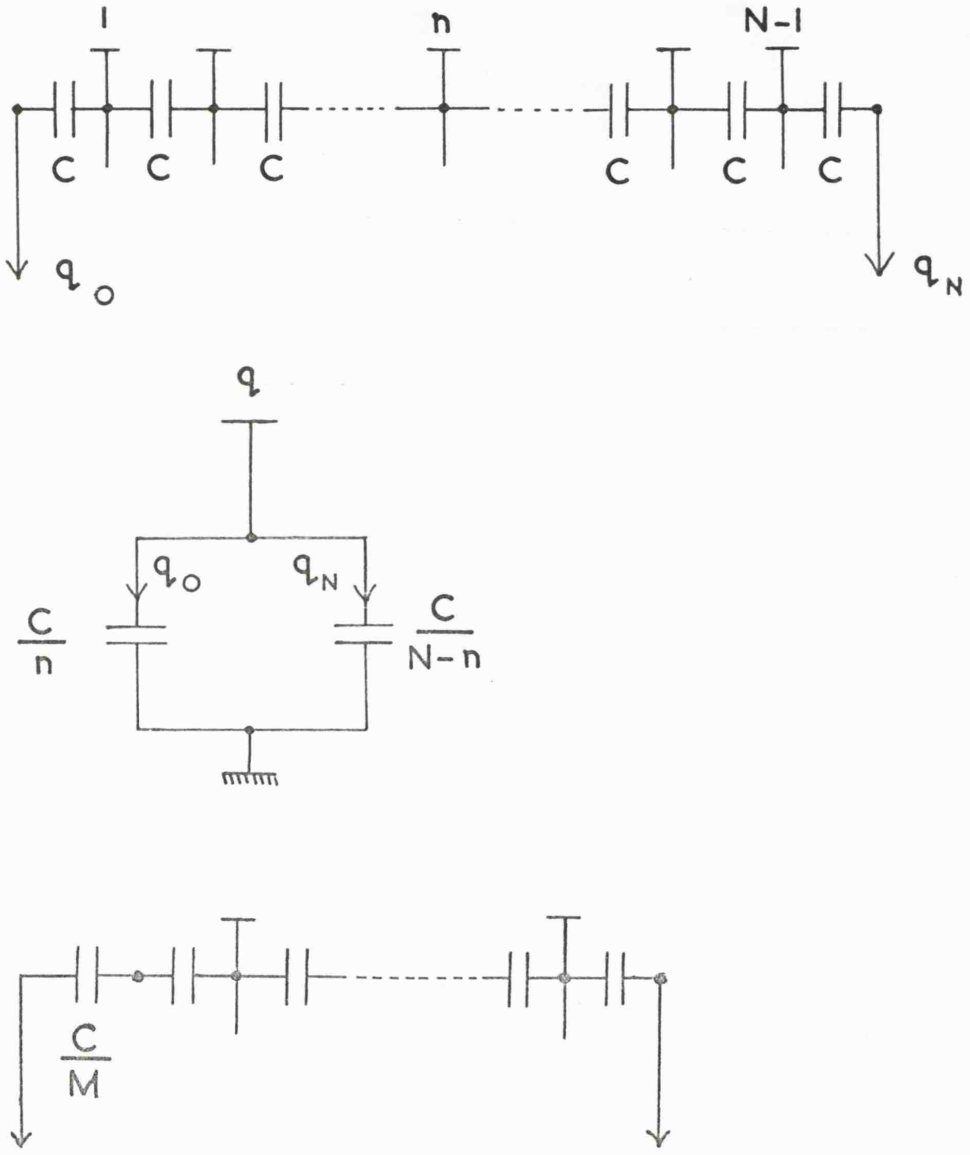

Fig. AP.3.1

by the natural capacitance existing between consecutive channels or, if this is insufficient, by external capacitors. This capacitive chain is terminated at each end with a low noise, high input capacitance, charge-sensitive amplifier. The two amplifiers detect the branching components, q_o and q_N, of the pulse q arising at the nth channel ($q=q_o+q_N$).

It can be easily shown that:

$$n/N = q_N/q_o+q_N$$

Thus a pulse of amplitude n/N could be produced by electronically obtaining the quotient q_N/q_o+q_N.

Fig. AP.3.2. shows how this would be carried out with the established logarithmic operational method.
Stage 1. Consists of the two low-noise charge amplifiers.
Stage 2. Forms Log q_o and Log q_N.
Stage 3. Forms (Log q_N- Log(q_o+q_N)).
Stage 4. Forms q_N/q_o+q_N.

The quotient pulse is recorded with a multichannel analyzer which therefore accumulates and stores the image information, photon by photon. No image information is lost, within the system live time limitation.

Fig. AP.3.3 shows the results obtained experimentally with a chain of 12 x 1,000pF capacitors, two Tennelec amplifiers and an Ortec pulser. The pulse amplitudes were measured with an oscilloscope and divided manually.

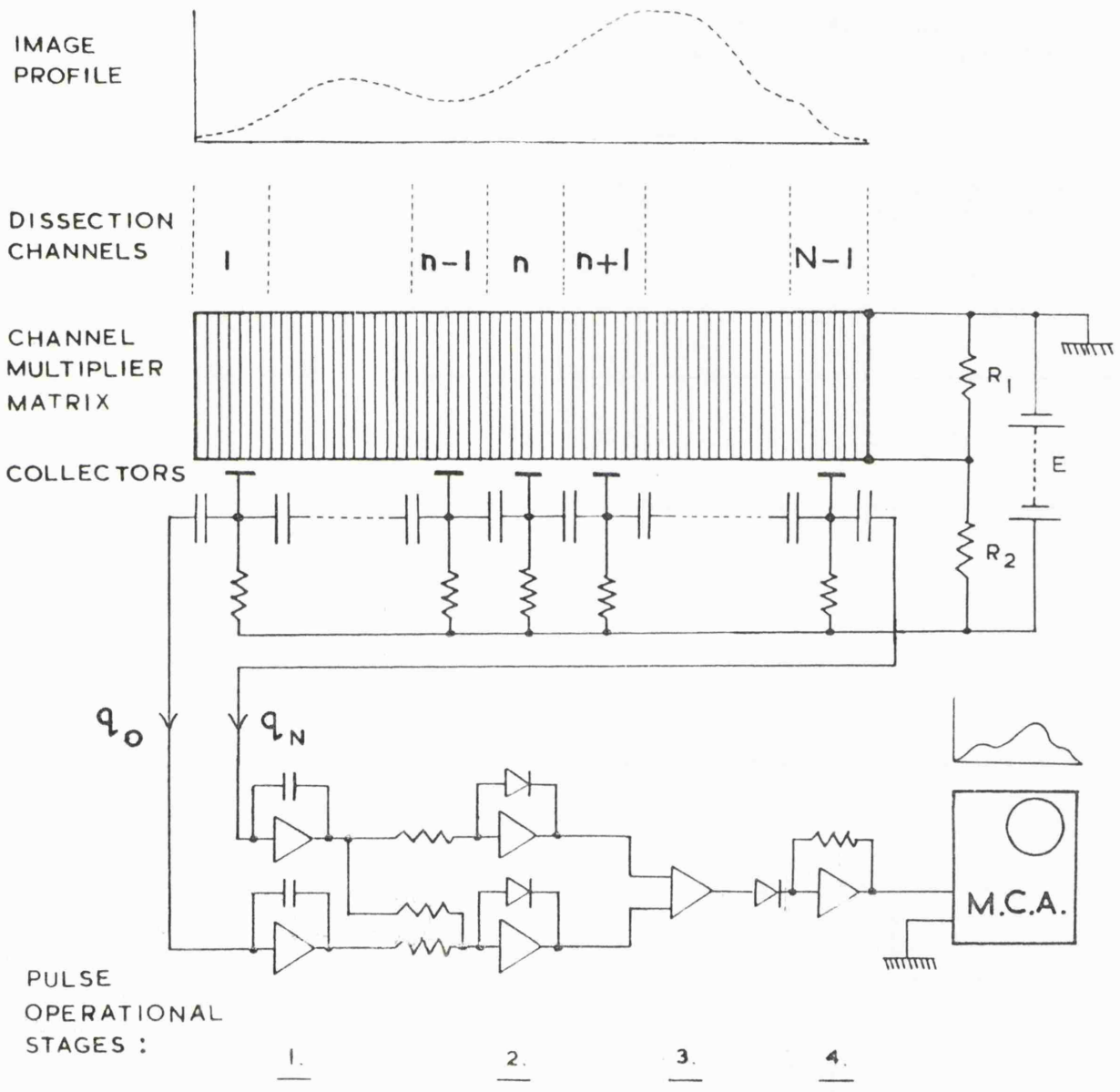
IMAGE
PROFILE
DISSECTION
CHANNELS
1
n-1
n
n+1
N-1
CHANNEL
MULTIPLIER
MATRIX
COLLECTORS
R1
E
R2
q0
qN
M.C.A.
PULSE
OPERATIONAL
STAGES :
1.
2.
3.
4.

Fig. AP. 3.2

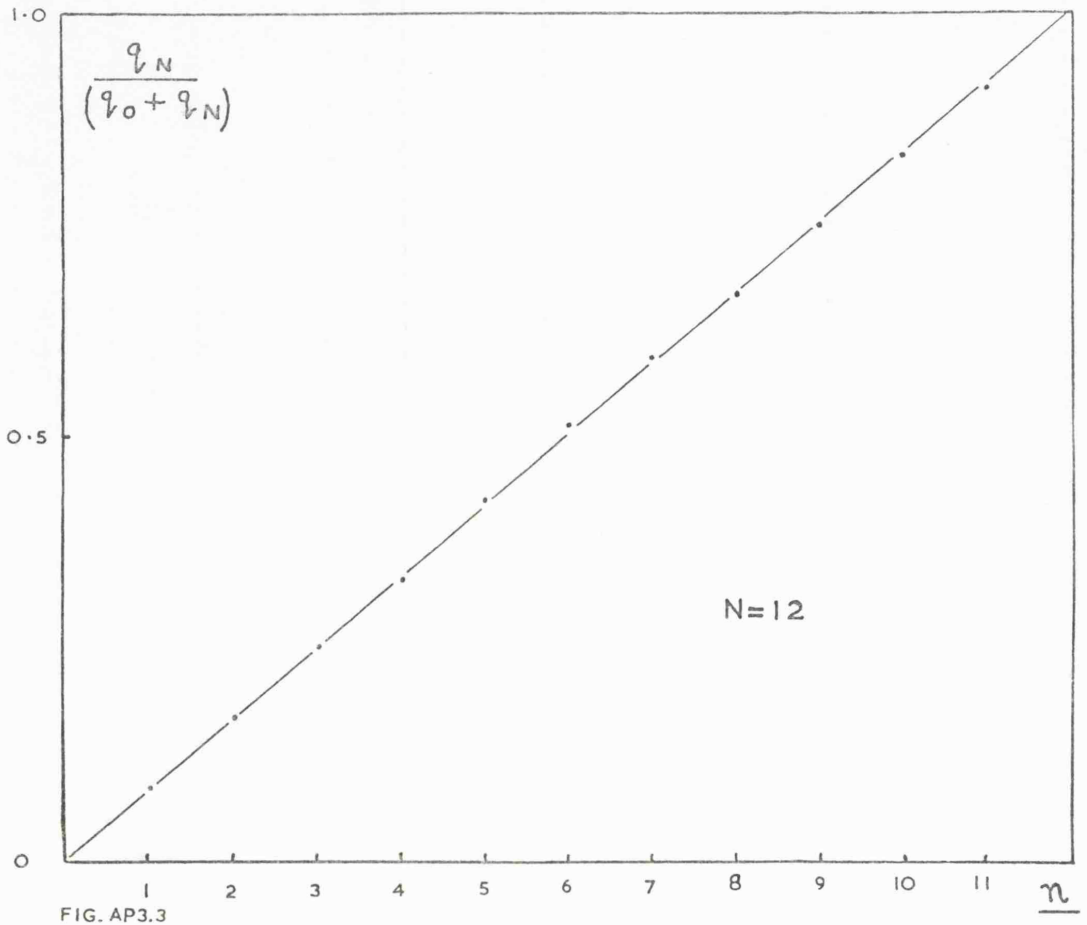

FIG. AP3.3

The amplitude dynamic range demanded of the electronics system can be decreased by employing a number of redundant channels at the n = 0 end of the chain. These could be M virtual channel, as represented by a fixed capacitor, of value C/M , added in series with the chain.

In the particular case of a field of point images, the method could be used for 2-dimensional dissection by rotating the detector with respect to the image. The position-coordinate of each point image will then vary sinusoidally with time. From a record of this variation, it will be possible to determine the location and intensity of each image point.

Appendix 4. The limitations imposed on electronic charge detection by electrical noise.

1. Shot Noise.

This noise will arise whenever the electron current consists of independently emitted electrons. This will occur as a result of the presence of the potential barrier in any solid-state detector.

The mean-square charge fluctuation arising at the input terminals of the pulse amplifier will be given by

$$\overline{q^2} = 2eI.\frac{dw.\ R^2C^2}{2\pi(1+w^2C^2R^2)}$$

(See Gillespie p. 32).

Where e = Electronic charge

I = Detector current

dw = Amplifier Bandwidth increment

R, C = Total shunt resistance and capacitance at input.

In a given charge amplifier, the total noise over all frequencies will be defined by the transmission characteristics of the pulse-shaping filter networks. Then,

$$\overline{q^2} = \frac{eI}{\pi}\int_0^{\infty} \frac{R^2C^2 \cdot w^2T_1^2 \cdot dw}{(1+w^2C^2R^2)(1+w^2T_1^2)(1+w^2T_2^2)}$$

Where T_1, and T_2 are the amplifier single-differentiating and single-integrating time-constants. Whence,

$$\overline{q^2} = \frac{eI}{2}.\frac{T_1^2R^2C^2}{(T_1+T_2)(RC+T_1)(RC+T_2)}$$

Under normal conditions $RC \gg T_1 = T_2$
(Time constants made equal for noise minimisation) and this expression reduces to:-

$$\overline{q^2} = e\, I\, T_2/4$$

e.g. For T_2 = 1μs and if pulses of 1000 electrons to be detected then q must not be greater than 200 electrons. Therefore I must be less than 25 nA.

2. Thermal Noise.

The mean square fluctuation in a bandwidth dw is now given by:

$$\overline{q^2} = \frac{4kT.\ RC^2\ .dw}{(1+w^2R^2C^2)2\pi}$$

Where T_{input} is the temperature of the detector and amplifier and k is Boltzmann's Constant.

After pulse shaping, the total noise over all frequencies is given, as before, by:

$$\overline{q^2} = \frac{2kT}{\pi R}\int_0^\infty \frac{R^2C^2}{(1+w^2C^2R^2)}\cdot\frac{w^2T_1^2}{(1+w^2T_1^2)(1+w^2T_2^2)}\cdot dw$$

whence,

$$\overline{q^2} = \frac{kT.T_1^2RC^2}{(T_1+T_2)(RC+T_1)(RC+T_2)}$$

For $RC \gg T_1 = T_2$,

$$\overline{q^2} = \frac{kT}{2}.\frac{T_2}{R}$$

e.g. For $T_2 = 1\mu s$ and $R = 10^6 \Omega$

$q = 280$ electrons, for $T = 293^{\circ}K$

and $q = 144$ electrons, for $T = 77^{\circ}$ K (LN_2).

References:

Adams, J., Manley, B.W., (1965) Electronic Engineering 37, 180 - 1.

Adams, J., Manley, B.W., (1966) IEEE Trans. N.S. 13, 3, 88 - 89.

Adams, J. (1967) Private Communication.

Adlam, J.H., Burcham, J.N., (1966), J. Sci. Insts., 43, 93 - 6.

Aitken, D.W., Marcum, A.I., and Zulliger, H.R., (1966) IEEE Trans., N.S. 13, 1, 287 - 96.

Aitken, D.W., Beron, B.L., Yenicay, G., and Zulliger,H.R., (1967) IEEE Trans., N.S. 14, 1, 468 - 78.

Alkhazov,G.D.,Komar,A.P., Vorob'ev,A.A., (1967),Nuclear Insts. and Methods, 48, 1 - 12.

Allen, J.S., (1947) Rev. Sci. Insts., 18, 739.

Aller, L.H. (1961)"Abundance of the Elements", Interscience Publishers Inc., New York.

Anderton, H.J., (1966) Advances in Electronics and Electronic Physics 22 B, 919 - 925.

A. S. E. (1967)"Report on the development programme of grazing incidence X-ray optics", 1967. American Science and Engineering, Cambridge, Mass.

Atkinson, P.A., Pounds, K.A., (1964) Journal of Photographic Science. 12.

Bathow, G., Freytag, E., Haensel, R., (1966) J. App. Phys. 37, 9, 3449 - 54.

Bearden, A.J. (1959) Bull. Am. Phys. Soc. 4, 2, 66 - 7.

Bearden, A.J., (1966) J. App. Phys., 37, 4, 1681 - 92.

Bell D.A. (1960) "Electrical Noise," Van Nostrand Co. Ltd.

Bethe, H.A., Salpeter, E.E., "Quantum Mechanics of One and Two Electron Atoms." Springer, Berlin, 1957.

Beyer, R.R., Green, M., Goetze, G.W., (1966) Advances in Electronics and Electronic Physics, 22A, 251 - 60.

Blake, R.L., Chubb, T.A., Friedman, H., Unzicker, A.E., (1964) Science, 146, 3647, 1037 - 8.

Blake, R.L., House, L.L., (1967) Ap. J. Letters, 148, L33 - 35.

Blodgett, K.E. and Langmuir, I. (1937) Phys. Rev. (51) 96.

Bowles, J.A., Culhane, J.L., Sanford, P.W., Shaw, M.L., Cooke, B.A., Pounds, K.A., (1967) Plan. Space. Sci. 15, 931 - 5.

Bowyer, S., Byram, E.T., Chubb, T.A., Friedman, H. (1964) Nature 201, 1307 - 8.

Bowyer, S., Byram, E.T., Chubb, T.A., Friedman, H. (1965 a) Science 146, 912.

Bowyer, S., Byram, E.T., Chubb, T.A., Friedman, H. (1965 b) Annales d'Astrophysique, 28, 4, 791.

Boyd, R.L.F., (1965) Space Science Reviews, 4, 1, 35.

Bryant, D.A., Johnstone, A.D., (1965) Rev. Sci. Insts. 36, 1662.

Burbidge, G.R., Gould, R.J., Tucker, W.H. (1965) Phys. Rev. Letters. 14, 289 - 92.

Burgess, A. (1964) Ap. J. 139, 776.

Burgess, A. (1965) Ap. J. 141, 1588.

Burkhalter, P.G., Brown, J.D., Myklehurst, R.L., (1966) Rev. Sci. Insts. 37, 9, 1267 - 8.

Burnight, T.R., (1949) Phys. Rev. 76, 165.

Byrne, J. (1962) Proc. Roy. Soc. Ed. 66 A, 33 - 51.

Cameron, A.G.W. (1959) Ap. J. 129, 676.

Campion (1960) "Metrology of Radio Nuclides, I.A.E.A. Vienna p. 6.

Caruso, A.J., Neupert, W.M., (1965) App. Optics, 4, 247 - 51.

Charalambus, St., Theodossiou, A., (1965) Nuclear Insts. and Methods 36, 331 - 2.

Charles, M.W. (1967) Private Communication.

Chevalier, P., Nussli, J., (1967 a) Comptes Rendus B, 264, 6, 462 - 6.

Chevalier, P., (1967 b) Nuclear Insts. and Methods 50, 2, 346 - 8.

Chodil, G., Mark, H., Rodrigues, R., Seward, F.D., Swift, C.D., (1967) Paper submitted for publication in Ap. J. University of California, Livermore Preprint UCRL - 70335.

Cooke, B.A., Stewardson, E.A., (1964), Brit. J. Appl. Phys., 15, 1315 - 19.

Culhane, J.L., Herring, J., Sanford, P.W., O'Shea, G., Phillips, R.D., (1966), J. Sci. Insts. 43, 12, 908 - 912.

Culhane, J.L. (1966) Thesis, unpublished. U.C. London.

Curran, S.C., Angus, J., Cockcroft, A.L., (1949)
Phil. Mag. 40, 929.

Dawber, K.R. (1960) Rev. Sci. Insts. 31, 210 - 11.

Day,R.B., Dearnaly, G. and Palms, J.M. (1966) 13th
Nuclear Science Symposium, Boston, Oct. 19 - 21,1966.

Denisov, E.P., Shchemelev, V.N., Mezhevich, A.N., Rumsh,
M.A., (1965). Soviet Physics Solid State. 6, 9,
2047 - 50.

Dolan, J.F. (1967) Space Science Reviews, 6, 5, 579 - 600.

Drexler, G., Perzl, F., (1967 a) Nuclear Insts. and Method,
48, 2, 332 - 5.

Drexler, G., Perzl, F., (1967 b) Atompraxis 13, 4/5,
185 - 7.

Eliseenko, L.G., Shchemelev, V.N., Rumsh, M.A., (1965)
Sov. Phys. Solid. State., 6, 12, 2973 - 4.

Efremov, A.I., Podmoshenskii, A.L., Efimov, O.N.,
Lebedev, A.A., (1962) Planet. Space. Sci. 9,
987 - 92.

Evans, D.S., (1965 a), IEEE. Trans., N.S. 12, 34 - 8.

Evans, D.S., (1965 b) Rev. Sci. Insts. 36, 3, 375 - 82.

Evans, K., Pounds, K.A., Culhane, J.L. (1967)
Nature 214, 41.

Evans, K., Pounds, K.A. (1968) Ap. J (April).

Evans, R.D. (1955) "The Atomic Nucleus". McGraw Hill.

Evatt H.R., (1967) Private Communication.

Fairstein, E., (1961) IRE Trans., N.S. 8, 129.

Fairstein, E., (1962), Nucleonics, 20, 8, 148 - 9.

Fano, U. (1947) Phys. Rev. 72, 26 - 9.

Felten, J.E., Morrison, P. (1963) Phys. Rev. Letters. 10, 10, 453 - 7.

Felten, J.E., Morrison, P. (1966) Ap. J., 146, 3, 686 - 708.

Felten, J.E., Gould, R.J. (1966) Phys. Rev. Letters., 17, 7, 401 - 5.

Felten, J.E. (1967) Nature, 216, 5117, 775 - 6.

Finn, R., Manley, O.P., Ouellette, G. (1966) Report 2017. A.S. and E. Corp., Cambridge, Mass.

Franks, J., (1961) A.E.I. Engineering, February, 1961, 71 - 5.

Frerichs, R., (1950) J. App. Phys. 21, 4, 312 - 7.

Friedman, H., Byram, E.T., Chubb, T.A., (1967) Science 156, 374 - 8.

Ganeev, A.S., and Izrailev, I.M., (1962) Soviet Physics Technical Physics 6, 270 - 4.

Giacconi, R., Gursky, H., Paolini, F.R., Rossi, B.B. (1962) Phys. Rev. Letters,9, 11, 439 - 43.

Giacconi, R., Gursky, H. (1965) Space Science Reviews.4.

Giacconi, R., Reidy, W.P., Zehnpfennig, T., Lindsay, J.C., Muney, W.S., (1965) Ap. J., 142, 3.

Giacconi, R., Gorenstein, P., Gursky, H., Waters, J.R., (1967) Paper submitted to Ap. J. American Science and Engineering Report No. 1587.

Gillespie, A.B. (1953) "Signals Noise and Resolution in Nuclear Counter Amplifiers" Pergamon.

Gold, A. and Knox, R.S. (1959) Phys. Rev. 113, 838.

Gould, R.J., Burbidge G.R. (1963) Ap. J., 138, 969.

Gould, R.J. (1967) Am. J. Phys. 35,5. May 1967, 376 - 393.

Grader, R.J., Hill, R.W., Seward, F.D., Toor, A., (1966) Science, 152, 3728, 1499 - 1504.

Grennberg, B., (1967) J. Sci. Insts. 44, 203 - 6.

Gursky, H., Giacconi, R., Paolini, F.R., Rossi, B.B., (1963) Phys. Rev. Letters, 11,530.

Gursky, H., Zehnpfennig, T., (1966) App. Optics., 5, 875 - 6.

Haitz, R.H., Smits, F.M., (1966) IEEE Trans., N.S. 13,3, 198 - 207.

Harries, J., McCracken, K.G., Francey, R.J., Fenton, A.G., (1967) University of Adelaide Report.

Henke, B.L., White, R. amd Lundberg, B. (1957) J.App. Phys. 28, 1, 98 - 105.

Henke, B.L., (1963) X-Ray Microanalysis, 157 - 72.

Henry, B.B., Cole, H., (1959), Rev. Sci. Insts. 30, 2, 90 - 2.

Heroux, L., Manson, J.E., Hinteregger, H.E., McMahon, W.J. (1965) J. Opt. Soc. Am. 55, 103.

Hicks, D.B., Reid Jr ., L., Petersen, L.E., (1965) IEEE Trans. NS 12, 1, 54 - 65.

Hinteregger, H.E., Hall, L.A., Schweizer, W., (1964) Ap. J. 140, 319.

Holland, L., (1956) "Vacuum deposition of thin films". Chapman and Hall.

Hunter, W.R., (1962) Space Res. III,1187 - 94.

Hunter, W.R., (1964) Le Journal de Physique 25, 154 - 60.

Huth, G.C., Trice, J.B., Shannon, J.A.. and McKinney, R.C. (1965) Trans. IEEE, N.S. 12, 275 - 80.

Huth, G.C. (1966) Trans. IEEE, N.S. 13, 1, 36 - 42.

Ipatkin, I.S., Bulatov, B.P., Antonov, E.A., (1966) Insts. and Exptl. Tech. 3, 577 - 80.

Izrailev, I.M., (1963) Soviet Physics Technical Physics, 7, 11, 1020 - 2.

Jacob, L., Noble, R., (1960) J. Sci. Insts. 37, 460 - 2.

Johann, H.H. (1931) Zeitschrift fur Physik, 69, 185.

Karzas, W.J., Latter, R., (1961), Ap. J. Suppl., 6, 167 - 212.

Korchak, A.A. (1967) Nature, 213, 5082, 1209 - 10.

Kupperian Jr., J.E., Byram, E.T., Chubb, T.A., Friedman, H. (1959) Planetary and Space Science, 1, 3.

Kvasnica, J., (1960) Czech. J. Phys., B 10, 14.

Lane, R.O., Zaffarano, D.J., (1954) Phys. Rev. 94,4, 960 - 4.

Langmann, H.J., Meyer, O., (1964) Nuclear Insts. and Methods, 30, 135.

Lifshits, T.M. (1956) Radioteknika i Elektronika, 1, 1271 - 83.

Lindsay, J.C., (1964) Planet. Space Sci. 12, 379 - 91.

Lukirskii, A.P. Karpovich, I.A., (1959) Optika i Spektroskopiya, 4, 685.

Lukirskii, A.P., Rumsh, M.A. and Smirnov, L.A. (1960 a) Optics and Spectroscopy, 9, 262 - 5.

Lukirskii, A.P., Rumsh, M.A., Smirnov, L.A., (1960 b) Optics and Spectroscopy 9, 265 - 7.

Lukirskii, A.P., Rumsh, M.A., Karpovich, I.A., (1960 c), Optics and Spectroscopy, 9, 5, 343 - 6.

Lukirskii, A.P., (1961) Bull.Acad. Sci. 25, 8, 926 - 31.

Lukirskii, A.P., Savinov, E.P., (1962) Optics and Spectroscopy 13, 480 - 1.

Lukirskii, A.P., Brytov, I.A. and Ershov, O.A. (1963) Bull. Acad. Sci., 27, 3, 447 - 52.

Lukirskii, A.P., Brytov, I.A., Zimkina, T.M., (1964 a) Optics and Spectroscopy 17, 234 - 7.

Lukirskii, A.P., Savinov, E.P., Brytov, I.A., Shepelev, Yu.F. (1964 b) Bull. Acad. Sci. (USSR) 28, 5. Translated 1965, 774 - 80.

Lukirskii, A.P., Savinov, E.P., Ershov, O.A., Shepelev, Yu.F., (1964 c) Optics and Spectroscopy 16, 168 - 72.

Lukirskii, A.P. and Brytov, I.A. (1965) Insts. Exp. Tech., 5, 1083 - 7.

Lukirskii, A.P., Ershov, O.A., Zimkina, T.M., Savinov, E.P. (1966) Soviet Physics Solid State, 8, 6, 1422 - 4.

Lukirsky, P. (1924 a) Z. Phys. 22, 6, 351 - 67.

Lukirsky, P. (1924 b) Phil. Mag. 47, 466.

Madden, R.P., Ederer, D.L., Codling, K. (1967) App. Optics, 6, 1, 31 - 8.

Mandel'stam, S.L., (1965) Space Science Reviews 4, 5/6, 587 - 665.

Mandel'stam, S.L., (1967), Applied Optics, 6, 11, 1834 - 44.

Manley, O.P., (1966), Ap. J., 144, 2, 628 - 34.

Marshall, Fitz-Hugh, Coltman, J.W., Hunter, L.P., (1947) Rev. Sci. Insts. 18, 7, 504 - 13.

Matsuoka, M., (1966) Jap. J. App.Phys. 5, 8, 671 - 88.

Mc.Ilraith, A.H., (1962) J. Sci. Insts. 39, 10, 504 - 8.

Mehlhorn, W., Albridge, R.G., (1964) Nuclear Insts. and Methods, 26, 37 - 41.

Melton,C.E.,Hurst,G.S.,Bortner,T.E.(1954) Phys.Rev.,96,3, 643-5.

Metchnik, V. (1964) Aust. J. Phys. 17, 200 - 4.

Meyerott, A.J., Fisher, P.C., Roethig, D.T., (1964) Rev. Sci. Insts. 35, 6, 669 - 672.

Misso, C.E.F., Karpinski, J.Z., (1964) IEEE Trans., N.S.11., 72 -75.

Morgan, R.H., (1942) Am. J. Roent. Rad.Ther. 47, 777.

Murcray, W.B. (1966) J. Geophys. Res., 71, 2739.

Nakhodkin, N.G., Mel'nik, P.V. (1963) Sov. Phys. Solid State, 1259 - 61.

Nakhodkin, N.G., Mel'nik, P.V., (1964), Bull. Acad. Sci., 28, 9.

Neufeldt, H. (1931) Z. fur Physik 68, 659 - 74.

Neupert, W.M., (1965) Annales d'Astrophysique 28, 2, 446 - 56.

Neupert, W.M., Gates, W., Swartz, M., Young, R., (1967) Ap. J. Letters, 149, 2, 2, L79 - 83.

Ogier, W.T., Ellis, D.V., (1965), J. App.Phys. 36, 12, 3788 - 90.

Ong, Poen Sing. (1965) Advances in X-ray Analysis Vol. 8, 341 - 51.

Oshchepkov, P.K., Skvortsov, B.N., Osanov, B.A., Siprikov, I.V., (1960) Insts. Exp. Tech. 4, 611 - 14.

Owen, R.B., Awcock, M., (1967) Report R.5393, A.E.R.E., Harwell, Berks.

Parratt, L.G., (1950) Paper presented at the Conference of Applications of X-Ray Spectroscopy to Solid State Problems. University of Wisconsin, October, 1950.

Pottasch, S.R. (1964) Space Science Reviews 3, 816 - 55.

Pounds, K.A., (1965) Journal of Photographic Science 13, 20 - 4.

Radeka, V., (1965) Nucleonics, 23, 7, 52 - 5.

Rees, M.J., Sciama, D.W. (1966) Nature, 211, 5051, 805 - 7.

Richardson, O.W., Chalkin, F.C., (1926) Proc. Roy. Soc. A., 110, 247 - 82.

Rompe, R., Schnürer, E., (1960), Sonderdruck aus Monatsberichte der Deutschen Akademie der Wissenschaften zu Berlin. Band 2, Heft 5, 280 - 6.

Rudberg, E. (1928) Proc. Roy. Soc. A. 120, 385 - 422.

Rumsh, M.A., Lukirskii, A.P., Karpovich, I.A., Shchemelev, V.N., (1960 a) Insts. Exp. Tech., 5., 755 - 761.

Rumsh, M.A., Lukirskii, A.P., Shchemelev, V.N., (1960 b) Sov. Phys. Dok. 135, 1, 1231 - 3.

Rumsh, M.A., Shchemelev, V.N., Lukirskii, A.P., (1961) Bull. Acad. Sci. 25, 8, 1069.

Rumsh, M.A., Shchemelev, V.N. (1962) J.E.T.P., 15, 3, 507 - 12.

Rumsh, M.A., Shchemelev, V.N., Prois, Kh., (1962 a) Soviet Physics Solid State 4, 1, 44 - 48.

Rumsh, M.A., Shchemelev, V.N., Prois, Kh., (1962 b) Soviet Physics Solid State 4, 1, 49 - 51.

Rumsh, M.A., Shchemelev, V.N., (1963 a) Soviet Physics Solid State, 5, 46 - 50.

Rumsh, M.A., Shchemelev, V.N., (1963 b) Bull. Acad. Sci. 27, 6, 812.

Rumsh, M.A., Shchemelev, V.N., (1963 c) Sov. Phys. Solid State, 4, 8, 1503 - 8.

Russell, P.C., (1965 a) Nature 205, 4972.

Russell, P.C., (1965 b) Nature 206, 4981, 281.

Russell, P.C., Pounds, K.A. (1966) Nature 209, 5022, 490.

Sanford, P.W., (1967) Private Communication.

Sanford, P.W. and Culhane, J.L. (1967) Proceedings of Second Symposium on low energy X and γ Sources and Applications held at Univ. of Texas, Austin, Texas, March 27 - 29.

Savinov, E.P., Lukirskii, A.P., Shepelev, Yu.F., (1965) Soviet Physics Solid State, 6, 11, 2624 - 30.

Schmidt, K.C., Hendee, C.F., (1966) IEEE Trans. N.S. 13, 3, 100 - 111.

Schumacher, B.W., Grodski, J.J., (1965) Proceedings of the Fourth National Meeting of the Society for Applied Spectroscopy. August 30 - Sept.3, 1965. Denver, Colorado. The device described is also the subject of Brit.Pat.No. 945, 621 - Jan. 2. 1964.

Schwinger, J. (1949) Phys. Rev., 75, 1912.

Seward, F.D., Toor, A., (1967) Paper submitted to Ap.J. Pre-print 70300, Lawrence Radiation Laboratory.

Seward, F., Chodil, G., Mark, H., Swift, C., Toor, A., (1967) Paper submitted to Ap. J. Pre-print 70425, Lawrence Radiation Laboratory.

Sharpe, J. (1955) "Nuclear Radiation Detectors". Methuen. 2nd. Ed.

Shchemelev, V.N. (1963) Rumsh, M.A., Soviet Physics Solid State, 4, 10, 2048 - 52.

Shchemelev, V.N., Eliseenko, L.G., Denisov, E.P., Rumsh,M.A., (1965) Soviet Physics Solid State, 6, 9, 2051 - 5.

Shea, M.F., Shook, G.B., Reagan, J.B., Smith, L.F., Sanders, T.C., (1967) IEEE Trans. N.S. 14, 96 - 102.

Smith, D.G. (1966) J. Sci. Insts. 43, 270 - 1.

Smith, D.G. (1967) J. Sci. Insts. 44, 12, 1053 - 5.

Spielberg, N., (1966) Rev. Sci. Insts. 37, 9, 1268 - 9.

Spindt, C.A., Shoulders, K.R., (1965) Rev. Sci. Insts., 36, 6, 775 - 9.

Stanford, J.L., Hamm, R.N., Arakawa, E.T. (1966) J. Opt. Soc. Amer. 56, No. 1, 124.

Stewardson, E.A., Underwood, J.H. (1965) Brit. J. App. Physics, 16, 1877 - 84.

Strom, S.E., Strom, K.M. (1961) Publ. Astrom. Soc. Pacific. 73, 43.

Theisen, R., Vollath, D. (1967) "Tables of Mass Attenuation Coefficients", Verlag Stahleisen, M.B.H. Dusseldorf.

Tiutikov, A.M., Efremov, A.I., (1958) Soviet Physics Doklady, 3, 154 - 6.

Tomboulian, D.H., Hartmann, P.L. (1956) Phys. Rev. 102, 1423 - 47.

Tomboulian, D.H. (1960) U.S.A.E.C. Report No. NP - 8475.

Tomboulian, D.H. (1964) "The determination of absolute photon fluxes and applications to laboratory calibration procedures in the 100 Å to 300 Å range." NASA - G.S.F.C. Report.

Tousey, R., (1967) Ap. J., 149, 2, 1, 239 - 52.

Trice, J.B. (1967) Private Communication.

Tsukerman, V.G., Gerasimov, V.A., Granitskii, L.V., Neermalov, A.F. (1966) Insts. Exp. Tech. 1, Jan - Feb. 174 - 9.

Tucker, W.H. and Gould R.J. (1966) Ap. J. 144, 1, 244 - 58.

Tucker, W.H. (1967) Ap. J. 148, 745 - 65.

Underwood, J.H., Muney, W.S., (1967) Solar Physics, 1, 129 - 44.

University of Leicester (1967) "Proposal for a neon-edge experiment."

Walker, S., Straw, H. (1962) "Spectroscopy" Vol. 2. Chapman and Hall.

Walker, W.C., Wainfain, N., Weissler, G.L., (1955) J. App. Phys. 26, 11, 1366 - 71.

Waters, J.R., (1964) Nuclear Insts and Methods, 30,336 - 40.

Weimer, P.K., Sadasiv, G., Borkan, H., Meray-Horvath, L., Meyer, Jr., J., Shallcross, F.V., (1966) Proceedings of the International Solid State Circuits Conference. University of Pennsylvania, Feb. 11, 1966.

Wilcock, W.L. (1967) Private Communication.

Wilson, J.E., (1966) Private Communication.

Wolfendale, A.W. (1963) "Cosmic Rays", Newnes, 129.

Zehnpfennig, T., (1966) App. Optics, 5, 1855 - 6.

Zizzo, S.G., Platt, J.B., (1949) Phys. Rev. 76, 704.

Zulliger, H.R., Aitken, D.W. (1967) Trans. IEEE, N.S. 14, 1, 563 - 9.

Reprinted from the *Journal of Scientific Instruments*, Vol. 43, pp. 270–271, April 1966

Gain variations in some channel multipliers

D. G. SMITH
Department of Physics, University of Leicester
MS. received 25*th November* 1965, *in revised form* 25*th January* 1966

Abstract. Three distinct types of gain variation observed in channel multiplier samples are described, and possible mechanisms of these variations are suggested.

1. Introduction

The channel multiplier (Wiley and Hendee 1962) has been used recently for the detection and measurement of both low-energy particles (Evans 1965) and ultra-violet radiation (Hunter 1963). Because of the unique geometry of the multiplier we have considered its application to the detection of soft x rays. The present note gives some interesting gain variations observed during the operation of these devices. The multipliers were operated in the pulse counting mode and count rates of between 10^2 and 10^3 counts per second were usual.

2. Gain fatigue

This effect was observed with three Bendix multipliers. Each multiplier was 1 cm in length, 170 μm internal diameter and had a d.c. resistance of 10^{10} Ω. The results obtained with each were sufficiently alike to warrant description of the measurements from one multiplier only.

The variation of pulse height distribution with channel voltage illustrates the gain saturation that occurs in some channel multipliers under certain conditions (figure 1). This phenomenon has been adequately discussed elsewhere (Evans 1965, Bryant 1965). Operation of the multiplier under such conditions, however, was found to lead to a reduction in gain. A typical reduction causes the output pulses to change from the state shown in figure 1 (curve C) to that in figure 1 (curve A), the multiplier then remaining comparatively stable with time. This fatiguing effect was found to be reversible, since the original conditions of gain saturation could be recovered by 'resting' the multiplier at a lower voltage or switching it off for a period of time. The effect was independent of the presence of incident radiation. The time required for the fatigue to take effect, however, was dependent on channel voltage. At voltages barely sufficient to cause gain saturation this took several hours, but at higher voltages fatiguing times as short as ten seconds were observed. On examining the multiplier under conditions of rapid fatigue (30 sec fatiguing time) it was found that the multiplier recovered its original gain within approximately $2\frac{1}{2}$ minutes of switching off irrespective of the time of operation in the fatigued condition.

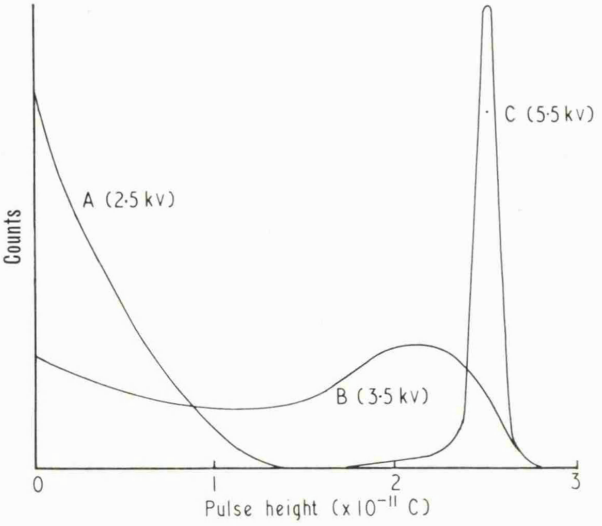

Figure 1. Variation of pulse height distribution with channel voltage. Pressure: 2×10^{-5} torr.

The multiplier seemed thus to possess a characteristic gain recovery time, and this was studied in the hope that it would indicate the mechanism responsible for the fatiguing effect.

A small calibrated thermocouple placed against the earthy end of the multiplier indicated a small rise in temperature (~1 degc) during operation. In view of the poor thermal contact existing and the relatively massive thermocouple that was used this apparently small temperature rise was significant enough to prompt further measurement.

A subsidiary experiment showed that the resistance of the multiplier could be represented by the expression

$$R_t = R_0(1 + \alpha t)$$

where $\alpha = -6{\cdot}75 \times 10^{-3}$ degc^{-1} over the range 10–70°c.

Independent measurements of the multiplier's current were then taken with a vibrating reed electrometer for a range of the multiplier's voltages. At each voltage, readings of the current were taken 1, 5 and 30 sec after the voltage had been switched on (very little increase occurring after 30 seconds had elapsed). The multiplier voltage was turned off for five minutes prior to taking readings at the next voltage (see figure 2). These measurements indicated that

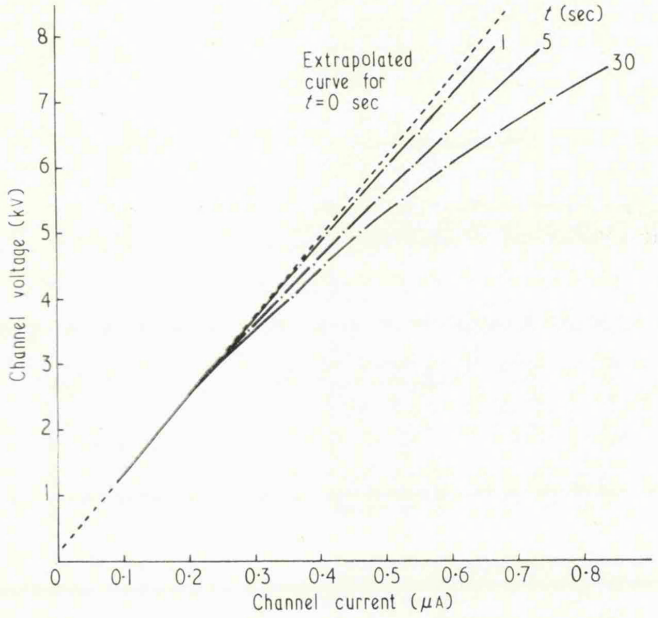

Figure 2. Channel voltage plotted against channel current.

at the operating conditions (6 kv, 2×10^{-5} torr) the multiplier not only fatigued over a period of 30 seconds but simultaneously suffered a decrease in channel resistance amounting to 22·5% of its original resistance. This represented an increase in the temperature of the multiplier of 33 degc above ambient.

It is concluded that gain fatigue coincides with the rise in temperature of the multiplier, the characteristic recovery time then corresponding to its cooling down period. Since the central sections of the channel are likely to suffer the greatest temperature increase, it is possible that the greatest reduction in channel resistance occurs here also. This would tend to lower the axial field strength of the channel at this point, thereby causing a reduction in gain.

3. Long-period gain reduction

A second effect has been observed over a period of eighteen months of intermittent operation of the multipliers. During this time a reduction of gain amounting to 20 db has taken place. The possibility of contamination of the secondary emitting surface exists, since the multiplier was operated for some time in the spectrometer prior to fitting a liquid nitrogen vapour trap. Conventional cleaning techniques have been applied to the multiplier but no significant recovery of initial operating characteristics has resulted. In support of the contamination hypothesis it is noted that intermittent operation of a Mullard multiplier for one year, entirely in the 'clean' vacuum type chamber, has resulted in no observed gain decay.

4. Gain variation at onset of operation

A third gain variation has been observed with the Mullard multiplier referred to in the previous paragraph. The multiplier measures 5 cm in length and 770 μm internal diameter and has a d.c. resistance of $10^{10}\ \Omega$. The overall performance was found to be similar to the Bendix multipliers with regard to gain, pulse height distribution and operating voltage. Immediately after switching on the multiplier a gradual decrease in gain has been found over the first 2000 or so counts. For an operating voltage of 4 kv the total gain loss was 6 db. Thereafter, continued operation of up to 50 hours showed no further gain variation greater than 1 db. The initial gain was recovered only after letting the spectrometer up to atmospheric pressure. Subsequent operations have shown this cycle to be strictly repeatable and to be unaffected by chemical cleaning of the multiplier prior to evacuation. The effect appears to be due to an absorbed gas layer on the multiplier surface, which is removed by the initial few thousand electron avalanches.

Acknowledgments

The author would like to acknowledge the generosity of Dr. H. Friedman of the Naval Research Laboratory, Washington D.C., for providing the Bendix multipliers, and of Mr. B. W. Manley of Mullard Research Laboratories, Redhill, for providing the Mullard multiplier.

References

Bryant, D. A., and Johnstone, A. D., 1965, *Rev. Sci. Instrum.*, **36**, 1662.

Evans, D. S., 1965, *Rev. Sci. Instrum.*, **36**, 375–82.

Hunter, W. R., 1963, *Space Research III: Proc. 3rd Int. Space Science Symp., Washington, D.C., 1962*, ed. W. Priestler (Amsterdam; North Holland,) pp. 1187–94.

Wiley, W. C., and Hendee, C. F., 1962, *I.R.E. Trans. Nucl. Sci.*, **9**, 103–6.

UNWIN BROTHERS LIMITED, WOKING AND LONDON (B 6139)

J. SCI. INSTRUM., 1967, VOL. 44

Channel multiplier life tests in ultra-high vacuum

D. G. SMITH†
Department of Physics, University of Leicester

MS. received 22*nd March* 1967, *in revised form* 15*th June* 1967

Abstract. The results of two-channel multiplier life tests in ultra-high vacuum are presented. In both cases the mean charge output was found to decrease progressively and to vary approximately as the reciprocal of the total number of counts for counts in excess of 10^{10}. A mechanism for this decrease is suggested.

1. Introduction

An earlier report (Smith 1966) described some gain variations experienced with channel multipliers. The results reported here form part of the continuation of this work to establish the suitability of the channel multiplier for laboratory and space experiments.

The two-channel multipliers tested in this work were examined individually in an ultra-high vacuum system. This testing environment was chosen to simulate as closely as possible the operating conditions in an orbiting satellite. The vacuum system consisted basically of a 2 l. stainless-steel chamber, fitted with an ionization gauge and a 15 l. sec^{-1} Penning pump. The system could be baked to 450°C, but in the present work no baking was attempted because of the unknown thermal stability of the channel multipliers.

A small tritium source mounted with the channel multiplier under test, provided a means of exciting pulses. In the first test the ionization gauge was also used for this purpose; the filament providing a convenient supply of electrons, the strength of which was dependent on the emission range used. In the second test the count rate was kept constant at a value considered to be reasonably typical of a satellite experiment.

The output pulses from the multiplier were displayed after amplification on an oscilloscope. Pulse amplitude analysis and count rate determination could be made with either a multichannel analyser or a single-channel analyser and counting unit. A precision pulser in series with a 2 pF calibration capacitor was used for a charge reference.

2. Results of the first test

The multiplier used for this test was a Mullard experimental type B400 A (channel length 7·5 cm, internal diameter 0·22 cm, d.c. resistance $1{\cdot}4 \times 10^{10}\ \Omega$). The multiplier was open at both ends and curved over 75% of its length to prevent positive ion feed back (Adams and Manley 1966, Schmidt and Hendee 1966). The independence of multiplier gain on environmental gas pressure was confirmed over the range 3 μtorr to 0·2 mtorr in a separate experiment beforehand.

The ultimate pressure attained by the end of the test was 0·4 ntorr. For most of the time, however, the pressure was of the order of 5 ntorr. The attainment of such pressures without baking of the vacuum system was attributed to the short time of exposure of the system to the atmosphere (30 minutes) during the mounting of the multiplier. The system had previously been evacuated and baked to 250°C by the manufacturer.

The multiplier was operated at 4 kv. This potential was insufficient to produce gain saturation, but was considered to be the maximum desirable in view of insulation requirements.

At the higher count rates decreases were observed in the mean output charge, due to current limitation in the channel multiplier (Adams and Manley 1965). To enable meaningful comparisons of multiplier gain to be made, therefore, the mean output charge was always measured at the same count rate (200 counts per sec approximately). In practice this meant switching the ionization gauge off and using only the tritium source to excite the multiplier. After the measurement had been made, the gauge was switched to the appropriate emission range and left on until the next measurement was due. Under these conditions, it was found the that oscilloscope display was adequate for the estimation of mean pulse height. Measurements could be reproduced to within ±10% even though the pulse height distribution was of exponential form.

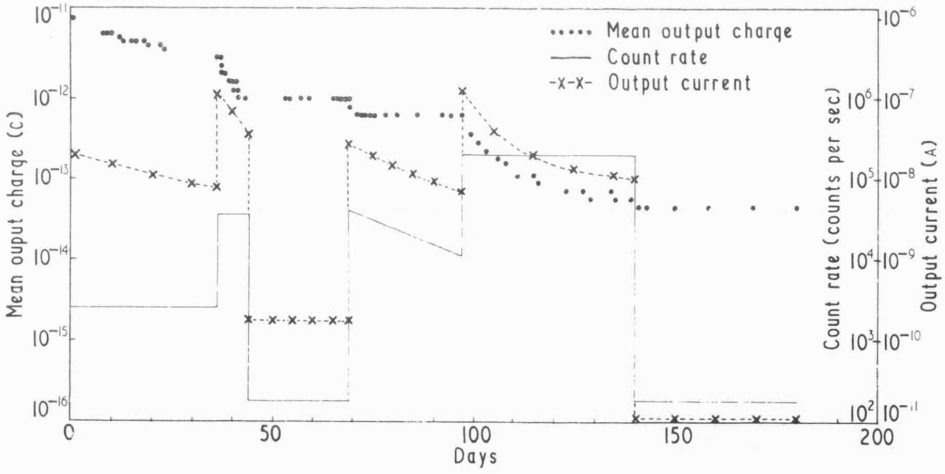

Figure 1. The variation of count rate, mean charge output and mean output current with time for first test.

† Now at Department of Physics, University of South Wales.

From figure 1 it is evident that the rate of decrease of mean charge output is a function of both count rate and time. A clearer picture emerges if the mean charge output is plotted against the integrated count total, as shown in figure 2. The plotted points represent ten-day integration intervals, from day 10 to day 140. The ionization gauge filament failed on day 140.

The multiplier was re-examined on day 240, having remained exposed to the laboratory atmosphere since the end of the life test on day 180. The mean charge output was found to have increased from $4{\cdot}5 \times 10^{-14}$ to $3{\cdot}2 \times 10^{-13}$ coulombs. The multiplier was then operated at a pressure of 10 μtorr for a further 4×10^7 counts at approximately 5000 counts per sec, but no measurable decrease in output was observed to take place.

The d.c. resistance of the channel measured at atmospheric pressure with a megohmeter on day 1 and day 180 was found to have remained constant to within 5% (the estimated accuracy of measurement).

3. Results of second test

The multiplier used in this test was a non-standard variation of the B400 type (channel length 11·5 cm, internal diameter 0·24 cm, d.c. resistance $2{\cdot}2 \times 10^{10}\ \Omega$). The additional length was accommodated as an extra turn on the curved section of the channel. The anode end of the multiplier was closed for reasons of practical convenience but the mode of operation was the same as that of the first test.

The initial pulse height distribution at 4 kv exhibited a broad peak which showed that the multiplier was operating into saturation. The count rate was approximately 3500 counts per sec. The pulse height distribution was observed not to change at lower count rates and it was concluded, therefore, that current limitation was not present at 3500 counts per sec.

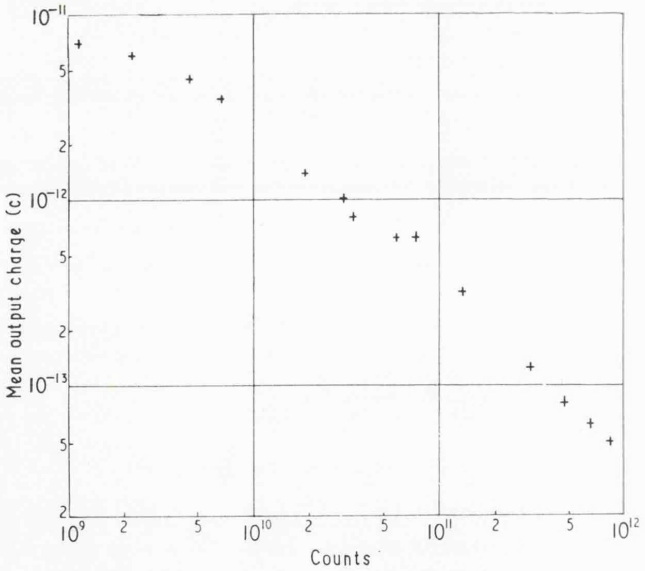

Figure 2. The variation of mean charge output with total number of counts for first test.

The change of pulse height distribution with time is shown in figure 3; the accumulation interval was 60 seconds for each distribution. The variation of mean charge output with the integrated count total is shown in figure 4.

The d.c. resistance of the multiplier was measured periodically during this test; the readings were found to differ by less than 2%.

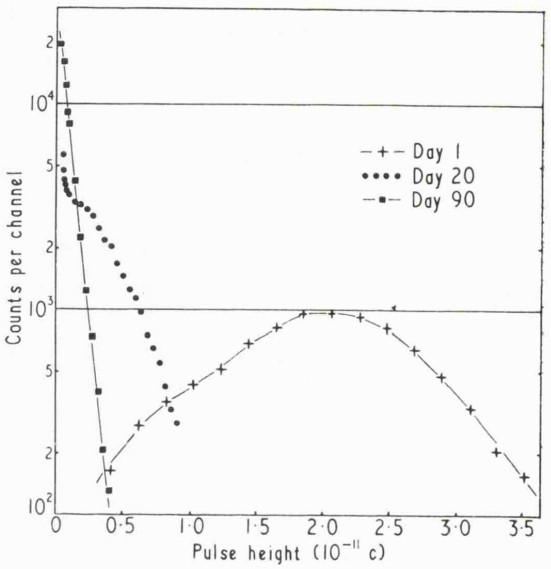

Figure 3. The change of pulse height distribution with time for second test.

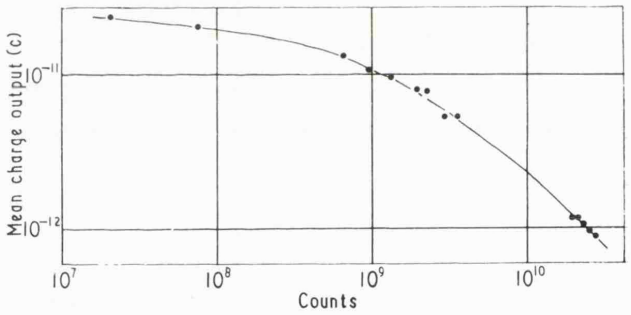

Figure 4. The variation of mean charge output with total number of counts for second test.

4. Discussion

Since only two multipliers have been examined, these results do not have great statistical significance. It is evident, however, that in both tests the multipliers exhibited a progressive decrease of mean charge output q in operation and that, in both cases, the decrease is related in some way to the integrated count total n. In fact for $n > 10^{10}$ there would appear to be an approximately reciprocal relationship between q and n of the form $q = A/n$; A was $4{\cdot}2\ (\pm 10\%) \times 10^{-2}$ coulombs in the first test and $2{\cdot}4\ (\pm 10\%) \times 10^{-2}$ coulombs in the second. The significance of the constant A is not clear for, although its value is lower in the second test, the multiplier used in this test was physically the larger of the two and possessed a slightly higher initial mean charge output.

Since the multipliers were operated at a fixed channel voltage a decrease in the mean charge output corresponds to a decrease in the secondary emission coefficient of the inside surfaces of the multipliers. Under conditions of ultra-high vacuum, it seems unlikely that contamination of the multipliers is the reason for such decreases. The alternative mechanism of surface modification would seem to be the removal of material during operation, leaving behind a cleaner surface with a lower secondary emission coefficient. The gain increase observed in the first test following exposure of the multiplier to the atmosphere would lend support to

this; the surface material removed being partly replaced by adsorbed atmospheric gas molecules. A similar effect was noted previously (Smith 1966). Then the increase in charge output was observed to fall to zero over the first few thousand counts, following the exposure of the multiplier to atmosphere. The fact that a subsequent decrease was not observed in the present work over 4×10^7 counts is thought to indicate that the multiplier surface was far more chemically active after the extensive life testing and therefore not so ready to release the atmospheric gas molecules attached to it. A measurable decrease would have been expected after a further 10^{11} counts, say, in view of the life test results. The fact that, in both tests, the channel resistance was found to remain substantially unaltered would indicate that the material removed from the surface did not contribute appreciably to the electrical conductivity of the surface. A consequence of the proposed model is a dependance of the output charge decrease on operating pressure according to the conditions of equilibrium existing between the adsorbed gas layers and the vapour phase of each gas component in the vacuum chamber. Thus, under ultra-high vacuum conditions, the rate of loss of surface material will be higher than that at higher pressures. It will not be possible to confirm this until extensive life tests are carried out at higher pressures. The present tests, however, have direct significance in the use of channel multipliers in satellite experiments. It would seem that a generous margin of amplifier gain in the electronic system is called for, if high count totals are anticipated in a particular experiment.

Acknowledgments

The author would like to thank Professor E. A. Stewardson for his encouragement and interest in the work; also B. W. Manley and J. Adams of Mullard Research Laboratories for many helpful discussions.

References

ADAMS, J., and MANLEY, B. W., 1965, *Electron. Engng*, **37**, 180–1.

—— 1966, *I.E.E.E. Trans. Nucl Sci.*, **NS 13, 3**, 88–99.

SCHMIDT, K. C., and HENDEE, C. F., 1966, *I.E.E.E. Trans. Nucl. Sci.* 3, **NS 13, 3**, 100–11.

SMITH, D. G., 1966, *J. Sci. Instrum.*, **43**, 270–1.